Charles University in Prague

Faculty of Science

Developmental and Cell Biology

Ing. Stanislav Vinopal

FUNCTIONAL CHARACTERIZATION OF SELECTED MICROTUBULE REGULATORY PROTEINS

Ph.D. Thesis

Supervisor: Assoc. Prof. RNDr. Pavel Dráber, Ph.D.

Department of Biology of Cytoskeleton

Institute of Molecular Genetics of the AS CR, v.v.i.

Prague, 2012

Prohlášení:

Prohlašuji, že jsem závěrečnou práci zpracoval samostatně a že jsem uvedl všechny použité informační zdroje a literaturu. Tato práce ani její podstatná část nebyla předložena k získání jiného nebo stejného akademického titulu.

V Praze 8. 3. 2012

Ing. Stanislav Vinopal

Prohlášení:

Jménem ostatních spoluautorů publikací, které tvoří základ disertační práce Ing. Stanislava Vinopala, potvrzuji, že podíl autora na jejich přípravě je popsaný v komentářích k jednotlivým publikacím pravdivě.

V Praze 8. 3. 2012

Doc. RNDr. Pavel Dráber, CSc.

Poděkování:

Předně chci poděkovat svému školiteli Pavlu Dráberovi za moudré vedení, inspirativní diskuze, podporu, trpělivost a důvěru v průběhu celého mého doktorského studia. Děkuji současným i bývalým členům Laboratoře biologie cytoskeletu, se kterými jsem mohl v průběhu let spolupracovat, za velmi příjemnou pracovní atmosféru, za všechnu pomoc a za vzácná přátelství. Také jsem vděčný mnoha dalším spolupracovníkům z Ústavu molekulární genetiky AV ČR, kteří mi vždy ochotně pomáhali. Dr. Jiřímu Janáčkovi z Fyziologického ústavu AV ČR děkuji za výbornou spolupráci při vývoji programů pro kvantifikaci dynamiky mikrotubulů a buněčné migrace.

Moc děkuji své milované ženě Mařence a všem svým blízkým za účinnou podporu, pochopení i za každodenní sdílení všech radostí i strastí doktorského studia.

TABLE OF CONTENTS

ABBREVIATIONS....1

ABSTRACT....3

SOUHRN....5

I. INTRODUCTION....7

I.1 Microtubules....7

I.1.1 Microtubule organization and functions....7

I.1.2 Microtubule structure and dynamic instability....11

I.1.3 Regulation of microtubule dynamics and functions....16

I.1.3.1 α- and β-tubulin isotypes....16

I.1.3.2 Tubulin post-translational modifications....18

I.1.3.3 Microtubule regulatory proteins....19

I.1.3.3.1 Microtubule destabilizing proteins....20

I.1.3.3.2 Microtubule (+) end tracking proteins....22

I.1.3.3.3 Microtubule (-) end capping proteins....23

I.2 γ-Tubulin....24

I.2.1 γ-Tubulin genes, structure and distribution....24

I.2.2 γ-Tubulin complexes and mechanism of microtubule nucleation....25

I.2.3 Other functions of γ-tubulin....28

I.2.4 γ-Tubulin regulation....29

I.3 Important model systems used in the study....31

I.3.1 Mast cells....31

I.3.2 Glioblastoma cells....32

II. AIMS OF THE STUDY....34

III. COMMENTS ON PRESENTED PUBLICATIONS....35

III.1 STIM1-directed reorganization of microtubules in activated mast cells....35

III.2 Microtubule-severing ATPase spastin in glioblastoma: increased expression in human glioblastoma cell lines and inverse roles in cell motility and proliferation....37

III.3 Nuclear γ-tubulin associates with nucleoli and interacts with tumor suppressor protein C53....38

III.4 γ-Tubulin 2 nucleates microtubules and is downregulated in mouse early embryogenesis 41

IV. CONCLUSIONS 45

V. REFERENCES 47

VI. PRESENTED PUBLICATIONS 61

VI.1 Hájková Z., Bugajev V., Dráberová E., **Vinopal S.**, Dráberová L., Janáček J., Dráber Pe., Dráber Pa. (2011). STIM1-directed reorganization of microtubules in activated mast cells. J Immunol. *186*, 913-923. 61

VI.1.1. Supplementary data 75

VI.2 Dráberová E., **Vinopal S**., Morfini G., Liu P.S., Sládková V., Sulimenko T., Burns M.R., Solowska J., Kulandaivel K., de Chadarévian J.P., Legido A., Mörk S.J., Janáček J., Baas P.W., Dráber P., Katsetos C.D. (2011). Microtubule-severing ATPase spastin in glioblastoma: increased expression in human glioblastoma cell lines and inverse roles in cell motility and proliferation. J Neuropathol Exp Neurol. *70*, 811-826. 81

VI.2.1. Supplementary data 99

VI.3 Hořejší B., **Vinopal S.**, Sládková V., Dráberová E., Sulimenko V., Sulimenko T., Vosecká V., Philimonenko A., Hozák P., Katsetos C. D., Dráber P. (2012). Nuclear γ-tubulin associates with nucleoli and interacts with tumor suppressor protein C53. J Cell Physiol. *227*, 367-382. 105

VI.3.1. Supplementary data 123

VI.4 **Vinopal S**., Černohorská M., Sulimenko V., Sulimenko T., Vosecká V., Flemr M., Dráberová E., Dráber P. (2012). γ-Tubulin 2 Nucleates Microtubules and Is Downregulated in Mouse Early Embryogenesis. PLoS ONE *7*: e29919. 135

VI.4.1. Supplementary data 151

ABBREVIATIONS

2D-PAGE	2 Dimensional-polyacrylamide gel electrophoresis
AAA	ATPases associated with various cellular activities
Ag	Antigen
BMMC	Bone marrow mast cell
CAP-Gly	Cytoskeleton-associated glycine-rich domain
CH	Calponin homology domain
CHMP	Charged multivesicular body protein
EB	End-binding protein
EBH	EB-homology domain
ECM	Extracellular matrix
EM	Electron microscopy
ER	Endoplasmic reticulum
ESCRT-III	Endosomal sorting complex required for transport-III
GA	Golgi apparatus
GCP	Gamma-tubulin complex protein
GMPCPP	Guanosine-5'-[(α,β)-methyleno]triphosphate
HSP	Hereditary spastic paraplegia
IF	Intermediate filament
KD	Knock-down (reduction of gene expression by RNAi technique)
MAP	Microtubule associated protein
MF	Microfilament
MT	Microtubule
MTOC	Microtubule organizing centre
NLS	Nuclear localization sequence
PCR	Polymerase chain reaction
PCM	Pericentriolar matrix
PTM	Post-translational modification
RT-qPCR	Reverse transcriptase-quantitative real-time PCR
SOCE	Store-operated Ca^{2+} entry
TIC	Tumor initiating cell
TTL	Tubulin-tyrosin ligase
γTuC	γ-Tubulin complex
γTuRC	γ-Tubulin ring complex
γTuSC	γ-Tubulin small complex
+TIP	Microtubule plus-end tracking protein

ABSTRACT

Microtubules (MTs) play crucial roles in intracellular organization and transport, cell polarity, motility, signalling, division and differentiation. MTs form complex arrays, which are, due to their highly dynamic nature, capable of rapid reorganization in response to cellular requirements. Dynamics, stability and spatial organization of MTs are regulated by many factors including MT regulatory proteins. In the presented study we functionally characterized three selected MT regulatory proteins: Ca^{2+}-sensor STIM1, MT severing protein spastin and γ-tubulin that is essential for MT nucleation.

We found out that activation of bone marrow mast cells (BMMCs) leads to the formation of plasma membrane protrusions containing MTs. Formation of these MT protrusions is dependent on an influx of extracellular Ca^{2+} regulated by protein STIM1, located in endoplasmic reticulum. STIM1 associates with MTs and its depletion prevents formation of MT protrusions. This indicates that Ca^{2+} ions might be involved in MT regulation. Since STIM1 depletion also causes defects in chemotaxis, we propose that MT protrusions might be involved in sensing of external signals recognized by BMMCs.

Glioblastoma multiforme is the most common and most aggressive malignant primary brain tumor in humans. We demonstrated that MT severing protein spastin is overexpressed in glioma and glioblastoma cell lines and that its expression level increases with tumor malignancy. Glioblastoma cells depleted of spastin exhibit significantly lower motility and an increased proliferation rate. Modulation of these spastin functions in cell migration and proliferation has a potential to become a part of novel approaches to treatment of invasive gliomas.

We showed for the first time that γ-tubulin is present in the nucleoli of various cell types. We identified new γ-tubulin interacting protein C53 in the nucleus using mass spectrometry and found out that γ-tubulin can modulate C53 function in G2/M checkpoint activation after DNA damage. Furthermore, we showed that mammalian γ-tubulin 2 is able to nucleate MTs and substitute for γ-tubulin 1 in cultured cells and that these γ-tubulins are differentially expressed in mouse early embryogenesis and in adult tissues. Based on our results we propose that mammalian γ-tubulins are functionally equivalent with respect to their MT nucleation activity.

SOUHRN

Mikrotubuly (MTs) hrají zásadní roli ve vnitřní organizaci buňky a vnitrobuněčném transportu, v regulaci polarity, pohyblivosti a přenosu signálů i v buněčném dělení a diferenciaci. MTs vytvářejí složité struktury, které jsou díky jejich dynamické povaze schopné rychlé reorganizace dle potřeb buňky. Dynamika, stabilita a prostorové uspořádání MTs jsou regulovány mnoha faktory. Jedním z nich jsou proteiny regulující MTs. V této práci jsme se zabývali funkční charakterizací tří proteinů regulujících MTs: Ca^{2+}-senzoru STIM1, spastinu, proteinu štěpícího MTs, a γ-tubulinu, který je zásadní pro nukleaci MTs.

Zjistili jsme, že aktivace žírných buněk kostní dřeně (BMMCs) vede ke tvorbě výběžků cytoplasmatické mebrány, které obsahují MTs. Tvorba těchto MT výběžků je závislá na transportu extracelulárních Ca^{2+} iontů do buňky, který je řízen proteinem STIM1 lokalizovaným na endoplasmatickém retikulu. STIM1 se váže na MTs a potlačení jeho exprese zabraňuje tvorbě MT výběžků. To naznačuje, že Ca^{2+} ionty mohou hrát roli při regulaci MTs. Jelikož snížení exprese STIM1 způsobuje také poruchy chemotaxe, popsané MT výběžky mohou být hypoteticky důležité pro vnímání vnějších signálů.

Glioblastoma multiforme je nejčastější a nejagresivnější maligní primární nádor mozku u člověka, jehož možnosti léčby jsou dosud velmi omezené. Ukázali jsme, že koncentrace proteinu spastinu, který katalyzuje štěpení MTs, je zvýšená u gliomů a glioblastomových buněčných linií a že jeho množství se zvyšuje se vzrůstající malignitou nádoru. Snížení exprese spastinu v glioblastomové linii vede k významnému snížení jejich pohyblivosti a zároveň ke zvýšené proliferaci. Ovlivnění funkce spastinu v buněčné migraci a proliferaci může potenciálně vést k zavedení nových přístupů k léčbě glioblastomů.

Jako první jsme ukázali, že klíčový protein pro nukleaci MTs γ-tubulin je přítomen v jadérkách různých typů buněk. Pomocí hmotnostní spektrometrie jsme v buněčném jádře identifikovali protein C53, který interaguje s γ-tubulinem. Zjistili jsme, že γ-tubulin může modulovat funkci C53 v G2/M kontrolním bodu po jeho aktivaci poškozením DNA. Dále jsme ukázali, že savčí γ-tubulin 2 je schopen nukleovat MTs a nahradit tak γ-tubulin 1. γ-Tubuliny jsou také rozdílně exprimované v průběhu časné myší embryogeneze i ve tkáních dospělce. Z našich výsledků vyplývá, že savčí γ-tubuliny jsou při nukleaci MTs funkčně ekvivalentní.

I. INTRODUCTION

Cytoskeleton is an intricate system of intracellular filaments essential for cell shape, internal organization and vital functions such as migration, proliferation, differentiation and responsiveness to external stimuli. There are two main types of filaments in eukaryotic cells, microtubules (MTs) and actin microfilaments (MFs). Intermediate filaments (IFs) are the third type of filaments found in metazoa, but not in all eukaryotic cells. Although prokaryotes also possess active and dynamic cytoskeletal structures, there is considerable diversity and no simple relationship between the cytoskeletons of prokaryotes and eukaryotes [1]. Despite structural and functional differences all cytoskeletal filaments closely cooperate and interact with each other.

As this thesis focuses on microtubule regulatory proteins in mammalian model systems, the structure and functions of MTs and their associated proteins in animal cells will be discussed further in greater detail.

I.1 Microtubules

I.1.1 Microtubule organization and functions

MTs are critically important for spatial and temporal organization of eukaryotic cells. They play crucial roles in intracellular transport, organelle positioning, establishment of cell polarity and shape, motility, signalling and cell division. In order to perform all of their functions, MTs are arranged in complex arrays that can be rapidly reorganized in response to cellular requirements. Such rapid rearrangements are possible due to the highly dynamic nature of MTs.

In the majority of interphase animal cells MTs form radial arrays emanating primarily from the centrosome, the microtubule-organizing centre (MTOC) localized near the nucleus. MTs explore cytoplasm with their free ends and reach the cell periphery (Fig. 1A). After the onset of cell division, they radically reorganize to form mitotic or meiotic spindle, very dynamic and distinct structure necessary for precise separation and delivery of sister chromatids or homologous chromosomes to future daughter cells (Fig. 1B). However, MT organization can be completely different in specialized cells. For instance in terminally differentiated neurons, the centrosome loses its function as a MTOC and radial MT arrays disappear. Neuronal MTs form stabilized bundles, which play an important role in

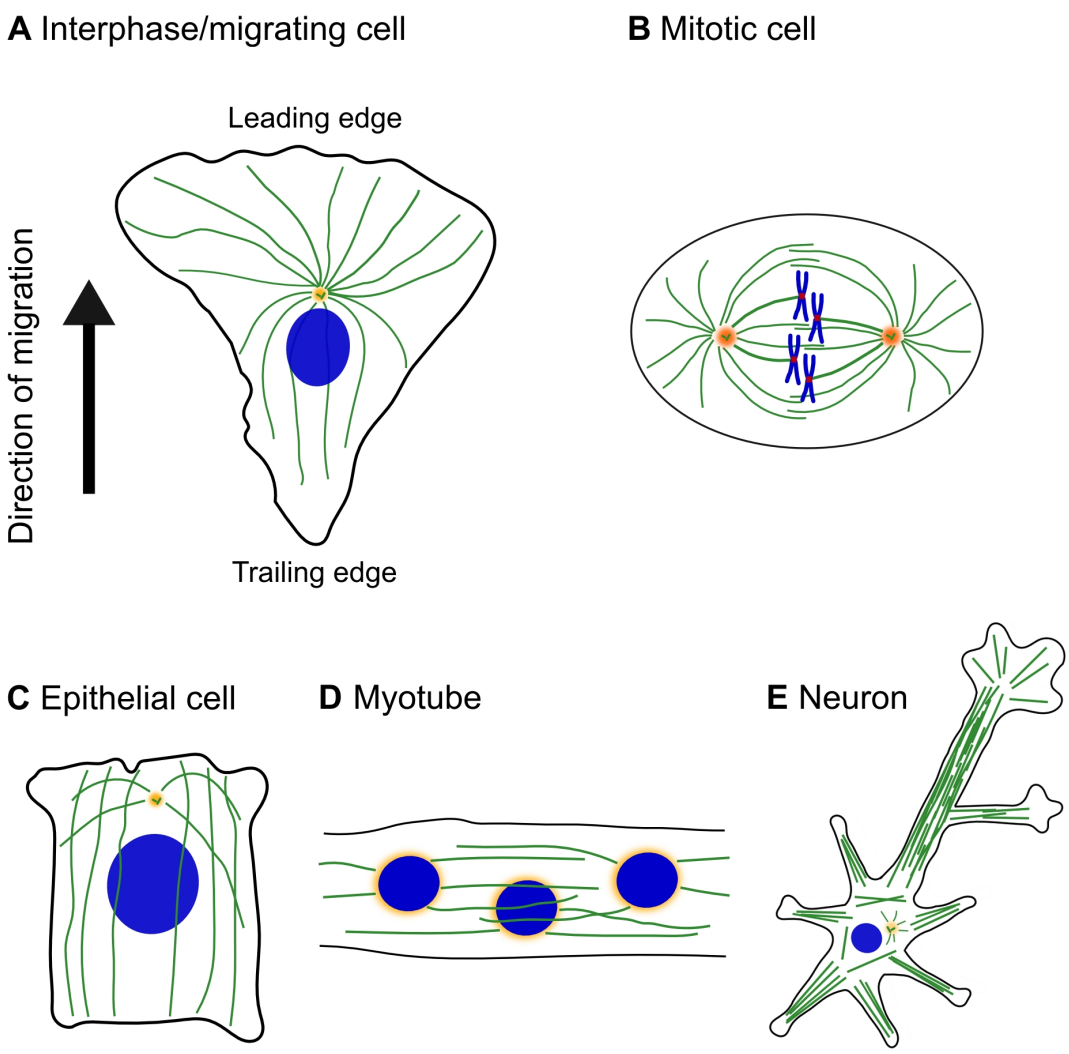

Figure 1. Microtubule arrays in various animal cell types. **A)** MTs are emanating mainly from the centrosome in the majority of interphase animal cells. Cells migrating in the mezenchymal mode stabilize MTs selectively in the direction of migration, whereas MTs near the retracting end of the cell are highly dynamic. **B)** During mitosis MTs form the mitotic spindle. MTs connected to chromosomal centromeres via multiprotein complex called kinetochore (red) are called kinetochore MTs (thick green lines), interpolar MTs are those not connected to kinetochores but directed to the cell center and overlapping. MTs pointing to the opposite direction, to the cell periphery, are termed astral MTs. **C)** MTs in epithelial cells are organized in apico-basal direction, being connected to both plasma membranes. **D)** MTs in myotubes are nucleated from nuclear envelopes. **E)** MTs in neurons form bundles that are not connected to the centrosome. *MTs are in green, MTOCs are in orange, nucleus/chromosomes are in blue.*

establishment of neuronal polarity. They initiate neurite outgrowth, guide axon elongation and branching and structurally support the shape of neuronal cells (Fig. 1E) [2]. Another examples are epithelial cells (Fig. 1C), where MTs are aligned in apicobasal direction or myotubes with linear arrays of MTs (Fig. 1D) [3, 4].

MTs serve as tracks for transport of various cellular components including membraneous vesicles, proteins and RNA as well as bacteria and viruses, which is mediated by MT motor proteins [4-6]. By the action of MT motors and other microtubule-associated proteins (MAPs) MTs organize intracellular space by precise positioning of organelles such as mitochondria, Golgi apparatus (GA) and endoplasmic reticulum (ER) [4]. In addition, MTs participate in nuclear positioning [7] and nuclear envelope break-down in prophase [8, 9]. There is an interplay between nuclear envelope proteins nesprins and MTs, MFs and IFs, which facilitates both centrosome and nuclear positioning [10, 11].

MTs and MFs are required for establishment and maintenance of cellular polarity in migrating cells. Migration is a complex and heterogeneous process executed by all nucleated cell types at a given time window of their development [12]. It is vital for tissue development and remodelling, wound healing or immunological surveillance. Cells migrating in the mesenchymal migration mode are strongly polarized with a leading edge and lamellipodia at the front, and a trailing edge at the rear. MTs are selectively stabilized in the leading edge direction, whereas at the rear they are highly dynamic (Fig. 1A). This selective stabilization is necessary for directional MT-based vesicular transport contributing to maintenance of cellular polarity [11]. Cells bind to extracellular matrix (ECM) via cell-substratum adhesion sites and use them for pushing or pulling themselves in order to move. MTs facilitate cell-to-substrate adhesion by interacting with cell-substratum adhesion sites such as focal adhesions or adhesion sites containing laminin and laminin receptor integrins [3]. On the other hand, destabilization of MTs can support a different, amoeboid migration mode common for several types of invasive cancers [13].

Besides described dynamic arrays, MTs form also highly stable and long-lived structures such as centrioles and axonemes. A pair of centrioles constitutes the structural core of animal centrosomes and their duplication controls duplication of centrosomes once and only once during cell cycle that is essential for proper bipolar spindle assembly and subsequent fidelity in chromosome separation during mitosis. Centrosomes serve as an important MTOC by nucleating and anchoring MTs [14, 15] and as a hub for many signalling molecules including those involved in cell cycle progression [16, 17]. Centrioles have 9-fold radial symmetry created by nine regularly spaced MT triplets organized around a cartwheel structure [18-20]. Centrioles are surrounded by a complicated layer of unknown ultrastructure composed of fibrillar proteins, and termed the pericentriolar matrix (PCM). MTs emanating from the centrosome are anchored at the PCM (Fig. 2A) [21, 22].

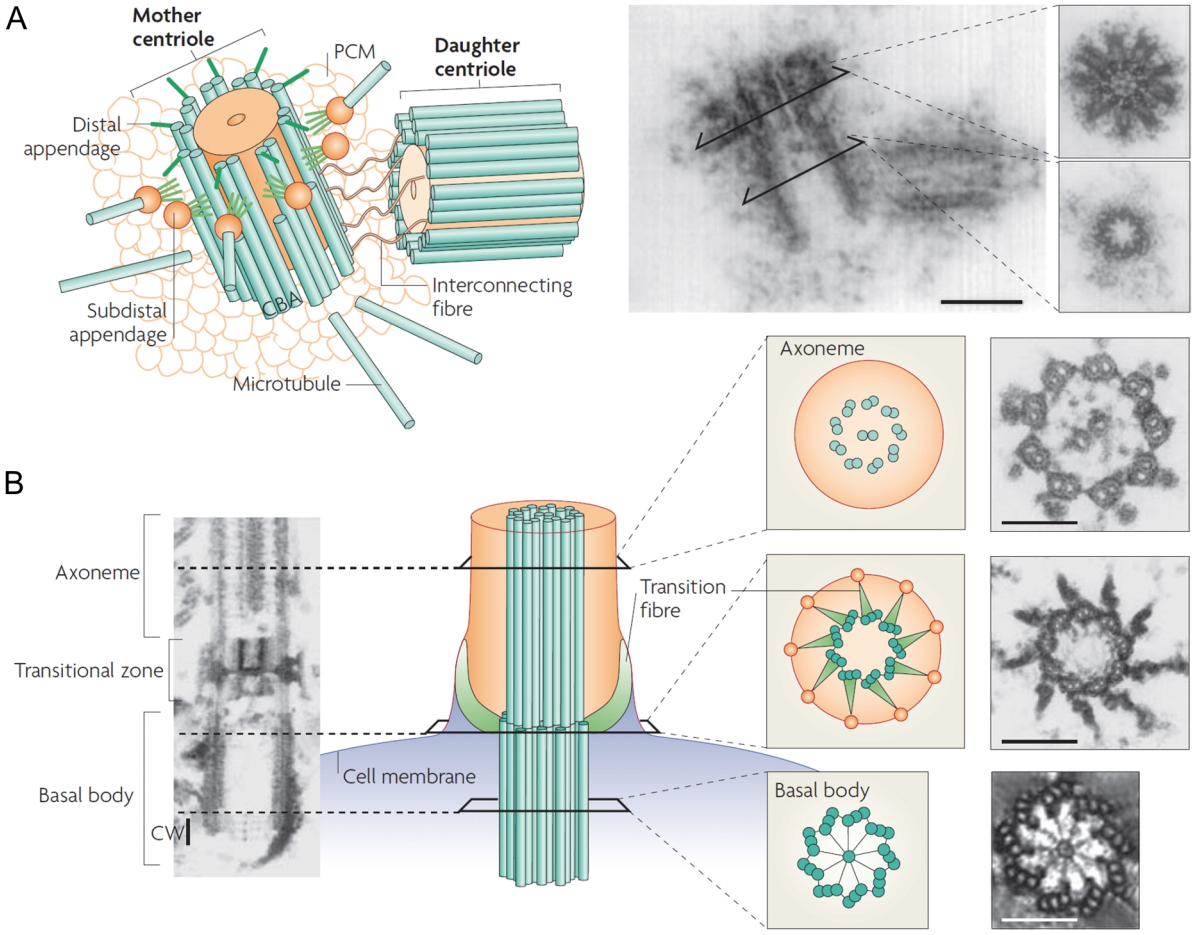

Figure 2. Structure of centrosomes, basal bodies and axonemes. **A)** The centrosome is composed of an older (mother) and a younger (daughter) centriole and the surrounding PCM. The PCM accumulates preferentially around the mother centriole. The mother centriole has several distal and subdistal appendages at its distal end, as highlighted by the EM micrograph, which are involved in MT anchoring. Centrioles comprise 9 triplet MTs that become dublets at their distal end and are structurally identical to basal bodies. **B)** Axonemes are cylindrical arrays of nine doublet MTs. Motile axonems contain a central MT pair and dynein, whereas non-motile axonemes in primary cilia lack dynein and the central MT pair. Transition fibres connect basal body to plasma membrane. Adapted from [22].

Axonemes surrounded by plasma membrane give rise to cilia and flagella. Cilia and flagella are structurally identical organelles. Motile organelles found on unicellular eukaryotes and sperm cells are termed flagella. On the other hand cilia can be found on almost every cell type in animals and are the key organelles in many physiologic and developmental processes. The motile axoneme is composed of a central pair of MTs and 9 parallel MT dublets. The central pair is connected with MT dublets by MT motor protein dynein that generates force needed for organelle movement (Fig. 2B). Motile cilia are usually

present in large numbers on the surface of epithelial cells and their coordinated movement generates flow of fluid. Primary cilia are immotile, but can act as sensoric organelles [23]. The immotile axoneme in the primary cilium lacks the MT central pair and dynein. Centriolar MT triplets and axonemal MT dublets are very stable and contain extensively post-translationally modified tubulins [24]. Axonemes elongate from the basal body that is structurally identical with the centriole and arise either from the existing centrosomal centriole or *de novo* (Fig. 2B).

Interestingly, only the older centriole in the pair, called the mother centriole, can be converted to the basal body. Moreover, maturation of the mother centriole is needed for this conversion and takes up one and half cell cycle resulting in functional differentiation of duplicated centrosomes. The older centrosome containing the mature mother centriole and the younger centrosome differ in their capability to become the cilia-nucleating basal body. The asymmetric inheritance of older and younger centrosomes by daughter cells is important for controlling cell fate during tissue differentiation [25].

I.1.2 Microtubule structure and dynamic instability

MTs are hollow tubes of about 25 nm in diameter composed of α- and β-tubulin heterodimers. Soluble tubulin heterodimers are abundant in the cytoplasm and can polymerize in a head-to-tail fashion into polarized protofilaments, which in turn associate laterally to form a cylindrical MT lattice (Fig. 3). The most ubiquitous form of the polymer is a singlet MT, however MTs can also form doublets or triplets as described in I.1.1.

While 11-16 protofilaments can form a MT *in vitro* [26], the majority of MTs grown *in vivo* consist of 13 protofilaments. 13-protofilament MTs have unique geometry; their protofilaments run straight along the MT length. This is especially important for movement of MT motor proteins along the MTs allowing them to remain always on the same face of the structure [27]. 13-protofilament MTs can be organized in two ways [28]. In the A-type lattice, α-tubulin form lateral bonds with β-tubulin from the adjacent protofilament. In the B-type lattice, lateral bonds are formed between the same types of tubulin monomers, ie. α-α, β-β. This arrangement results in a left-handed helix with a seam between the 1st and the 13th protofilament formed from lateral bonds between α-tubulin and β-tubulin (Fig. 3). Although some proteins can induce formation of A-lattice *in vitro*, e.g. EB1 homolog Mal3p [29], only the B-type lattice was found *in vivo* [30].

There are fenestrations of about 1.5 x 2 nm between the contact regions of protofilaments creating a direct access to the MT lumen [31]. Astonishingly, MT lumen is not vacant. Several independent studies reported luminal particles inside MTs of different origin [32-34]. Nevertheless, the nature of these particles is still unknown.

As a consequence of head-to-tail polymerization of tubulin heterodimer and a unidirectional arrangement of protofilaments, MTs are intrinsically polar. The end with exposed β-tubulin is called the plus (+) end, the other end with exposed α-tubulin is called the minus (-) end. The (+) end is the fast growing end both *in vitro* and *in vivo*. On the other hand the (-) end can grow only slowly *in vitro*, while in cells it is usually capped and stabilized, for example by anchoring at a MTOC. Uncapped (-) ends mostly rapidly depolymerize *in vivo*. Stochastical switching between periods of growth and rapid shortening of (+) ends, occurring both *in vitro* and *in vivo,* is termed „dynamic instability“ [35]. Historically, the transition between the growth to the shrinkage is called *catastrophe*, the opposite transition is called *rescue* (Fig. 4).

Electron microscopy (EM) studies have revealed distinct morphology of growing and shrinking MT ends. Growing MTs have an open protofilament sheet at the tip with the open seam closing back into a tube toward the (-) end, whereas shrinking MTs have frayed ends

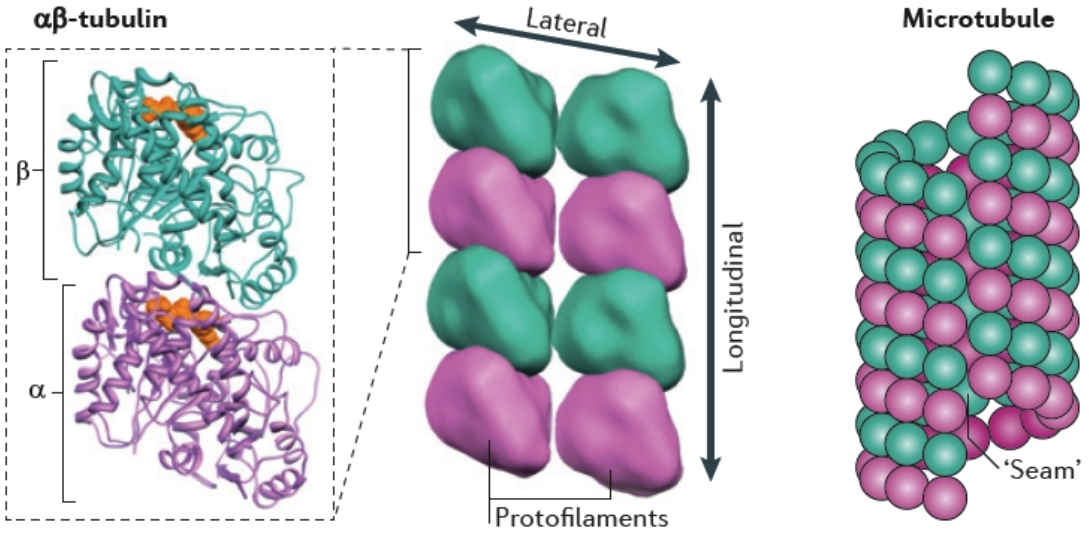

Figure 3. Molecular structure of microtubules. α- and β-tubulin heterodimers polymerize longitudinally into protofilaments. *In vivo*, MTs predominantly consist of 13 protofilaments and lateral bonds are formed between two α-tubulins and two β-tubulins, each of adjacent protofilaments. Since protofilaments are slightly staggered, there is a “seam” formed by lateral interactions between α- and β-tubulins. *α-Tubulin is in violet, β-tubulin in green, GTP in orange*. Adapted from [27].

with individual protofilaments curved and peeling away from the fast depolymerizing end (Fig. 4) [34, 36, 37]. However, a recent study on fission yeasts indicated that structures of growing (+) ends might be more diverse. Growing (+) ends inspected by electron tomography exhibited mostly flared, funnel-like structures [38]. The authors propose a model of MT growth, when the protofilaments first elongate and then successively „zip up" with their neighbours. Interestingly, recent computer simulations suggested a very similar model of (+) end growth [39].

Each tubulin monomer contains one binding site for a guanine nucleotide coordinated with Mg^{2+} cation(s) on the N-terminal domain (Fig. 3) [40]. Since GTP bound to α-tubulin is physically traped at the dimer interface, it cannot be exchanged and hydrolyzed. On the other hand, guanine nucleotide binding site of β-tubulin is accessible. Thus, β-tubulin-bound GTP can be hydrolyzed and resulting GDP can be exchanged for GTP. Tubulin heterodimers with bound GTP (GTP-tubulin) are essential for MT growth. GTP-tubulin is incorporated into a growing MT and GTP is hydrolyzed to GDP few moments after polymerization yielding GDP-tubulin, which forms the majority of the MT lattice (Fig. 4).

Depolymerizing protofilaments are frayed and curved reflecting the bent conformation of GDP-tubulin adopted also by non-polymerized GDP-tubulin in solution [41]. While GDP-tubulin increases the curvature of protofilaments putting strain on the lattice, fluctuating layers of GTP-tubulin on the (+) end, termed „GTP cap", stabilize the MT due to the strong interactions among GTP-tubulin subunits. If GTP cap is lost or a crack develops between protofilaments at the end, they peel apart and curl outward, finally releasing the stored free energy from GTP hydrolysis [39, 42]. Curled protofilaments subsequently depolymerize, GDP is exchanged for GTP in free tubulin dimers and GTP-tubulin can take part in the next round of MT polymerization (Fig. 4).

MT growth rate considerably fluctuates at a sub-second time-scale both *in vitro* and *in vivo* [43]. It has been proposed that tubulin oligomers from solution are being incorporated into the growing (+) end [44, 45], which could explain the observed fluctuations. Higher-resolution studies have revealed though that apparent oligomer additions are in fact very rapid events of polymerization of individual tubulin dimers [46, 47]. Several lines of evidence indicate the GTP cap at the MT (+) end is highly dynamic and its length changes in time [46, 47]. GTP cap grows and shrinks independently on GTP hydrolysis, with perhaps 90% of the GTP–tubulin dimers that bind to the (+) end dissociating before they are incorporated stably into the MT lattice. The combined association (On) and dissociation (Off) rates of GTP-tubulin were estimated to occur at nearly 1000/s both *in vitro* and *in vivo*. In addition, GTP-

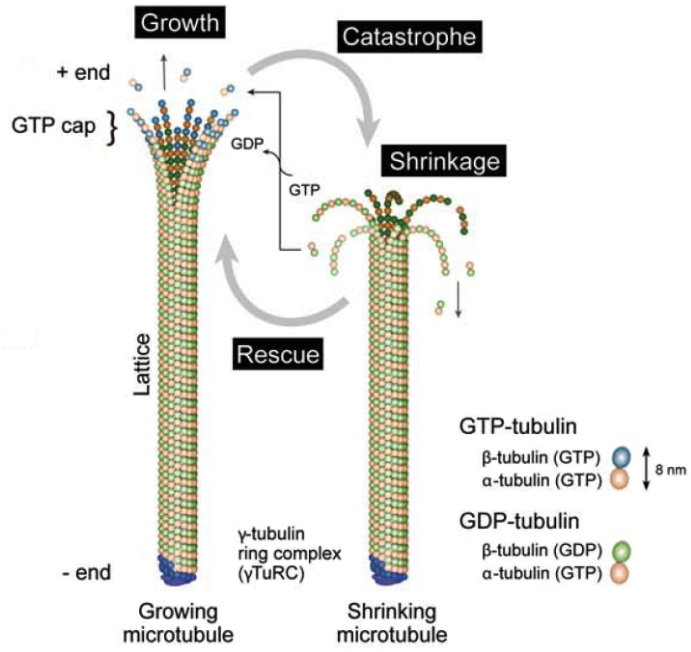

Figure 4. Dynamic instability of microtubules. Assembly and disassembly of MTs are driven by binding, hydrolysis and exchange of a guanine nucleotide on the β-tubulin. GTP bound to α-tubulin is non-exchangeable and is never hydrolyzed, whereas β-tubulin GTP undergoes hydrolysis soon after incorporation. As a consequence, a 'cap' of GTP-tubulin subunits (GTP cap) forms at the (+) end. When free GTP-tubulin concentration decreases or the (+) end structure is disrupted, MTs rapidly start depolymerizing. Consequently, GDP in the disassembled tubulin subunits is exchanged for GTP. This stochastic assembly-disassembly cycle is termed ''dynamic instability''. (-) ends are mostly stabilized *in vivo* by capping. Typical (-) end stabilizer is the γ-tubulin ring complex (γTuRC), which also serves as a template for MT nucleation. Modified from [3].

tubulin On and Off rates are nearly equal to each other at all concentrations and in contrast to previous models, the Off rate is dependent on free GTP-tubulin concentration. These findings indicate that MAPs or drugs promoting net MT assembly or disassembly could work through only modest changes in GTP-tubulin kinetics [47].

It was initially thought that GTP-tubulin adopts straight conformation upon GTP binding and so fits well into the relatively straight protofilament sheets on the (+) end [48, 49]. However, there is increasing evidence that unassembled GTP-tubulin is also curved similarly to GDP-tubulin [50-52]. This strongly supports the lattice model of MT assembly postulating that straightening of GTP-tubulin conformation occur predominantly upon polymerization. GTP bound to β-tubulin is supposed to lower the unfavourable free energy difference between the curved soluble tubulin and the straight microtubular tubulin [50, 53]. GTP hydrolysis is not required for MT polymerization *per se*, but for the destabilization of a MT lattice, as MTs assembled from tubulin containing slowly hydrolyzable GTP analog guanosine-5'-[(α,β)-

methyleno]triphosphate (GMPCPP) can grow and are resistant to depolymerization [54]. Interestingly, GDP-tubulin can also directly incorporate into growing MTs *in vitro*, however, only when mixed with GTP-tubulin [55].

While the mechanisms of catastrophe are becoming increasingly understood [56], the nature of rescue events had been unclear until recently. A specific antibody was generated recognizing conformation of GTP-tubulin in the polymer [57]. This antibody stained segments a few hundred nanometers long at the (+) ends indicating the presence of GTP cap and also short segments in the middle of cellular MTs. Since the regions of GTP-tubulin (or GDP-tubulin in an alternative, stable structural state of the lattice) within MT lattice coincided with rescue events, it was proposed that these regions are rescue promoters [57, 58]. This hypothesis was recently supported by an *in vitro* study, where GMPCPP-tubulin was used to mimic the GTP-tubulin structures within the lattices of dynamic cellular MTs [59]. The study clearly showed that regions containing GMPCPP-tubulin promoted rescue and resisted depolymerization. Another rescue promoting factors are CLASP family proteins [60].

MTs with uncapped (-) ends are subjected to a specific turnover termed treadmilling. Due to structural constraints in tubulin dimers and in the MT lattice described above, GTP-tubulin strongly prefers the (+) end for polymerization. As a result, the concentration of GTP-tubulin needed for polymerization (critical concentration, C_c) is much higher for the (-) end than for the (+) end. When tubulin concentration is adjusted so as it is higher then C_c for the (+) end and lower than C_c for the (-) end, MTs start treadmilling by polymerizing at the (+) end and depolymerizing at the (-) end creating a flux of tubulin dimers through the MT. Treadmilling rarely occurs in interphase cells of different origin [61, 62], however in mitotic cells it contributes to MT flux in the mitotic spindle [63, 64].

In addition to above described α- and β-tubulin, tubulin superfamily comprises γ, δ, ε, ζ, η, θ, ι and κ-tubulin [65, 66]. They account together for less than 1% of the total tubulin content in the cell. While α-, β- and γ-tubulin are found in all eukaryotes and are highly conserved across species, the other tubulins are not as ubiquitous. It seems that the primary function of these less ubiquitous tubulins is the regulation of centriole and basal body stability and duplication [65, 67, 68]; only α- and β-tubulin are capable of polymerizing into MTs. γ-Tubulin has additional vital functions including nucleation of MT and their anchoring at MTOCs. As it is the most studied molecule in the presented work, it will be discussed in greater detail later on in the chapter I.2.

I.1.3 Regulation of microtubule dynamics and functions

Dynamics, stability and spatial organization of MTs are regulated by many factors including expression of different tubulin isotypes, tubulin post-translational modifications (PTMs), MT regulatory proteins such as MAPs, MT severing proteins and MT motor proteins. Small ligands like specific tubulin drugs and mechanical forces also affect MT stability. Some aspects of MT regulation will be discussed in this chapter.

I.1.3.1 α- and β-tubulin isotypes

Both α- and β-tubulin are encoded by multiple genes in vertebrates. 9 genes for α-tubulin and 8 genes for β-tubulin were identified in human [69], whereas other organisms, such as some yeasts, contain only one to two genes for each tubulin. α- and β-tubulin share 40% amino-acid sequence identity, however their tertiary structures are almost identical [70]. While the majority of both α- and β-tubulin amino-acid sequence is highly conserved to maintain the essential tubulin fold, their unstructured C-terminal tails are more divergent. Thus, the conserved differences among α- and β-tubulin isotypes are located mainly in their C-termini. α- and β-tubulin C-terminal tails are located on the exterior of the MT, where are the putative binding site for MAPs (Fig. 5) [71]. Sequential differences among individual α-tubulins are much lower than among β-tubulins [72].

Although *in vitro* studies using purified β-tubulin isotypes indicated the existence of differences in MT assembly, GTPase activity and drug binding [73-75], *in vivo* studies showed various results whose interpretation is not straightforward [76-80]. The picture that emerges from recent studies is that different tubulins are all able to coassemble, and in doing so they may, or may not, alter the properties and functions of the MTs that they form [81].

Some of β-tubulin isotypes are expressed ubiquitously, the others are expressed in a tissue-specific manner [72, 82]. βI-tubulin expression is essentially ubiquitous. βII-tubulin is expressed particularly in brain, peripheral nerves and muscles. It was also detected in cell nuclei of various cancer types [83, 84]. βIII-tubulin occurs predominantly in neurons and testicular Sertoli cells. In spite of its absence in glial cells, βIII was found in gliomas; its expression correlates with the tumor grade [85]. βIVa-tubulin is expressed only in brain, whereas βIVb-tubulin is widespread among cell types being especially prominent in axonemes [86]. βVI-tubulin is restricted to hematopoietic-specific cell types. The distribution

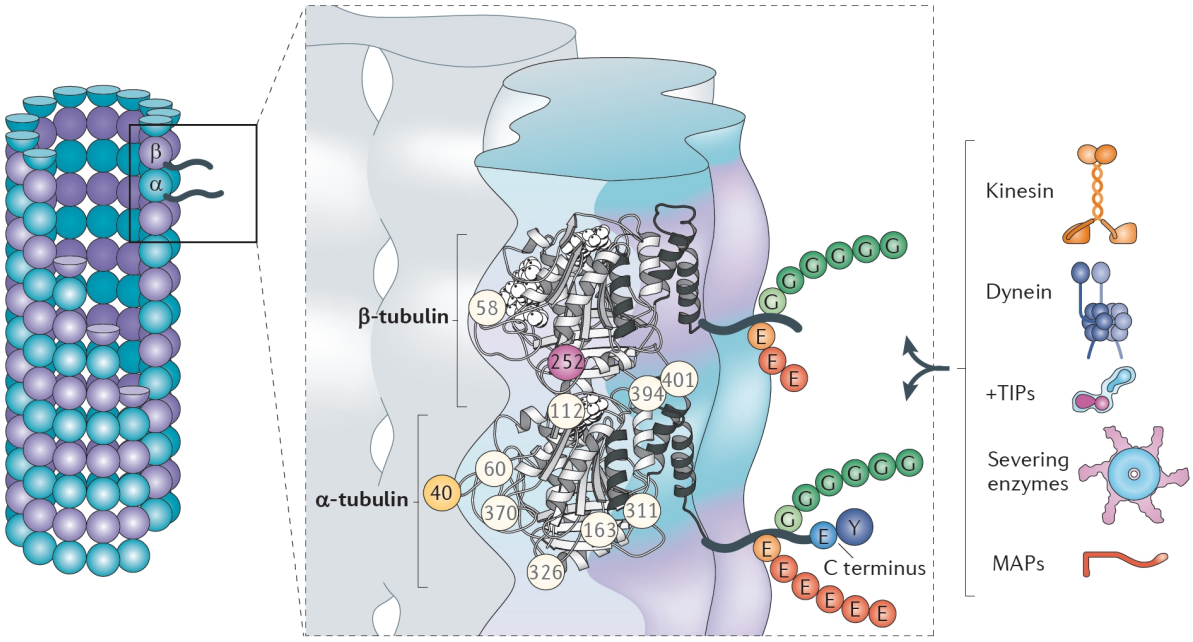

Figure 5. Localization of tubulin PTMs and their effectors. C-terminal tails of α- and β-tubulin subunits are accessible from the surface of a MT. Polyglutamylation, polyglycinylation, detyrosination and Δ2-tubulin modifications occur on these C-terminal tails. Acetylation sites are highlighted as circles with numbers indicating amino acid position. Acetylation of α-tubulin Lys40 (yellow) and β-tubulin Lys252 (magenta) have been confirmed. Unconfirmed acetlyation sites are shown as white circles. Tubulin PTMs affect binding and action of MT motor proteins (kinesins and dyneins), MAPs and severing enzymes. Adapted from [24].

of βV is ubiquitous but its levels are generally very low [81]. Remarkably, tissue distribution of α-tubulin isotypes is much less heterogeneous when compared to β-tubulin.

Mutations in genes TUBA1A (α1A), TUBA8 (α8), TUBB2B (β2), and TUBB3 (β3) encoding different isotypes of α-tubulin and β-tubulin were recently linked to various neurological disorders, some of them being isotype specific [87]. Moreover, altered expression of tubulin isotypes contributes to drug resistance in several cancer types [88]. The functional differences of tubulin isotypes can also be coordinated with tubulin PTMs. Heterogeneous C-terminal tails of tubulin isotypes could display altered patterns of PTMs due to the divergent amino-acid sequence. For instance, some α-tubulin isotypes are missing the gene-encoded C-terminal tyrosine (Tyr), thus their expression would strongly increase the pool of detyrosinated MTs even in the absence of detyrosinating enzymes [24]. Collectively, recent findings indicate that there might be significant functional differences between some tubulin isotypes *in vivo*.

I.1.3.2 Tubulin post-translational modifications

Tubulin PTMs have a strong impact on MT functions. In addition to unique composition of MTs based on different tubulin isotypes, PTMs represent another level of complexity enabling generation of defined MT identities with specific properties. An exciting hypothesis was proposed postulating that tubulin PTMs alone or in combination have the potential to generate complex molecular signals that can serve as a readable code on MTs [89]. MAPs, MT severing enzymes and MT motor proteins are the best known downstream effectors of this code (Fig. 5). Some tubulin PTMs are characteristic for stable MTs. Patterns of PTMs are not uniform and have various subcellular and submicrotubular distribution [24, 90].

The most characterized tubulin PTM is tubulin detyrosination and the generation of Δ2-tubulin. Most α-tubulin genes encode C-terminal Tyr, which can be specifically removed by an unknown carboxypeptidase. The reverse reaction is catalyzed by Tubulin-tyrosin ligase (TTL). The detyrosinating enzyme(s) act(s) on tubulin polymerized into MTs, whereas TTL works exclusively on soluble tubulin heterodimers. As TTL is highly effective, almost all GTP-tubulin incorporated into growing MTs is tyrosinated. Deglutamylases of the cytosolic carboxypeptidases (CCP) family can generate Δ2-tubulin by removing C-terminal glutamate (Glu) from detyrosinated α-tubulin. This reaction seems to be irreversible in cells [24].

Detyrosination is typical for long-lived MTs in many cell types. Tubulin detyrosination does not stabilize MTs *per se*, but it prevents binding of several MAPs and motor proteins to the α-tubulin tail such as MT depolymerizing motors from kinesin-13 family [91] and MT (+) end interacting proteins (+TIPs) containing a cytoskeleton-associated glycine-rich (CAP-Gly) domain [92-94]. CAP-Gly domain specifically recognizes EEY/F motif, which is present on tyrosinated but lost from detyrosinated tubulin. By contrast, kinesin-1 (KIF5) walks preferentially on detyrosinated MTs [95, 96]. Thus, tubulin tyrosination regulates stability of MTs and intracellular transport by recruiting or repulsing different MT motors and MAPs [97]. Since Δ2-tubulin modification is irreversible, it can lock MTs in a detyrosinated state and stabilize them for very long time. Consistently, Δ2-tubulin is found in differentiated MT structures such as centrioles, axonemes or neuronal MTs [24].

While detyrosination occurs only on α-tubulin, both α- and β-tubulin C-terminal tails can be extensively polyglutamylated or polyglycylated on Glu residues, with polyglutamate or polyglycin chains of various length. Since both PTMs use overlapping modification sites, they can compete with one another [24, 90]. Polyglycination is restricted to axonemes, whereas polyglutamylation is widespread. In axonemes, glycylation stabilizes the structure,

while glutamylation modulates beating behaviour. Polyglutamylation is a key regulatory mechanism controlling MT-based motor traffic not only in axonemes but also in neurons [24].

Surprisingly, polyglutamate chains attract MT severing enzymes such as spastin and katanin [98, 99]. It suggests that polyglutamylated MTs need to be protected from uncontrolled severing in stable MT structures. Indeed, a structural MAP Tau binds to polyglutamylated MTs and protects them from severing activity in neurons [100]. On the other hand polyglutamylation is found on highly dynamic MTs in mitotic spindle, where MT severing by katanin is imporant for regulation of spindle architecture. Well-controlled glutamylation/ deglutamylation cycle is vital for normal neuronal development, since inhibition of tubulin deglutamylation leads to neuronal degeneration [24, 90, 97].

Acetylation of lysine (Lys) 40 on α-tubulin is the only PTM located in the MT lumen. This acetylation is also found on stable MTs, but again, it is not the cause of their stability. Additional acetylation sites on α- and β-tubulin were recently identified, but they need to be further verified [24]. It was shown that tubulin acetylation might play a part in neuronal migration, differentiation and synaptic targeting or in regulation of ciliary assembly [97]. However, the conserved α-tubulin acetylation at Lys40 has only a subtle effect on MT dynamics and *in vivo* studies on the function of tubulin acetylation produce conflicting results. Taken together, there has been no direct evidence linking tubulin acetylation to any MT function or stability yet [24, 90].

There are also many other less studied tubulin PTMs. α- and β-tubulin can be phosphorylated, palmitoylated or glycosylated, α-tubulin itself can be methylated on Lys, ubiquitinylated or sumoylated [90]. Polyglutamylation or polyglycylation can be modulated by methylation of Glu residues on C-terminal tails of α- or β-tubulin [101]. Finally, nitration of α-tubulin on a tyrosine residue was detected in differentiating mouse P12 cells implicating its putative role in neuronal differentiation [102].

I.1.3.3 Microtubule regulatory proteins

MTs can be regulated by an astonishing number of interacting proteins. MT motor proteins kinesins and dyneins use MTs as tracks for moving their cargo such as membrane vesicles, proteins, RNA or organelles to desired destinations. Moreover, they create force needed for mitotic spindle assembly and function. They position organelles and organize MT arrays also in interphase cells [4].

Structural MAPs bind along the length of MTs to stabilize the lattice. They usually carry a highly positive net charge facilitating their interaction with negatively charged tubulin. They are thermostable and have repeating conserved MT-binding domains in their C-terminal parts allowing each MAP to interact with more than one tubulin dimer. N-terminal domains of various length projecting towards cytoplasm are capable of interacting with variety of proteins. As a result, structural MAPs can cross-link individual MTs creating stabilized MT bundles or connect MTs to membranes, MFs or IFs. MAPs binding to MTs can attract signalling molecules, alter the MT binding sites for motor proteins and protect MTs from severing. Binding of the structural MAPs to MTs is controlled by kinases and phosphatases and dramatically decreases dynamic instability of MTs. Some MAPs stabilize interphase MTs in different cell types, others are predominantly found in non-dividing neuronal cells [103].

One of the best known structural MAPs are proteins from MAP2/Tau family MAP2(A,B,C), MAP4, and Tau. MAP2 and Tau are neuronal proteins. While MAP2 is located mainly in dendrites, Tau is concentrated in axons. By contrast, MAP4 is almost absent in neurons and is found in other tissues. Remarkably, Tau hyperphosphorylation leading to formation of large Tau aggregates has been linked to Alzheimer disease [104]. MAP1A, MAP1B and MAP1S constitute the MAP1 family [105]. These proteins are also neuronal and stabilize MTs. Generally, these structural MAPs are important for normal development and function of the nervous system. There are also other structural MAPs with different mechanisms of MT binding and impact on MT dynamics such as doublecortin [106], ensconsin [107], stable tubulin only proteins (STOPs) [108] or tektins [109].

I.1.3.3.1 Microtubule destabilizing proteins

Proteins specialized on MT destabilization work through different mechanisms. Two specialized kinesin classes, kinesin-13 and kinesin-8 bind directly to MT ends and use ATP hydrolysis to depolymerize MTs, probably by bending protofilaments into an unstable conformation [110]. Some kinesins have lost their ability to move processively along MTs, like MCAK/Kif2C (kinesin-13 family), whereas others, like Kip3 (kinesin-8 family), have not. Catalyzed MT depolymerization occurs on both MT ends. MT (-) end depolymerization catalyzed by Klp10A/Kif2A (kinesin-13 family) during anaphase generates tubulin flux and is important for chromosome poleward movement [64, 111].

Another strategy for MT destabilization has stathmin/Op18, which is selectively sequestering soluble tubulin dimers, effectively lowering the pool of polymerization-

competent tubulin and thus inducing MT depolymerization. Alternatively, it can bind directly to MTs and destabilize both their ends [112, 113].

Katanin, spastin, fidgetin and VPS4 are members of AAA (ATPases associated with various cellular activities) protein family and use energy from ATP hydrolysis to sever MT lattice. Both katanin and spastin form hexameric ring complexes with a hole in the centre that specifically interacts with tubulin C-terminal tails [114]. Katanin and spastin are crucial for neuronal development and maintenance, because their MT severing activities induce growth and branching of neurites [2]. Spastin influences mainly axon branching, whereas katanin plays a more important role in neurite outgrowth [115]. In non-neuronal cells, katanin regulates cortical MT (+) end and cell migration [116]. During mitosis, katanin controls mitotic and meiotic spindle length [117]. It has been shown that tubulin glutamylation, particularly long polyglutamate chains, attracts spastin and promotes MT severing [99].

Mutations in spastin are the most common cause of hereditary spastic paraplegia (HSP). This neurodegenerative disorder affects axons of corticospinal neurons and cause progressive spastic paralysis of the legs [118]. Mammalian spastin has 4 isoforms, longer M1 isoform, shorter M87 isoform lacking the first 86 amino acids present in M1 and truncated versions of each M1 and M87, both lacking 32 amino acids encoded by exon 4. M87 arises either from alternative translation initiation from a second start codone in M1 transcript or from a shorter alternative transcript driven by a cryptic promoter in the exon 1 of the spastin gene [119].

All spastin isoforms possess C-terminal AAA ATPase domain, MT-binding domain (MTB) and a domain present in MT interacting and trafficking proteins (MIT), that is involved in interactions with charged multivesicular body protein (CHMP) family of proteins. CHMP family members form a highly conserved complex termed endosomal sorting complex required for transport-III (ESCRT-III) that is involved in membrane scission in a variety of membrane modelling processes. The ubiquitously expressed M87 variant is found in cytoplasm, partially co-localizes with MTs, and can be recruited to endosomes and to the cytokinetic midbody during cell division in via ESCRT-III [119]. Interestingly, spastin is probably not required for MT severing within intercellular bridge during abscission of daughter cells, instead it regulates MT organization and endosome trafficking [120, 121]. The M87 isoform has also been reported in the nucleus [119], where it acts as a transcriptional co-repressor of HOXA10 [122].

Only the M1 variants have a N-terminal hydrophobic domain (HD) that targets these spastin isoforms to the ER, early secretory pathway, and possibly also to the very early ER-to-GA intermediate compartment. Expression of ATPase-defective version of M1, which is

unable to cut MTs, leads to profound tubulation of the ER, implicating spastin as an ER morphogen [123]. Since MTs influence ER remodelling, either by ER-sliding on existing MTs or by attachment to growing MT (+) ends, M1 spastin might influence ER morphogenesis by severing MTs connected to the ER. Strikingly, ER proteins REEP1, atlastin-1 and RTN2 interacting with M1 spastin are also mutated in HSP. These findings indicate that HSP might be coupled with M1 spastin and support the hypothesis that abnormal ER morphogenesis is the pathogenic mechanism in HSP [119, 124]. A recent study showed that M1 has higher expression in axons of corticospinal neurons [125], however, since M87 variant is also present, precise mechanisms of HSP remain to be elucidated.

I.1.3.3.2 Microtubule (+) end tracking proteins

MT (+) end tracking proteins (+TIPs) are a conserved group of MAPs that preferentially accumulate at growing MT (+) ends and regulate MT dynamics. +TIPs link MTs to various intracellular structures such as vesicles, cell membrane, focal adhesions, MFs, IFs and kinetochores. +TIPs are structurally and functionally diverse, use different (+) end tracking mechanisms and are regulated by various signalling pathways [3, 126].

End binding (EB) protein family (EB1, EB2, EB3) can track MT (+) end autonomously by binding directly to tubulin via their N-terminal calponin homology domain (CH). It was suggested that EB proteins specifically recognize the GTP-cap on MTs [127, 128]. Alternatively, EBs (+) end tracking mechanism could be based on electrostatic repulsion between MT lattice and EBs that is not taking place at the (+) end [129]. A linker region connects the CH domain with the C-terminal domain that is composed of a coiled coil EB-homology domain (EBH) and an acidic tail. EB proteins can homo- or heterodimerize through coiled coil domains, which enhances their (+) end tracking ability [130]. EBH specifically recognizes a conserved SxIP motif present in many +TIPs. The ultimate C-terminal amino acids of EBs form the EEY/F motif found also on tyrosinated α-tubulin subunits and serving as a recruitment signal for proteins carrying CAP-Gly motifs. EBs boost both MT growth and frequency of catastrophes *in vitro*. However, they promote growth and suppress catastrophes *in vivo*. The different results could be caused by the action of other +TIPs in the cell [126].

Cytoplasmic linker protein (CLIP)-170, CLIP-115 and $p150^{glued}$ (a component of dynactin complex regulating MT motor proteins) contain multiple CAP-Gly domains. They can bind to tyrosinated tubulin and also to EBs. CLIP-170 has a C-terminal EEY/F that is involved in its

autoinhibition mechanism. In addition to EEY/F motif, CLIPs can bind to EBH in EBs as well. CLIPs are positive regulators of MT growth [126].

Many +TIPs contain short SxIP motif that is required for interaction with EBH domain. The most important +TIPs with SxIP motif are CLIP-170-associated proteins (CLASPs), Adenomatous Polyposis Coli (APC), Microtubule-Actin Crosslinking Factor (MACF), CDK5 regulatory subunit associated protein 2 (CDK5RAP2) and Stromal Interaction Molecule 1 (STIM1). A special type of a SxIP-motif-containing +TIP is MT depolymerizing kinesin-13 (MCAK/Kif2C) [126].

Members of XMAP215/Dis1/Tog and also CLASP protein family can bind directly to MT (+) end, since their N-termini contain 250 residue sequence repeats, termed tumor overexpressed gene (TOG) domains (named after human ortholog ch-TOG) capable of direct binding to tubulin. XMAP215/ch-TOG is a MT polymerase attached to the MT (+) end catalyzing addition of tubulin dimers [131, 132]. Interestingly, many +TIPs accumulate at MTOCs where they might take part in MT nucleation and anchoring [133].

I.1.3.3.3 Microtubule (-) end capping proteins

MT (-) ends are commonly stabilized by specialized proteins or protein complexes in living cells. The best known (-) end capping complexes are the γ-tubulin complexes (γ-TuCs) that are also crucial for MT nucleation and their anchoring at various MTOCs. γ-Tubulin and its complexes will be described in greater detail in the chapter I.2. MT (-) ends can be also protected by newly described proteins from Patronin/Nezha family [134, 135]. In epithelial cells, Nezha binds to MT (-) ends and tethers them to zonula adherens in adherens junctions. As C-terminal part of Nezha is capable of binding to MT (-) ends *in vitro*, its (-) end capping ability is probably independent of γ-tubulin [134]. Patronin, a *Drosophila* homolog of Nezha, was also shown to bind directly to MT (-) ends and to protect them from depolymerization induced by a kinesin-13 family protein Klp10A [135]. Interestingly, MTs with uncapped (-) end in Patronin-depleted cells showed not only treadmilling behaviour or depolymerization from both ends, but also growth on both ends. Another very surprising finding was that the both growing ends were marked by EB1 indicating that GTP-tubulin addition to the growing (-) end might occur also *in vivo* [135].

I.2 γ-Tubulin

I.2.1 γ-Tubulin genes, structure and distribution

γ-Tubulin is a highly conserved member of tubulin superfamily essential for nucleation of MTs [136-138]. Initially it was discovered in a filamentous fungus *Aspergillus nidulans* [139] and later on it was found in all examined eukaryotes. The conservation of γ-tubulin is remarkable, for example fission yeast γ-tubulin Tug1 (former Gtb-1) share 71% protein sequence identity with human γ-tubulin TUBG1 [140]. The most distant homologs of human TUBG1 (in terms of sequence divergence) are the budding yeast γ-tubulin Tub4p and *Ceanorhabditis elegans* γ-tubulin TBG-1. Tub4p and TBG-1 share 40% and 43% protein sequence identity with TUBG1, respectively [141-144].

While many species have a single γ-tubulin gene, several organisms including *Arabidopsis* [145], *Zea* [146], *Paramecium* [147], *Euplotes* [148, 149], *Drosophila* [150] and mammals [151-153] posses two genes encoding γ-tubulin. Nevertheless, phylogenetic analyses revealed that γ-tubulin gene duplications occurred independently during evolution [151, 153]. Mammalian γ-tubulin genes *TUBG1* and *TUBG2* are located on the same chromosome in tandem and their protein products are almost identical (>97% protein sequence identity in human). They are also highly conserved, e.g. mouse TUBG1 and TUBG2 share with their human orthologs 98.9% and 97.6% protein sequence identity, respectively.

Although TUBG1 and TUBG2 were initially assumed to be functionally equivalent [152], a gene knock-out analysis of *Tubg1* and *Tubg2* in mice suggested that they might have different functions [151]. While TUBG1 was expressed ubiquitously, TUBG2 was primarily detected in the brain. *Tubg1*$^{-/-}$ embryos stopped their development at the morula/blastocyst stage because of severe mitotic defects. In contrast, *Tubg*2$^{-/-}$ mice developed normally and had fertile offsprings, but adults exhibited behavioural changes including abnormalities in circadian rhythm and reaction to painful stimulations. The authors concluded that TUBG1 is a conventional γ-tubulin, whereas TUBG2, which was not able to substitute for TUBG1 in *Tubg1*$^{-/-}$ blastocysts, might have some unknown function(s) in the brain [151]. However, the molecular basis of the suggested functional difference has been unknown.

Despite only 30-40% protein sequence identity which γ-tubulin is sharing with α- and β-tubulin, their tertiary structures are very similar [53, 154]. There are no significant differences in the structure of GDP- and GTP-bound γ-tubulin [53], however the significance and function of γ-tubulin GTPase activity remains to be elucidated. The individual γ-tubulins in

the crystals make lateral contacts with each other through the same contact regions as α- and β-tubulins in MT lattice suggesting their preferred mode of interaction [53, 154].

γ-Tubulin is concentrated at various MTOCs in cells, but its majority is soluble in the cytoplasm [155]. Many proteins are involved in γ-tubulin anchoring at MTOCs and will be described in the following chapter. At the centrosome, γ-tubulin is associated with the PCM [156, 157] and also with the core of centrioles [155, 158, 159]. γ-Tubulin was detected at many other MTOCs including GA, apical and basal membranes of epithelial cells, midbody, basal body, along MTs in mitotic and meiotic spindles, on condensed mitotic chromosomes and on nuclear membranes in myotubes [15]. MT nucleation from GA is important for directional mezenchymal migration [160]. MT nucleation from spindle MTs [161-164] and condensed chromosomes [165-167] is needed for establishment and maintenance of proper spindle architecture and subsequent normal progression of cell division. Noticeably, various patterns of γ-tubulin distribution along interphase MTs were observed in *Drosophila* [168] and in human cancer cells [169]. In addition, we and others described γ-tubulin localization in the nucleus and nucleolus [169-172].

I.2.2 γ-Tubulin complexes and mechanism of microtubule nucleation

γ-Tubulin assembles together with other conserved proteins, named Gamma-tubulin complex proteins (GCP) in human, into γTuCs. The 2.2 MDa γ-tubulin ring complex (γTuRC) consists of γ-tubulin, GCP2, GCP3 [173-175], GCP4 [176], GCP5 and GCP6 [177] and looks like a ring structure when observed using EM [156, 178]. Two molecules of γ-tubulin and one molecule each of GCP2 and GCP3 constitute γ-tubulin small complex (γTuSC), which is the basic subunit of γTuRC [179]. γ-Tubulin, GCP2 and GCP3 are present in all eukaryots. GCP4 and GCP5 are in most eukaryotes with the exception of yeasts and GCP6 is found only in animals and fungi [27]. γTuRC was estimated to comprise 14 copies of γ-tubulin, 12 copies of GCP2 or GCP3, 2–3 copies of GCP4, a single copy of GCP5 and one half of a copy of GCP6 indicating that GCP6 is probably absent in a large fraction of the isolated γTuRCs [180].

Purified *Drosophila* γTuRC was able to nucleate MTs *in vitro*, whereas *Drosophila* γTuSC was inefficient [181], indicating that γTuSCs need to be assembled into the γTuRC for efficient MT nucleation. In contrast, depletion of GCP4, GCP5 or GCP6, the core components of γ-TuRC, in *Drosophila* and *Aspergillus* did not prevent centrosomal targeting of γTuSC and MT nucleation *in vivo* [182, 183]. In line with these findings is the fact that budding yeasts contain only γTuSCs. These results suggest that γTuSC without GCP4-6 is sufficient to

nucleate MTs from the centrosome or spindle pole body *in vivo*. The conflicting reports can be explained by the recently discovered ability of γTuSCs to self-assemble into ring-like structures, which, however, need to be activated by additional proteins to become active MT nucleating factors [27].

It was shown that purified budding yeast γTuSCs were able to form ring-like structures with 13-fold symmetry *in vitro,* resembling the MT 13-protofilament lattice [184]. Purified γTuSCs interacted latterally through γ-tubulins as predicted by crystalographic studies [53, 154]. However, individual γ-tubulin molecules bound to GCP3 were not positioned precisely to form longitudinal bonds with α-tubulin and were therefore inefficient in MT nucleation *in vitro* [184]. EM revealed that γTuSC is a Y-shaped structure with elongated body connected to two arms (Fig. 6). GCP2 and GCP3 form the body and arms directly interacting with each other and with γ-tubulins located in lobes at the ends of the arms. The conformational change in the GCP3 is presumably needed to bring both γ-tubulins in the γTuSC in the right position to match MT lattice [185]. This activating conformational switch could explain why MT nucleation is observed only at MTOCs and not in the cytoplasm, where the majority of cellular γTuCs can be found [155].

Solution of the GCP4 crystal structure revealed that all GCPs have a similar fold. Moreover, C-terminus of GCP4 bound directly to γ-tubulin in the same way as GCP2 and GCP3 [186]. GCP5 and GCP6 were also suggested to bind γ-tubulin directly implicating that all GCPs are capable of interacting with γ-tubulin directly in the γTuRC [187]. Fitting of GCP4 structure into γ-TuSC density maps suggested that all GCPs can fit into the γTuSC. 3D models of GCP2 and GCP3 were created based on GCP4 structure and a hinge in GCP3 was discovered, which is probably responsible for expected conformational changes of GCP3 inducing nucleation-competent positioning of γ-tubulin [186].

A new refined template model of MT nucleation was proposed in which seven γTuSCs assemble to give rise a γTuRC with a half-subunit overlap between the first and the seventh subunit (Fig 6). The resulting γTuRC exhibits 13-fold symmetry matching perfectly the MT lattice after activation via GCP3 conformational change. Special γTuSCs presumably exist containing GCP4, GCP5 or GCP6 [27].

Many proteins participate in the activation and targeting of γTuRC to MTOCs. Some of them co-purify with γTuRC such as GCP-WD/NEDD1 [188, 189], MOZART1 [190], MOZART2 [191], others are fibrillar PCM proteins like pericentrin [192], ninein [193], Nlp [194], CDK5RAP2 [180, 195], Cep192 [196] or AKAP450/CG-NAP [197]. Besides its cytoplasmic function as a chaperon for tubulin folding, Tubulin folding cofactor D (TBCD)

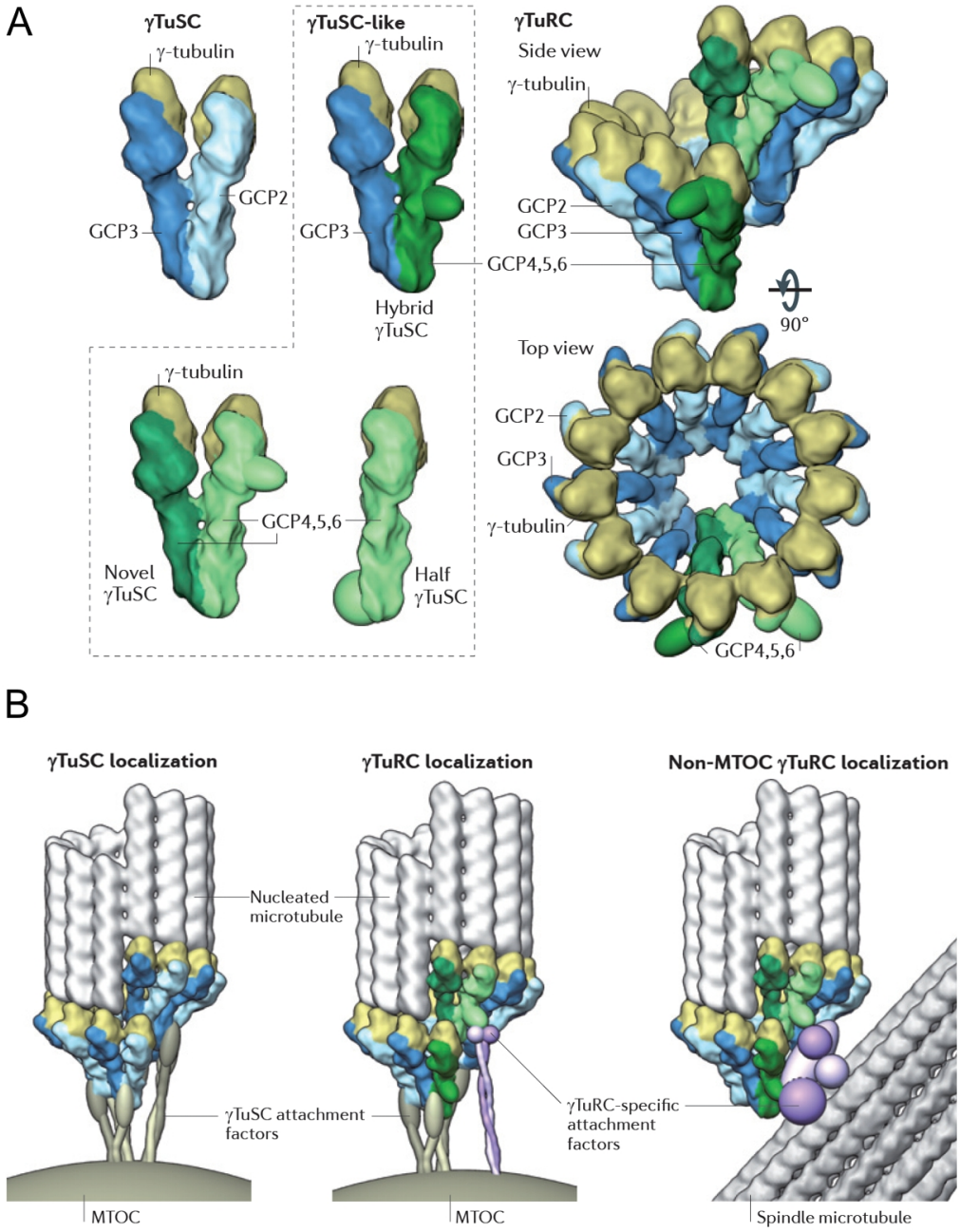

Figure 6. The template model of MT nucleation. **A)** Seven γTuSCs interact laterally to form a γTuRC. Since GCP4, 5, 6 can directly bind γ-tubulin and have a similar fold as GCP2/GCP3, they might form hybrid γTuSCs with GCP2, GCP3 or with each other. γTuRC has a 13-fold symmetry with 13 exposed γ-tubulins for longitudinal interactions with α-tubulins in B-lattice type MTs. **B)** MTs are anchored at various MTOCs by attachment factors specific either for γTuSC or γTuRC only components. A typical example of γTuSC-specific attachment factor is Spc110p in budding yeast or ninein in animals. A typical example of γTuRC-specific attachment factor is the augmin complex. Adapted from [27].

has been found on centrosomes where it participates in pericentrin and γTuRC recruitment [198]. On the other hand, γ-tubulin can serve as a centrosomal recruitment factor itself. The

centrosomal localization of Cep70, a protein involved in mitotic spindle assembly and MT organization, is γ -tubulin-dependent [199]. Specialized proteins facilitate targeting of γ-tubulin to non-centrosomal MTOCs and its regulation. For example, a multiprotein complex augmin connects γTuRC via GCP-WD to the mitotic or meiotic spindle MTs [161-163, 200-202], while AKAP-450, CLASPs, GM130, GMAP210 and CAP350 are required for MT nucleation and anchoring of γTuRC at GA [160, 203-205].

Although γTuRC-specific GCP4-6 are dispensable for centrosomal targeting and MT nucleation, they are necessary for binding of γTuRC to some non-centrosomal MTOCs. An intact γTuRC is required for binding along spindle [182] and interphase MTs [168]. Interestingly, a conserved region in CDK5RAP2 and its homologs named γ -TuNA binds directly to γTuRC and when overexpressed in cells, it induces abnormal non-centrosomal MT nucleation [180]. It suggests that one of the possible mechanisms of γTuRC activation might be its binding by recruitment factors [27].

I.2.3 Other functions of γ-tubulin

Besides MT nucleation and their anchoring at MTOCs, γ-tubulin is important for capping of MT (-) ends [156, 178, 206, 207], protecting them from depolymerization. Nucleation incompetent γTuC in fission yeast is still capable of capping unanchored MT (-) ends and of stabilizing them [208]. Further, γ -tubulin is involved in centriole biogenesis, presumably as a nucleator of centriolar MTs [189, 209-211]. γ-Tubulin also modulates MT (+) end dynamics in yeast [212, 213]. Interestingly, *Drosophila* γTuRC was detected along interphase MTs and its presence coincided with switching from a shortening or a growing phase to a pause [168] indicating that γTuRC could play a role as a catastrophe and rescue stopper. Remarkably, γTuRC did not co-localize with GTP-tubulin islands previously described to promote rescue event [57, 168]. By interacting with a (-) end-directed kinesin-14 Pkl1, γ -tubulin regulates bipolar spindle assembly in fission yeast [214].

Several studies suggested that γ-tubulin regulates cell cycle progression independently of MT nucleation. γ -Tubulin regulates anaphase-promoting complex/cyclosome during interphase in *Aspergillus* [215] and affects E2F transcriptional activity and S-phase progression in mammalian cells [171]. γ-Tubulin interacts with Cdc20 and BubRI in *Drosophila* [216], however its direct involvement in the spindle assembly checkpoint (SAC) remains controversial [217, 218]. Several lines of evidence implicate γ -tubulin role in DNA damage signalling. γ -Tubulin was found in complexes with Rad51 [219], ATR and BRCA1

[220]. Nevertheless it remains to be elucidated whether γ-tubulin regulates DNA damage proteins or vice-versa.

Some mutations in γ-tubulin resulted in an unexpected stabilization of MTs in fission yeast [221, 222] and *Aspergillus* [223] indirectly indicating that γ-tubulin can modulate MT dynamics. At present it is unknown whether the stabilization effect is achieved by γ-tubulin action at the MT (+) end similar to what was observed in *Drosophila* [168] or whether mutation-induced structural changes in the γTuC at the MT (-) end might propagate across the MT lattice and influence MT (+) end dynamics.

I.2.4 γ-Tubulin regulation

γ-Tubulin function and timely localization is regulated by PTMs. BRCA1/BARD1 complex was capable of catalyzing γ-tubulin ubiquitinylation *in vitro* [224]. Expression of mutant γ-tubulin unable to be ubiquitinylated led to the increased MT nucleation and centrosome amplification *in vivo*. BRCA1/BARD1-dependent ubiquitinylation also negatively regulated γTuRC recruitment to centrosomes resulting in diminished MT nucleation. However, it is unclear whether it was caused by ubiquitinylation of γ-tubulin or other γTuRC component [225].

γ-Tubulin forms complexes with several kinases including Wee1 [226], PI3-K [227] or Src family kinases Lyn [228], Syk [229] and Fyn [230]. Phosphorylation of the budding yeast γ-tubulin Tub4p on the Y445 by an unknown kinase increases assembly rate of MTs and influences MT organization [231]. Phosphorylation of Tub4p on Ser74 and Ser100 is important for functions of MTs, phosphorylation on highly conserved Ser360 regulates γ-tubulin stability [232]. γ-Tubulin is phosphorylated in Wee1-dependent manner in *Drosophila*, however functional recombinant Wee1 was not able to phosphorylate γ-tubulin *in vitro* indicating either indirect phoshorylation or requirement of some unknown cofactor [226]. γ-Tubulin phosphorylation was decribed also in mammalian cells [211, 233]. Phosphorylation of human γ-tubulin on Ser131 by SADB kinase is needed for centriole duplication [211].

γ-Tubulin PTMs are not the only way how to tune γTuRC function. As noted above, interactions with recruitment factors and MTOC localization play an important role in regulation of γTuRC function. Sequential phosphorylation of GCP-WD by Cdk1 and Plk1 at the onset of mitosis directs γTuRC to mitotic centrosomes and spindle MTs [188, 189, 202, 234, 235]. Large-scale analysis of Plk1 phosphoproteome of the early mitotic spindle in HeLa

cells revealed GCP2, GCP3, GCP5 and GCP6 as substrates of Plk1 [236]. Phosphorylation of GCP2 was also reported in connection with human sperm motility. Hypophosphorylation of GCP2 and lower expression of γ-tubulin was found in abberantly motile sperms in comparison to sperms from healthy donors [237]. Phosphorylation of GCP5 by GSK3-β prevents over-accumulation of γTuRC on spindle poles during mitosis [238]. Phosphorylation of GCP6 by Plk4 regulates centriole duplication [239]. Remarkably, androgen and Src signalling promote MT nucleation and accumulation of γ-tubulin at the centrosome during interphase [240]. Integrin-induced formation of androgen receptor-Src signalling complexes has been recently shown to activate the MEK/ERK signalling pathway regulating centrosomal localization of γTuRC, which links cell membrane events with centrosomal MT nucleation [241].

Another level of control is modulation of γTuRC structural stability and stability of its individual components. Chaperon TCP-1, with the help of a protein prefoldin, assists in γ-tubulin folding [242-244]. A prefoldin-like protein UXT, overexpressed in several tumor tissues [245], also interacts with γ-tubulin and its overexpression leads to dislocation of centrosomal γ-tubulin and centrosome organization [246]. Depletion of any γTuSC component in *Drosophila* resulted in a dramatic reduction of protein levels of the other two components, but the γTuRC-specific components were affected only slightly. On the other hand, depletion of any γTuRC-specific component did not change the protein levels of γTuSC-specific components and altered only the protein levels of the other γTuRC-specific components. It suggests that (i) coregulation and stabilization of γTuSC proteins is independent of γTuRC assembly, (ii) generally, proteins incorporated in γTuRC are stabilized and protected from degradation [168]. It is in good agreement with other studies showing that multisubunit complexes are often unstable when one component is absent [161, 247]. A nucleolar and centrosomal protein HCA66 was shown to affect the stability of γTuSC *in vivo* [248].

γ-Tubulin is abberantly expressed, usually overexpressed, in many cancer types including glioblastoma and medulloblastoma [85, 249, 250], breast cancer, [251, 252], prostate cancer [253], thyroid carcinoma [254] or pediatric pilocytic astrocytoma [255]. Although there are many compounds modulating MTs, there have been no γ-tubulin-specific drugs available. However, it has been recently reported that colchicine and combrestatin A 4 bind to γ-tubulin *in vitro* [256].

I.3 Important model systems used in the study

I.3.1 Mast cells

Mast cells are derived from hematopoietic stem cells. They circulate in the form of precursors, but their terminal differentiation and maturation occur locally in peripheral tissues. They exhibit high phenotypic plasticity called „mast cell heterogeneity“ that is presumably a result of the tissue-specific maturation and that is also dynamically changing in accordance with microenvironmental conditions [257-260].

In vertebrates, mast cells are widely distributed throughout the body, but they are especially located in tissues surrounding blood vessels, nerves and tissues in contact with external environment such as skin, respiratory and gastrointestinal tract. They are, together with dendritic cells, well positioned to be the first cell types of the immune system to detect and initiate responses against invading pathogens, environmental antigens (Ag) or environmentally derived toxins [258-260].

Mast cells participate in many physiological and pathophysiological processes. They are involved e.g. in tissue remodelling, wound healing, angiogenesis and in both innate and adaptive immunity. There has been increasing evidence that mast cells function not only as effector and immunomodulatory cells in turning the immune response on, but also in turning it off [261]. From a pathological perspective, mast cells are involved in allergic disorders, autoimmune diseases, innate and adaptive immunity [259, 260], and play a complex and in many aspects unknown role in modulating tumor microenvironment [262].

Various stimuli can activate mast cells to release a wide variety of biologically active products including histamine, proteases and other enzymes, cytokines, chemokines, growth factors, arachidonic acid metabolites and reactive oxygen and nitrogen species, many of which can potentially mediate physiological or pathophysiological functions of mast cells [261]. Since these mediators are stored in cytoplasmic granules and vesicles, their release is called degranulation. In addition, mast cells release exosomes containing exosomal proteins and exosomal shuttle RNA (mRNA and microRNA) that are transferable to other cells. However, their exact functions remain to be elucidated [259]. Interestingly, mast cells can participate in multiple cycles of activation for mediator release and can be differentially activated to release distinct patterns of mediators or cytokines, depending on the type and strength of the activating stimuli. Therefore, there are more than only two - off/on (resting/activated) - functional configurations of mast cells [257].

The most known mechanism of mast cell activation is through Ag- and IgE-dependent aggregation of the high-affinity IgE receptor (FcεRI). Ag crosslinks IgE antibodies connected to the FcεRI on the plasma membrane, which starts a complex signalling cascade leading to Ca^{2+} efflux from ER stores. STIM1 is an ER membrane protein sensing intralumenal Ca^{2+} concentration. The intralumenal part of STIM1 has a low affinity EF-hand Ca^{2+} binding site. When ER Ca^{2+} stores are depleted, the vacant EF-hand induces STIM1 conformational changes leading to STIM1 oligomerization and aggregation. Aggregates of STIM1 in the close proximity to plasma membrane physically associate with highly selective calcium release–activated calcium channels (CRAC) such as Orai1 and induce prolonged influx of extracellular Ca^{2+}. This extracellular Ca^{2+} influx is essential for mast cell activation and release of inflammatory mediators stored in cytoplasmic granules [258, 259, 263]. STIM1 also represents a special type of a +TIP. It contains SxIP motif and binds to growing MT (+) ends via EB1. However, its MT-dependent movement is restricted to diffusion in the ER membrane [264, 265].

MTs are required for mast cell degranulation and very rapidly reorganize in the course of mast cell activation [230, 266, 267]. Bone marrow mast cells (BMMCs) thus represent excellent model system for studying rapid MT changes. Nevertheless, regulatory mechanisms responsible for MT reorganization in BMMCs during activation events are largely unknown.

I.3.2 Glioblastoma cells

Gliomas are central nervous system tumors arising from glial cells. They are the most frequent group of primary brain tumors [268]. When sorted according to the original cell type, there are astrocytomas, oligodenrogliomas and ependymomas. Gliomas are categorized according to the level of malignancy. Low grade gliomas (WHO grade I-II) are still not anaplastic and carry a better prognosis for patients. High-grade gliomas (WHO grade III-IV) are anaplastic, malignant, diffuse and highly invasive multifocal tumors that have a very poor prognosis. Glioblastoma multiforme (GBM) arises from astrocytes and it is the most common grade IV tumor in adults and also the deadliest primary brain tumor in human.

Glioblastomas are incurable by conventional therapies, since they are radioresistant, chemoresistant, and tend to recur in a local fashion despite surgical resection [269]. Glioblastoma form tendrils extending several centimetres away from the main tumor mass which makes their complete surgical excision impossible [270]. It has been shown that a subpopulation of glioma cells, so called tumor initiating cells (TICs), were able to initiate

new tumors *in vivo* when transplanted into immunocompromised mice at low cell numbers [271]. They possess stem-cell-like properties, including extensive self-renewal, multipotency and the proliferative potential for generation of many progeny. Several coordinated cellular programs are activated in TICs resulting in increased migration, invasion, reduced proliferation and marked resistance to apoptosis, which render them highly resistant to conventional treatments [269, 272]. Remarkably, TICs are present also in glioblastoma cell lines such as U87MG and T98G [273].

Highly motile and invasive glioblastoma cells specifically use the mesenchymal mode of migration and invasion [274]. Several signalling pathways involved in regulation of cell migration and closely related cytoskeleton remodelling such as integrin signalling and phosphatidylinositol-3 kinase (PI3-K) pathway are aberrant in glioblastoma [274, 275]. The regulation of cytoskeleton in glioblastoma cells is largely unknown. Some glioblastoma cell lines exhibit unusual regulation of cytoskeletal filaments, e.g. glioblastoma cells U87MG remain motile even in the absence of MFs and create MT-based protrusions. On the other hand, depolymerization of MTs stops their migration completely [276]. Furthermore, βIII-tubulin and γ-tubulin are highly overexpressed in glioma and glioblastoma cell lines. Moreover, γ-tubulin forms aggregates, which accumulate in the cytoplasm and at the cell periphery [85, 249]. Why particular tubulins are overexpressed and how MTs are regulated in glioblastoma cells remains to be elucidated.

II. AIMS OF THE STUDY

The long-term goal of the Laboratory of biology of cytoskeleton is to elucidate at the molecular level how MTs are regulated in various cellular processes. We have focused on nucleation and reorganization of MT in cells under normal and pathological conditions. In particular, we have been studying γ-tubulin, the essential protein for MT nucleation. A panel of monoclonal antibodies against various MT proteins including α-, β- and γ-tubulins has been prepared in our laboratory and these antibodies represent a powerful tool in studying MT organization and properties. Nevertheless, microscopic analysis of living cells could provide new insights into the subcellular localization, dynamics and function of studied proteins. In the presented study we aimed to characterize novel functions of important MT regulatory proteins: γ-tubulin, MT severing protein spastin and MT-interacting Ca^{2+} sensor STIM1. We also intended to develop live cell imaging methods for quantitative measurement of MT dynamics and cell migration, which would be applicable for functional analysis of the selected MT regulatory proteins.

Partial aims of this Ph.D. thesis were following:

1) Development of new tools for quantification of MT dynamics and cell migration

2) Analysis of MT reorganization in the course of mast cell activation and the role of STIM1 in this process.

3) Functional characterization of MT severing protein spastin in glioblastoma

4) Analysis of novel functions of mammalian γ-tubulins

III. COMMENTS ON PRESENTED PUBLICATIONS

III.1 STIM1-directed reorganization of microtubules in activated mast cells

Hájková Z., Bugajev V., Dráberová E., **Vinopal S.**, Dráberová L., Janáček J., Dráber Pe., Dráber Pa. (2011). STIM1-directed reorganization of microtubules in activated mast cells. J Immunol. *186*, 913-923.

MTs are involved in processes leading to degranulation of mast cells [266, 277, 278]. We and others have previously shown that activation of mast cells either via specific aggregation of FcεRI or by unspecific activation with pervanadate leads to significant changes in MT organization [230, 267]. However, the precise role of MTs in degranulation is still incompletely understood.

In this work, we showed that activation of BMMCs induced by FcεRI aggregation or treatment with pervanadate or thapsigargin results in generation of plasma membrane protrusions containing MTs (MT protrusions). Quantification of MT (+) end dynamics after activation revealed increased density of MT tracks near the cell periphery. Formation of MT protrusions and changes in MT (+) end dynamics were dependent on extracellular Ca^{2+} influx, as they could be induced also by thapsigargin, an inhibitor of sarco/endoplasmic reticulum Ca^{2+} ATPases. Thapsigargin treatment causes depletion of Ca^{2+} from ER stores, which in turn induce an influx of extracellular Ca^{2+} controlled by store-operated Ca^{2+} entry (SOCE) [279]. It is well established that SOCE is essential for mast cell activation both *in vitro* and *in vivo* [280, 281] and can be triggered by FcεRI aggregation. Knock-down (KD) of STIM1, the key regulator of SOCE, impaired Ca^{2+} signalling, formation of MT protrusions and prevented redistribution of growing MTs after activation. Expression of siRNA-resistant STIM1 in STIM1-depleted BMMCs rescued the wild-type phenotype.

In accordance with previous studies [264, 265], we observed co-localization of STIM1 with a +TIP protein EB1 in resting BMMCs. Interestingly, we noticed that the typical submembrane STIM1 puncta, which form due to STIM1 oligomerization and aggregation during the first minute after activation, are associated with MTs in the protrusions. This led us to hypothesize that MTs might be important for relocation of STIM1 oligomers to the plasma membrane, where they trigger opening of Orai channels and influx of extracellular Ca^{2+}.

However, using TIRF microscopy-based live cell imaging, we directly showed that MTs are dispensable for relocation of STIM1 oligomers to the plasma membrane in BMMCs. While depolymerization of MTs had a significant impact on degranulation measured by β-glucuronidase release, Ca^{2+} uptake was only slightly affected, which correlated with our live cell imaging data.

STIM1-depleted cells exhibited defective chemotaxis toward Ag. Although we still do not know exactly, what is the function of the MT protrusions in activated BMMCs, the defective chemotaxis indicates a possible role of MT protrusions in sensing external chemotactic gradients of Ag or other signals recognized by mast cells. MT protrusions also significantly enlarge the cell surface. That might facilitate directional sorting of the membrane receptors and enhance the specific responsiveness of mast cells to various stimuli, since mast cells can participate in multiple cycles of activation and can be differentially activated to release distinct patterns of mediators, depending on the type and strength of the activating stimuli.

Taken together, we showed that STIM1-induced SOCE and following enhanced levels of free cytoplasmic Ca^{2+} concentration are vital for degranulation, chemotactic response and MT reorganization in BMMCs. This reorganization of MTs results in the formation of MT protrusions considerably enlarging the surface of activated cells. We have also demonstrated, that the early relocation of STIM1 oligomers to the plasma membrane after activation is MT-independent process in BMMCs. Our findings open new area for investigation of novel rational approaches to treatment of inflammatory and allergic diseases. Research on the role of Ca^{2+} signalling in MT growth and nucleation continues in our laboratory.

In this project, I established and performed live cell imaging experiments including analysis of MT (+) end dynamics and real-time observations of STIM1 puncta formation under different conditions. I also acquired and prepared images showing co-localization of STIM1 and EB1 on MT (+) ends and association of STIM1 with MT protrusions in activated mast cells. I participated in planning of experiments and manuscript preparation. For quantification of MT dynamics, I participated in development of a semi-automatic particle tracking plugin for Ellipse program (ViDiTo, Systems, Košice Slovakia) in collaboration with Dr. Jiří Janáček (Institute of Physiology of the AS CR, v.v.i., Prague).

III.2 Microtubule-severing ATPase spastin in glioblastoma: increased expression in human glioblastoma cell lines and inverse roles in cell motility and proliferation

Dráberová E., **Vinopal S**., Morfini G., Liu P.S., Sládková V., Sulimenko T., Burns M.R., Solowska J., Kulandaivel K., de Chadarévian J.P., Legido A., Mörk S.J., Janáček J., Baas P.W., Dráber P., Katsetos C.D. (2011). Microtubule-severing ATPase spastin in glioblastoma: increased expression in human glioblastoma cell lines and inverse roles in cell motility and proliferation. J Neuropathol Exp Neurol. *70*, 811-826.

Previously, we described overexpression and aberrant patterns of noncentrosomal γ-tubulin in high-grade gliomas and showed that its expression level increases with the tumor grade [249]. βIII-tubulin is also abberantly expressed in glioma [282] and forms complexes with soluble γ-tubulin [85]. Since components of MT cytoskeleton are overexpressed in high-grade glioma, we started investigating glioma-specific expression and function of other proteins involved in MT regulation.

In this work we studied the expression and distribution of the MT severing protein spastin in 3 human glioblastoma cell lines (U87MG, U138MG, and T98G) and in clinical tissue samples representative of all grades of diffuse astrocytic gliomas. Although spastin has four isoforms in human, M87 variant was the most prevalent in the studied cells. Spastin expression was increased in neoplastic glial phenotypes, especially in glioblastoma when compared with lower grade glioma and with normal mature brain tissues. RT-qPCR and immunoblotting experiments revealed increased levels of spastin mRNA and protein expression in the glioblastoma cell lines versus normal human astrocytes.

Interestingly, we observed enrichment of spastin in the leading edges of cells in T98G glioblastoma cell cultures and in neoplastic cell populations in tumor specimens. This prompted us to test whether spastin contributes to increased motility of glioblastoma cells. We depleted spastin by siRNA (KD) and measured free migration of control and KD T98G cells. By quantification of cell motility we showed that depletion of spastin leads to a highly significant reduction of T98G motility. Surprisingly, we noticed that cells depleted of spastin proliferate significantly faster than control cells. These inverse roles of spastin in cell motility and proliferation are intriguing, especially its role in proliferation. Our findings indicate that (i) spastin might have an unknown MT-independent function in regulation of cell proliferation

or (ii) that disruption of MT regulation resulting in decreased motility might activate cellular programs switching the cell to the proliferative mode.

Increased migration, invasion and reduced proliferation belong to hallmarks of glioma TICs [269, 283]. Further investigation of spastin function in glioma will be important to elucidate mechanisms that could be potentially used for reprogramming of glioblastoma cells to the proliferative mode, which might increase their susceptibility to chemo- and radiotherapy.

In conclusion, we showed that spastin is overexpressed in glioma and its expression level rises with the grade of tumor. We also demonstrated for the first time that spastin is involved in regulation of cell motility and that its expression contributes to high motility and relatively reduced proliferation of T98G glioblastoma cells. Our work suggests new possible directions in research on MT arrangement and functions in glioblastoma cells. Currently, other MT severing proteins katanin and fidgetin are studied in respect of their role in cell motility and proliferation of glioblastoma cells in our laboratory.

For the purpose of this study, I performed bioinformatic study on human spastin variants and based on its results ordered and tested suitable siRNAs for KD. Two best performing siRNAs were used in further experiments. My main contribution to this work was development and application of a program for semi-automatic cell tracking. We developed it in collaboration with Dr. Jiří Janáček (Institute of Physiology of the AS CR, v.v.i., Prague), who did all programming. I processed all time-lapse sequences, analyzed corresponding datasets and prepared several figures and a movie for publication.

III.3 Nuclear γ-tubulin associates with nucleoli and interacts with tumor suppressor protein C53

Hořejší B., **Vinopal S.**, Sládková V., Dráberová E., Sulimenko V., Sulimenko T., Vosecká V., Philimonenko A., Hozák P., Katsetos C. D., Dráber P. (2012). Nuclear γ-tubulin associates with nucleoli and interacts with tumor suppressor protein C53. J Cell Physiol. *227*, 367-382.

γ-Tubulin is a typical centrosomal protein, however, it can be found also in the cytoplasm, on cell membranes, condensed mitotic chromosomes, midbodies and along MTs in mitotic

spindles [15]. In addition, γ-tubulin presence in the nucleus was reported in plants [170] and several studies suggested that γ-tubulin is a nuclear protein in animals as well [219, 220].

In this paper, we showed for the first time that γ-tubulin is present in the nucleolus. During our previous work on human glioblastoma cell lines exhibiting high expression of γ-tubulin, we repeatedly observed γ-tubulin immunostaining in the nucleus/nucleolus. The intensity of staining was dependent on used fixation procedures. We have found out that γ-tubulin can be reproducibly visualized in the nucleolus after methanol-acetic acid fixation or prolonged wash-out after methanol fixation. Immunostaining with antibodies against γ-tubulin and markers of nucleoli (UBF, nucleolin, fibrillarin) revealed γ-tubulin nucleolar localization not only in glioblastoma cells but also in other cell lines including normal human astrocytes, representing a non-transformed primary cell line.

We further confirmed γ-tubulin nucleolar localization by different anti-γ-tubulin antibodies, by expressing exogenous FLAG-tagged γ-tubulin in cultured cells and by depletion of γ-tubulin using siRNA. Immunoelectron microscopy revealed γ-tubulin localization outside fibrillar centres where transcription of ribosomal DNA takes place. In addition, γ-tubulin was detected using immunoblotting and immunofluorescence on isolated nucleoli.

Proteins can get into the nucleus during mitosis when the nuclear envelope is broken-down. A similar mechanism of nuclear entry was proposed for βII-tubulin [83]. By analysis of γ-tubulin localization during mitosis using confocal microscopy, we showed that γ-tubulin remains associated with nucleolar remnants suggesting that γ-tubulin can enter the nucleus/nucleolus during mitosis. γ-Tubulin contains putative nuclear localization sequence (NLS) and nuclear export sequence (NES); NLS has been recently experimentally verified [169, 171]. We tested, whether γ-tubulin is actively transported into the nucleus during interphase by blocking nuclear export via nuclear pores using nuclear export inhibitor leptomycin B. No significant accumulation of γ-tubulin in the nucleus was observed after leptomycin B treatment indicating that γ-tubulin is not transported to the nucleus by fast nuclear import mechanisms.

Additional experiments with γ-tubulin fused to a photoconvertible protein DendraII and heterokaryon assays also excluded fast nuclear import during interphase. However, faint staining of γ-tubulin-FLAG in the nuclei of untransfected mouse NIH-3T3 cells, forming heterokaryons with human U2OS cells transfected with γ-tubulin-FLAG, was detected 6 hours after the initiation of the experiment. It indicates that slow nuclear import of γ-tubulin occurs also in interphase.

Immunoprecipitation with anti-γ-tubulin antibody from nuclear extracts combined with mass spectrometry led to a discovery of a novel γ-tubulin interacting protein C53, also known as CDK5 regulatory subunit associated protein 3 (CDK5RAP3) or LXXLL/leucine-zipper-containing ARF-binding protein (LZAP). C53 is located at multiple subcellular compartments including nucleoli and participates in many cellular processes including NF-κB [284], G1/S [285, 286] and G2/M checkpoint signalling [287]. Overexpression of C53 in cultured cells weakens DNA damage induced G2/M checkpoint activation. Interestingly, co-expression of γ-tubulin with C53 neutralizes the inhibitory effect of C53 on DNA damage G2/M checkpoint activation. These results suggest that γ-tubulin regulates C53 function and participates in G2/M checkpoint signalling.

Recently, the nucleolar localization of γ-tubulin has been confirmed independently by another research group [169]. A detailed description of γ-tubulin translocation to the nucleus and its novel nuclear function in regulation of S-phase progression have been also reported [171].

Collectively taken, we showed for the first time that γ-tubulin is present in the nucleolus. We identified a novel γ-tubulin interacting protein C53 and showed that, via its interaction with C53, γ-tubulin participates in the regulation of G2/M checkpoint. Our results support the increasingly accepted picture of γ-tubulin as a multifunctional protein whose role is not restricted only to MT (-) ends. Characterization of molecular mechanisms of γ-tubulin interaction with C53 and their functional consequences is underway in our laboratory.

I prepared C-terminally FLAG-tagged human γ-tubulin 1, which was used for verification of γ-tubulin localization in the nucleolus. I performed high-throughput imaging on Olympus ScanR screening station to quantify dynamics of γ-tubulin nucleo-cytoplasmic shuttling and analyzed the data. Further, I examined distribution of γ-tubulin during mitosis using confocal microscopy, performed studies with γ-tubulin-DendraII in living cells, prepared pC53-EGFP vector and established U2OS cell line stably expressing C53-EGFP. I participated in planning of experiments, formulation of hypotheses, preparation of the manuscript and response to reviewers.

III.4 γ-Tubulin 2 nucleates microtubules and is downregulated in mouse early embryogenesis

Vinopal S., Černohorská M., Sulimenko V., Sulimenko T., Vosecká V., Flemr M., Dráberová E., Dráber P. (2012). γ-Tubulin 2 Nucleates Microtubules and Is Downregulated in Mouse Early Embryogenesis. PLoS ONE *7*: e29919.

In this work, we wanted to identify and characterize molecular mechanisms underlying functional differences between TUBG1 and TUBG2 suggested by Yuba-Kubo *et al.* [151]. At first, we had to prepare FLAG-tagged human and mouse TUBG1 and TUBG2, because no specific antibodies distinguishing between TUBG1 and TUBG2 have been available. We examined their subcellular localization and interactions with GCP2 and GCP4. All recombinant proteins localized properly to MTOCs such as centrosomes and mitotic spindle MTs and formed immunocomplexes with GCP2 and GCP4 being indistinguishable from each other.

Next, we tested whether TUBG2 can substitute for TUBG1 *in vivo*. We depleted endogenous TUBG1 in U2OS cells using siRNA and performed phenotypic rescue experiments by expressing siRNA-resistant mouse TUBG1-FLAG, mouse TUBG2-FLAG or human TUBG2-FLAG in these cells. The used siRNA was TUBG1-specific and immunobloting with anti-γ-tubulin antibody recognizing both TUBG1 and TUBG2 revealed that TUBG1 is a predominant γ-tubulin in U2OS cells. Depletion of TUBG1 resulted in severe mitotic spindle defects including monopolar and collapsed spindles, very similar to those observed in *Tubg1*$^{-/-}$ blastocysts [151], and induced accumulation of TUBG1-depleted cells in metaphase. As expected, mouse TUBG1-FLAG rescued wild-type phenotype and normal mitotic progression. Importantly, the same was true for both mouse and human TUBG2-FLAG indicating that TUBG2 is able to replace TUBG1 *in vivo*.

The above results indirectly implicated that TUBG2 is able to nucleate MTs. To prove it directly, we used the same experimental set-up and examined MT nucleating capability of TUBG2 by MT regrowth experiments. We focused on mitotic cells, because γ-tubulin is enriched on prophase and metaphase centrosomes [288] and we could expect a prominent effect on MT nucleation. In accordance with our previous results, mouse TUBG1-FLAG as a positive control, mouse TUBG2-FLAG and human TUBG2-FLAG rescued MT aster

formation in TUBG1-depleted cells. These findings suggested that mammalian TUBG2 is capable of centrosomal MT nucleation in mitotic cells.

To strengthen the evidence of MT nucleation capability of TUBG2, we quantified MT formation *in vivo* by the tracking of MT (+) ends marked by EB1-GFP in interphase U2OS cells. For live cell imaging we prepared mouse TUBG1 and human TUBG2 tagged with a red fluorescent protein TagRFP and use shRNA-based system. MT formation was quantified in negative control cells, TUBG1-depleted cells and in TUBG1-depleted cells expressing either mouse TUBG1-TagRFP or human TUBG2-TagRFP. We observed a significant reduction in the number of MT (+) end tracks in TUBG1-depleted cells. Both exogenous TUBG1 and TUBG2 rescued MT formation indicating that TUBG2 can take the place of TUBG1 also in interphase cells.

We showed by several methods that TUBG2 was able to nucleate MTs and substitute for TUBG1 in cultured cells. The inability of TUBG2 to do so in TUBG1-deficient blastocysts, where TUBG2 should have been present [151], was intriguing. Therefore we analyzed the expression of TUBG2 in wild-type mouse blastocysts in greater detail. Using RT-qPCR, we quantified mRNA levels of *Tubg1*, *Tubg2*, *Tubgcp2* and *Tubgcp5* in mouse oocytes, 2-cell stage embryos, 8-cell stage embryos and blastocysts. Surprisingly, *Tubg2* mRNA level decreased dramatically in the course of mouse preimplantation development, unlike mRNA levels of *Tubg1*, *Tubgcp2* and *Tubgcp5,* resulting in a very low amount of *Tubg2* transcript in the blastocyst.

Although there had been no antibodies available distinguishing specifically between mammalian γ-tubulins, we were able to separate TUBG1 and TUBG2 using 2D-PAGE and identify their specific positions on the gel. By this method, we found out that while TUBG1 was abundant, there was a very low level of TUBG2 protein in the wild-type blastocyst, which was in a good agreement with our RT-qPCR data. In line with previous studies, we also detected high levels of TUBG2 mRNA and protein in the brain [151, 153] .

Based on our data, we proposed an alternative interpretation of *Tubg1*$^{-/-}$ and *Tubg2*$^{-/-}$ phenotypes previously described in mice [151]. Endogenous TUBG2 could not replace missing TUBG1 in *Tubg1*$^{-/-}$ blastocyst, even though it can nucleate MTs, because it was not present in a sufficient amount. Nevertheless, our data did not directly exclude the possibility that TUBG2 expression was upregulated in *Tubg1*$^{-/-}$ blastocysts in response to TUBG1 deficiency as it was observed for several other duplicate gene pairs [289, 290]. It that case, TUBG2 would not be functionally equivalent to TUBG1 in mouse blastocysts. However, we consider this possibility unlikely for several reasons. First, although upregulation of

a duplicate gene by transcriptional reprogramming occurs after its paralog deletion, it is not a genome-wide phenomenon [291]. A recent genome-wide study on yeasts revealed that only 11% of duplicate genes responded by increased expression to the deletion of their paralogs [290]. Second, such paralog responsiveness occurred with almost no exceptions only when the duplicate genes were synthetic lethal [290], which is not the case of γ-tubulin genes (TUBG1 knock-out is lethal itself). Third, Yuba-Kubo *et al.* speculated that TUBG2 was unable to be recruited to centrosomes in the absence TUBG1, because they did not detect any γ-tubulin signal on centrosomes in *Tubg1*$^{-/-}$ blastocysts [151]. Our alternative and simpler interpretation of their observation is that TUBG2 is expressed neither in the wild-type nor in *Tubg1*$^{-/-}$ blastocysts.

Behavioural abnormalities of *Tubg2*$^{-/-}$ mice do not necessarily imply just unknown function of TUBG2. They might also reflect the reduction of total γ-tubulin in the brain of *Tubg2*$^{-/-}$ mice, as TUBG2 is highly expressed in the brain [151, 153]. Yet, we cannot directly exclude the possibility that TUBG2 has some additional still unknown function(s).

The question is, how almost identical and functionally redundant γ-tubulin genes are maintained in mammalian genomes? Analyses of expression of TUBG1 and TUBG2 showed that they are differentially expressed in many tissues [151, 153], the same holds also for this study. Partitioning of tissue-specific patterns of expression of the ancestral gene [292] or expression reduction [293] are special types of subfunctionalization facilitating retention of duplicates and conservation of their ancestral functions.

In addition, it was reported that some gene segments of TUBG1 and TUBG2 had been evolving together in the process known as „concerted evolution“ [153]. It was proposed that concerted evolution might have been operative to maintain perfect homology at essential binding sites. Indeed, exons 2-3 and 7-10 of both γ-tubulin genes homogenized by gene conversion [153] encode regions which are likely critical for interaction of γ-tubulin with GCP2 and GCP3 [186]. Thus, concerted evolution together with subfunctionalization foster the preservation of highly similar and functionally redundant γ-tubulin genes in mammalian genomes [153].

In conclusion, we demonstrated that TUBG2 is able to nucleate MTs and substitute for TUBG1 *in vivo*. Further, we showed at both mRNA and protein level that TUBG2 expression is dramatically reduced in blastocysts in contrast to TUBG1. Our data indicate that TUBG2 cannot rescue TUBG1 deficiency in *Tubg1*$^{-/-}$ blastocysts, because it is not present in a sufficient amount. We propose that mammalian γ-tubulins are functionally redundant with respect to their MT nucleation activity.

In this project, I cloned all described constructs, established protocols for γ-tubulin depletion by RNAi, performed RT-qPCR, immunofluorescence and quantification of MT (+) end dynamics. I participated in conceiving and designing all experiments, formulation of hypotheses and in preparation of the majority of images for publication. I analyzed all data, wrote the manuscript draft and participated in the response to rewievers comments.

IV. CONCLUSIONS

1. We developed a new method for quantification of MT (+) end dynamics in living cells. The method is based on semi-automatic tracking of MT (+) ends marked by a +TIP EB1-GFP. To quantify migration of glioblastoma cells, we developed a method for measuring of free cell migration by tracking their nuclei visualized by a vital DNA dye. These methods were successfully used in the presented publications and are now routinely used in our laboratory.

2. We found out that activation of BMMCs leads to the formation of plasma membrane protrusions containing MTs. These MT protrusions do not form in the absence of STIM1-induced SOCE suggesting that Ca^{2+} signalling might modulate MTs in activated BMMCs. Although STIM1 is associated with MTs in both resting and activated BMMCs, MTs are not required for STIM1-regulated SOCE. STIM1 depletion prevents not only formation of MT protrusion, but also causes defects in chemotaxis. We propose that MT protrusions might be involved in sensing external chemotactic gradients of antigen or other signals in mast cells.

3. We found out that spastin is overexpressed in glioma and glioblastoma cell lines and its overexpression can be linked to a trend toward high-grade malignancy. Glioblastoma cells depleted of spastin exhibit significantly lower motility but at the same time an increased proliferation rate. These novel and inverse roles of spastin in cell migration and proliferation need to be further investigated, as therapeutic targeting of spastin might be a novel approach to treatment of invasive gliomas.

4. We showed for the first time that γ-tubulin is present in the nucleoli of various cell lines of different tissue and species origin. γ-Tubulin can get into the nucleus during mitosis and interphase as well, however its interphase nuclear transport is very slow. We identified the multifunctional protein C53 as a new γ-tubulin interacting protein in the nucleus. We found out that γ-tubulin antagonizes the inhibitory effect of C53 on DNA damage G2/M checkpoint activation. Our results suggest that γ-tubulin has also other functions in addition to MT nucleation.

5. We demonstrated that mammalian TUBG2 is able to nucleate MTs and substitute for TUBG1 in cultured cells. Further, we found out that almost identical mammalian γ-tubulins

can be reliably discriminated according to their electrophoretic properties by 2D-PAGE. We showed at both mRNA and protein level that, unlike TUBG1, TUBG2 expression is dramatically downregulated in mouse preimplantation development, which results in very low amount of TUBG2 in blastocysts. Our data indicate that TUBG2 cannot rescue TUBG1 deficiency in *Tubg1*$^{-/-}$ blastocysts, because it is not present in a sufficient amount. Based on our results we propose that mammalian γ-tubulins are functionally equivalent with respect to their MT nucleation activity.

V. REFERENCES

1. Wickstead, B., and Gull, K. (2011). The evolution of the cytoskeleton. J Cell Biol *194*, 513-525.
2. Stiess, M., and Bradke, F. (2011). Neuronal polarization: the cytoskeleton leads the way. Dev Neurobiol *71*, 430-444.
3. Mimori-Kiyosue, Y. (2011). Shaping microtubules into diverse patterns: molecular connections for setting up both ends. Cytoskeleton (Hoboken) *68*, 603-618.
4. de Forges, H., Bouissou, A., and Perez, F. (2012). Interplay between microtubule dynamics and intracellular organization. Int J Biochem Cell Biol *44*, 266-274.
5. Henry, T., Gorvel, J.P., and Meresse, S. (2006). Molecular motors hijacking by intracellular pathogens. Cell Microbiol *8*, 23-32.
6. Dodding, M.P., and Way, M. (2011). Coupling viruses to dynein and kinesin-1. EMBO J *30*, 3527-3539.
7. Razafsky, D., and Hodzic, D. (2009). Bringing KASH under the SUN: the many faces of nucleo-cytoskeletal connections. J Cell Biol *186*, 461-472.
8. Beaudouin, J., Gerlich, D., Daigle, N., Eils, R., and Ellenberg, J. (2002). Nuclear envelope breakdown proceeds by microtubule-induced tearing of the lamina. Cell *108*, 83-96.
9. Salina, D., Bodoor, K., Eckley, D.M., Schroer, T.A., Rattner, J.B., and Burke, B. (2002). Cytoplasmic dynein as a facilitator of nuclear envelope breakdown. Cell *108*, 97-107.
10. Mellad, J.A., Warren, D.T., and Shanahan, C.M. (2011). Nesprins LINC the nucleus and cytoskeleton. Curr Opin Cell Biol *23*, 47-54.
11. Luxton, G.W., and Gundersen, G.G. (2011). Orientation and function of the nuclear-centrosomal axis during cell migration. Curr Opin Cell Biol *23*, 579-588.
12. Friedl, P., and Wolf, K. (2010). Plasticity of cell migration: a multiscale tuning model. J Cell Biol *188*, 11-19.
13. Belletti, B., Nicoloso, M.S., Schiappacassi, M., Berton, S., Lovat, F., Wolf, K., Canzonieri, V., D'Andrea, S., Zucchetto, A., Friedl, P., et al. (2008). Stathmin activity influences sarcoma cell shape, motility, and metastatic potential. Mol Biol Cell *19*, 2003-2013.
14. Azimzadeh, J., and Bornens, M. (2007). Structure and duplication of the centrosome. J Cell Sci *120*, 2139-2142.
15. Luders, J., and Stearns, T. (2007). Microtubule-organizing centres: a re-evaluation. Nat Rev Mol Cell Biol *8*, 161-167.
16. Doxsey, S., Zimmerman, W., and Mikule, K. (2005). Centrosome control of the cell cycle. Trends Cell Biol *15*, 303-311.
17. Lindqvist, A., Rodriguez-Bravo, V., and Medema, R.H. (2009). The decision to enter mitosis: feedback and redundancy in the mitotic entry network. J Cell Biol *185*, 193-202.
18. Azimzadeh, J., and Marshall, W.F. (2010). Building the centriole. Curr Biol *20*, R816-825.
19. Kitagawa, D., Vakonakis, I., Olieric, N., Hilbert, M., Keller, D., Olieric, V., Bortfeld, M., Erat, M.C., Fluckiger, I., Gonczy, P., et al. (2011). Structural basis of the 9-fold symmetry of centrioles. Cell *144*, 364-375.
20. van Breugel, M., Hirono, M., Andreeva, A., Yanagisawa, H.A., Yamaguchi, S., Nakazawa, Y., Morgner, N., Petrovich, M., Ebong, I.O., Robinson, C.V., et al. (2011). Structures of SAS-6 suggest its organization in centrioles. Science *331*, 1196-1199.
21. Bettencourt-Dias, M., and Glover, D.M. (2007). Centrosome biogenesis and function: centrosomics brings new understanding. Nat Rev Mol Cell Biol *8*, 451-463.
22. Mahen, R., and Venkitaraman, A.R. (2012). Pattern formation in centrosome assembly. Curr Opin Cell Biol *24*, 14-23.
23. Ishikawa, H., and Marshall, W.F. (2011). Ciliogenesis: building the cell's antenna. Nat Rev Mol Cell Biol *12*, 222-234.
24. Janke, C., and Bulinski, J.C. (2011). Post-translational regulation of the microtubule cytoskeleton: mechanisms and functions. Nat Rev Mol Cell Biol *12*, 773-786.
25. Nigg, E.A., and Stearns, T. (2011). The centrosome cycle: Centriole biogenesis, duplication and inherent asymmetries. Nat Cell Biol *13*, 1154-1160.

26. Chretien, D., and Wade, R.H. (1991). New data on the microtubule surface lattice. Biol Cell *71*, 161-174.
27. Kollman, J.M., Merdes, A., Mourey, L., and Agard, D.A. (2011). Microtubule nucleation by gamma-tubulin complexes. Nat Rev Mol Cell Biol *12*, 709-721.
28. Amos, L., and Klug, A. (1974). Arrangement of subunits in flagellar microtubules. J Cell Sci *14*, 523-549.
29. des Georges, A., Katsuki, M., Drummond, D.R., Osei, M., Cross, R.A., and Amos, L.A. (2008). Mal3, the Schizosaccharomyces pombe homolog of EB1, changes the microtubule lattice. Nat Struct Mol Biol *15*, 1102-1108.
30. McIntosh, J.R., Morphew, M.K., Grissom, P.M., Gilbert, S.P., and Hoenger, A. (2009). Lattice structure of cytoplasmic microtubules in a cultured Mammalian cell. J Mol Biol *394*, 177-182.
31. Meurer-Grob, P., Kasparian, J., and Wade, R.H. (2001). Microtubule structure at improved resolution. Biochemistry *40*, 8000-8008.
32. Garvalov, B.K., Zuber, B., Bouchet-Marquis, C., Kudryashev, M., Gruska, M., Beck, M., Leis, A., Frischknecht, F., Bradke, F., Baumeister, W., et al. (2006). Luminal particles within cellular microtubules. J Cell Biol *174*, 759-765.
33. Bouchet-Marquis, C., Zuber, B., Glynn, A.M., Eltsov, M., Grabenbauer, M., Goldie, K.N., Thomas, D., Frangakis, A.S., Dubochet, J., and Chretien, D. (2007). Visualization of cell microtubules in their native state. Biol Cell *99*, 45-53.
34. Koning, R.I., Zovko, S., Barcena, M., Oostergetel, G.T., Koerten, H.K., Galjart, N., Koster, A.J., and Mieke Mommaas, A. (2008). Cryo electron tomography of vitrified fibroblasts: microtubule plus ends in situ. J Struct Biol *161*, 459-468.
35. Mitchison, T., and Kirschner, M. (1984). Dynamic instability of microtubule growth. Nature *312*, 237-242.
36. Chretien, D., Fuller, S.D., and Karsenti, E. (1995). Structure of growing microtubule ends: two-dimensional sheets close into tubes at variable rates. J Cell Biol *129*, 1311-1328.
37. Arnal, I., Karsenti, E., and Hyman, A.A. (2000). Structural transitions at microtubule ends correlate with their dynamic properties in Xenopus egg extracts. J Cell Biol *149*, 767-774.
38. Hoog, J.L., Huisman, S.M., Sebo-Lemke, Z., Sandblad, L., McIntosh, J.R., Antony, C., and Brunner, D. (2011). Electron tomography reveals a flared morphology on growing microtubule ends. J Cell Sci *124*, 693-698.
39. Margolin, G., Gregoretti, I.V., Cickovski, T.M., Li, C., Shi, W., Alber, M.S., and Goodson, H.V. (2012). The Mechanisms of Microtubule Catastrophe and Rescue: Implications from analysis of a dimer-scale computational model. Mol Biol Cell *23*, 642-656.
40. Menendez, M., Rivas, G., Diaz, J.F., and Andreu, J.M. (1998). Control of the structural stability of the tubulin dimer by one high affinity bound magnesium ion at nucleotide N-site. J Biol Chem *273*, 167-176.
41. Ravelli, R.B., Gigant, B., Curmi, P.A., Jourdain, I., Lachkar, S., Sobel, A., and Knossow, M. (2004). Insight into tubulin regulation from a complex with colchicine and a stathmin-like domain. Nature *428*, 198-202.
42. Kueh, H.Y., and Mitchison, T.J. (2009). Structural plasticity in actin and tubulin polymer dynamics. Science *325*, 960-963.
43. Howard, J., and Hyman, A.A. (2009). Growth, fluctuation and switching at microtubule plus ends. Nat Rev Mol Cell Biol *10*, 569-574.
44. Kerssemakers, J.W., Munteanu, E.L., Laan, L., Noetzel, T.L., Janson, M.E., and Dogterom, M. (2006). Assembly dynamics of microtubules at molecular resolution. Nature *442*, 709-712.
45. Mozziconacci, J., Sandblad, L., Wachsmuth, M., Brunner, D., and Karsenti, E. (2008). Tubulin dimers oligomerize before their incorporation into microtubules. PLoS One *3*, e3821.
46. Schek, H.T., 3rd, Gardner, M.K., Cheng, J., Odde, D.J., and Hunt, A.J. (2007). Microtubule assembly dynamics at the nanoscale. Curr Biol *17*, 1445-1455.
47. Gardner, M.K., Charlebois, B.D., Janosi, I.M., Howard, J., Hunt, A.J., and Odde, D.J. (2011). Rapid microtubule self-assembly kinetics. Cell *146*, 582-592.
48. Muller-Reichert, T., Chretien, D., Severin, F., and Hyman, A.A. (1998). Structural changes at microtubule ends accompanying GTP hydrolysis: information from a slowly hydrolyzable analogue of GTP, guanylyl (alpha,beta)methylenediphosphonate. Proc Natl Acad Sci U S A *95*, 3661-3666.
49. Wang, H.W., and Nogales, E. (2005). Nucleotide-dependent bending flexibility of tubulin regulates microtubule assembly. Nature *435*, 911-915.

50. Buey, R.M., Diaz, J.F., and Andreu, J.M. (2006). The nucleotide switch of tubulin and microtubule assembly: a polymerization-driven structural change. Biochemistry *45*, 5933-5938.
51. Barbier, P., Dorleans, A., Devred, F., Sanz, L., Allegro, D., Alfonso, C., Knossow, M., Peyrot, V., and Andreu, J.M. (2010). Stathmin and interfacial microtubule inhibitors recognize a naturally curved conformation of tubulin dimers. J Biol Chem *285*, 31672-31681.
52. Nawrotek, A., Knossow, M., and Gigant, B. (2011). The determinants that govern microtubule assembly from the atomic structure of GTP-tubulin. J Mol Biol *412*, 35-42.
53. Rice, L.M., Montabana, E.A., and Agard, D.A. (2008). The lattice as allosteric effector: structural studies of alphabeta- and gamma-tubulin clarify the role of GTP in microtubule assembly. Proc Natl Acad Sci U S A *105*, 5378-5383.
54. Hyman, A.A., Salser, S., Drechsel, D.N., Unwin, N., and Mitchison, T.J. (1992). Role of GTP hydrolysis in microtubule dynamics: information from a slowly hydrolyzable analogue, GMPCPP. Mol Biol Cell *3*, 1155-1167.
55. Valiron, O., Arnal, I., Caudron, N., and Job, D. (2010). GDP-tubulin incorporation into growing microtubules modulates polymer stability. J Biol Chem *285*, 17507-17513.
56. Gardner, M.K., Zanic, M., Gell, C., Bormuth, V., and Howard, J. (2011). Depolymerizing kinesins Kip3 and MCAK shape cellular microtubule architecture by differential control of catastrophe. Cell *147*, 1092-1103.
57. Dimitrov, A., Quesnoit, M., Moutel, S., Cantaloube, I., Pous, C., and Perez, F. (2008). Detection of GTP-tubulin conformation in vivo reveals a role for GTP remnants in microtubule rescues. Science *322*, 1353-1356.
58. Cassimeris, L. (2009). Microtubule assembly: lattice GTP to the rescue. Curr Biol *19*, R174-176.
59. Tropini, C., Roth, E.A., Zanic, M., Gardner, M.K., and Howard, J. (2012). Islands containing slowly hydrolyzable GTP analogs promote microtubule rescues. PLoS One *7*, e30103.
60. Al-Bassam, J., and Chang, F. (2011). Regulation of microtubule dynamics by TOG-domain proteins XMAP215/Dis1 and CLASP. Trends Cell Biol *21*, 604-614.
61. Rodionov, V.I., and Borisy, G.G. (1997). Microtubule treadmilling in vivo. Science *275*, 215-218.
62. Waterman-Storer, C.M., and Salmon, E.D. (1997). Actomyosin-based retrograde flow of microtubules in the lamella of migrating epithelial cells influences microtubule dynamic instability and turnover and is associated with microtubule breakage and treadmilling. J Cell Biol *139*, 417-434.
63. Kwok, B.H., and Kapoor, T.M. (2007). Microtubule flux: drivers wanted. Curr Opin Cell Biol *19*, 36-42.
64. Rath, U., and Sharp, D.J. (2011). The molecular basis of anaphase A in animal cells. Chromosome Res *19*, 423-432.
65. Dutcher, S.K. (2003). Long-lost relatives reappear: identification of new members of the tubulin superfamily. Curr Opin Microbiol *6*, 634-640.
66. Luduena, R.F., and Banerjee, A. (2008). The tubulin superfamily. In The role of microtubules in cell biology, neurobiology and oncology., T. Fojo, ed. (Totowa, NJ: Humana Press), pp. 177-191.
67. Chang, P., and Stearns, T. (2000). Delta-tubulin and epsilon-tubulin: two new human centrosomal tubulins reveal new aspects of centrosome structure and function. Nat Cell Biol *2*, 30-35.
68. Chang, P., Giddings, T.H., Jr., Winey, M., and Stearns, T. (2003). Epsilon-tubulin is required for centriole duplication and microtubule organization. Nat Cell Biol *5*, 71-76.
69. Verdier-Pinard, P., Pasquier, E., Xiao, H., Burd, B., Villard, C., Lafitte, D., Miller, L.M., Angeletti, R.H., Horwitz, S.B., and Braguer, D. (2009). Tubulin proteomics: towards breaking the code. Anal Biochem *384*, 197-206.
70. Nogales, E., Wolf, S.G., and Downing, K.H. (1998). Structure of the alpha beta tubulin dimer by electron crystallography. Nature *391*, 199-203.
71. Downing, K.H., and Nogales, E. (1998). Tubulin and microtubule structure. Curr Opin Cell Biol *10*, 16-22.
72. Luduena, R.F., and Banerjee, A. (2008). The isotypes of tubulin: Distribution and functional significance. In The role of microtubules in cell biology, neurobiology and oncology, T. Fojo, ed. (Totowa, NJ: Humana Press), pp. 123-177.
73. Banerjee, A., and Luduena, R.F. (1992). Kinetics of colchicine binding to purified beta-tubulin isotypes from bovine brain. J Biol Chem *267*, 13335-13339.

74. Lu, Q., and Luduena, R.F. (1994). In vitro analysis of microtubule assembly of isotypically pure tubulin dimers. Intrinsic differences in the assembly properties of alpha beta II, alpha beta III, and alpha beta IV tubulin dimers in the absence of microtubule-associated proteins. J Biol Chem *269*, 2041-2047.

75. Panda, D., Miller, H.P., Banerjee, A., Luduena, R.F., and Wilson, L. (1994). Microtubule dynamics in vitro are regulated by the tubulin isotype composition. Proc Natl Acad Sci U S A *91*, 11358-11362.

76. May, G.S. (1989). The highly divergent beta-tubulins of Aspergillus nidulans are functionally interchangeable. J Cell Biol *109*, 2267-2274.

77. Takahashi, M., Shiraishi, H., Ishibashi, Y., Blade, K.L., McDermott, P.J., Menick, D.R., Kuppuswamy, D., and Cooper, G.t. (2003). Phenotypic consequences of beta1-tubulin expression and MAP4 decoration of microtubules in adult cardiocytes. Am J Physiol Heart Circ Physiol *285*, H2072-2083.

78. Hoyle, H.D., and Raff, E.C. (1990). Two Drosophila beta tubulin isoforms are not functionally equivalent. J Cell Biol *111*, 1009-1026.

79. Savage, C., Hamelin, M., Culotti, J.G., Coulson, A., Albertson, D.G., and Chalfie, M. (1989). mec-7 is a beta-tubulin gene required for the production of 15-protofilament microtubules in Caenorhabditis elegans. Genes Dev *3*, 870-881.

80. Schwer, H.D., Lecine, P., Tiwari, S., Italiano, J.E., Jr., Hartwig, J.H., and Shivdasani, R.A. (2001). A lineage-restricted and divergent beta-tubulin isoform is essential for the biogenesis, structure and function of blood platelets. Curr Biol *11*, 579-586.

81. Bhattacharya, R., Yang, H., and Cabral, F. (2011). Class V beta-tubulin alters dynamic instability and stimulates microtubule detachment from centrosomes. Mol Biol Cell *22*, 1025-1034.

82. Luduena, R.F. (1998). Multiple forms of tubulin: different gene products and covalent modifications. Int Rev Cytol *178*, 207-275.

83. Walss-Bass, C., Xu, K., David, S., Fellous, A., and Luduena, R.F. (2002). Occurrence of nuclear beta(II)-tubulin in cultured cells. Cell Tissue Res *308*, 215-223.

84. Yeh, I.T., and Luduena, R.F. (2004). The betaII isotype of tubulin is present in the cell nuclei of a variety of cancers. Cell Motil Cytoskeleton *57*, 96-106.

85. Katsetos, C.D., Draberova, E., Smejkalova, B., Reddy, G., Bertrand, L., de Chadarevian, J.P., Legido, A., Nissanov, J., Baas, P.W., and Draber, P. (2007). Class III beta-tubulin and gamma-tubulin are co-expressed and form complexes in human glioblastoma cells. Neurochem Res *32*, 1387-1398.

86. Jensen-Smith, H.C., Luduena, R.F., and Hallworth, R. (2003). Requirement for the betaI and betaIV tubulin isotypes in mammalian cilia. Cell Motil Cytoskeleton *55*, 213-220.

87. Tischfield, M.A., Cederquist, G.Y., Gupta, M.L., Jr., and Engle, E.C. (2011). Phenotypic spectrum of the tubulin-related disorders and functional implications of disease-causing mutations. Curr Opin Genet Dev *21*, 286-294.

88. Kavallaris, M. Microtubules and resistance to tubulin-binding agents. Nat Rev Cancer *10*, 194-204.

89. Verhey, K.J., and Gaertig, J. (2007). The tubulin code. Cell Cycle *6*, 2152-2160.

90. Wloga, D., and Gaertig, J. (2010). Post-translational modifications of microtubules. J Cell Sci *123*, 3447-3455.

91. Peris, L., Wagenbach, M., Lafanechere, L., Brocard, J., Moore, A.T., Kozielski, F., Job, D., Wordeman, L., and Andrieux, A. (2009). Motor-dependent microtubule disassembly driven by tubulin tyrosination. J Cell Biol *185*, 1159-1166.

92. Peris, L., Thery, M., Faure, J., Saoudi, Y., Lafanechere, L., Chilton, J.K., Gordon-Weeks, P., Galjart, N., Bornens, M., Wordeman, L., et al. (2006). Tubulin tyrosination is a major factor affecting the recruitment of CAP-Gly proteins at microtubule plus ends. J Cell Biol *174*, 839-849.

93. Weisbrich, A., Honnappa, S., Jaussi, R., Okhrimenko, O., Frey, D., Jelesarov, I., Akhmanova, A., and Steinmetz, M.O. (2007). Structure-function relationship of CAP-Gly domains. Nat Struct Mol Biol *14*, 959-967.

94. Bieling, P., Kandels-Lewis, S., Telley, I.A., van Dijk, J., Janke, C., and Surrey, T. (2008). CLIP-170 tracks growing microtubule ends by dynamically recognizing composite EB1/tubulin-binding sites. J Cell Biol *183*, 1223-1233.

95. Dunn, S., Morrison, E.E., Liverpool, T.B., Molina-Paris, C., Cross, R.A., Alonso, M.C., and Peckham, M. (2008). Differential trafficking of Kif5c on tyrosinated and detyrosinated microtubules in live cells. J Cell Sci *121*, 1085-1095.

96. Konishi, Y., and Setou, M. (2009). Tubulin tyrosination navigates the kinesin-1 motor domain to axons. Nat Neurosci *12*, 559-567.

97. Janke, C., and Kneussel, M. (2010). Tubulin post-translational modifications: encoding functions on the neuronal microtubule cytoskeleton. Trends Neurosci *33*, 362-372.

98. Sharma, N., Bryant, J., Wloga, D., Donaldson, R., Davis, R.C., Jerka-Dziadosz, M., and Gaertig, J. (2007). Katanin regulates dynamics of microtubules and biogenesis of motile cilia. J Cell Biol *178*, 1065-1079.

99. Lacroix, B., van Dijk, J., Gold, N.D., Guizetti, J., Aldrian-Herrada, G., Rogowski, K., Gerlich, D.W., and Janke, C. (2010). Tubulin polyglutamylation stimulates spastin-mediated microtubule severing. J Cell Biol *189*, 945-954.

100. Qiang, L., Yu, W., Andreadis, A., Luo, M., and Baas, P.W. (2006). Tau protects microtubules in the axon from severing by katanin. J Neurosci *26*, 3120-3129.

101. Xiao, H., El Bissati, K., Verdier-Pinard, P., Burd, B., Zhang, H., Kim, K., Fiser, A., Angeletti, R.H., and Weiss, L.M. (2010). Post-translational modifications to Toxoplasma gondii alpha- and beta-tubulins include novel C-terminal methylation. J Proteome Res *9*, 359-372.

102. Cappelletti, G., Maggioni, M.G., Tedeschi, G., and Maci, R. (2003). Protein tyrosine nitration is triggered by nerve growth factor during neuronal differentiation of PC12 cells. Exp Cell Res *288*, 9-20.

103. Amos, L.A., and Schlieper, D. (2005). Microtubules and maps. Adv Protein Chem *71*, 257-298.

104. Dehmelt, L., and Halpain, S. (2005). The MAP2/Tau family of microtubule-associated proteins. Genome Biol *6*, 204.

105. Halpain, S., and Dehmelt, L. (2006). The MAP1 family of microtubule-associated proteins. Genome Biol *7*, 224.

106. Reiner, O., Coquelle, F.M., Peter, B., Levy, T., Kaplan, A., Sapir, T., Orr, I., Barkai, N., Eichele, G., and Bergmann, S. (2006). The evolving doublecortin (DCX) superfamily. BMC Genomics *7*, 188.

107. Faire, K., Waterman-Storer, C.M., Gruber, D., Masson, D., Salmon, E.D., and Bulinski, J.C. (1999). E-MAP-115 (ensconsin) associates dynamically with microtubules in vivo and is not a physiological modulator of microtubule dynamics. J Cell Sci *112*, 4243-4255.

108. Bosc, C., Andrieux, A., and Job, D. (2003). STOP proteins. Biochemistry *42*, 12125-12132.

109. Amos, L.A. (2008). The tektin family of microtubule-stabilizing proteins. Genome Biol *9*, 229.

110. Howard, J., and Hyman, A.A. (2007). Microtubule polymerases and depolymerases. Curr Opin Cell Biol *19*, 31-35.

111. Ems-McClung, S.C., and Walczak, C.E. (2010). Kinesin-13s in mitosis: Key players in the spatial and temporal organization of spindle microtubules. Semin Cell Dev Biol *21*, 276-282.

112. Steinmetz, M.O. (2007). Structure and thermodynamics of the tubulin-stathmin interaction. J Struct Biol *158*, 137-147.

113. Cassimeris, L. (2002). The oncoprotein 18/stathmin family of microtubule destabilizers. Curr Opin Cell Biol *14*, 18-24.

114. Roll-Mecak, A., and McNally, F.J. (2010). Microtubule-severing enzymes. Curr Opin Cell Biol *22*, 96-103.

115. Yu, W., Qiang, L., Solowska, J.M., Karabay, A., Korulu, S., and Baas, P.W. (2008). The microtubule-severing proteins spastin and katanin participate differently in the formation of axonal branches. Mol Biol Cell *19*, 1485-1498.

116. Zhang, D., Grode, K.D., Stewman, S.F., Diaz-Valencia, J.D., Liebling, E., Rath, U., Riera, T., Currie, J.D., Buster, D.W., Asenjo, A.B., et al. (2011). Drosophila katanin is a microtubule depolymerase that regulates cortical-microtubule plus-end interactions and cell migration. Nat Cell Biol *13*, 361-370.

117. McNally, K., Audhya, A., Oegema, K., and McNally, F.J. (2006). Katanin controls mitotic and meiotic spindle length. J Cell Biol *175*, 881-891.

118. Hazan, J., Fonknechten, N., Mavel, D., Paternotte, C., Samson, D., Artiguenave, F., Davoine, C.S., Cruaud, C., Durr, A., Wincker, P., et al. (1999). Spastin, a new AAA protein, is altered in the most frequent form of autosomal dominant spastic paraplegia. Nat Genet *23*, 296-303.

119. Lumb, J.H., Connell, J.W., Allison, R., and Reid, E. (2012). The AAA ATPase spastin links microtubule severing to membrane modelling. Biochim Biophys Acta *1823*, 192-197.

120. Connell, J.W., Lindon, C., Luzio, J.P., and Reid, E. (2009). Spastin couples microtubule severing to membrane traffic in completion of cytokinesis and secretion. Traffic *10*, 42-56.

121. Schiel, J.A., Park, K., Morphew, M.K., Reid, E., Hoenger, A., and Prekeris, R. (2011). Endocytic membrane fusion and buckling-induced microtubule severing mediate cell abscission. J Cell Sci *124*, 1411-1424.

122. Daftary, G.S., Tetrault, A.M., Jorgensen, E.M., Sarno, J., and Taylor, H.S. (2011). A novel role for the AAA ATPase spastin as a HOXA10 transcriptional corepressor in Ishikawa endometrial cells. Mol Endocrinol *25*, 1539-1549.

123. Sanderson, C.M., Connell, J.W., Edwards, T.L., Bright, N.A., Duley, S., Thompson, A., Luzio, J.P., and Reid, E. (2006). Spastin and atlastin, two proteins mutated in autosomal-dominant hereditary spastic paraplegia, are binding partners. Hum Mol Genet *15*, 307-318.

124. Montenegro, G., Rebelo, A.P., Connell, J., Allison, R., Babalini, C., D'Aloia, M., Montieri, P., Schule, R., Ishiura, H., Price, J., et al. (2012). Mutations in the ER-shaping protein reticulon 2 cause the axon-degenerative disorder hereditary spastic paraplegia type 12. J Clin Invest *122*, 538-544.

125. Solowska, J.M., Garbern, J.Y., and Baas, P.W. (2010). Evaluation of loss of function as an explanation for SPG4-based hereditary spastic paraplegia. Hum Mol Genet *19*, 2767-2779.

126. Galjart, N. (2010). Plus-end-tracking proteins and their interactions at microtubule ends. Curr Biol *20*, R528-537.

127. Zanic, M., Stear, J.H., Hyman, A.A., and Howard, J. (2009). EB1 recognizes the nucleotide state of tubulin in the microtubule lattice. PLoS One *4*, e7585.

128. Maurer, S.P., Bieling, P., Cope, J., Hoenger, A., and Surrey, T. (2011). GTPgammaS microtubules mimic the growing microtubule end structure recognized by end-binding proteins (EBs). Proc Natl Acad Sci U S A *108*, 3988-3993.

129. Buey, R.M., Mohan, R., Leslie, K., Walzthoeni, T., Missimer, J.H., Menzel, A., Bjelic, S., Bargsten, K., Grigoriev, I., Smal, I., et al. (2011). Insights into EB1 structure and the role of its C-terminal domain for discriminating microtubule tips from the lattice. Mol Biol Cell *22*, 2912-2923.

130. Akhmanova, A., and Steinmetz, M.O. (2008). Tracking the ends: a dynamic protein network controls the fate of microtubule tips. Nat Rev Mol Cell Biol *9*, 309-322.

131. Brouhard, G.J., Stear, J.H., Noetzel, T.L., Al-Bassam, J., Kinoshita, K., Harrison, S.C., Howard, J., and Hyman, A.A. (2008). XMAP215 is a processive microtubule polymerase. Cell *132*, 79-88.

132. Widlund, P.O., Stear, J.H., Pozniakovsky, A., Zanic, M., Reber, S., Brouhard, G.J., Hyman, A.A., and Howard, J. (2010). XMAP215 polymerase activity is built by combining multiple tubulin-binding TOG domains and a basic lattice-binding region. Proc Natl Acad Sci U S A *108*, 2741-2746.

133. Jiang, K., and Akhmanova, A. (2010). Microtubule tip-interacting proteins: a view from both ends. Curr Opin Cell Biol *23*, 94-101.

134. Meng, W., Mushika, Y., Ichii, T., and Takeichi, M. (2008). Anchorage of microtubule minus ends to adherens junctions regulates epithelial cell-cell contacts. Cell *135*, 948-959.

135. Goodwin, S.S., and Vale, R.D. (2010). Patronin regulates the microtubule network by protecting microtubule minus ends. Cell *143*, 263-274.

136. Oakley, B.R., Oakley, C.E., Yoon, Y., and Jung, M.K. (1990). Gamma-tubulin is a component of the spindle pole body that is essential for microtubule function in Aspergillus nidulans. Cell *61*, 1289-1301.

137. Stearns, T., Evans, L., and Kirschner, M. (1991). Gamma-tubulin is a highly conserved component of the centrosome. Cell *65*, 825-836.

138. Joshi, H.C., Palacios, M.J., McNamara, L., and Cleveland, D.W. (1992). Gamma-tubulin is a centrosomal protein required for cell cycle-dependent microtubule nucleation. Nature *356*, 80-83.

139. Oakley, C.E., and Oakley, B.R. (1989). Identification of gamma-tubulin, a new member of the tubulin superfamily encoded by mipA gene of Aspergillus nidulans. Nature *338*, 662-664.

140. Horio, T., and Oakley, B.R. (1994). Human gamma-tubulin functions in fission yeast. J Cell Biol *126*, 1465-1473.

141. Sobel, S.G., and Snyder, M. (1995). A highly divergent gamma-tubulin gene is essential for cell growth and proper microtubule organization in Saccharomyces cerevisiae. J Cell Biol *131*, 1775-1788.

142. Spang, A., Geissler, S., Grein, K., and Schiebel, E. (1996). gamma-Tubulin-like Tub4p of Saccharomyces cerevisiae is associated with the spindle pole body substructures that organize microtubules and is required for mitotic spindle formation. J Cell Biol *134*, 429-441.

143. Hannak, E., Oegema, K., Kirkham, M., Gonczy, P., Habermann, B., and Hyman, A.A. (2002). The kinetically dominant assembly pathway for centrosomal asters in Caenorhabditis elegans is gamma-tubulin dependent. J Cell Biol *157*, 591-602.

144. Strome, S., Powers, J., Dunn, M., Reese, K., Malone, C.J., White, J., Seydoux, G., and Saxton, W. (2001). Spindle dynamics and the role of gamma-tubulin in early Caenorhabditis elegans embryos. Mol Biol Cell *12*, 1751-1764.

145. Liu, B., Joshi, H.C., Wilson, T.J., Silflow, C.D., Palevitz, B.A., and Snustad, D.P. (1994). gamma-Tubulin in Arabidopsis: gene sequence, immunoblot, and immunofluorescence studies. Plant Cell *6*, 303-314.

146. Lopez, I., Khan, S., Sevik, M., Cande, W.Z., and Hussey, P.J. (1995). Isolation of a full-length cDNA encoding Zea mays gamma-tubulin. Plant Physiol *107*, 309-310.

147. Ruiz, F., Beisson, J., Rossier, J., and Dupuis-Williams, P. (1999). Basal body duplication in Paramecium requires gamma-tubulin. Curr Biol *9*, 43-46.

148. Tan, M., and Heckmann, K. (1998). The two gamma-tubulin-encoding genes of the ciliate Euplotes crassus differ in their sequences, codon usage, transcription initiation sites and poly(A) addition sites. Gene *210*, 53-60.

149. Marziale, F., Pucciarelli, S., Ballarini, P., Melki, R., Uzun, A., Ilyin, V.A., Detrich, H.W., and Miceli, C. (2008). Different roles of two gamma-tubulin isotypes in the cytoskeleton of the Antarctic ciliate Euplotes focardii - Remodelling of interaction surfaces may enhance microtubule nucleation at low temperature. Febs Journal *275*, 5367-5382.

150. Wilson, P.G., Zheng, Y., Oakley, C.E., Oakley, B.R., Borisy, G.G., and Fuller, M.T. (1997). Differential expression of two gamma-tubulin isoforms during gametogenesis and development in Drosophila. Dev Biol *184*, 207-221.

151. Yuba-Kubo, A., Kubo, A., Hata, M., and Tsukita, S. (2005). Gene knockout analysis of two gamma-tubulin isoforms in mice. Dev Biol *282*, 361-373.

152. Wise, D.O., Krahe, R., and Oakley, B.R. (2000). The gamma-tubulin gene family in humans. Genomics *67*, 164-170.

153. Carson, A.R., and Scherer, S.W. (2009). Identifying concerted evolution and gene conversion in mammalian gene pairs lasting over 100 million years. BMC Evol Biol *9*, 156.

154. Aldaz, H., Rice, L.M., Stearns, T., and Agard, D.A. (2005). Insights into microtubule nucleation from the crystal structure of human gamma-tubulin. Nature *435*, 523-527.

155. Moudjou, M., Bordes, N., Paintrand, M., and Bornens, M. (1996). gamma-Tubulin in mammalian cells: the centrosomal and the cytosolic forms. J Cell Sci *109 (Pt 4)*, 875-887.

156. Zheng, Y., Wong, M.L., Alberts, B., and Mitchison, T. (1995). Nucleation of microtubule assembly by a gamma-tubulin-containing ring complex. Nature *378*, 578-583.

157. Moritz, M., Braunfeld, M.B., Sedat, J.W., Alberts, B., and Agard, D.A. (1995). Microtubule nucleation by gamma-tubulin-containing rings in the centrosome. Nature *378*, 638-640.

158. Fuller, S.D., Gowen, B.E., Reinsch, S., Sawyer, A., Buendia, B., Wepf, R., and Karsenti, E. (1995). The core of the mammalian centriole contains gamma-tubulin. Curr Biol *5*, 1384-1393.

159. Guichard, P., Chretien, D., Marco, S., and Tassin, A.M. (2010). Procentriole assembly revealed by cryo-electron tomography. EMBO J *29*, 1565-1572.

160. Efimov, A., Kharitonov, A., Efimova, N., Loncarek, J., Miller, P.M., Andreyeva, N., Gleeson, P., Galjart, N., Maia, A.R., McLeod, I.X., et al. (2007). Asymmetric CLASP-dependent nucleation of noncentrosomal microtubules at the trans-Golgi network. Dev Cell *12*, 917-930.

161. Goshima, G., Mayer, M., Zhang, N., Stuurman, N., and Vale, R.D. (2008). Augmin: a protein complex required for centrosome-independent microtubule generation within the spindle. J Cell Biol *181*, 421-429.

162. Uehara, R., Nozawa, R.S., Tomioka, A., Petry, S., Vale, R.D., Obuse, C., and Goshima, G. (2009). The augmin complex plays a critical role in spindle microtubule generation for mitotic progression and cytokinesis in human cells. Proc Natl Acad Sci U S A *106*, 6998-7003.

163. Uehara, R., and Goshima, G. (2010). Functional central spindle assembly requires de novo microtubule generation in the interchromosomal region during anaphase. J Cell Biol *191*, 259-267.

164. Hughes, S.E., Beeler, J.S., Seat, A., Slaughter, B.D., Unruh, J.R., Bauerly, E., Matthies, H.J., and Hawley, R.S. (2011). Gamma-tubulin is required for bipolar spindle assembly and for proper kinetochore microtubule attachments during prometaphase I in Drosophila oocytes. PLoS Genet *7*, e1002209.

165. Carazo-Salas, R.E., Guarguaglini, G., Gruss, O.J., Segref, A., Karsenti, E., and Mattaj, I.W. (1999). Generation of GTP-bound Ran by RCC1 is required for chromatin-induced mitotic spindle formation. Nature *400*, 178-181.

166. Maiato, H., and Sunkel, C.E. (2004). Kinetochore-microtubule interactions during cell division. Chromosome Res *12*, 585-597.

167. Mishra, R.K., Chakraborty, P., Arnaoutov, A., Fontoura, B.M., and Dasso, M. (2010). The Nup107-160 complex and gamma-TuRC regulate microtubule polymerization at kinetochores. Nat Cell Biol *12*, 164-169.

168. Bouissou, A., Verollet, C., Sousa, A., Sampaio, P., Wright, M., Sunkel, C.E., Merdes, A., and Raynaud-Messina, B. (2009). gamma-Tubulin ring complexes regulate microtubule plus end dynamics. J Cell Biol *187*, 327-334.

169. Hubert, T., Vandekerckhove, J., and Gettemans, J. (2011). Cdk1 and BRCA1 target gamma-tubulin to microtubule domains. Biochem Biophys Res Commun *414*, 240-245.

170. Binarova, P., Cenklova, V., Hause, B., Kubatova, E., Lysak, M., Dolezel, J., Bogre, L., and Draber, P. (2000). Nuclear gamma-tubulin during acentriolar plant mitosis. Plant Cell *12*, 433-442.

171. Hoog, G., Zarrizi, R., von Stedingk, K., Jonsson, K., and Alvarado-Kristensson, M. (2011). Nuclear localization of gamma-tubulin affects E2F transcriptional activity and S-phase progression. FASEB J.

172. Horejsi, B., Vinopal, S., Sladkova, V., Draberova, E., Sulimenko, V., Sulimenko, T., Vosecka, V., Philimonenko, A., Hozak, P., Katsetos, C.D., et al. (2012). Nuclear gamma-tubulin associates with nucleoli and interacts with tumor suppressor protein C53. J Cell Physiol *227*, 367-382.

173. Knop, M., Pereira, G., Geissler, S., Grein, K., and Schiebel, E. (1997). The spindle pole body component Spc97p interacts with the gamma-tubulin of Saccharomyces cerevisiae and functions in microtubule organization and spindle pole body duplication. EMBO J *16*, 1550-1564.

174. Geissler, S., Pereira, G., Spang, A., Knop, M., Soues, S., Kilmartin, J., and Schiebel, E. (1996). The spindle pole body component Spc98p interacts with the gamma-tubulin-like Tub4p of Saccharomyces cerevisiae at the sites of microtubule attachment. EMBO J *15*, 3899-3911.

175. Murphy, S.M., Urbani, L., and Stearns, T. (1998). The mammalian gamma-tubulin complex contains homologues of the yeast spindle pole body components spc97p and spc98p. J Cell Biol *141*, 663-674.

176. Fava, F., Raynaud-Messina, B., Leung-Tack, J., Mazzolini, L., Li, M., Guillemot, J.C., Cachot, D., Tollon, Y., Ferrara, P., and Wright, M. (1999). Human 76p: A new member of the gamma-tubulin-associated protein family. J Cell Biol *147*, 857-868.

177. Murphy, S.M., Preble, A.M., Patel, U.K., O'Connell, K.L., Dias, D.P., Moritz, M., Agard, D., Stults, J.T., and Stearns, T. (2001). GCP5 and GCP6: two new members of the human gamma-tubulin complex. Mol Biol Cell *12*, 3340-3352.

178. Moritz, M., Braunfeld, M.B., Guenebaut, V., Heuser, J., and Agard, D.A. (2000). Structure of the gamma-tubulin ring complex: a template for microtubule nucleation. Nat Cell Biol *2*, 365-370.

179. Moritz, M., Zheng, Y., Alberts, B.M., and Oegema, K. (1998). Recruitment of the gamma-tubulin ring complex to Drosophila salt-stripped centrosome scaffolds. J Cell Biol *142*, 775-786.

180. Choi, Y.K., Liu, P., Sze, S.K., Dai, C., and Qi, R.Z. (2010). CDK5RAP2 stimulates microtubule nucleation by the gamma-tubulin ring complex. J Cell Biol *191*, 1089-1095.

181. Oegema, K., Wiese, C., Martin, O.C., Milligan, R.A., Iwamatsu, A., Mitchison, T.J., and Zheng, Y. (1999). Characterization of two related Drosophila gamma-tubulin complexes that differ in their ability to nucleate microtubules. J Cell Biol *144*, 721-733.

182. Verollet, C., Colombie, N., Daubon, T., Bourbon, H.M., Wright, M., and Raynaud-Messina, B. (2006). Drosophila melanogaster gamma-TuRC is dispensable for targeting gamma-tubulin to the centrosome and microtubule nucleation. J Cell Biol *172*, 517-528.

183. Xiong, Y., and Oakley, B.R. (2009). In vivo analysis of the functions of gamma-tubulin-complex proteins. J Cell Sci *122*, 4218-4227.

184. Kollman, J.M., Polka, J.K., Zelter, A., Davis, T.N., and Agard, D.A. (2010). Microtubule nucleating gamma-TuSC assembles structures with 13-fold microtubule-like symmetry. Nature *466*, 879-882.

185. Kollman, J.M., Zelter, A., Muller, E.G., Fox, B., Rice, L.M., Davis, T.N., and Agard, D.A. (2008). The structure of the gamma-tubulin small complex: implications of its architecture and flexibility for microtubule nucleation. Mol Biol Cell *19*, 207-215.

186. Guillet, V., Knibiehler, M., Gregory-Pauron, L., Remy, M.H., Chemin, C., Raynaud-Messina, B., Bon, C., Kollman, J.M., Agard, D.A., Merdes, A., et al. (2011). Crystal structure of gamma-tubulin complex protein GCP4 provides insight into microtubule nucleation. Nat Struct Mol Biol *18*, 915-919.

187. Gunawardane, R.N., Martin, O.C., and Zheng, Y. (2003). Characterization of a new gammaTuRC subunit with WD repeats. Mol Biol Cell *14*, 1017-1026.

188. Luders, J., Patel, U.K., and Stearns, T. (2006). GCP-WD is a gamma-tubulin targeting factor required for centrosomal and chromatin-mediated microtubule nucleation. Nat Cell Biol *8*, 137-147.

189. Haren, L., Remy, M.H., Bazin, I., Callebaut, I., Wright, M., and Merdes, A. (2006). NEDD1-dependent recruitment of the gamma-tubulin ring complex to the centrosome is necessary for centriole duplication and spindle assembly. J Cell Biol *172*, 505-515.

190. Hutchins, J.R., Toyoda, Y., Hegemann, B., Poser, I., Heriche, J.K., Sykora, M.M., Augsburg, M., Hudecz, O., Buschhorn, B.A., Bulkescher, J., et al. (2010). Systematic analysis of human protein complexes identifies chromosome segregation proteins. Science *328*, 593-599.

191. Teixido-Travesa, N., Villen, J., Lacasa, C., Bertran, M.T., Archinti, M., Gygi, S.P., Caelles, C., Roig, J., and Luders, J. (2010). The gammaTuRC revisited: a comparative analysis of interphase and mitotic human gammaTuRC redefines the set of core components and identifies the novel subunit GCP8. Mol Biol Cell *21*, 3963-3972.

192. Zimmerman, W.C., Sillibourne, J., Rosa, J., and Doxsey, S.J. (2004). Mitosis-specific anchoring of gamma tubulin complexes by pericentrin controls spindle organization and mitotic entry. Mol Biol Cell *15*, 3642-3657.

193. Delgehyr, N., Sillibourne, J., and Bornens, M. (2005). Microtubule nucleation and anchoring at the centrosome are independent processes linked by ninein function. J Cell Sci *118*, 1565-1575.

194. Casenghi, M., Meraldi, P., Weinhart, U., Duncan, P.I., Korner, R., and Nigg, E.A. (2003). Polo-like kinase 1 regulates Nlp, a centrosome protein involved in microtubule nucleation. Dev Cell *5*, 113-125.

195. Fong, K.W., Choi, Y.K., Rattner, J.B., and Qi, R.Z. (2008). CDK5RAP2 is a pericentriolar protein that functions in centrosomal attachment of the gamma-tubulin ring complex. Mol Biol Cell *19*, 115-125.

196. Gomez-Ferreria, M.A., Rath, U., Buster, D.W., Chanda, S.K., Caldwell, J.S., Rines, D.R., and Sharp, D.J. (2007). Human Cep192 is required for mitotic centrosome and spindle assembly. Curr Biol *17*, 1960-1966.

197. Takahashi, M., Yamagiwa, A., Nishimura, T., Mukai, H., and Ono, Y. (2002). Centrosomal proteins CG-NAP and kendrin provide microtubule nucleation sites by anchoring gamma-tubulin ring complex. Mol Biol Cell *13*, 3235-3245.

198. Cunningham, L.A., and Kahn, R.A. (2008). Cofactor D functions as a centrosomal protein and is required for the recruitment of the gamma-tubulin ring complex at centrosomes and organization of the mitotic spindle. J Biol Chem *283*, 7155-7165.

199. Shi, X., Sun, X., Liu, M., Li, D., Aneja, R., and Zhou, J. CEP70 protein interacts with gamma-tubulin to localize at the centrosome and is critical for mitotic spindle assembly. J Biol Chem *286*, 33401-33408.

200. Lawo, S., Bashkurov, M., Mullin, M., Ferreria, M.G., Kittler, R., Habermann, B., Tagliaferro, A., Poser, I., Hutchins, J.R., Hegemann, B., et al. (2009). HAUS, the 8-subunit human Augmin complex, regulates centrosome and spindle integrity. Curr Biol *19*, 816-826.

201. Petry, S., Pugieux, C., Nedelec, F.J., and Vale, R.D. (2011). Augmin promotes meiotic spindle formation and bipolarity in Xenopus egg extracts. Proc Natl Acad Sci U S A *108*, 14473-14478.

202. Johmura, Y., Soung, N.K., Park, J.E., Yu, L.R., Zhou, M., Bang, J.K., Kim, B.Y., Veenstra, T.D., Erikson, R.L., and Lee, K.S. (2011). Regulation of microtubule-based microtubule nucleation by mammalian polo-like kinase 1. Proc Natl Acad Sci U S A *108*, 11446-11451.

203. Rios, R.M., Sanchis, A., Tassin, A.M., Fedriani, C., and Bornens, M. (2004). GMAP-210 recruits gamma-tubulin complexes to cis-Golgi membranes and is required for Golgi ribbon formation. Cell *118*, 323-335.

204. Hoppeler-Lebel, A., Celati, C., Bellett, G., Mogensen, M.M., Klein-Hitpass, L., Bornens, M., and Tassin, A.M. (2007). Centrosomal CAP350 protein stabilises microtubules associated with the Golgi complex. J Cell Sci *120*, 3299-3308.

205. Rivero, S., Cardenas, J., Bornens, M., and Rios, R.M. (2009). Microtubule nucleation at the cis-side of the Golgi apparatus requires AKAP450 and GM130. EMBO J *28*, 1016-1028.

206. O'Toole, E.T., McDonald, K.L., Mantler, J., McIntosh, J.R., Hyman, A.A., and Muller-Reichert, T. (2003). Morphologically distinct microtubule ends in the mitotic centrosome of Caenorhabditis elegans. J Cell Biol *163*, 451-456.

207. Hoog, J.L., Schwartz, C., Noon, A.T., O'Toole, E.T., Mastronarde, D.N., McIntosh, J.R., and Antony, C. (2007). Organization of interphase microtubules in fission yeast analyzed by electron tomography. Dev Cell *12*, 349-361.

208. Anders, A., and Sawin, K.E. (2011). Microtubule stabilization in vivo by nucleation-incompetent gamma-tubulin complex. J Cell Sci *124*, 1207-1213.

209. Kleylein-Sohn, J., Westendorf, J., Le Clech, M., Habedanck, R., Stierhof, Y.D., and Nigg, E.A. (2007). Plk4-induced centriole biogenesis in human cells. Dev Cell *13*, 190-202.

210. Dammermann, A., Maddox, P.S., Desai, A., and Oegema, K. (2008). SAS-4 is recruited to a dynamic structure in newly forming centrioles that is stabilized by the gamma-tubulin-mediated addition of centriolar microtubules. J Cell Biol *180*, 771-785.

211. Alvarado-Kristensson, M., Rodriguez, M.J., Silio, V., Valpuesta, J.M., and Carrera, A.C. (2009). SADB phosphorylation of gamma-tubulin regulates centrosome duplication. Nat Cell Biol *11*, 1081-1092.

212. Zimmerman, S., and Chang, F. (2005). Effects of gamma-tubulin complex proteins on microtubule nucleation and catastrophe in fission yeast. Mol Biol Cell *16*, 2719-2733.

213. Cuschieri, L., Miller, R., and Vogel, J. (2006). Gamma-tubulin is required for proper recruitment and assembly of Kar9-Bim1 complexes in budding yeast. Mol Biol Cell *17*, 4420-4434.

214. Rodriguez, A.S., Batac, J., Killilea, A.N., Filopei, J., Simeonov, D.R., Lin, I., and Paluh, J.L. (2008). Protein complexes at the microtubule organizing center regulate bipolar spindle assembly. Cell Cycle *7*, 1246-1253.

215. Nayak, T., Edgerton-Morgan, H., Horio, T., Xiong, Y., De Souza, C.P., Osmani, S.A., and Oakley, B.R. (2010). Gamma-tubulin regulates the anaphase-promoting complex/cyclosome during interphase. J Cell Biol *190*, 317-330.

216. Muller, H., Fogeron, M.L., Lehmann, V., Lehrach, H., and Lange, B.M. (2006). A centrosome-independent role for gamma-TuRC proteins in the spindle assembly checkpoint. Science *314*, 654-657.

217. Weaver, B.A., and Cleveland, D.W. (2007). Comment on "A centrosome-independent role for gamma-TuRC proteins in the spindle assembly checkpoint". Science *316*, 982; author reply 982.

218. Taylor, S.S., Hardwick, K.G., Sawin, K.E., Biggins, S., Piatti, S., Khodjakov, A., Rieder, C.L., Salmon, E.D., and Musacchio, A. (2007). Comment on "A centrosome-independent role for gamma-TuRC proteins in the spindle assembly checkpoint". Science *316*, 982; author reply 982.

219. Lesca, C., Germanier, M., Raynaud-Messina, B., Pichereaux, C., Etievant, C., Emond, S., Burlet-Schiltz, O., Monsarrat, B., Wright, M., and Defais, M. (2005). DNA damage induce gamma-tubulin-RAD51 nuclear complexes in mammalian cells. Oncogene *24*, 5165-5172.

220. Zhang, S., Hemmerich, P., and Grosse, F. (2007). Centrosomal localization of DNA damage checkpoint proteins. J Cell Biochem *101*, 451-465.

221. Hendrickson, T.W., Yao, J., Bhadury, S., Corbett, A.H., and Joshi, H.C. (2001). Conditional mutations in gamma-tubulin reveal its involvement in chromosome segregation and cytokinesis. Mol Biol Cell *12*, 2469-2481.

222. Tange, Y., Fujita, A., Toda, T., and Niwa, O. (2004). Functional dissection of the gamma-tubulin complex by suppressor analysis of gtb1 and alp4 mutations in Schizosaccharomyces pombe. Genetics *167*, 1095-1107.

223. Jung, M.K., Prigozhina, N., Oakley, C.E., Nogales, E., and Oakley, B.R. (2001). Alanine-scanning mutagenesis of Aspergillus gamma-tubulin yields diverse and novel phenotypes. Mol Biol Cell *12*, 2119-2136.

224. Starita, L.M., Machida, Y., Sankaran, S., Elias, J.E., Griffin, K., Schlegel, B.P., Gygi, S.P., and Parvin, J.D. (2004). BRCA1-dependent ubiquitination of gamma-tubulin regulates centrosome number. Mol Cell Biol *24*, 8457-8466.

225. Sankaran, S., Starita, L.M., Groen, A.C., Ko, M.J., and Parvin, J.D. (2005). Centrosomal microtubule nucleation activity is inhibited by BRCA1-dependent ubiquitination. Mol Cell Biol *25*, 8656-8668.

226. Stumpff, J., Kellogg, D.R., Krohne, K.A., and Su, T.T. (2005). Drosophila Wee1 interacts with members of the gammaTURC and is required for proper mitotic-spindle morphogenesis and positioning. Curr Biol *15*, 1525-1534.

227. Macurek, L., Draberova, E., Richterova, V., Sulimenko, V., Sulimenko, T., Draberova, L., Markova, V., and Draber, P. (2008). Regulation of microtubule nucleation from membranes by complexes of membrane-bound gamma-tubulin with Fyn kinase and phosphoinositide 3-kinase. Biochem J.

228. Draberova, L., Draberova, E., Surviladze, Z., and Draber, P. (1999). Protein tyrosine kinase p53/p56(lyn) forms complexes with gamma-tubulin in rat basophilic leukemia cells. Int Immunol *11*, 1829-1839.

229. Zyss, D., Montcourrier, P., Vidal, B., Anguille, C., Merezegue, F., Sahuquet, A., Mangeat, P.H., and Coopman, P.J. (2005). The Syk tyrosine kinase localizes to the centrosomes and negatively affects mitotic progression. Cancer Res *65*, 10872-10880.

230. Sulimenko, V., Draberova, E., Sulimenko, T., Macurek, L., Richterova, V., and Draber, P. (2006). Regulation of microtubule formation in activated mast cells by complexes of gamma-tubulin with Fyn and Syk kinases. J Immunol *176*, 7243-7253.

231. Vogel, J., Drapkin, B., Oomen, J., Beach, D., Bloom, K., and Snyder, M. (2001). Phosphorylation of gamma-tubulin regulates microtubule organization in budding yeast. Dev Cell *1*, 621-631.

232. Lin, T.C., Gombos, L., Neuner, A., Sebastian, D., Olsen, J.V., Hrle, A., Benda, C., and Schiebel, E. (2011). Phosphorylation of the yeast gamma-tubulin Tub4 regulates microtubule function. PLoS One *6*, e19700.

233. Kukharskyy, V., Sulimenko, V., Macurek, L., Sulimenko, T., Draberova, E., and Draber, P. (2004). Complexes of gamma-tubulin with nonreceptor protein tyrosine kinases Src and Fyn in differentiating P19 embryonal carcinoma cells. Exp Cell Res *298*, 218-228.

234. Zhang, X., Chen, Q., Feng, J., Hou, J., Yang, F., Liu, J., Jiang, Q., and Zhang, C. (2009). Sequential phosphorylation of Nedd1 by Cdk1 and Plk1 is required for targeting of the gammaTuRC to the centrosome. J Cell Sci *122*, 2240-2251.

235. Haren, L., Stearns, T., and Luders, J. (2009). Plk1-dependent recruitment of gamma-tubulin complexes to mitotic centrosomes involves multiple PCM components. PLoS One *4*, e5976.

236. Santamaria, A., Wang, B., Elowe, S., Malik, R., Zhang, F., Bauer, M., Schmidt, A., Sillje, H.H., Korner, R., and Nigg, E.A. (2011). The Plk1-dependent phosphoproteome of the early mitotic spindle. Mol Cell Proteomics *10*, M110 004457.

237. Chan, C.C., Shui, H.A., Wu, C.H., Wang, C.Y., Sun, G.H., Chen, H.M., and Wu, G.J. (2009). Motility and protein phosphorylation in healthy and asthenozoospermic sperm. J Proteome Res *8*, 5382-5386.

238. Izumi, N., Fumoto, K., Izumi, S., and Kikuchi, A. (2008). GSK-3beta regulates proper mitotic spindle formation in cooperation with a component of the gamma-tubulin ring complex, GCP5. J Biol Chem *283*, 12981-12991.

239. Bahtz, R., Seidler, J., Arnold, M., Haselmann-Weiss, U., Antony, C., Lehmann, W.D., and Hoffmann, I. (2012). GCP6 is a substrate of Plk4 and required for centriole duplication. J Cell Sci *in press*.

240. Colello, D., Reverte, C.G., Ward, R., Jones, C.W., Magidson, V., Khodjakov, A., and LaFlamme, S.E. (2010). Androgen and Src signaling regulate centrosome activity. J Cell Sci *123*, 2094-2102.

241. Colello, D., Mathew, S., Ward, R., Pumiglia, K., and Laflamme, S.E. (2012). Integrins Regulate Microtubule Nucleating Activity of Centrosome through Mitogen-activated Protein Kinase/Extracellular Signal-regulated Kinase Kinase/Extracellular Signal-regulated Kinase (MEK/ERK) Signaling. J Biol Chem *287*, 2520-2530.

242. Melki, R., Vainberg, I.E., Chow, R.L., and Cowan, N.J. (1993). Chaperonin-mediated folding of vertebrate actin-related protein and gamma-tubulin. J Cell Biol *122*, 1301-1310.

243. Geissler, S., Siegers, K., and Schiebel, E. (1998). A novel protein complex promoting formation of functional alpha- and gamma-tubulin. EMBO J *17*, 952-966.

244. Vainberg, I.E., Lewis, S.A., Rommelaere, H., Ampe, C., Vandekerckhove, J., Klein, H.L., and Cowan, N.J. (1998). Prefoldin, a chaperone that delivers unfolded proteins to cytosolic chaperonin. Cell *93*, 863-873.

245. Schroer, A., Schneider, S., Ropers, H., and Nothwang, H. (1999). Cloning and characterization of UXT, a novel gene in human Xp11, which is widely and abundantly expressed in tumor tissue. Genomics *56*, 340-343.

246. Zhao, H., Wang, Q., Zhang, H., Liu, Q., Du, X., Richter, M., and Greene, M.I. (2005). UXT is a novel centrosomal protein essential for cell viability. Mol Biol Cell *16*, 5857-5865.

247. De Wulf, P., McAinsh, A.D., and Sorger, P.K. (2003). Hierarchical assembly of the budding yeast kinetochore from multiple subcomplexes. Genes Dev *17*, 2902-2921.

248. Fant, X., Gnadt, N., Haren, L., and Merdes, A. (2009). Stability of the small gamma-tubulin complex requires HCA66, a protein of the centrosome and the nucleolus. J Cell Sci *122*, 1134-1144.

249. Katsetos, C.D., Reddy, G., Draberova, E., Smejkalova, B., Del Valle, L., Ashraf, Q., Tadevosyan, A., Yelin, K., Maraziotis, T., Mishra, O.P., et al. (2006). Altered cellular distribution and subcellular sorting of gamma-tubulin in diffuse astrocytic gliomas and human glioblastoma cell lines. J Neuropathol Exp Neurol *65*, 465-477.

250. Caracciolo, V., D'Agostino, L., Draberova, E., Sladkova, V., Crozier-Fitzgerald, C., Agamanolis, D.P., de Chadarevian, J.P., Legido, A., Giordano, A., Draber, P., et al. (2010). Differential expression and cellular distribution of gamma-tubulin and betaIII-tubulin in medulloblastomas and human medulloblastoma cell lines. J Cell Physiol *223*, 519-529.

251. Orsetti, B., Nugoli, M., Cervera, N., Lasorsa, L., Chuchana, P., Ursule, L., Nguyen, C., Redon, R., du Manoir, S., Rodriguez, C., et al. (2004). Genomic and expression profiling of chromosome 17 in breast cancer reveals complex patterns of alterations and novel candidate genes. Cancer Res *64*, 6453-6460.

252. Niu, Y., Liu, T., Tse, G.M., Sun, B., Niu, R., Li, H.M., Wang, H., Yang, Y., Ye, X., Wang, Y., et al. (2009). Increased expression of centrosomal alpha, gamma-tubulin in atypical ductal hyperplasia and carcinoma of the breast. Cancer Sci *100*, 580-587.

253. Li, Y., Hussain, M., Sarkar, S.H., Eliason, J., Li, R., and Sarkar, F.H. (2005). Gene expression profiling revealed novel mechanism of action of Taxotere and Furtulon in prostate cancer cells. BMC Cancer *5*, 7.

254. Montero-Conde, C., Martin-Campos, J.M., Lerma, E., Gimenez, G., Martinez-Guitarte, J.L., Combalia, N., Montaner, D., Matias-Guiu, X., Dopazo, J., de Leiva, A., et al. (2008). Molecular profiling related to poor prognosis in thyroid carcinoma. Combining gene expression data and biological information. Oncogene *27*, 1554-1561.

255. Potter, N., Karakoula, A., Phipps, K.P., Harkness, W., Hayward, R., Thompson, D.N., Jacques, T.S., Harding, B., Thomas, D.G., Palmer, R.W., et al. (2008). Genomic deletions correlate with underexpression of novel candidate genes at six loci in pediatric pilocytic astrocytoma. Neoplasia *10*, 757-772.

256. Friesen, D.E., Barakat, K.H., Semenchenko, V., Perez-Pineiro, R., Fenske, B.W., Mane, J., Wishart, D.S., and Tuszynski, J.A. (2012). Discovery of small molecule inhibitors that interact with gamma-tubulin. Chem Biol Drug Des *in press*.

257. Galli, S.J., Kalesnikoff, J., Grimbaldeston, M.A., Piliponsky, A.M., Williams, C.M., and Tsai, M. (2005). Mast cells as "tunable" effector and immunoregulatory cells: recent advances. Annu Rev Immunol *23*, 749-786.

258. Kalesnikoff, J., and Galli, S.J. (2008). New developments in mast cell biology. Nat Immunol *9*, 1215-1223.

259. Moon, T.C., St Laurent, C.D., Morris, K.E., Marcet, C., Yoshimura, T., Sekar, Y., and Befus, A.D. (2010). Advances in mast cell biology: new understanding of heterogeneity and function. Mucosal Immunol *3*, 111-128.

260. Galli, S.J., and Tsai, M. (2010). Mast cells in allergy and infection: versatile effector and regulatory cells in innate and adaptive immunity. Eur J Immunol *40*, 1843-1851.

261. Galli, S.J., Grimbaldeston, M., and Tsai, M. (2008). Immunomodulatory mast cells: negative, as well as positive, regulators of immunity. Nat Rev Immunol *8*, 478-486.

262. Liu, J., Zhang, Y., Zhao, J., Yang, Z., Li, D., Katirai, F., and Huang, B. (2011). Mast cell: insight into remodeling a tumor microenvironment. Cancer Metastasis Rev *30*, 177-184.

263. Wang, Y., Deng, X., and Gill, D.L. (2010). Calcium signaling by STIM and Orai: intimate coupling details revealed. Sci Signal *3*, pe42.

264. Grigoriev, I., Gouveia, S.M., van der Vaart, B., Demmers, J., Smyth, J.T., Honnappa, S., Splinter, D., Steinmetz, M.O., Putney, J.W., Jr., Hoogenraad, C.C., et al. (2008). STIM1 is a MT-plus-end-tracking protein involved in remodeling of the ER. Curr Biol *18*, 177-182.

265. Sampieri, A., Zepeda, A., Asanov, A., and Vaca, L. (2009). Visualizing the store-operated channel complex assembly in real time: identification of SERCA2 as a new member. Cell Calcium *45*, 439-446.

266. Smith, A.J., Pfeiffer, J.R., Zhang, J., Martinez, A.M., Griffiths, G.M., and Wilson, B.S. (2003). Microtubule-dependent transport of secretory vesicles in RBL-2H3 cells. Traffic *4*, 302-312.

267. Nishida, K., Yamasaki, S., Ito, Y., Kabu, K., Hattori, K., Tezuka, T., Nishizumi, H., Kitamura, D., Goitsuka, R., Geha, R.S., et al. (2005). FcεRI-mediated mast cell degranulation requires calcium-independent microtubule-dependent translocation of granules to the plasma membrane. J Cell Biol *170*, 115-126.

268. Ohgaki, H., and Kleihues, P. (2005). Population-based studies on incidence, survival rates, and genetic alterations in astrocytic and oligodendroglial gliomas. J Neuropathol Exp Neurol *64*, 479-489.

269. Hadjipanayis, C.G., and Van Meir, E.G. (2009). Tumor initiating cells in malignant gliomas: biology and implications for therapy. J Mol Med (Berl) *87*, 363-374.

270. Giese, A., Bjerkvig, R., Berens, M.E., and Westphal, M. (2003). Cost of migration: invasion of malignant gliomas and implications for treatment. J Clin Oncol *21*, 1624-1636.

271. Galli, R., Binda, E., Orfanelli, U., Cipelletti, B., Gritti, A., De Vitis, S., Fiocco, R., Foroni, C., Dimeco, F., and Vescovi, A. (2004). Isolation and characterization of tumorigenic, stem-like neural precursors from human glioblastoma. Cancer Res *64*, 7011-7021.

272. Molina, J.R., Hayashi, Y., Stephens, C., and Georgescu, M.M. (2010). Invasive glioblastoma cells acquire stemness and increased Akt activation. Neoplasia *12*, 453-463.

273. Chua, C., Zaiden, N., Chong, K.H., See, S.J., Wong, M.C., Ang, B.T., and Tang, C. (2008). Characterization of a side population of astrocytoma cells in response to temozolomide. J Neurosurg *109*, 856-866.

274. Zhong, J., Paul, A., Kellie, S.J., and O'Neill, G.M. (2010). Mesenchymal migration as a therapeutic target in glioblastoma. J Oncol *2010*, 430142.

275. Lino, M.M., and Merlo, A. (2011). PI3Kinase signaling in glioblastoma. J Neurooncol *103*, 417-427.

276. Panopoulos, A., Howell, M., Fotedar, R., and Margolis, R.L. (2011). Glioblastoma motility occurs in the absence of actin polymer. Mol Biol Cell *22*, 2212-2220.

277. Martin-Verdeaux, S., Pombo, I., Iannascoli, B., Roa, M., Varin-Blank, N., Rivera, J., and Blank, U. (2003). Evidence of a role for Munc18-2 and microtubules in mast cell granule exocytosis. J Cell Sci *116*, 325-334.

278. Oka, T., Hori, M., and Ozaki, H. (2005). Microtubule disruption suppresses allergic response through the inhibition of calcium influx in the mast cell degranulation pathway. J Immunol *174*, 4584-4589.

279. Derler, I., Schindl, R., Fritsch, R., and Romanin, C. (2012). Gating and permeation of Orai channels. Front Biosci *17*, 1304-1322.

280. Baba, Y., Nishida, K., Fujii, Y., Hirano, T., Hikida, M., and Kurosaki, T. (2008). Essential function for the calcium sensor STIM1 in mast cell activation and anaphylactic responses. Nat Immunol *9*, 81-88.

281. Vig, M., DeHaven, W.I., Bird, G.S., Billingsley, J.M., Wang, H., Rao, P.E., Hutchings, A.B., Jouvin, M.H., Putney, J.W., and Kinet, J.P. (2008). Defective mast cell effector functions in mice lacking the CRACM1 pore subunit of store-operated calcium release-activated calcium channels. Nat Immunol *9*, 89-96.

282. Katsetos, C.D., Del Valle, L., Geddes, J.F., Assimakopoulou, M., Legido, A., Boyd, J.C., Balin, B., Parikh, N.A., Maraziotis, T., de Chadarevian, J.P., et al. (2001). Aberrant localization of the neuronal class III beta-tubulin in astrocytomas. Arch Pathol Lab Med *125*, 613-624.

283. Stiles, C.D., and Rowitch, D.H. (2008). Glioma stem cells: a midterm exam. Neuron *58*, 832-846.

284. Wang, J., An, H., Mayo, M.W., Baldwin, A.S., and Yarbrough, W.G. (2007). LZAP, a putative tumor suppressor, selectively inhibits NF-kappaB. Cancer Cell *12*, 239-251.

285. Wang, J., He, X., Luo, Y., and Yarbrough, W.G. (2006). A novel ARF-binding protein (LZAP) alters ARF regulation of HDM2. Biochem J *393*, 489-501.

286. Shiwaku, H., Yoshimura, N., Tamura, T., Sone, M., Ogishima, S., Watase, K., Tagawa, K., and Okazawa, H. (2010). Suppression of the novel ER protein Maxer by mutant ataxin-1 in Bergman glia contributes to non-cell-autonomous toxicity. EMBO J *29*, 2446-2460.

287. Jiang, H., Wu, J., He, C., Yang, W., and Li, H. (2009). Tumor suppressor protein C53 antagonizes checkpoint kinases to promote cyclin-dependent kinase 1 activation. Cell Res *19*, 458-468.

288. Khodjakov, A., and Rieder, C.L. (1999). The sudden recruitment of gamma-tubulin to the centrosome at the onset of mitosis and its dynamic exchange throughout the cell cycle, do not require microtubules. J Cell Biol *146*, 585-596.

289. Kafri, R., Levy, M., and Pilpel, Y. (2006). The regulatory utilization of genetic redundancy through responsive backup circuits. Proc Natl Acad Sci U S A *103*, 11653-11658.

290. DeLuna, A., Springer, M., Kirschner, M.W., and Kishony, R. (2010). Need-based up-regulation of protein levels in response to deletion of their duplicate genes. PLoS Biol *8*, e1000347.

291. He, X., and Zhang, J. (2006). Transcriptional reprogramming and backup between duplicate genes: is it a genomewide phenomenon? Genetics *172*, 1363-1367.

292. Lynch, M., and Force, A. (2000). The probability of duplicate gene preservation by subfunctionalization. Genetics *154*, 459-473.

293. Qian, W., Liao, B.Y., Chang, A.Y., and Zhang, J. (2010). Maintenance of duplicate genes and their functional redundancy by reduced expression. Trends Genet *26*, 425-430.

VI. PRESENTED PUBLICATIONS

VI.1

Hájková, Z., Bugajev, V., Dráberová, E., **Vinopal, S.**, Dráberová, L., Janáček, J., Dráber, Pe., Dráber, Pa. (2011). STIM1-directed reorganization of microtubules in activated mast cells. J Immunol. *186*, 913-923.

STIM1-Directed Reorganization of Microtubules in Activated Mast Cells

Zuzana Hájková,*[,1] Viktor Bugajev,[†,1] Eduarda Dráberová,* Stanislav Vinopal,* Lubica Dráberová,[†] Jiří Janáček,[‡] Petr Dráber,[†] and Pavel Dráber*

Activation of mast cells by aggregation of the high-affinity IgE receptors (FcεRI) initiates signaling events leading to the release of inflammatory and allergic mediators stored in cytoplasmic granules. A key role in this process play changes in concentrations of intracellular Ca^{2+} controlled by store-operated Ca^{2+} entry (SOCE). Although microtubules are also involved in the process leading to degranulation, the molecular mechanisms that control microtubule rearrangement during activation are largely unknown. In this study, we report that activation of bone marrow-derived mast cells (BMMCs) induced by FcεRI aggregation or treatment with pervanadate or thapsigargin results in generation of protrusions containing microtubules (microtubule protrusions). Formation of these protrusions depended on the influx of extracellular Ca^{2+}. Changes in cytosolic Ca^{2+}concentration also affected microtubule plus-end dynamics detected by microtubule plus-end tracking protein EB1. Experiments with knockdown or reexpression of STIM1, the key regulator of SOCE, confirmed the important role of STIM1 in the formation of microtubule protrusions. Although STIM1 in activated cells formed puncta associated with microtubules in protrusions, relocation of STIM1 to a close proximity of cell membrane was independent of growing microtubules. In accordance with the inhibition of Ag-induced Ca^{2+} response and decreased formation of microtubule protrusions in BMMCs with reduced STIM1, the cells also exhibited impaired chemotactic response to Ag. We propose that rearrangement of microtubules in activated mast cells depends on STIM1-induced SOCE, and that Ca^{2+} plays an important role in the formation of microtubule protrusions in BMMCs. ***The Journal of Immunology*****, 2011, 186: 913–923.**

Mast cells play a pivotal role in innate immunity, allergy, and inflammation; they express plasma membrane-associated FcεRIs, the aggregation of which by multivalent Ag–IgE complexes triggers mast cell activation resulting in the degranulation and release of inflammatory mediators such as histamine, proteases, lipid mediators, and cytokines. The first defined step in FcεRI signaling is tyrosine phosphorylation of the FcεRI β and γ subunits by Src family kinase Lyn. This step is followed by enhanced activity of Syk kinase and phosphorylation of transmembrane adaptor linker for activation of T cells. Phosphorylated linker for activation of T cells is an anchor site for phospholipase Cγ. After membrane anchoring and activation, phospholipase Cγ produces inositol 1,4,5,-triphosphate that binds to its receptors in the endoplasmic reticulum (ER). This results in Ca^{2+} efflux from the ER (1). Subsequently, depletion of Ca^{2+} from ER lumen induces Ca^{2+} influx across the plasma membrane through store-operated Ca^{2+} channels (SOCs). The influx leads to enhancement of free cytoplasmic Ca^{2+} concentration, a step that is substantial in further signaling events. The store-operated Ca^{2+} entry (SOCE) is also important for the replenishment of intracellular stores by means of sarcoendoplasmatic reticulum Ca^{2+}-ATPase (SERCA) pumps located in the ER membrane (2, 3).

The stromal interacting molecule 1 (STIM1) is a pivotal component of the SOCE pathway (4, 5). It represents the Ca^{2+} sensor responsible for communicating the depleted state of intracellular Ca^{2+} compartments to SOCs. In quiescent cells with ER filled with Ca^{2+}, STIM1 is distributed homogenously throughout the ER (6), but relocates upon release of Ca^{2+} from ER stores to distinct puncta on the ER in close proximity to the plasma membrane (5). Aggregated STIM1 activates members of the Orai family of SOCs, resulting in the opening of the plasma membrane Ca^{2+} channels and Ca^{2+} influx into the cell (7); in this way STIM1 serves as a major regulator of SOCE.

STIM1 is a microtubule-tracking protein (8, 9) and interacts with the end-binding protein 1 (EB1) that associates with the tips of growing microtubules (10, 11). Although microtubules are necessary for positioning of membrane-enclosed organelles in-

*Department of Biology of Cytoskeleton, Institute of Molecular Genetics, Academy of Sciences of the Czech Republic, 142 20 Prague, Czech Republic; [†]Department of Signal Transduction, Institute of Molecular Genetics, Academy of Sciences of the Czech Republic, 142 20 Prague, Czech Republic; and [‡]Department of Biomathematics, Institute of Physiology, Academy of Sciences of the Czech Republic, 142 20 Prague, Czech Republic

[1]Z.H. and V.B. contributed equally to this work

Received for publication June 25, 2010. Accepted for publication November 13, 2010.

This work was supported in part by Grants 204/09/H084, 204/09/1777, 301/09/1826, and P302/10/1759 from the Grant Agency of the Czech Republic, Grants LC545, LC06063, and 1M6837805001 from the Ministry of Education, Youth and Sports of the Czech Republic, Grants KAN200520701 and M200520901 from the Grant Agency of the Czech Academy of Sciences, Grant 11109 from the Grant Agency of Charles University, and by the Institutional Research Supports (AVOZ 50520514 and 50110509). S.V. was supported in part by the Department of Cell Biology, Faculty of Science, Charles University, Prague, Czech Republic.

Address correspondence and reprint requests to Dr. Pavel Dráber or Dr. Petr Dráber, Department of Biology of Cytoskeleton, Institute of Molecular Genetics, AS CR v.v.i., Vídeňská 1083, 142 20 Prague, Czech Republic (Pavel Dráber), or Department of Signal Transduction, Institute of Molecular Genetics, AS CR v.v.i., Vídeňská 1083, 142 20 Prague, Czech Republic (Petr Dráber). E-mail addresses: paveldra@img.cas.cz (Pavel Dráber) and draberpe@img.cas.cz (Petr Dráber)

The online version of this article contains supplemental material.

Abbreviations used in this article: BMMC, bone marrow-derived mast cell; BMMCL, BMMC line; BSS, buffered saline solution; $[Ca^{2+}]_i$, concentration of free intracellular calcium; EB1, end-binding protein 1; ER, endoplasmic reticulum; KD, knockdown; SCF, stem cell factor; SERCA, sarcoendoplasmatic reticulum Ca^{2+}-ATPase; shRNA, short hairpin RNA; SOC, store-operated Ca^{2+} channels; SOCE, store-operated Ca^{2+} entry; STIM1, stromal interacting molecule 1; Tg, thapsigargin; TIRF, total internal reflection fluorescence; TIRFM, total internal reflection fluorescence microscopy; YFP, yellow fluorescent protein.

cluding ER (12), the role of microtubules in regulating SOCE is not fully understood. Whereas inhibition of microtubule dynamics by taxol, a microtubule stabilizer, or by knockdown (KD) of EB1 had no significant effect on SOCE (11), Ca^{2+} influx in different cell types was inhibited by microtubule depolymerizing drug nocodazole (13, 14). It has been suggested that microtubules play a facilitative role in SOCE signaling pathway by optimizing the localization of STIM1 (15).

Microtubules are involved in mast cell degranulation, because the movement of secretory granules depends on intact microtubules (16, 17). This finding is supported by demonstrations that agents inhibiting tubulin polymerization also suppress degranulation (18–20). Importantly, FcεRI aggregation triggers reorganization of microtubules and their concentration in cell periphery (17, 21). It has also been reported that translocation of granules along microtubules to plasma membranes occurred independently of Ca^{2+}, whereas the release of mediators and granule-plasma membrane fusion were dependent on Ca^{2+} (17). Although these data confirm that a microtubule network is required for mast cell degranulation, our understanding of the mechanisms responsible for microtubule formation in bone marrow-derived mast cells (BMMCs) during activation events is still limited.

In this study, we investigated the interplay between Ca^{2+} signaling and changes in microtubule distribution in the course of BMMC activation. Our results indicate that microtubules in activated cells are in protrusions that depend on STIM1 activity and Ca^{2+} influx. Whereas microtubules are not necessary for the relocation of STIM1 to puncta in close proximity to the plasma membrane in activated cells, changes in the concentration of cytoplasmic Ca^2 affect microtubule plus-end dynamics and result in dramatic modifications in cell physiology documented by chemotactic response. The results support the concept of a tight crosstalk between microtubular network and Ca^{2+} signaling machinery in the course of mast cell activation.

Materials and Methods

Reagents

Fibronectin, nocodazole, thapsigargin, probenecid, DNP-albumin, and DNP-lysine were acquired from Sigma-Aldrich (St. Louis, MO). Src-family selective tyrosine kinase inhibitor PP2 and the negative control, PP3, were obtained from Calbiochem (Darmstadt, Germany). Fluo 3-AM, Fura Red-AM, 4-methylumbelliferyl β-D-glucuronide, and Lipofectamine 2000 were purchased from Invitrogen (Carlsbad, CA), and puromycin was acquired from InvivoGen (San Diego, CA). IL-3 and stem cell factor (SCF) were from PeproTech (Rocky Hill, NJ). Restriction enzymes were bought from New England Biolabs (Ipswich, MA). SuperSignal WestPico Chemiluminescent reagents were bought from Pierce (Rockford, IL).

Abs

Mouse mAb PY-20 (IgG_{2b}) labeled with HRP and anti-STIM1(GOK) mAb (IgG_{2a}) were acquired from BD Biosciences (San Jose, CA). Rabbit Ab to α-tubulin was acquired from GeneTex (Irvine, CA). Rabbit Ab to actin, mAb TUB 2.1 (IgG_1) to β-tubulin labeled with indocarbocyanate (Cy3) and mAb SPE-7 (IgE) specific for DNP were acquired from Sigma-Aldrich. Anti-mouse and anti-rabbit Abs conjugated with HRP were purchased from Promega Biotec (Madison, WI), Alexa Fluor 488-conjugated anti-rabbit IgG Ab was acquired from Invitrogen (Carlsbad, CA), and FITC-conjugated anti-mouse IgG cross-reacting with mouse IgE were acquired from Jackson ImmunoResearch Laboratories (West Grove, PA).

To prepare mouse mAb specific for STIM1, 29-aa oligopeptide DNGSIGEETDSSPGRKKFPLKIFKKPLKK corresponding to the mouse STIM1 sequence 657-685 from the C-terminal end of the molecule (22) was synthesized by Clonestar Peptide Service (Brno, Czech Republic). A cysteine had been added to the N terminus of the peptide to allow oriented covalent coupling to the carrier proteins, maleimide-activated keyhole limpet hemocyanin, or BSA (Imject Activated Immunogen Conjugation Kit, Pierce, Rockford, IL), according to the manufacturer's directions. BALB/c mice were immunized with the peptide-keyhole limpet hemocyanin conjugate, and sera were monitored for Ab activity by ELISA on peptide-BSA conjugate as described (23). Fusion of splenocytes with mouse myeloma cells Sp2/0, screening by ELISA, cloning and production of ascitic fluids in BALB/c mice have been described previously (24). The subclasses of mAbs were identified by ISO1 isotyping kit (Sigma-Aldrich). The selected hybridoma cell line ST-01 produced Ab of the IgG_1 class.

Cell cultures and transfection

Bone marrow cells were isolated from the femurs and tibias of 6–8-wk-old BALB/c mice. All mice were maintained and used in accordance with the Institute of Molecular Genetics guidelines. The cells were differentiated in suspension cultures in freshly prepared culture medium (IMDM supplemented with antibiotics [100 U/ml penicillin, 100 μg/ml streptomycin] 10% FCS, 35 μM 2-ME, IL-3 [36 ng/ml] and SCF [36 ng/ml]). Cells were grown at 37˚C in 10% CO_2 in air and passaged every 2–3 d. After 6–8 wk, ~99% of cells were identified as mast cells, expressing FcεRI and c-Kit as detected by flow cytometry. BMMCs isolated from at least three mice were used for each experiment.

Mouse BMMC line (BMMCL) was by M. Hibbs (Ludwig Institute for Cancer Research, Melbourne, Australia). In this study, the cells are denoted as BMMCL and were cultured in freshly prepared culture medium (RPMI 1640 supplemented with 20 mM HEPES, pH 7.5, 100 U/ml penicillin, 100 μg/ml streptomycin, 100 μM MEM nonessential amino acids, 1 mM sodium pyruvate, 10% FCS, and 10% WEHI-3 cell supernatant as a source of IL-3). Cells were grown at 37˚C in 5% CO_2 in air and passaged every 2 d.

HEK 293FT packaging cells (Invitrogen) were grown at 37˚C in 5% CO_2 in DMEM supplemented with 10% FCS and antibiotics. The cells used for lentivirus production were at passage 4–15.

BMMCL cells were transfected with DNA constructs by nucleofection using Mouse Macrophage Kit and program Y-001 on Amaxa Nucleofector II (Lonza Cologne AG, Cologne, Germany) according to the manufacturer's instructions. After nucleofection, cells were transferred into culture media supplemented with IL-3 and cultured for 24–48 h before analysis.

DNA constructs

Full-length human STIM1 cloned into pDS_XB-YFP vector (pYFP-hSTIM1) was provided by Dr. T. Meyer (5). The signal-peptide region (22), sequence 1–23 aa, of STIM1 was recloned from this vector into pmCherry_N1 from Clontech Laboratories (Mountain View, CA) upstream of mCherry, using *Eco*RI and AgeI restriction sites. The remaining part of STIM1 was recloned downstream of mCherry into the BsrGI site. The construct was verified by DNA sequencing. Expression plasmid coding mouse EB1 fused with GFP (pEB1-GFP) was obtained from Dr. Y. Mimori-Kiyosue (25). Expression plasmid coding human EB3 fused with mRFP1 (26) was obtained from Dr. A. Akhmanova (11).

Lentivirus short hairpin RNAs and virus transduction

A set of five murine STIM1 (GenBank accession number: NM_ 009287) short hairpin RNA (shRNA) constructs cloned into the pLKO.1 vector (TRCN0000175139, TRCN0000175008, TRCN0000193877, TRCN0000193400, and TRCN0000173765) were purchased from Open Biosystems (Huntsville, AL). Aliquots of 1.4 ml Opti-MEM medium (Invitrogen) were mixed with 21 μl ViraPower Lentiviral Packaging Mix (Invitrogen), 14 μg STIM1 shRNA constructs, and 82 μl Lipofectamine 2000. The mixture was incubated for 20 min at room temperature before it was added to semiconfluent HEK-293FT packaging cells in a 150-cm^2 tissue-culture flask. After 3 d, viruses in culture supernatants were concentrated by centrifugation at 25,000 rpm for 2 h using a JA-25.50 rotor (Beckman Coulter, Palo Alto, CA). The pellets were resuspended in 1 ml of culture medium and added to 29 ml of medium, supplemented with 5 μg/ml puromycin containing 5×10^7 BMMCs or BMMCL cells. Stable selection was achieved by culturing cells for 1 wk in the presence of puromycin. Cells were pooled and analyzed for STIM1 expression by immunoblotting. Cells with the highest reduction of STIM1 protein, obtained with TRCN0000175008 (KD1) and TRCN0000193400 (KD2), were selected for additional experiments. Cells transfected with empty pLKO.1 vector were used as negative controls.

Cell activation

Cells at a concentration of 6×10^6 cells/ml were sensitized for 2 h at 37˚C in IL-3– and SCF-free culture medium supplemented with DNP-specific IgE mAb (SPE-7; 1 μg/ml). The cells were then washed in buffered saline solution (BSS; 20 mM HEPES, pH 7.4, 135 mM NaCl, 5 mM KCl, 1.8 mM $CaCl_2$, 5.6 mM glucose, 2 mM $MgCl_2$), supplemented with 0.1% BSA (BSS-BSA), and challenged with various concentrations of Ag (DNP-albumin; 30–40 mol of DNP per mole of albumin) or thapsigargin.

For immunofluorescence experiments, cells at a concentration of 6×10^6 cells/ml were sensitized in suspension for 1 h at 37˚C with DNP-specific

IgE (1 μg/ml) and diluted to a concentration of 1.5×10^6 cells/ml. The suspension (1 ml) was then overlaid on fibronectin-coated coverslips (immersed for 1 h at 37°C in 50 μg/ml fibronectin in 50 mM $NaHCO_3$ and rinsed in PBS) placed in a 3.5-cm tissue culture dish. Cells were allowed to attach for 1 h at 37°C, washed in BSS-BSA, and challenged for 3–5 min with Ag (DNP-albumin) at a final concentration of 100 ng/ml. To determine the time course of activation, cells were challenged with Ag for 1–10 min. For dose response curve construction, the concentration of Ag ranged from 10 to 1000 ng/ml.

Alternatively, cells were activated by pervanadate or thapsigargin, in which case the sensitization step was omitted. Pervanadate solution was prepared fresh by mixing sodium orthovanadate solution with hydrogen peroxide to get a final concentration (10 mM) of both components. The pervanadate solution was incubated for 15 min at room temperature and then diluted 1:100 in BSS-BSA. Attached cells were incubated with pervanadate solution for 15 min at 37°C. Cells were also incubated for 20 min with BSS-BSA containing 2 μM thapsigargin. To determine the time course of activation, cells were activated with thapsigargin for 5–20 min. Dose response measurements were done at thapsigargin concentrations ranging from 0.01 to 2 μM. In some experiments, $[Ca^{2+}]$-free BSS was used. Trypan blue exclusion test was used to evaluate the effect of pervanadate and thapsigargin on viability of cells.

To depolymerize microtubules, cells were treated for 1 h at 37°C with 10 μM nocodazole and activated with pervanadate or thapsigargin in the presence of nocodazole. To inhibit the activity of Src family kinases, IgE-sensitized cells were pretreated for 60 min with Src family selective tyrosine kinase inhibitor PP2 at a concentration of 10 μM before incubation with DNP-albumin. Cells treated for 60 min with 10 μM PP3 were used as controls.

Flow cytometry analysis of FcεRI

To determine the surface FcεRI expression, cells (5×10^5/ml) were exposed for 30 min on ice to 1 μg/ml anti-DNP IgE followed by 30 min incubation with FITC-conjugated anti-mouse Ab (cross-reacting with mouse IgE). After incubation the cells were washed in ice-cold BSS-BSA. Mean fluorescence intensities were determined in the FL1 channel of FACSCalibur (BD Biosciences, Mountain View, CA).

Degranulation assay

The degree of degranulation was quantified as the release of β-glucuronidase from anti-DNP IgE-sensitized and DNP-albumin or thapsigargin-activated cells, using 4-methylumbelliferyl β-D-glucuronide as a substrate (27). The total content of the enzyme was evaluated in supernatants from cells lysed by 0.1% Triton X-100.

Determination of intracellular Ca^{2+} concentrations and $^{45}Ca^{2+}$ uptake

Concentrations of free intracellular calcium ($[Ca^{2+}]_i$) were determined using Fluo3 as a reporter. Cells were sensitized with anti-DNP IgE (1 μg/ml) at 37°C in culture medium supplemented with 10% FCS, but devoid of SCF and IL-3. After 4 h, the cells were washed and resuspended at a concentration of 1×10^7 cells/ml in the same medium supplemented with Fluo3 and probenecid at final concentrations of 1 μg/ml and 2.5 mM, respectively. After 30 min, the cells were washed in BSS-BSA supplemented with probenecid and put on ice for 10 min. Before measurement, the cells (5×10^5) were briefly centrifuged, resuspended in 200 μl BSS-BSA, and preincubated for 4 min at 37°C. Cells were activated by adding 100 ng/ml DNP-albumin or 2 μM thapsigargin. Calcium mobilization was determined in the FL1 channel of a FACSCalibur Flow Cytometer (BD Biosciences, San Jose, CA) using FlowJo software (Ashland, OR). In the yellow fluorescent protein (YFP)-hSTIM1 rescue experiments, calcium responses were measured 48 h after nucleofection. STIM1 KD cells nucleofected with pYFP alone (Clontech Laboratories, Mountain View, CA) were used as a mock control. The experimental procedure was similar to that described above with some differences. Cells were loaded with the calcium reporter Fura Red (5 μg/ml), and changes in fluorescence intensity were monitored on an LSRII flow cytometer (BD Biosciences). Populations of live cells were selected based on forward and side scatters. In live nucleofected cells, YFP-positive cells were gated based on fluorescence in the FL1 channel. Fura Red was excited with 406- and 488-nm lasers, and data were collected separately using 675/45 BP and 675/20 BP filters, respectively.

Uptake of extracellular calcium was determined as described previously (28). Cells were sensitized with anti-DNP IgE (1 μg/ml) and activated for various time intervals with 100 ng/ml DNP-albumin or 2 μM thapsigargin in the presence of extracellular $^{45}Ca^{2+}$ (1 mM). Cell-bound radioactivity was measured in 10 ml scintillation liquid (EcoLite; ICN Biomedicals, Costa Mesa, CA) using a QuantaSmart TM counter.

Chemotaxis assay

Chemotactic responses of BMMCs were examined using 96-well chemotaxis plates (ChemoTx system; Neuro Probe, Gaithersburg, MD) with 8-μm pore size polycarbonate filters. Chemoatractant (DNP-BSA) at concentrations of 50–250 ng/ml in RPMI 1640 supplemented with 20 mM HEPES and 1% BSA (assay buffer), or assay buffer alone was added in 305 μl to the lower wells, and IgE-sensitized BMMCs (0.15×10^6) in 60-μl assay buffer were added on top of the membrane above each well. After 8 h incubation at 37°C and 5% CO_2 in humidified air, cells on the upper membrane surface were removed with suction, and the plates with membrane frames were centrifuged ($156 \times g$, 4 min). After centrifugation, 200 μl media above the cells was removed and 100 μl of water containing 0.1% Triton X-100 and 10 μM SYTOX Green nucleic acid stain (Invitrogen) was added to the well. Fluorescence was determined at 485-nm excitation and 530-nm emission, using TECAN Infinite M200 fluorescence microplate reader (Grödig, Austria). A linear standard curve with serial dilutions of the cells (400–50,000 cells) was included in each experiment to equate fluorescence intensity with cell number. Four independent experiments were run in triplicates.

Gel electrophoresis and immunoblotting

Whole-cell extracts were prepared by washing the cells in cold PBS, solubilizing them in hot SDS-sample buffer (29), and boiling for 5 min. SDS-PAGE on 7.5% gels, electrophoretic transfer of separated proteins onto nitrocellulose, and details of the immunostaining procedure have been described elsewhere (30). Abs against STIM1 and actin were diluted 1:2000 and 1:3000, respectively. Bound primary Abs were detected after incubation of the blots with HRP-conjugated secondary Ab diluted 1:10,000. Phosphotyrosine was detected by PY-20–HRP conjugate (dilution 1:2000). HRP signal was detected with chemiluminescence reagents in accordance with the manufacturer's directions and quantified using LAS 3000 imaging system (Fujifilm, Tokyo, Japan).

Immunofluorescence microscopy

Immunofluorescence microscopy was performed on fixed cells as described previously (31). Cells attached to fibronectin-coated coverslips were rinsed with microtubule-stabilizing buffer (0.1 M MES, pH 6.9, 2 mM EGTA, 2 mM $MgCl_2$, 4% polyethylene glycol 6000), fixed for 20 min in 3% formaldehyde in microtubule-stabilizing buffer, and extracted for 4 min with 0.5% Triton X-100 in microtubule-stabilizing buffer. TUB 2.1 mAb conjugated with Cy3 and polyclonal Ab to α-tubulin were diluted 1:600 and 1:200, respectively. AlexaFluor 488-conjugated anti-rabbit Ab was diluted 1:300. The preparations were mounted in MOWIOL 4-88 (Merck, Darmstadt, Germany), supplemented with DAPI to label nuclei, and examined with an Olympus A70 Provis microscope equipped with ×60 water-immersion or ×100 oil-immersion objectives. Images were recorded with a SensiCam cooled CCD camera (PCO IMAGING, Kelheim, Germany). Conjugated secondary Ab did not give any detectable staining.

Alternatively, samples were examined with a confocal laser scanning microscope Leica TCS SP5 equipped with an ×63/1.4.N.A. oil-immersion objective. Excitation and emission wavelengths were 561 nm and 566 to 633 nm for Cy3 (diode pumped solid-state laser). Optical sections were acquired in 125-nm steps, and z-series were made from 70 sections. Deconvolution and rotation was performed using Huygens Deconvolution Software (Scientific Volume Imaging, Hilversum, The Netherlands).

To estimate the number of cells that responded to activation events by generation of microtubule protrusions, three independent immunofluorescence experiments were performed. In each experiment usually 500 cells were examined, and cells with five and more microtubule protrusions after activation were counted up. These protrusions were not discernible in nonactivated cells. Statistical comparison of data was conducted with Student *t* test.

Time-lapse imaging by total internal reflection fluorescence microscopy

Control BMMCL cells, BMMCL cells with empty pLKO.1 vector, or cells with STIM1 KD were nucleofected with pEB1-GFP. Alternatively, BMMCL cells were nucleofected with YFP-hSTIM1 or simultaneously with YFP-hSTIM1 and EB3-mRFP1. Twenty-four hours later, 100 μl of cell suspension at concentration 1.5×10^6 cells/ml was overlaid on 35-mm glass-bottom culture dishes (MatTek, Ashland, MA; Cat. No. P35G-1.5-14-C) precoated with fibronectin (see above), and cells were allowed to attach for 1 h at 37°C. Perfusion insert for the 35-mm culture dish was

inserted (Warner Instruments, Hamden, CT; model RC-37F), and cells were washed and subsequently incubated in RPMI medium for live cell imaging (RPMI 1640 without phenol red, riboflavin, folic acid, pyridoxal, $Fe[NO_3]_3$) supplemented with 20 mM HEPES. Cells were imaged on the Leica AM total internal reflection fluorescence (TIRF) MC (Leica Microsystems) at 37˚C. Time-lapse sequences of EB1-GFP or YFP-hSTIM1 were acquired in TIRF mode (GFP cube, laser line 488 nm; Ex, 470/40; Em, 525/50; penetration depth, 150 nm) using HCX PL APO ×100/1.46 NA oil-immersion TIRF objective. Images were taken for 3 min at 1-s intervals with 30–40% laser power and exposure times ranging from 500–800 ms. Time-lapse sequences of EB3-mRFP1 in combination with YFP-hSTIM1 were acquired in TIRF mode (laser lines 561 nm or 488 nm, Em: 640/40 or 530/30, respectively; the same penetration depth 150 nm for both channels) using the same objective as above. Individual channels were imaged sequentially. Images were taken for 3 min at 2-s intervals with 50–80% (561 nm) or 30–40% (488 nm) laser power and exposure times ranging from 500–800 ms. Cells were scanned before, during, and after thapsigargin or nocodazole addition to final concentrations of 2 μM and 10 μM, respectively.

Time-lapse sequences were adjusted and analyzed with a particle tracking plug-in written in house. The images were smoothed to remove noise (σ 80 nm). The particles were then enhanced by subtracting the images obtained by Gaussian smoothing (σ 300 nm). The coordinates of particles were detected as centers of mass of maxima of the image intensity found by morphologic reconstruction (32). Regions of pixels with distance less than 3 μm from cell boundary were detected by thresholding the Euclidean distance transform (33) of the cell binary image. Only the particles in the selected region were evaluated. The corresponding particles in subsequent images were detected by pairing the closest particles, and the particle trajectories were constructed by continuation. The speed of the particles was calculated as the ratio of particle trajectory length and trajectory duration. The histogram of the particles speed was calculated from the trajectory speed weighted by the trajectory duration. The algorithms were implemented as plug-in modules of the Ellipse program, version 2.07 (ViDiTo, Systems, Košice Slovakia). Statistical analysis was done in Microsoft Excel.

Results

Reorganization of microtubules during activation of BMMCs

To compare microtubule organization in resting and activated mast cells, BMMCs were attached to fibronectin-coated coverslips and then activated by various means before fixation and immunofluorescence labeling for β-tubulin. Data showed a clear difference between resting and activated cells in microtubule distribution. Quiescent cells were characterized by rounded morphology and microtubules in cell periphery running predominantly alongside the plasma membrane (Fig. 1*A*, *a*, *b*; −Ag). When activated by FcεRI aggregation, many cells had multiple protrusions containing microtubules, in the following text denoted as microtubule protrusions (Fig. 1*A*, *c*, *d*; +Ag). Similarly, activation by pervanadate, a potent protein tyrosine phosphatase inhibitor (34) that mimics in part the stimulatory effect of Ag (35), gave rise to multiple microtubule protrusions (Fig. 1*A*, *e*, *f*; +Pv). Surprisingly, generation of robust microtubule protrusions was also found in cells treated with thapsigargin, a compound that discharges intracellular Ca^{2+} stores by inhibition of the SERCA (36) (Fig. 1*A*, *g*, *h*; +thapsigargin [Tg]). Microtubule protrusions do not reflect only the spreading of cells during activation events, because they are also found on the dorsal side of cells as clearly documented on deconvoluted three-dimensional images from laser scanning confocal microscopy. Although no protrusions were found in resting cells (Fig. 2*A*, 2*B*, –Ag), they were clearly discernible in cells activated by Ag-mediated FcεRI aggregation (Fig. 2*C*, 2*D*, +Ag), pervnadate (Fig. 2*E*, 2*F*, +Pv) or thapsigargin (Fig. 2*G*, 2*H*, +Tg). To determine whether the number of cells with protrusions depends on the mode of activation, BMMCs were evaluated for the presence of protrusions in three independent experiments (each included 500 cells). Activation of the cells with Ag, pervanadate, or thapsigargin resulted in 37 ± 9, 59 ± 8, and 94 ± 3% (mean ± SD; n = 3), respectively, of cells with microtubule protrusions (Fig. 1*B*). To prove that the generation of microtubule protrusion is not restricted only to cells of primary cultures, activations were repeated with an established cell line, BMMCL. In that case the rates of activation with Ag, pervanadate, or thapsigargin were 55 ± 10, 64 ± 3, and 80 ± 5% (mean ± SD; n = 3), respectively. The microtubule protrusions in cells activated by FcεRI aggregation were most prominent ~5 min after crosslinking. In contrast, cells stimulated by pervanadate or thapsigargin reached the maximum after 15 and 20 min, respectively.

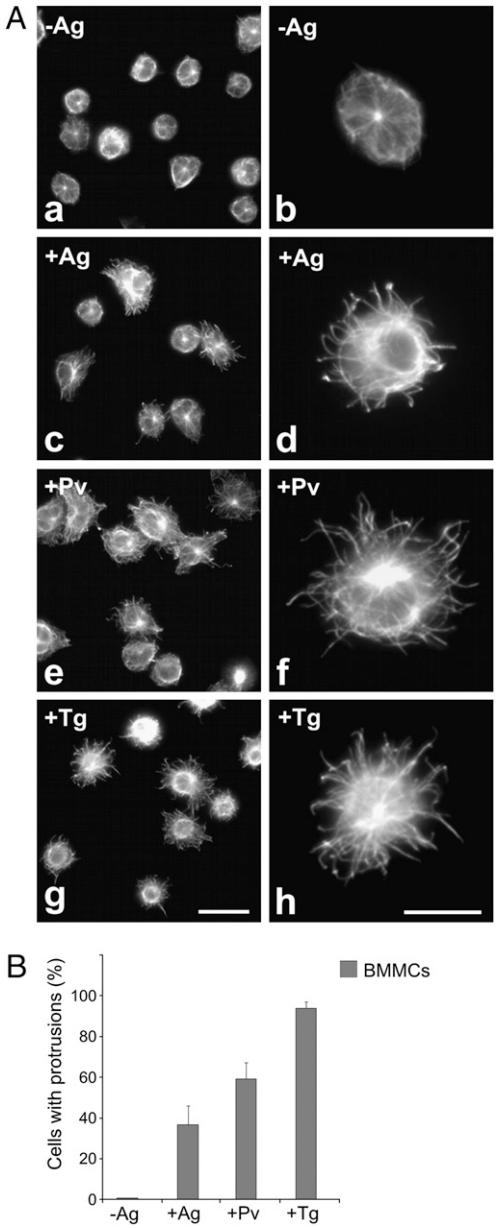

FIGURE 1. Organization of microtubules in resting and activated mast cells. *A*, Resting BMMCs (*a*, *b*; −Ag), the cells activated by FcεRI aggregation (*c*, *d*; +Ag), pervanadate (*e*, *f*; +Pv), or thapsigargin (*g*, *h*; +Tg) were fixed and stained for β-tubulin. The preparations were imaged by fluorescence microscopy. Scale bars, 20 μm (*g*) and 10 μm (*h*). Comparable magnifications are in (*a*, *c*, *e*, *g*) and in (*b*, *d*, *f*, *h*). *B*, Quantitative analysis of the frequency of microtubule protrusions in BMMCs. Resting cells (−Ag), cells activated by FcεRI aggregation (+Ag), pervanadate (+Pv) or thapsigargin (+Tg). Three independent experiments were performed, each involving 500 BMMCs examined for the presence of microtubule protrusions. Values indicate means ± SD (n = 3).

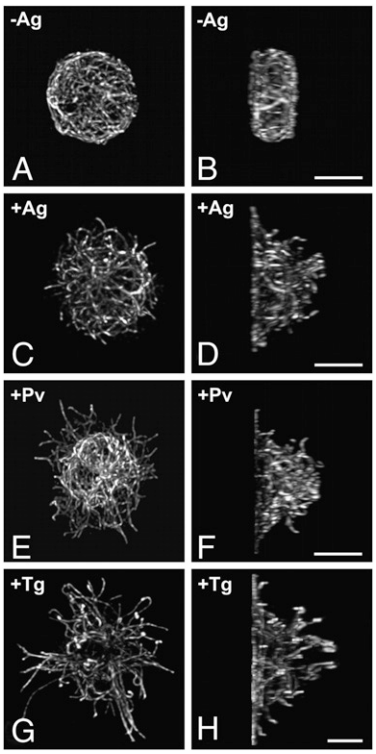

FIGURE 2. Changes in the spatial distribution of microtubules in resting and activated BMMCs. Resting cells (*A*, *B*; −Ag), cells activated by FcεRI aggregation (*C*, *D*; +Ag), pervanadate (*E*, *F*; +Pv), or thapsigargin (*G*, *H*; +Tg) were fixed and stained for β-tubulin. The preparations were imaged by laser scanning confocal microscopy. The stacks of confocal sections were deconvoluted and subjected to three-dimensional reconstruction. Resulting three-dimensional images viewed from top of the cells (*A*, *C*, *E*, *G*) and from the plane perpendicular to the plane of cell adhesion (*B*, *D*, *F*, *H*). Each pair (*A–B*, *C–D*, *E–F*, and *G–H*) represents the same cells. Scale bars, 5 μm.

Dose response curves demonstrating the relations between the formation of microtubule protrusions and the degree of degranulation, quantified as the release of β-glucuronidase, in BMMCL activated by FcεRI aggregation for 5 min and by thapsigargin for 20 min are shown in Supplemental Fig. 1A and 1B, respectively. There were dose response correlations between formation of microtubule protrusions and degranulation. Correlations between the time course of microtubule protrusion formation and the degree of degranulation after activation by FcεRI aggregation at Ag concentration 100 ng/ml and by thapsigargin at concentration 2 μM are shown in Supplemental Fig. 1C and 1D, respectively. Although there was a correlation between morphologic changes and degranulation in case of thapsigargin activation, cells activated by Ag reached the maximum of microtubule protrusions at 5 min, whereas the increase in β-glucuronidase release persisted to 10 min. Activation by either pervanadate or thapsigargin had no effect on viability of the cells (not shown). When the cells were pretreated with microtubule inhibitor nocodazole and activated in its presence, protrusions were not formed (not shown). This implies that microtubules are essential in this process.

Formation of microtubule protrusions in FcεRI-activated cells was substantially reduced if a monovalent hapten causing receptor disengagement (50 μM DNP-lysine) (37) was added together with or 1 min after Ag (not shown). Inhibition of protrusion formations was also observed in IgE-sensitized cells pretreated for 60 min with Src family inhibitor PP2 (10 μM) and then activated by Ag. Pretreatment with PP3 (negative control for PP2) failed to affect protrusion formation (not shown). This finding suggests that the activity of Src family protein tyrosine kinases is essential for this process. Interestingly, when the cells were activated by FcεRI aggregation, pervanadate, or thapsigargin in Ca^{2+}-free media, microtubule protrusions were basically not detectable. A typical example of the effect of extracellular Ca^{2+} on generation of microtubule protrusions in cells after their activation by FcεRI aggregation is shown in Fig. 3*A*. Statistical evaluation of these and other experiments is documented by histogram (Fig. 3*B*). Collectively, these data suggest that dramatic changes in microtubule arrangement during activation of BMMCs by FcεRI aggregation depend on the activity of Src family kinases and are modulated by Ca^{2+} influx.

Changes of microtubule dynamics in activated cells

Microtubule plus-end dynamics in BMMCL cells expressing EB1-GFP was monitored by means of time-lapse imaging using TIRF microscopy (TIRFM). Cells were activated or not by thapsigargin, and the distribution of growing microtubules in cell periphery was evaluated after collecting 180 frames in 1-s intervals for 3 min total time. In activated cells, time-lapse imaging started 13 min after thapsigargin addition. Data from a typical experiment are shown in Fig. 4*A*. A comparison of single-frame or 20-frame projections obtained either from control (Fig. 4*A*, *a*, *b*; –Tg) or thapsigargin-activated (Fig 4A, *c*, *d*; + Tg) cell indicated more growing microtubules in cell periphery of the latter. This finding was confirmed by statistical data evaluation and documented with

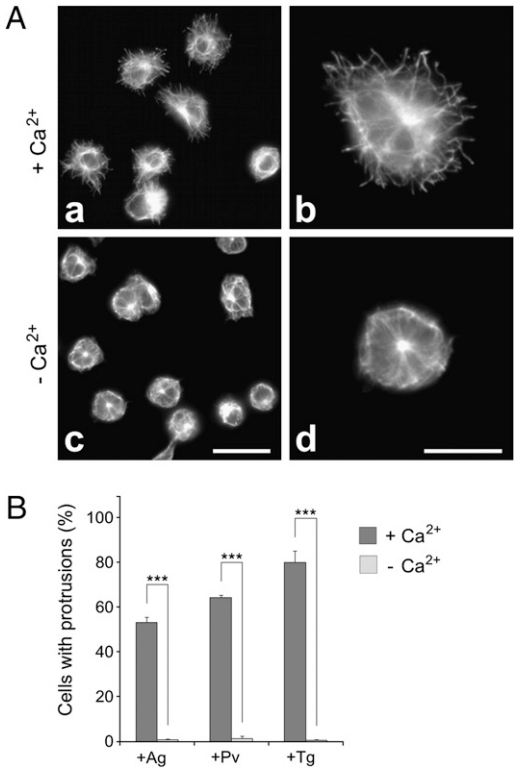

FIGURE 3. Effect of extracellular Ca^{2+} on generation of microtubule protrusions. *A*, BMMCL cells activated by FcεRI aggregation in the presence (*a*, *b*; $+Ca^{2+}$) or absence (*c*, *d*; $–Ca^{2+}$) of extracellular Ca^{2+} (1.8 mM) were fixed and stained for β-tubulin. Scale bars, 20 μm (*c*) and 10 μm (*d*). Comparable magnifications are in (*a*, *c*) and in (*b*, *d*). *B*, Statistical analysis of the frequency of microtubule protrusions in BMMCL cells. Cells activated by FcεRI aggregation (+Ag), pervanadate (+Pv), or thapsigargin (+Tg) in the presence ($+Ca^{2+}$) or absence ($-Ca^{2+}$) of extracellular Ca^{2+}. Three independent experiments were performed, each involving 500 cells, and examined for the presence of microtubule protrusions. Values indicate means ± SD, $n = 3$; $^{***}p < 0.001$.

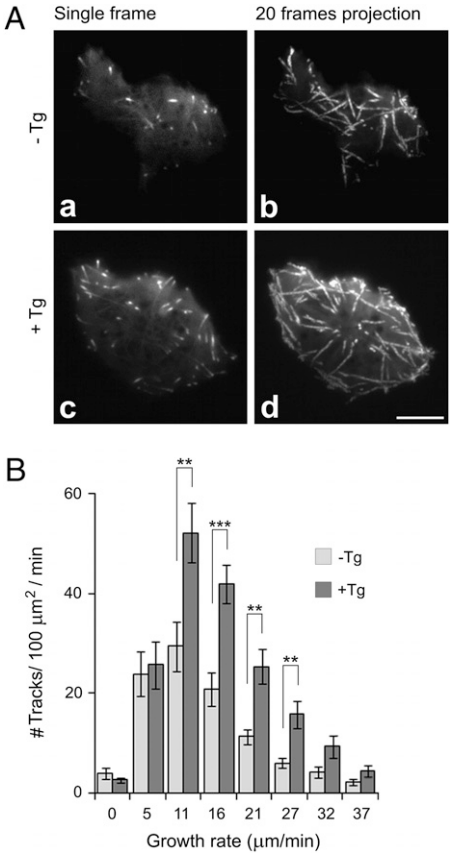

FIGURE 4. Activation of mast cells increases the number of growing microtubules in cell periphery as determined by TIRFM time-lapse imaging. *A*, Time-lapse imaging of resting (*a*, *b*) and thapsigargin-activated (*c*, *d*) BMMCL cells expressing EB1-GFP. Still images of EB1 (*a*, *c*) and tracks of EB1 comets over 20 s created by maximum intensity projection of the 20 consecutive frames (*b*, *d*). Scale bar, 5 μm. *B*, Histogram of microtubule growth rates in cell periphery of resting (−Tg) and thapsigargin-activated (+Tg) cells. A total of 15 different cells were tracked in five independent experiments. Values indicate mean ± SE, $n = 15$; $^{**}p < 0.01$; $^{***}p < 0.001$.

a histogram of the microtubule growth rates (Fig. 4*B*). Typical time-lapse imaging of control (Supplemental Video 1) and activated (Supplemental Video 2) cells are shown in the supplemental material. These data suggest that activation increases the number of growing microtubules in the cell periphery where microtubule protrusions are formed. More growing microtubules at cell periphery, compared with nonactivated cells, were also observed after activation of cells by FcεRI aggregation (Supplemental Fig. 2).

Reduced degranulation, Ca^{2+} influx, and free cytoplasmic Ca^{2+} concentration in cells with reduced level of STIM1

STIM1 represents the key regulator in the SOCE pathway leading to an influx of extracellular Ca^{2+}. To discover whether STIM1 is involved in the generation of microtubule protrusion, we first isolated cells with reduced levels of STIM1 and characterized their properties. STIM1-deficient cells were produced in both BMMCs and BMMCL cells using lentiviral vectors. At the best silencing, the amount of STIM1 in BMMCs and BMMCL cells reached 20 ± 12% and 10 ± 9% (means ± SD; n = 5-8), respectively, when compared with the expression level in control cells with an empty pLKO.1 vector. A typical immunoblotting experiment is shown in Fig. 5*A*, and evaluation of all data obtained is shown in Fig. 5*B*. Cells with the highest STIM1 reduction (denoted KD2) were selected for further experiments. As detected by flow cytometry, the

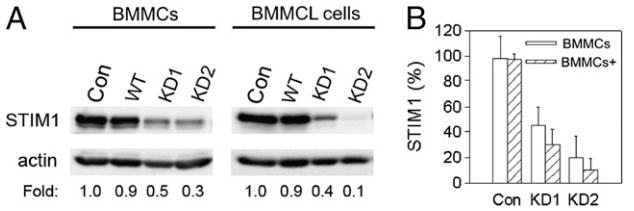

FIGURE 5. Characterization of mast cells with reduced level of STIM1. *A*, Immunoblots of whole cell lysates from BMMCs or BMMCL cells probed with anti-STIM1 and anti-actin (loading control) Abs. Control cells infected with empty pLKO.1 vector (Con), noninfected wild-type cells (WT), cells selected after KD of STIM1 by shRNA1 (KD1), or shRNA2 (KD2). Numbers under the blots indicate relative amounts of STIM1 normalized to control cells (Con) and to the amount of actin in individual samples (Fold). *B*, Comparison of STIM1 expression levels in control and STIM1 KD BMMCs or BMMCL cells. Values indicate means ± SD from independent experiments (n = 6 for controls; n = 3 for KD1; n = 5 for KD2).

expression levels of surface FcεRI were similar in cells with normal and reduced amount of STIM1 (not shown). No substantial changes in the profile of total tyrosine-phosphorylated proteins were detected in STIM1 KD2 cells (not shown).

It is well established that an increase in $[Ca^{2+}]_i$ is a prerequisite for mast cell degranulation (1). To confirm the functional relevance of STIM1 KD, we determined the degree of degranulation by measuring the release of β-glucuronidase in cells activated by FcεRI aggregation or by thapsigargin. As expected, a substantial decrease in degranulation was observed in BMMCs with STIM1 KD compared with control cells. The inhibition of degranulation was observed in cells activated by both FcεRI aggregation (Supplemental Fig. 3*A*) and by thapsigargin (Supplemental Fig. 3*B*). The uptake of $^{45}Ca^{2+}$ after activation by FcεRI aggregation (Supplemental Fig. 3*C*) or by thapsigargin (Supplemental Fig. 3*D*) was also inhibited in STIM1 KD cells. Finally, a substantially lower concentration of free intracellular calcium $[Ca^{2+}]_i$ was detected in STIM1 KD cells, after activation by both FcεRI aggregation (Supplemental Fig. 3*E*) and thapsigargin (Supplemental Fig. 3*F*; thapsigargin). Similar results were obtained with BMMCL cells (not shown). Collectively, these data clearly demonstrate that STIM1 is essential for Ca^{2+} mobilization and degranulation in cells used in this study.

Generation of microtubule protrusions is dependent on STIM1

When BMMCs carrying empty pLKO.1 vector were activated with thapsigargin, the formation of microtubule protrusions was prominent (Fig. 6*A*, *a*, *c*; control + Tg) and essentially the same as in BMMCs without vector (not shown). Alternatively, thapsigargin-induced activation in BMMCs with STIM1 KD failed to generate microtubule protrusions, and the cell shape was spherical (Fig. 6*A*, *b*, *d*; STIM1 KD + Tg). Significant inhibition of protrusion formations in STIM1 KD cells was also found after stimulation with pervanadate or Ag in both BMMCs and BMMCL cells (Fig. 6*B*). No obvious change in microtubule dynamics was detected by time-lapse imaging in BMMCL cells with STIM1 KD after activation by thapsigargin. Data from a typical experiment of time-lapse imaging are shown in Fig. 7*A*. Comparison of still images (single frame or 20 frames projections) from nonactivated (Fig. 7*A*, *a*, *b*; STIM1 KD – Tg) or activated (Fig 7A, *c*, *d*; STIM1 KD + Tg) cells disproved the notion that more microtubules grow in the cell periphery of activated cells. This finding was confirmed by the histogram comparing microtubule growth rates (Fig 7*B*). Although thapsigargin-activated cells exhibited some increase in the number of growing microtubules in the cell periphery, it was insignificant except for the fast-growing group (27 μm/min). In control

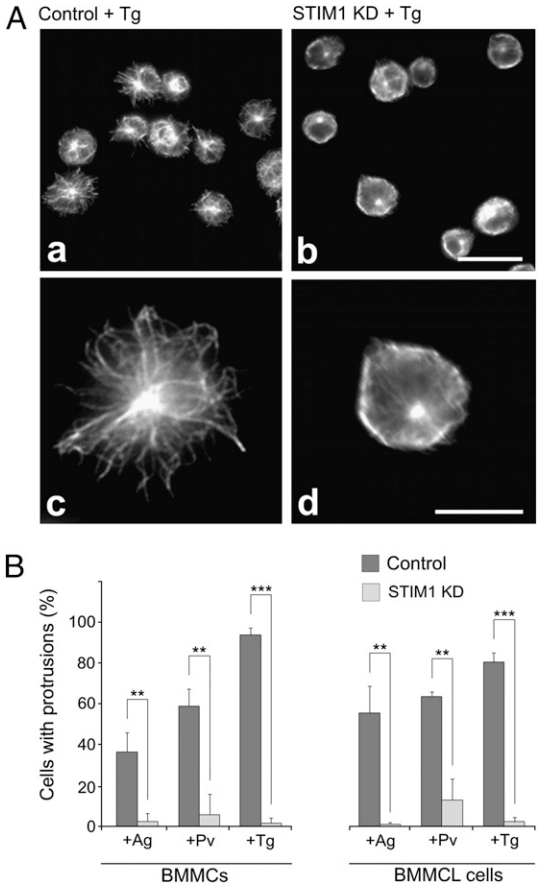

FIGURE 6. Decreased expression of STIM1 inhibits the generation of microtubule protrusions in activated cells. *A*, Control BMMCs, carrying empty pLKO.1 vector (*a*, *c*) or STIM1 KD2 cells (*b*, *d*) were activated by thapsigargin, fixed, and stained for β-tubulin. Scale bars, 20 μm (*a*, *b*) and 10 μm (*c*, *d*). *B*, Statistical analysis of the frequency of microtubule protrusions in control cells (carrying empty pLKO.1 vector) and STIM1 KD2 cells activated by FcεRI aggregation (+Ag), pervanadate (+Pv), or thapsigargin (+Tg). Three independent experiments were performed, each involving 500 BMMCs or BMMCL cells, and examined for the presence of microtubule protrusions. Values indicate means ± SD, $n = 3$; $^{**}p < 0.01$; $^{***}p < 0.001$.

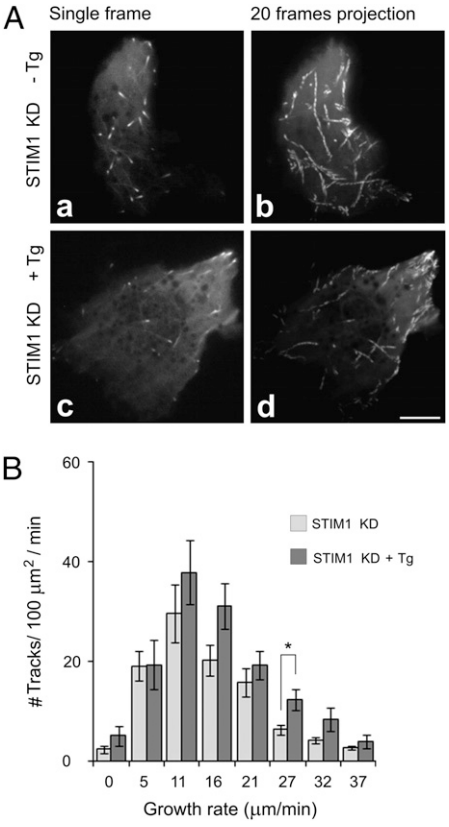

FIGURE 7. KD of STIM1 prevents changes in microtubule dynamics in activated cells as determined by TIRFM time-lapse imaging. STIM1 KD2 cells were nucleofected with EB1-GFP and used for time-lapse imaging. *A*, Resting (*a*, *b*) and thapsigargin-activated (*c*, *d*) STIM1 KD2 cells. Still images of EB1 (*a*, *c*) and tracks of EB1 comets over 20 s created by a maximum intensity projection of 20 consecutive frames (*b*, *d*). Scale bar, 5 μm. *B*, Histogram of microtubule growth rates in the cell periphery of resting (STIM1 KD) and thapsigargin-activated (STIM1 KD +Tg) cells. A total of nine different cells were tracked in three independent experiments. Values indicate means ± SE, $n = 9$; $^{*}p < 0.05$.

BMMCL cells carrying empty pLKO.1 vector, the distribution of growing microtubules in resting and thapsigargin-treated cells was similar as in BMMCL cells (Fig. 4).

To strengthen the evidence of STIM1-dependent formation of microtubule protrusions during activation, a rescue experiment was performed with construct-encoding mCherry-tagged human STIM1. Proper localization of mCherry-hSTIM1 was demonstrated in cells expressing EB1-GFP. It has been shown previously that STIM1 associates with the plus ends of growing microtubules (11); in addition, the mCherry-hSTIM1 localized in quiescent cells both in the ER and in the growing ends of microtubules labeled with EB1 (Fig. 8*A*, *a–c*). When BMMCL cells with STIM1 KD were nucleofected with mCherry-hSTIM1 and activated by thapsigargin, the formation of typical microtubule protrusions was recovered (Fig. 8*B*, *a–c*). Alternatively, no protrusions were generated after activation of cells nucleofected with empty mCherry vector (Fig. 8*B*, *d–f*). Control experiments revealed that no microtubule protrusions were evident in nonactivated BMMCL cells nucleofected either with mCherry-hSTIM1 or mCherry vector alone (not shown). The formation of microtubule protrusions was also recovered when YFP-hSTIM1 was used in rescue experiments as documented by quantitative data (Fig. 8*C*). Nucleofection of YFP-hSTIM1 into STIM1 KD2 cells also restored calcium mobilization upon triggering with thapsigargin (Fig. 8*D*) or aggregation of the FcεRI (not shown). Collectively, these data strongly suggest that STIM1 is essential for the generation of microtubule protrusions during activation of BMMCs.

Microtubules are not essential for STIM1 puncta formation

To address the question of whether microtubules in BMMCs have a role in activating SOCE, we investigated the effect of nocodazole, a microtubule-depolymerizing drug, on the distribution of STIM1 in the absence or presence of thapsigargin. In control cells, a typical comet-like movement was observed in quiescent BMMCs expressing YFP-hSTIM1 (Supplemental Video 3). After activation by thapsigargin, STIM1 formed puncta (Supplemental Video 4) similar to those previously described in other cells (5, 15). The addition of 10 μM nocodazole led to the rapid disappearance of comet-like movement of YFP-hSTIM1 as well as EB3-mRFP1, used as marker of growing microtubules. YFP-hSTIM1 was located only on the ER. When the nocodazole-treated cells were then activated with thapsigargin, YFP- hSTIM1 formed robust puncta (Supplemental Video 5). Staining of parallel samples for tubulin confirmed that most microtubules were disassembled (not shown). This finding suggests that initial STIM1 aggregation does not require intact microtubules. Interestingly, the disruption of microtubules only moderately inhibited the $^{45}Ca^{2+}$ uptake in

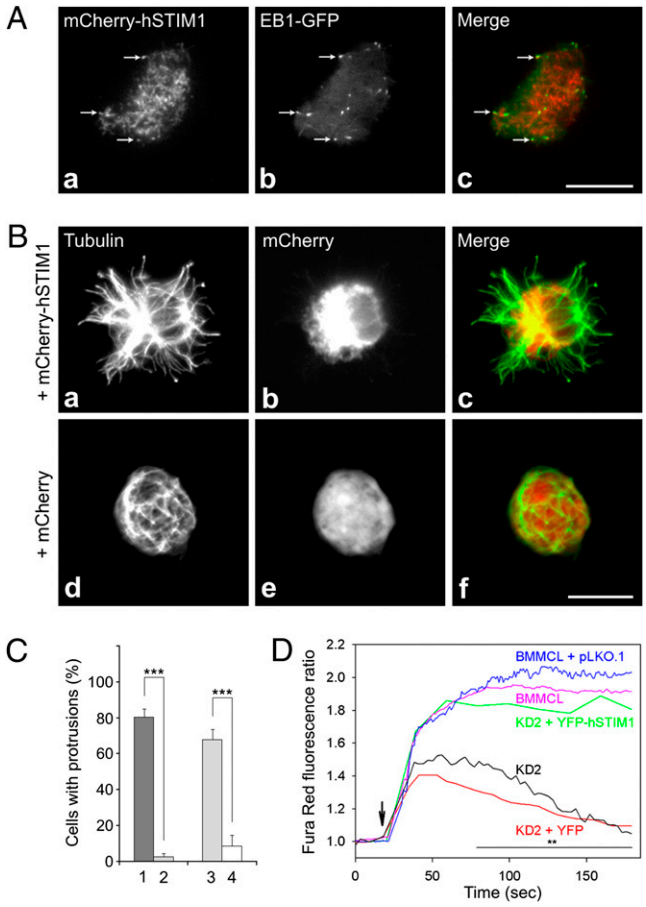

FIGURE 8. Phenotype rescue of STIM1 KD2 BMMCL cells after introduction of human STIM1. *A*, Localization of mCherry-tagged human STIM1 during TIRFM time-lapse imaging of resting cells expressing EB1-GFP. Still images of mCherry-hSTIM1 (*a*) EB1-GFP (*b*) and superposition of images (*c*; mCherry, red; GFP, green). Arrows indicate the same positions. Scale bar, 10 μm. *B*, STIM1 KD2 cells were nucleofected with mCherry-hSTIM1 (*a–c*) or mCherry vector alone (*d–f*; control) and activated by thapsigargin. Microtubules in fixed cells stained with anti-α-tubulin Ab (*a*, *d*). Fluorescence of nucleofected mCherry vectors (*b*, *e*). Superposition of images (*c*, *f*; tubulin, green; mCherry, red). The preparations were imaged by fluorescence microscopy; *a–c* and *d–f* represent the same cells. Scale bar, 10 μm. *C*, Statistical analysis of the frequency of microtubule protrusions in thapsigargin-activated control cells (1), STIM1 KD2 cells (2), STIM1 KD2 cells nucleofected with pYFP-hSTIM1 (3) and STIM1 KD2 cells nucleofected with pYFP empty vector (4). Three independent experiments were performed, each involving 500 (1, 2) or 100 (3, 4) cells examined for the presence of microtubule protrusions. Values indicate means ± SD, $n = 3$; $***p < 0.001$. *D*, Changes in intracellular Ca^{2+} mobilization. KD2 cells were nucleofected with pYFP-hSTIM1 (green line) or with pYFP empty vector (red line). Nontransfected cells (pink line), cells transfected with pLKO.1 (blue line) and STIM1 KD2 cells (black line) served as controls. The arrow indicates activation by 2 μM thapsigargin. The extent of activation is expressed as a ratio of Fura Red fluorescence intensity induced with 406- and 488-nm lasers. Representative curves are plotted against time. The line below the asterisks indicates the time interval of significant differences between STIM1 KD2 cell transfected with pYFP-hSTIM1 or with pYFP empty vector; $**p < 0.01$; $n = 3$.

thapsigargin-activated cells (Fig. 9*A*), but degranulation was substantially reduced (Fig. 9*B*).

STIM1 associates with microtubule protrusions and plays a role in chemotactic response

The movement of YFP-hSTIM1, not associated with growing tips of microtubules, was observable at later stages of activation when microtubule protrusions started to form. Association of YFP-hSTIM1 with microtubule protrusions was evident in thapsigargin-activated BMMCs and was detectable by confocal microscopy on cells stained for β-tubulin (Fig. 10*A*, *a–c*). Similarly, FcεRI aggregation led to partial association of YFP-hSTIM1 with microtubule protrusions (not shown).

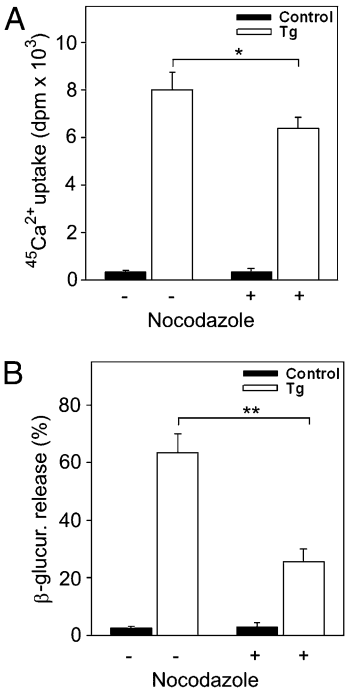

FIGURE 9. Effect of microtubule depolymerization on Ca^{2+} uptake and degranulation. *A*, Effect of nocodazole on Ca^{2+} uptake. BMMCs were treated or not with nocodazole (10 μM) for 30 min and then exposed to thapsigargin (2 μM; Tg) or BSS-BSA alone (Control) for 15 min in the presence of extracellular $^{45}Ca^{2+}$ (1 mM) and nocodazole (10 μM). *B*, Effect of nocodazole on degranulation. BMMCs were treated with nocodazole and exposed to thapsigargin as in *A*, and the release of β-glucuronidase was determined. Data in *A* and *B* represent means ± SD, $n = 6–8$; $*p < 0.05$; $**p < 0.01$.

The observed formation of STIM1-dependent microtubule protrusions could be related to enhanced movement of the activated cells. Therefore, in additional experiments, we investigated the chemotactic response of STIM1-deficient BMMCs. The data presented in Fig. 10*B* indicate that at low concentrations of Ag (25–100 ng/ml), the chemotactic response is contingent on STIM1 in a dose-dependent manner. At a higher concentration (250 ng/ml), the difference disappears mainly because of the high-dose–mediated inhibition of chemotaxis in control cells. This finding demonstrates that STIM1-dependent Ca^{2+} influx promotes chemotaxis.

Discussion

FcεRI stimulation of mast cells leads to rapid cytoskeleton rearrangement that is important for cell activation and degranulation. Accumulating recent data point to an important role of microtubules in these processes (38). Previous studies focused primarily on the role of microtubules in granular transport (13, 16, 17, 20) or on the initial stages of SOCE signaling pathway (13, 15, 39). In this study, we show that microtubule network rearrangement in activated BMMCs and formation of microtubule protrusions is dependent on the activity of Ca^{2+} sensor STIM1. This conclusion is supported by several lines of evidence. First, microtubule protrusions were found in cells stimulated by three types of activators that induced depletion of Ca^{2+} from internal stores (FcεRI aggregation, pervanadate, or thapsigargin treatment). Second, the generation of protrusions was impaired when multivalent Ag-

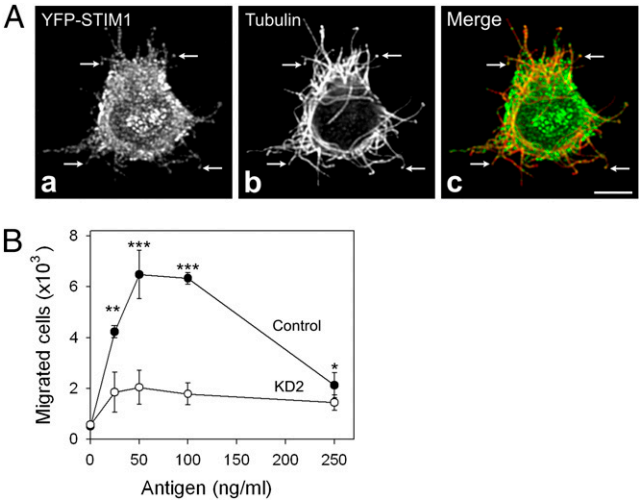

FIGURE 10. STIM1 associates with microtubule protrusions in activated cells and is essential for chemotactic response. *A*, Laser scanning confocal microscopy of BMMCL cells expressing YFP-hSTIM1 after activation by thapsigargin. Cells were fixed and immunostained for β-tubulin, and both STIM1 (*a*) and tubulin (*b*) were visualized in a single confocal section. Superposition of STIM1 and tubulin staining is shown in *c*. Association of YFP-hSTIM1 with microtubule protrusions is depicted (arrows). Scale bar, 5 μm. *B*, Chemotactic response in activated cells. Various concentrations of DNP-BSA (chemoattractant) were added to the lower wells of ChemoTx system plate, and IgE-sensitized BMMCs infected with empty pLKO.1 vector (Control) or STIM1 KD2 cells (KD2) were added on top of the membrane above each well. The numbers of cells migrated to the lower well were determined as described in *Materials and Methods*. Values indicate mean ± SD, $n = 12$; $*p < 0.05$; $**p < 0.01$; $***p < 0.001$.

induced FcεRI aggregation and signaling were inhibited either by monovalent hapten or by Src family specific inhibitor; this implies that early, physiologically relevant signaling events leading to STIM1 aggregation are important for microtubule rearrangement. Third, the formation of protrusions was also inhibited in cells with a decreased level of STIM1 and with correspondingly diminished influx of extracellular Ca^{2+}. Fourth, microtubule protrusions were restored in STIM1 KD cells after the introduction of hSTIM1. Finally, microtubule protrusions were not observed in cells activated in Ca^{2+}-free media. Thus, STIM1-regulated Ca^{2+} influx plays a crucial role in the generation of microtubule protrusions.

We have shown previously that, compared with resting cells, FcεRI- or pervanadate-induced activation of BMMCs attached to poly-L-lysine-coated coverslips resulted in more intense staining of microtubules. However, no obvious microtubule protrusions were detected (21). Similarly, activation and fixation of BMMCs in suspension followed by attachment to glass slides by cytospin intensified the tubulin immunostaining, but microtubule protrusions were not reported (17). In this study, the cells were attached to fibronectin before activation, resembling more closely the natural conditions in connective tissue where mast cells are congregated (40). Although the attachment of BMMCs to fibronectin alone did not generate microtubule protrusions, they were observable after cell triggering. It is known that engagement of integrins by their ligands activates some signaling pathways that modulate signals originating from other receptors (41). It has been reported that, when mast cells were activated simultaneously via both FcεRI and integrins, phosphorylation events were prolonged and intensified (42). Thus, generation of microtubule protrusions could reflect such integrated signals in activated cells.

To discover whether the generation of microtubule protrusions is limited to BMMCs, several other cell types were tested. However, thapsigargin treatment failed to induce formation of protrusions in any other cell type examined, including mouse embryonal fibroblasts 3T3, human osteosarcoma cell line U2OS or human glioblastoma T98G (Z. Hájková, unpublished data). By contrast, in BMMCL cells, which are grown for many years in the absence of SCF, the formation of protrusions was observed after triggering with cell activators (Ag, pervanadate, thapsigargin). The reduction of STIM1 expression both in BMMCs and BMMCL cells had a detrimental impact on the formation of microtubule protrusions. This finding indicates that protrusion formation could be a typical feature of mast cells that are characterized by immediate response to outer stimuli. However, we cannot rule out at present that the generation of microtubule protrusions can also be observable in the other cell types.

Colocalization of ER-embedded STIM1 with microtubules has been described for several cell types, including rat basophilic leukemia RBL-2H3 (8, 9, 15, 43), and comet-like movement of STIM1 was also reported (11). Furthermore, STIM1 contains a short sequence (SxIP) responsible for direct binding to EB1 (44). Thus, STIM1 can associate with growing microtubules, a mechanism that might facilitate the transport of STIM1 to plasma membrane. Using TIRFM we have confirmed the comet-like movement of STIM1 and its association with EB1 in resting BMMCL cells. This movement was substantially reduced after the addition of thapsigargin, which is in agreement with the impaired association of STIM1 with microtubules in Ag-activated RBL-2H3 cells (43). Recent data on FRET imaging of EB1 and STIM1 in HEK293 cells showed that, upon store depletion of Ca^{2+}, STIM1 dissociated from EB1 and associated with SERCA. This process was reversible, because the replenishment of intracellular Ca^{2+} stores also restored the STIM1–EB1 interactions (45). Moreover, no effect on SOCE was observed in HeLa cells with depleted EB1 (11). Taking these findings together, it is likely that the interaction of STIM1 with EB1 on growing microtubules is not essential for the transport of STIM1 to plasma membrane during mast cell activation.

After depletion of intracellular Ca^{2+} stores, STIM1 accumulates into puncta, discrete subregions of ER located in a close proximity (10–25 nm) to the plasma membrane (46). STIM1 puncta are formed several seconds before the opening of calcium channels (47), and one could expect that microtubules are involved in this process. However, our data demonstrate that although microtubule disruption by nocodazole abolished the comet-like movement of STIM1, it had no effect on puncta formation in activated cells. This finding is in line with our observation that the uptake of extracellular Ca^{2+} was only partially inhibited in nocodazole-pretreated and thapsigargin-activated BMMCs. This suggests that STIM1 aggregation beneath the plasma membrane and subsequent opening of Ca^{2+} release-activated Ca^{2+} channels does not require intact microtubules in activated mast cells. Previous studies often reported discordant effects of nocodazole treatment on SOCE or I_{CRAC}, the current most frequently associated with SOCE, in various cell types. Whereas there was no effect of nocodazole treatment observed in NIH 3T3 (48), RBL-1 (15, 39), and DT40 cells (8), an inhibitory effect was demonstrated for other cell types, such as RBL-2H3 cells, BMMCs (13), and HEK 293 (15). It appears that different factors, including cell type, treatment protocol and the way of Ca^{2+} depletion might modify the results of the experiments. It is also possible that microtubules play a supporting role in SOCE signaling by optimizing the location of ER containing STIM1 before cell activation (15).

Nocodazole treatment, in contrast, effectively suppressed degranulation in BMMCs, suggesting that microtubules have a key role in the intracellular transport of granules. This finding is in accordance with previously published data demonstrating

microtubule-dependent movement of secretory vesicles during exocytotic response (16, 17, 20) and studies documenting a dramatic decrease in degranulation, but not in Ca^{2+} response in nocodazole treated cells (49). Our observation that STIM1 puncta are associated with microtubules in protrusions (Fig. 10*A*) indicates that microtubules might be important for translocation of clustered STIM1 as well. This process could possibly be dependent on the movement of ER components to protrusions via microtubule motor proteins; an important role of kinesin and dynein in the distribution of ER has already been reported (14).

Compared with quiescent cells or cells with decreased expression of STIM1, the number of growing microtubules at the periphery of activated BMMCL cells is substantially increased. This finding suggests the stabilization of microtubule plus ends. It is known that an important role in stabilization of growing microtubules is to be assigned to the plus end-tracking proteins whose interactions with microtubules are regulated by phosphorylation (10). Ca^{2+}-dependent kinases (e.g., conventional protein kinases C, calcium-calmodulin–dependent kinases) or phosphatases (e.g., PP2B) might participate in the regulation of microtubule stability in activated BMMCs. It has been reported that calcium-dependent activation of Rac (from the RhoA family of small GTPases) depends on the activity of conventional protein kinase C (50). FcεRI stimulation induced in BMMCs the activation of RhoA (17), which participates in the stabilization of microtubule plus ends through its target mDia (51). It remains to be determined whether stimulated kinases, small GTPases, or both have a stabilizing role in thapsigargin-treated BMMCs.

Nishida et al. (17) reported that FcεRI stimulation of BMMCs triggered the formation of microtubules and the translocation of granules in a manner independent of Ca^{2+}. Alternatively, our results demonstrate Ca^{2+}-dependent formation of microtubule protrusions. This discrepancy could be explained by differences in cell activation (the absence or presence of integrin engagement) and unlike methods of preparation of samples for microscopic evaluation, as discussed above. However, it is also possible that the initial stages of microtubule formation and transport of granules along microtubules are independent of Ca^{2+}, but later stages of activation and formation of microtubule protrusions depend on sustained influx of Ca^{2+}. The presence of aggregated STIM1 in protrusion could help to organize Ca^{2+} release-activated Ca^{2+} channels (46) and open locally these channels to cause SOCE. These interactions could be modulated by Ca^{2+} channel regulators, such as calmodulin (52) and the recently discovered CRACR2A (53). Our finding that STIM1-deficient BMMCs exhibited defective chemotaxis toward Ag is in line with these interpretations, and it supports previous data on the role of Ca^{2+} in chemotaxis (54, 55). We propose that microtubule protrusions might be involved in sensing external chemotactic gradients of Ag or other signals reaching mast cells at inflammatory sites.

In conclusion, our data indicate that the activation of mast cells leads to microtubule rearrangements and formation of microtubule protrusions. This process is dependent on STIM1-induced SOCE and enhanced levels of free cytoplasmic Ca^{2+} concentration, which have an important role in the regulation of microtubule dynamics, degranulation, and chemotactic response. Interference with the microtubular network via STIM1 or other Ca^{2+} regulators could potentially open new rational approaches to the treatment of inflammatory and allergic diseases.

Acknowledgments

We thank Dr. M. Hibbs (Ludwig Institute for Cancer Research, Melbourne, Australia) for BMMCL cells, Dr. T. Meyer (Department of Molecular Pharmacology, Stanford University Medical School, Stanford, CA) for YFP–hSTIM1 construct, Dr. Y. Mimori-Kiyosue (KAN Research Institute, Kyoto, Japan) for EB1-GFP construct, and Dr. A. Akhmanova (Department of Cell Biology, Erasmus Medical Center, Rotterdam, The Netherlands) for EB3-mRFP1.

Disclosures

The authors have no financial conflicts of interest.

References

1. Rivera, J., N. A. Fierro, A. Olivera, and R. Suzuki. 2008. New insights on mast cell activation via the high affinity receptor for IgE. *Adv. Immunol.* 98: 85–120.
2. Parekh, A. B., and J. W. Putney, Jr. 2005. Store-operated calcium channels. *Physiol. Rev.* 85: 757–810.
3. Smyth, J. T., W. I. Dehaven, B. F. Jones, J. C. Mercer, M. Trebak, G. Vazquez, and J. W. Putney, Jr. 2006. Emerging perspectives in store-operated Ca^{2+} entry: roles of Orai, Stim and TRP. *Biochim. Biophys. Acta* 1763: 1147–1160.
4. Roos, J., P. J. DiGregorio, A. V. Yeromin, K. Ohlsen, M. Lioudyno, S. Zhang, O. Safrina, J. A. Kozak, S. L. Wagner, M. D. Cahalan, et al. 2005. STIM1, an essential and conserved component of store-operated Ca^{2+} channel function. *J. Cell Biol.* 169: 435–445.
5. Liou, J., M. L. Kim, W. D. Heo, J. T. Jones, J. W. Myers, J. E. Ferrell, Jr., and T. Meyer. 2005. STIM is a Ca^{2+} sensor essential for Ca^{2+}-store-depletion-triggered Ca^{2+} influx. *Curr. Biol.* 15: 1235–1241.
6. Dziadek, M. A., and L. S. Johnstone. 2007. Biochemical properties and cellular localisation of STIM proteins. *Cell Calcium* 42: 123–132.
7. Prakriya, M., S. Feske, Y. Gwack, S. Srikanth, A. Rao, and P. G. Hogan. 2006. Orai1 is an essential pore subunit of the CRAC channel. *Nature* 443: 230–233.
8. Baba, Y., K. Hayashi, Y. Fujii, A. Mizushima, H. Watarai, M. Wakamori, T. Numaga, Y. Mori, M. Iino, M. Hikida, and T. Kurosaki. 2006. Coupling of STIM1 to store-operated Ca^{2+} entry through its constitutive and inducible movement in the endoplasmic reticulum. *Proc. Natl. Acad. Sci. USA* 103: 16704–16709.
9. Mercer, J. C., W. I. Dehaven, J. T. Smyth, B. Wedel, R. R. Boyles, G. S. Bird, and J. W. Putney, Jr. 2006. Large store-operated calcium selective currents due to co-expression of Orai1 or Orai2 with the intracellular calcium sensor, Stim1. *J. Biol. Chem.* 281: 24979–24990.
10. Akhmanova, A., and M. O. Steinmetz. 2008. Tracking the ends: a dynamic protein network controls the fate of microtubule tips. *Nat. Rev. Mol. Cell Biol.* 9: 309–322.
11. Grigoriev, I., S. M. Gouveia, B. van der Vaart, J. Demmers, J. T. Smyth, S. Honnappa, D. Splinter, M. O. Steinmetz, J. W. Putney, Jr., C. C. Hoogenraad, and A. Akhmanova. 2008. STIM1 is a MT-plus-end-tracking protein involved in remodeling of the ER. *Curr. Biol.* 18: 177–182.
12. Terasaki, M., L. B. Chen, and K. Fujiwara. 1986. Microtubules and the endoplasmic reticulum are highly interdependent structures. *J. Cell Biol.* 103: 1557–1568.
13. Oka, T., M. Hori, and H. Ozaki. 2005. Microtubule disruption suppresses allergic response through the inhibition of calcium influx in the mast cell degranulation pathway. *J. Immunol.* 174: 4584–4589.
14. Wu, S., H. Chen, M. F. Alexeyev, J. A. King, T. M. Moore, T. Stevens, and R. D. Balczon. 2007. Microtubule motors regulate ISOC activation necessary to increase endothelial cell permeability. *J. Biol. Chem.* 282: 34801–34808.
15. Smyth, J. T., W. I. DeHaven, G. S. Bird, and J. W. Putney, Jr. 2007. Role of the microtubule cytoskeleton in the function of the store-operated Ca^{2+} channel activator STIM1. *J. Cell Sci.* 120: 3762–3771.
16. Smith, A. J., J. R. Pfeiffer, J. Zhang, A. M. Martinez, G. M. Griffiths, and B. S. Wilson. 2003. Microtubule-dependent transport of secretory vesicles in RBL-2H3 cells. *Traffic* 4: 302–312.
17. Nishida, K., S. Yamasaki, Y. Ito, K. Kabu, K. Hattori, T. Tezuka, H. Nishizumi, D. Kitamura, R. Goitsuka, R. S. Geha, et al. 2005. FcεRI-mediated mast cell degranulation requires calcium-independent microtubule-dependent translocation of granules to the plasma membrane. *J. Cell Biol.* 170: 115–126.
18. Urata, C., and R. P. Siraganian. 1985. Pharmacologic modulation of the IgE or Ca^{2+} Ionophore A23187 mediated Ca^{2+} influx, phospholipase activation, and histamine release in rat basophilic leukemia cells. *Int. Arch. Allergy Immunol.* 78: 92–100.
19. Tasaka, K., M. Mio, K. Fujisawa, and I. Aoki. 1991. Role of microtubules on Ca^{2+} release from the endoplasmic reticulum and associated histamine release from rat peritoneal mast cells. *Biochem. Pharmacol.* 41: 1031–1037.
20. Martin-Verdeaux, S., I. Pombo, B. Iannascoli, M. Roa, N. Varin-Blank, J. Rivera, and U. Blank. 2003. Evidence of a role for Munc18-2 and microtubules in mast cell granule exocytosis. *J. Cell Sci.* 116: 325–334.
21. Sulimenko, V., E. Dráberová, T. Sulimenko, L. Macurek, V. Richterová, P. Dráber, and P. Dráber. 2006. Regulation of microtubule formation in activated mast cells by complexes of γ-tubulin with Fyn and Syk kinases. *J. Immunol.* 176: 7243–7253.
22. Oritani, K., and P. W. Kincade. 1996. Identification of stromal cell products that interact with pre-B cells. *J. Cell Biol.* 134: 771–782.
23. Nováková, M., E. Dráberová, W. Schürmann, G. Czihak, V. Viklický, and P. Dráber. 1996. γ-Tubulin redistribution in taxol-treated mitotic cells probed by monoclonal antibodies. *Cell Motil. Cytoskeleton* 33: 38–51.
24. Dráber, P., J. Zikán, and M. Vojtíšková. 1980. Establishment and characterization of permanent murine hybridomas secreting monoclonal anti-thy-1 antibodies. *J. Immunogenet.* 7: 455–474.

25. Mimori-Kiyosue, Y., N. Shiina, and S. Tsukita. 2000. The dynamic behavior of the APC-binding protein EB1 on the distal ends of microtubules. *Curr. Biol.* 10: 865–868.
26. Campbell, R. E., O. Tour, A. E. Palmer, P. A. Steinbach, G. S. Baird, D. A. Zacharias, and R. Y. Tsien. 2002. A monomeric red fluorescent protein. *Proc. Natl. Acad. Sci. USA* 99: 7877–7882.
27. Surviladze, Z., L. Dráberová, M. Kovářová, M. Boubelík, and P. Dráber. 2001. Differential sensitivity to acute cholesterol lowering of activation mediated via the high-affinity IgE receptor and Thy-1 glycoprotein. *Eur. J. Immunol.* 31: 1–10.
28. Dráberová, L. 1990. Cyclosporin A inhibits rat mast cell activation. *Eur. J. Immunol.* 20: 1469–1473.
29. Laemmli, U. K. 1970. Cleavage of structural proteins during the assembly of the head of bacteriophage T_4. *Nature* 227: 680–685.
30. Dráber, P., L. A. Lagunowich, E. Dráberová, V. Viklický, and I. Damjanov. 1988. Heterogeneity of tubulin epitopes in mouse fetal tissues. *Histochemistry* 89: 485–492.
31. Dráberová, E., and P. Dráber. 1993. A microtubule-interacting protein involved in coalignment of vimentin intermediate filaments with microtubules. *J. Cell Sci.* 106: 1263–1273.
32. Soile, P. 2003. *Morphological Image Analysis – Principles and Applications.* Springer Verlag, Berlin.
33. Breu, H., D. Kirkpatrick, and M. Werman. 1995. Linear time euclidean distance transform algorithms. *IEEE Trans. Pattern Anal. Mach. Intell.* 17: 529–533.
34. Zick, Y., and R. Sagi-Eisenberg. 1990. A combination of H_2O_2 and vanadate concomitantly stimulates protein tyrosine phosphorylation and polyphosphoinositide breakdown in different cell lines. *Biochemistry* 29: 10240–10245.
35. Teshima, R., H. Ikebuchi, M. Nakanishi, and J. Sawada. 1994. Stimulatory effect of pervanadate on calcium signals and histamine secretion of RBL-2H3 cells. *Biochem. J.* 302: 867–874.
36. Thastrup, O., P. J. Cullen, B. K. Drøbak, M. R. Hanley, and A. P. Dawson. 1990. Thapsigargin, a tumor promoter, discharges intracellular Ca^{2+} stores by specific inhibition of the endoplasmic reticulum Ca^{2+}-ATPase. *Proc. Natl. Acad. Sci. USA* 87: 2466–2470.
37. Paolini, R., M. H. Jouvin, and J. P. Kinet. 1991. Phosphorylation and dephosphorylation of the high-affinity receptor for immunoglobulin E immediately after receptor engagement and disengagement. *Nature* 353: 855–858.
38. Gilfillan, A. M., and J. Rivera. 2009. The tyrosine kinase network regulating mast cell activation. *Immunol. Rev.* 228: 149–169.
39. Bakowski, D., M. D. Glitsch, and A. B. Parekh. 2001. An examination of the secretion-like coupling model for the activation of the Ca^{2+} release-activated Ca^{2+} current I_{CRAC} in RBL-1 cells. *J. Physiol.* 532: 55–71.
40. Galli, S. J., M. Tsai, and A. M. Piliponsky. 2008. The development of allergic inflammation. *Nature* 454: 445–454.
41. Schwartz, M. A., M. D. Schaller, and M. H. Ginsberg. 1995. Integrins: emerging paradigms of signal transduction. *Annu. Rev. Cell Dev. Biol.* 11: 549–599.
42. Lam, V., J. Kalesnikoff, C. W. Lee, V. Hernandez-Hansen, B. S. Wilson, J. M. Oliver, and G. Krystal. 2003. IgE alone stimulates mast cell adhesion to fibronectin via pathways similar to those used by IgE + antigen but distinct from those used by Steel factor. *Blood* 102: 1405–1413.
43. Calloway, N., M. Vig, J. P. Kinet, D. Holowka, and B. Baird. 2009. Molecular clustering of STIM1 with Orai1/CRACM1 at the plasma membrane depends dynamically on depletion of Ca^{2+} stores and on electrostatic interactions. *Mol. Biol. Cell* 20: 389–399.
44. Honnappa, S., S. M. Gouveia, A. Weisbrich, F. F. Damberger, N. S. Bhavesh, H. Jawhari, I. Grigoriev, F. J. van Rijssel, R. M. Buey, A. Lawera, et al. 2009. An EB1-binding motif acts as a microtubule tip localization signal. *Cell* 138: 366–376.
45. Sampieri, A., A. Zepeda, A. Asanov, and L. Vaca. 2009. Visualizing the store-operated channel complex assembly in real time: identification of SERCA2 as a new member. *Cell Calcium* 45: 439–446.
46. Cahalan, M. D. 2009. STIMulating store-operated Ca^{2+} entry. *Nat. Cell Biol.* 11: 669–677.
47. Wu, M. M., J. Buchanan, R. M. Luik, and R. S. Lewis. 2006. Ca^{2+} store depletion causes STIM1 to accumulate in ER regions closely associated with the plasma membrane. *J. Cell Biol.* 174: 803–813.
48. Ribeiro, C. M., J. Reece, and J. W. Putney, Jr. 1997. Role of the cytoskeleton in calcium signaling in NIH 3T3 cells. An intact cytoskeleton is required for agonist-induced $[Ca^{2+}]$i signaling, but not for capacitative calcium entry. *J. Biol. Chem.* 272: 26555–26561.
49. Hesketh, T. R., M. A. Beaven, J. Rogers, B. Burke, and G. B. Warren. 1984. Stimulated release of histamine by a rat mast cell line is inhibited during mitosis. *J. Cell Biol.* 98: 2250–2254.
50. Price, L. S., M. Langeslag, J. P. ten Klooster, P. L. Hordijk, K. Jalink, and J. G. Collard. 2003. Calcium signaling regulates translocation and activation of Rac. *J. Biol. Chem.* 278: 39413–39421.
51. Palazzo, A. F., T. A. Cook, A. S. Alberts, and G. G. Gundersen. 2001. mDia mediates Rho-regulated formation and orientation of stable microtubules. *Nat. Cell Biol.* 3: 723–729.
52. Mullins, F. M., C. Y. Park, R. E. Dolmetsch, and R. S. Lewis. 2009. STIM1 and calmodulin interact with Orai1 to induce Ca^{2+}-dependent inactivation of CRAC channels. *Proc. Natl. Acad. Sci. USA* 106: 15495–15500.
53. Srikanth, S., H. J. Jung, K. D. Kim, P. Souda, J. Whitelegge, and Y. Gwack. 2010. A novel EF-hand protein, CRACR2A, is a cytosolic Ca^{2+} sensor that stabilizes CRAC channels in T cells. *Nat. Cell Biol.* 12: 436–446.
54. Hartmann, K., B. M. Henz, S. Krüger-Krasagakes, J. Köhl, R. Burger, S. Guhl, I. Haase, U. Lippert, and T. Zuberbier. 1997. C3a and C5a stimulate chemotaxis of human mast cells. *Blood* 89: 2863–2870.
55. Hofstra, C. L., P. J. Desai, R. L. Thurmond, and W. P. Fung-Leung. 2003. Histamine H4 receptor mediates chemotaxis and calcium mobilization of mast cells. *J. Pharmacol. Exp. Ther.* 305: 1212–1221.

VI.1.1

Supplementary data for:

Hájková Z., Bugajev V., Dráberová E., **Vinopal S.**, Dráberová L., Janáček J., Dráber Pe., Dráber Pa. (2011). STIM1-directed reorganization of microtubules in activated mast cells. J Immunol. *186*, 913-923.

Fig. S1

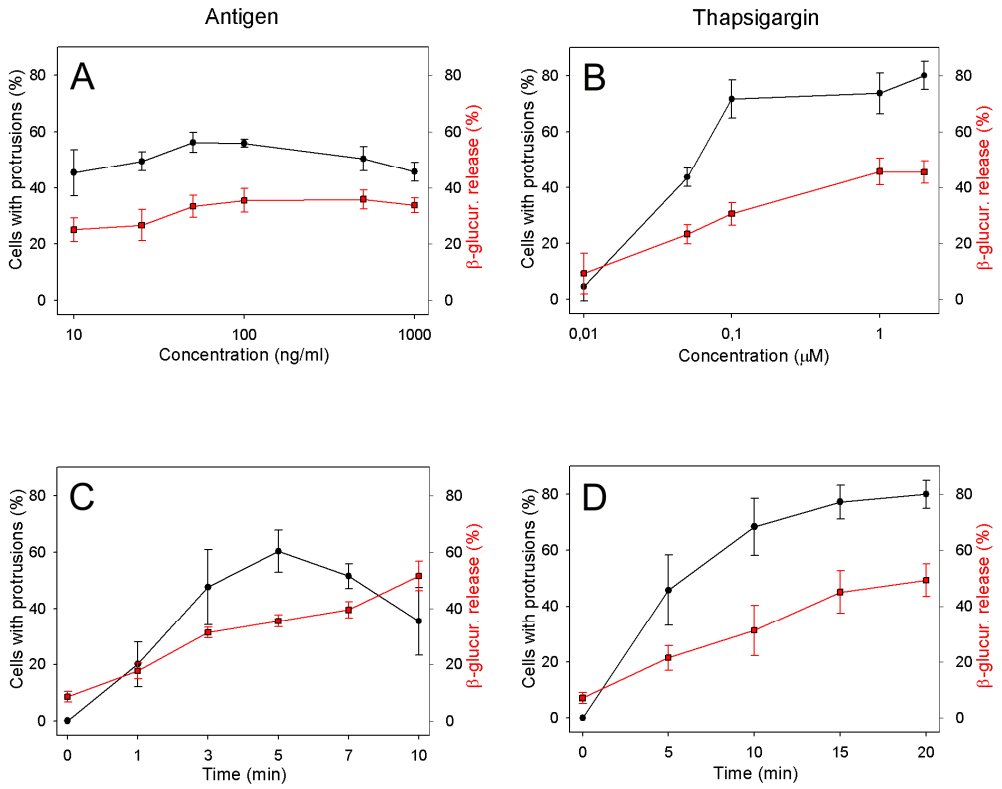

FIGURE S1. Correlation between formation of microtubule protrusions and degranulation in activated mast cells. Control or activated BMMCL cells were either fixed and stained for β-tubulin or used for determination of β-glucuronidase release. (A) IgE-sensitized (1 μg/ml) cells activated with different concentrations of Ag for 5 min. (B) Cells activated with different concentration of thapsigargin for 20 min. (C) IgE-sensitized cells activated with Ag (100 ng/ml) for various time intervals. (D) Cells activated with thapsigargin (2 μM) for various time. Three independent experiments were performed, each involving 500 cells and examined for the presence of microtubule protrusions. Values indicate means ± SD (n=3). Data for β-glucuronidase release represent means ± SD (n=3).

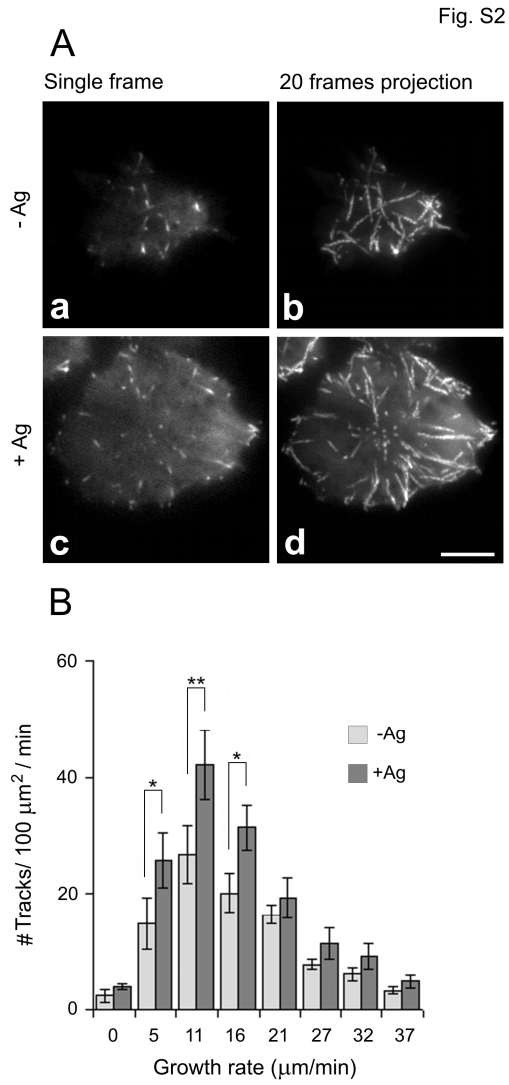

FIGURE S2. Activation of mast cells with Ag increases the number of growing microtubules in cell periphery as determined by TIRFM time-lapse imaging. (A) Time-lapse imaging of resting (a-b) and FcεRI aggregation-activated (c-d) BMMCL cells expressing EB1-GFP. Still images of EB1 (a, c) and tracks of EB1 comets over 20 sec created by maximum intensity projection of the 20 consecutive frames (b, d). Scale bar, 5 µm. (B) Histogram of microtubule growth rates in cell periphery of resting (-Ag) and Ag-activated (+Ag) cells. Total 10 different cells were tracked in 3 independent experiments. Values indicate mean ± SE, n=10 (*, $p<0.05$;**, $p<0.01$).

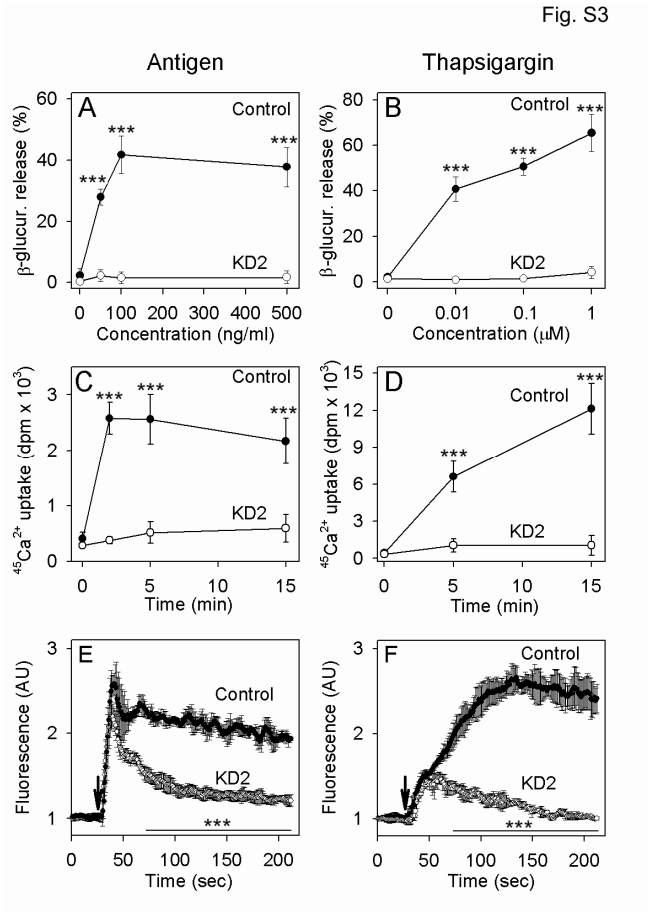

FIGURE S3. Degranulation and Ca^{2+} responses in cells with reduced STIM1 levels. (A-B) Changes in the degree of degranulation quantified as β-glucuronidase release. IgE-sensitized (1 μg/ml) cells infected with empty pLKO.1 vector (Control) or cells with reduced STIM1 after infection with shRNA2 (KD2) were activated with different concentrations of DNP-albumin for 30 min (A) or thapsigargin for 20 min (B) and the release of β-glucuronidase was determined. Data in (A) and (B) represent means ± SD (n=3, both for controls and KD2). (C-D) Changes in $^{45}Ca^{2+}$ uptake. IgE-sensitized (1 μg/ml) control cells (empty pLKO.1vector) or STIM1 KD2 cells were activated for various time intervals with 100 ng/ml DNP-albumin (C) or 2 μM thapsigargin (D) in the presence of extracellular $^{45}Ca^{2+}$ (1 mM). Data in (C) and (D) represent means ± SD (n=6, both for controls and KD2). (E-F) Changes in intracellular Ca^{2+} mobilization. IgE-sensitized (1 μg/ml) control cells (empty pLKO.1vector) or STIM1 KD2 cells loaded with Fluo 3-AM were activated (arrows) by 100 ng/ml DNP-albumin (E) or 2 μM thapsigargin (F). Data in (E) and (F) represent means ± SD (n=3, both for controls and KD2). (***, $p<0.001$; in E and F the line under asterisks indicate time interval of significant differences).

Movie S1. Time-lapse imaging of EB1-GFP in quiescent cells. BMMCL cells were imaged, with 0.5 s exposure time and 1 s interval between frames, for 3 min in TIRFM.
(http://www.jimmunol.org/content/suppl/2010/12/15/jimmunol.1002074.DC1/1.mov)

Movie S2. Time-lapse imaging of EB1-GFP in thapsigargin activated cells. BMMCL cells were imaged, with 0.5s exposure time and 1 s interval between frames, for 3 min in TIRFM. Imaging started 13 min after addition of thapsigargin at final concentration 2 μM.
(http://www.jimmunol.org/content/suppl/2010/12/15/jimmunol.1002074.DC1/2.mov)

Movie S3. Time-lapse imaging of YFP-hSTIM1 in quiescent cells. BMMCL cells were imaged, with 0.5s exposure time and 1 s interval between frames, for 3 min in TIRFM.
(http://www.jimmunol.org/content/suppl/2010/12/15/jimmunol.1002074.DC1/3.mov)

Movie S4. Time-lapse imaging of YFP-hSTIM1 in the course of thapsigargin activation of cells. BMMCL cells were imaged, with 0.5s exposure time and 1 s interval between frames, for 3 min in TIRFM. Thapsigargin was added 30s after starting the movie.
http://www.jimmunol.org/content/suppl/2010/12/15/jimmunol.1002074.DC1/4.mov)

Movie S5. Time-lapse imaging of YFP-hSTIM1 and EB3-mRFP1 in the course of nocodazole treatment of cells, folowed by thapsigargin activation. BMMCL cells were imaged, with exposure time ranging from 0.5-0.8s and 2 s interval between frames, for 3 min in TIRFM. Nocodazole and thapsigargin were added to the final concentration of 10 μM and 2 μM, respectively. Elapsed time in minutes and seconds is depicted in the upper right.
(http://www.jimmunol.org/content/suppl/2010/12/15/jimmunol.1002074.DC1/5.mov)

VI.2

Dráberová E., **Vinopal S**., Morfini G., Liu P.S., Sládková V., Sulimenko T., Burns M.R., Solowska J., Kulandaivel K., de Chadarévian J.P., Legido A., Mörk S.J., Janáček J., Baas P.W., Dráber P., Katsetos C.D. (2011). Microtubule-severing ATPase spastin in glioblastoma: increased expression in human glioblastoma cell lines and inverse roles in cell motility and proliferation. J Neuropathol Exp Neurol. *70*, 811-826.

J Neuropathol Exp Neurol

Vol. 70, No. 9
September 2011
pp. 811–826

ORIGINAL ARTICLE

Microtubule-Severing ATPase Spastin in Glioblastoma: Increased Expression in Human Glioblastoma Cell Lines and Inverse Roles in Cell Motility and Proliferation

Eduarda Dráberová, PhD, Stanislav Vinopal, MSc, Gerardo Morfini, PhD, Pei S. Liu, MMS, Vladimíra Sládková, MSc, Tetyana Sulimenko, MSc, Matthew R. Burns, BA, Joanna Solowska, PhD, Kandan Kulandaivel, MD, Jean-Pierre de Chadarévian, MD, FRCPC, Agustin Legido, MD, PhD, Sverre J. Mörk, MD, PhD, Jiří Janáček, PhD, Peter W. Baas, PhD, Pavel Dráber, PhD, and Christos D. Katsetos, MD, PhD, FRCPath

Abstract

We studied the expression and distribution of the microtubule-severing enzyme spastin in 3 human glioblastoma cell lines (U87MG, U138MG, and T98G) and in clinical tissue samples representative of all grades of diffuse astrocytic gliomas (n = 45). In adult human brains, spastin was distributed predominantly in neurons and neuropil puncta and, to a lesser extent, in glia. Compared with normal mature brain tissues, spastin expression and cellular distribution were increased in neoplastic glial phenotypes, especially in glioblastoma ($p < 0.05$ vs low-grade diffuse astrocytomas). Overlapping punctate and diffuse patterns of localization were identified in tumor cells in tissues and in interphase and mitotic cells of glioblastoma cell lines. There was enrichment of spastin in the leading edges of cells in T98G glioblastoma cell cultures and in neoplastic cell populations in tumor specimens. Real-time polymerase chain reaction and immunoblotting experiments revealed greater levels of spastin messenger RNA and protein expression in the glioblastoma cell lines versus normal human astrocytes. Functional experiments indicated that spastin depletion resulted in reduced cell motility and higher cell proliferation of T98G cells. To our knowledge, this is the first report of spastin involvement in cell motility. Collectively, our results indicate that spastin expression in glioblastomas might be linked to tumor cell motility, migration, and invasion.

Key Words: Astrocyte, Brain tumor, Cell motility, Glioblastoma, Glioma, Microtubule severing, Spastin.

From the Department of the Biology of Cytoskeleton, Institute of Molecular Genetics (ED, SV, VS, TS, PD) and Department of Biomathematics, Institute of Physiology, Academy of Sciences of the Czech Republic (JJ), Prague, Czech Republic; Departments of Neurology (PSL, KK, AL, CDK), Pediatrics (AL, CDK), Pathology and Laboratory Medicine (J-PdC, CDK), and Neurobiology and Anatomy (JS, PWB), Drexel University College of Medicine, St. Christopher's Hospital for Children (J-PdC, AL, CDK) and Hahnemann University Hospital (CDK), Philadelphia, PA; Department of Anatomy and Cell Biology (GM, MRB), University of Illinois at Chicago, Chicago, IL; The Gade Institute, Department of Pathology (SJM), University of Bergen, Haukeland University Hospital, Bergen, Norway.

Send correspondence and reprint requests to: Christos D. Katsetos, MD, PhD, FRCPath, Section of Neurology, St. Christopher's Hospital for Children, Erie Ave at Front St, Philadelphia, PA 19134; E-mail: Christos.Katsetos@drexelmed.edu

Drs Dráberová and Katsetos contributed equally to this work.

This study was supported in part by grants from the Czech Science Foundation (P302/10/1701 to Eduarda Dráberová, 204/09/1777 to Pavel Dráber, and 204/09/H084 to Stanislav Vinopal), from the Grant Agency ASCR (KAN200520701 to Vladimíra Sládková), and from the Ministry of Education, Youth and Sports of the Czech Republic (LC545). This study was also supported by institutional research grants to Pavel Dráber (AVOZ 50520514) and Jiří Janáček (AVOZ 50110509); by a National Institutes of Health grant (R01 NS066942A) and an ALS Therapy Alliance research grant to Gerardo Morfini; by a National Institutes of Health grant (RO1 NS28785), a National Science Foundation grant (0841245), and a grant from the State of Pennsylvania Tobacco Settlement Funds to Peter W. Baas; and by a grant from the St. Christopher's Foundation for Children to Christos D. Katsetos (203).

Supplemental digital content is available for this article. Direct URL citations appear in the printed text and are provided in the HTML and PDF versions of this article on the journal's Web site (www.jneuropath.com).

INTRODUCTION

Gliomas are the most frequent group of central nervous system (CNS) neoplasms, accounting for more than 70% of all brain tumors (1). Diffuse gliomas are particularly ominous forms because they are highly invasive within the brain and are difficult to treat. Glioblastoma multiforme (GBM) is the most common and malignant, as well as the deadliest, glioma in adults (1).

One of the most effective strategies for treating malignant tumors has focused on disrupting the integrity of the microtubule system and preventing mitotic division (2–4). Microtubules are dynamic polymers that undergo rapid bouts of assembly and disassembly during interphase and then reorganize into a bipolar spindle during mitosis (5). Targeting microtubules represents a strategy for attenuating the invasive properties of tumor cells because these cytoskeletal structures are implicated in tumor cell motility, the formation of long dynamic protrusions (6), and the elongation of invadopodia (7). Unfortunately, despite the potential usefulness of a new generation of tubulin-binding agents from the bench to the bedside, the emergence of drug-resistant tumor cells remains an overriding problem that contributes to treatment failures (8). As a result, the efficacy of drugs such as the taxanes, which aggressively stabilize microtubules in tumor

cells, is hindered by the development of resistance ascribed, in part, to cytoskeletal alterations; these include the aberrant overexpression of class III β-tubulin isotype (4, 9–11). Moreover, many of these drugs do not readily cross the blood-brain barrier (12), whereas they also exert deleterious effects on host neural tissues, as exemplified in paclitaxel-induced peripheral neuropathy (13). Hence, there is great urgency in expanding the body of knowledge about the regulation of microtubules in cancer cells so that more sophisticated strategies can be developed.

A number of different proteins affect the dynamic properties of the microtubules, such as stathmin, which promotes microtubule disassembly, and the classic microtubule-associated proteins, which promote their assembly and stabilization (14). Molecular motor proteins are also needed to organize microtubules into higher-level structures such as the mitotic spindle; motor proteins such as kinesin-5 have recently been proposed as potential targets for anticancer drugs (15, 16). Another category of microtubule-related proteins is endowed with the specialized property of severing or breaking the lattice of microtubules, but to date, these proteins have received little attention in the context of cancer. These so-called microtubule-severing proteins are enzymes capable of severing long microtubules generated at the centrosome by breaking the microtubules into short pieces that are able to translocate through the axonal and glial cytoplasm (5, 17).

The microtubule-severing protein spastin, encoded by the *SPG4* gene, is a member of the ATPases associated with various cellular activities (AAA) family of proteins. Spastin has a 220-amino acid AAA domain at its carboxy terminus, as well as other functional domains (18). A microtubule-interacting and endosomal-trafficking domain is located at the amino terminus; whereas the microtubule-binding domain comprises amino acids 270 to 328 (19). Two functional nuclear localization signals responsible for targeting to the nucleus and 2 nuclear export signals have also been identified, but their functional significance is not understood (18). Biochemical and cell biologic experiments demonstrated that both microtubule-binding domain and AAA domains are essential for the microtubule-severing activity of spastin (19).

Various spastin isoforms with heterogeneous patterns of distribution among different tissues have been demonstrated (20). These isoforms mainly result from a combination of translation at 2 different start codons (18, 21) and the inclusion/exclusion of exons 4, 8, and 15 within these transcripts (20). Distribution studies in rat tissue showed that the longest spastin isoform (hereafter referred to as M1) is selectively expressed in the adult spinal cord, whereas the shorter isoform (referred to as M87) has a more ubiquitous tissue distribution (22). To date, the main interest in spastin has derived from the fact that mutations in this gene account for 40% of cases of hereditary spastic paraplegias (23).

In the normal human and mouse CNS, spastin is expressed constitutively in neurons (24, 25), but induced spastin expression has been reported in reactive astrocytes of the hippocampus in pilocarpine-induced status epilepticus (25). To our knowledge, the expression of spastin in brain tumors, in general, and in gliomas, in particular, is hitherto unknown. Given the role of microtubules on the invasive properties of tumor cells and the high propensity of GBM cells for brain invasion, we hypothesized that the microtubule-severing ATPase spastin might be aberrantly expressed and/or regulated in these cells. To test this hypothesis, we evaluated the expression levels and the intracellular distribution of spastin in human GBM cell lines and in surgically excised tumor samples representative of all grades of diffuse astrocytic gliomas. In addition, we performed functional experiments to evaluate the effects of spastin depletion on cell motility and proliferation in GBM cells.

MATERIALS AND METHODS

Cell Lines

All cell lines were obtained from American Type Culture Collection (Manassas, VA). Human GBM cell lines T98G, U87MG, and U138MG; human neuroblastoma cell lines SH-SY5Y and SK-N-SH; as well as human embryonic kidney (HEK) cells were maintained in Dulbecco modified Eagle medium (Invitrogen, Prague, Czech Republic) containing 10% fetal bovine serum (PAA Laboratories, Cölbe, Germany), 4 mmol/L L-glutamine, and antibiotics. SH-SY5Y cells were cultivated for 4 days in the presence of 1 μmol/L of all *trans*-retinoic acid (Sigma-Aldrich, Prague, Czech Republic) to induce neurite formation (26). Proliferating non-immortalized, nontransformed human fetal astrocytes, isolated from the cerebral hemisphere of an 18 gestational week human male fetus were purchased as ''Clonetics Astrocyte Cell System'' from Cambrex Bio Science (Walkersville, MD) and cultivated as previously described (27).

Antibodies

A rabbit polyclonal antibody (Sp/AAA) (22) and 2 mouse monoclonal antibodies, Sp3G11/1 (catalog no. MAB5634; Millipore, Temecula, CA) and Sp6C6 (catalog no. S7074 [Sigma-Aldrich] and catalog no. sc-81624 [Santa Cruz Biotechnology, Santa Cruz, CA]), were used for immunohistochemistry, immunofluorescence, and immunoblotting experiments. The Sp/AAA antibody was raised against the recombinant fragment coding mouse spastin polypeptide (amino acids [a.a.] 337–446) (22); the Sp3G11/1 (IgG2a) was prepared using full-length recombinant human spastin for immunization. For the preparation of antibody Sp6C6 (IgG2a), the recombinant human M87 spastin lacking the 32 amino acids encoded by exon 4 (a.a. 197–228) was used as an immunogen (21) (Fig. 1). Mouse monoclonal antibody TU-01 to α-tubulin (IgG1) (28, 29) and affinity-purified polyclonal rabbit antibody to αβ-tubulin dimer (30) were described previously. A rabbit antibody to actin and a mouse monoclonal antibody to Golgi matrix protein GM-130 were purchased from Sigma-Aldrich and BD Biosciences (San Jose, CA), respectively. A rabbit antibody to kinesin-like protein KIF11 (Eg5) was from Cytoskeleton, Inc (Denver, CO). 5Cy3-conjugated anti-mouse and anti-rabbit antibodies and DY 488–conjugated anti-mouse and anti-rabbit antibodies for multiple staining were obtained from Jackson Immunoresearch Laboratories (West Grove, PA). Horseradish peroxidase (HRP)–conjugated anti-mouse and anti-rabbit antibodies were obtained from Promega (Madison, WI).

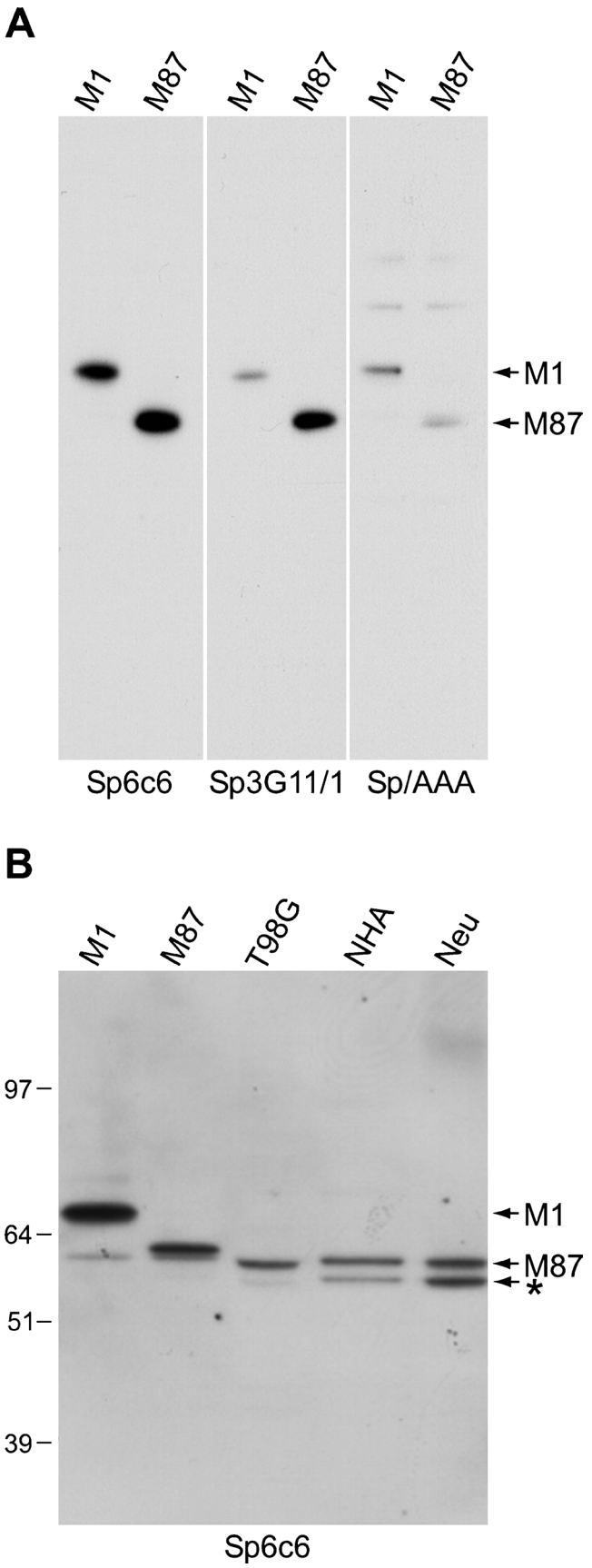

RNA Silencing

T98G cells in 24-well plates were transfected with small interfering RNAs (siRNA; final concentration, 20 nmol/L) using Lipofectamine RNAi MAX (Invitrogen) according to the manufacturer's instructions. Two Silencer Select siRNAs (Applied Biosystems/Ambion, Prague, Czech Republic) that target regions present in all human spastin isoforms (siRNA 1, 5′-CAACCTTGCTAACCTTATA-3′; and siRNA 2, 5′-GGA AGUCCATTGACCCAAA-3′) were used. dTdT overhangs were added to the 3′ of the oligomers with the exception of siRNA 1 antisense strand where dCdT overhang was used. The maximal depletion was reached 48 to 72 hours after siRNA transfection. Negative control siRNA was from Ambion (Silencer Negative Control 1 siRNA).

Real-Time Quantitative Polymerase Chain Reaction

Total RNA from GBM cell lines and normal human astrocytes (NHAs) was isolated by the RNeasy Mini kit (QIAGEN, Valencia, CA). Aliquots of 1 μg of total RNA in a 20-μl reaction mixture were converted to complementary DNA (cDNA) using the ImProm-II RT kit (Promega) with random hexamers in a 20-μL reaction volume. These cDNA reaction mixtures were diluted 5 times in diethyl pyrocarbonate-treated water to prevent inhibition of Taq polymerase in a subsequent polymerase chain reaction (PCR). One microliter of diluted cDNA product was used for each PCR. Amplifications were performed in 10-μL PCR mixtures containing QuantiTect SYBR Green PCR Master Mix (QIAGEN) and 0.5 μmol/L of each human gene-specific primers for spastin (*SPAST*; National Center for Biotechnology Information RefSeq ID: NM_014946 and NM_199436; primers anneal to both M1 and M87 transcript isoforms) or β-actin (*ACTB*; National Center for Biotechnology Information RefSeq ID: NM_001101). Primer sequences were as follows: spastin forward 5′-TCAGGCTGGT CTTGAACTCC-3′, reverse 5′-ATGCATCTTCTGGCTGGG-3′; and β-actin forward 5′-TCCTTCCTGGGCATGGAGT-3′, reverse 5′-AAAGCCATGCCAATCTCATC-3′. Oligonucleotides

FIGURE 1. (A) Reactivity of antibodies used in this study with spastin isoforms. Human embryonic kidney (HEK) cells were infected with lentiviral vectors encoding full-length versions of human M1 and M87 spastin isoforms; lysates derived from these cells were probed with anti-spastin antibodies Sp6C6, Sp3G11/1, and Sp/AAA. All antibodies similarly recognized overexpressed M1 and M87 spastin isoforms. **(B)** Lysates of HEK cells overexpressing full-length M1 or M87 spastin as in **A** were run along with lysates derived from T98G human glioblastoma cells, normal human astrocytes (NHAs), and cultured cortical neurons (Neu). Samples were run on Bis-Tris sodium dodecyl sulfate–polyacrylamide gel electrophoresis to increase M1/M87 separation. Under these gel conditions, immunoblotting with Sp6C6 antibody indicates that T98G cells, NHA, and cultured cortical neurons all predominantly express the spastin M87 isoform. A faint Sp6C6-immunoreactive band running at a slightly lower molecular weight than full-length M87 (asterisk) was observed in T98G cells. This band likely represents the M87 isoform without exon 4 (M87 Δ Ex. 4) (20) and was more prominent in NHA and cultured cortical neurons.

were from East Port (Prague, Czech Republic). Real-time quantitative PCRs were carried out on MasterCycler RealPlex (Eppendorf, Wesseling-Berzdorf, Germany) as described (27). Experiments were performed twice with triplicate samples (cDNA isolated from 3 separate cultures of tested cells). The expression of analyzed genes was normalized to the expression of β-actin. Levels of β-actin did not differ significantly between cell lines and NHAs. The identity of spastin PCR product was verified by cDNA sequencing. Statistical analysis was performed with the Student unpaired *t*-test.

Spastin Constructs

Full-length human spastin constructs M1 (Swiss-Prot identifier Q9UBP0-1, 616 a.a.) and M87 (Swiss-Prot identifier Q9UBP0-3, 530 a.a) were subcloned in the lentiviral plasmid vector FCbAGW-IRES-GFP (D. Huang and G. Morfini, unpublished data). Lentiviral constructs were cotransfected into 293T HEK cells, along with VSVg and ΔR8.9 envelope and packaging plasmids by calcium phosphate transfection. Viral supernatants were harvested 24 to 36 hours after transfection, concentrated by ultracentrifugation, resuspended in sterile phosphate-buffered saline (PBS), and stored at −80°C. HEK cells were then infected with functional lentivirus at a multiplicity of infection of 100. HEK cells lysates were obtained 72 hours after infection. Lysates derived from HEK cells overexpressing full-length M1 and M87 spastin isoforms facilitated the identification of specific spastin isoforms in immunoblots.

Gel Electrophoresis and Immunoblotting

Whole-cell extracts were prepared by washing the cells in cold PBS, solubilizing them in hot sodium dodecyl sulfate (SDS) sample buffer (31) and boiling for 5 minutes. Proteins were separated by SDS–polyacrylamide gel electrophoresis (PAGE) on 7.5% Tris gels and transferred to nitrocellulose membranes. Cultured T98G cells, NHA, and cortical neurons were lysed in 1% SDS, and protein concentration was measured using a BCA protein assay kit (catalog no. 23225; Pierce, Rockford, IL). Lysates were run on NuPAGE Novex 4% to 12% Bis-Tris gels (to increase M1/M87 separation) and were transferred to PDF membranes. Details on the immunoblotting procedure have been described elsewhere (32). Monoclonal antibodies to spastin (Sp6C6, Sp3G11/1) and polyclonal antibody to actin were diluted 1:1000 and 1:3000, respectively. The polyclonal anti-spastin antibody (Sp/AAA) was diluted from 1:2000 to 1:20000. The polyclonal antibody to Eg5 was diluted 1:5000. Monoclonal antibody to α-tubulin (TU-01) was used as an undiluted hybridoma culture supernatant. Primary antibodies were detected after incubating the blots with HRP-conjugated secondary antibody diluted 1:10,000. The HRP signal was detected with chemiluminescence reagents (Pierce) in accordance with the manufacturer's instructions.

Immunofluorescence on Cell Lines

Immunofluorescence microscopy on fixed cells was performed as described previously (33). Briefly, cells grown on coverslips were rinsed with a microtubule-stabilizing buffer (MSB; 1 mol/L Mes adjusted to pH 6.9 with KOH, 2 mM EGTA, 2 mM $MgCl_2$) supplemented with 4% polyethylene glycol 6000, fixed for 20 minutes in 3% formaldehyde in MSB, and thereafter extracted for 4 minutes in 0.5% Triton X-100 in MSB. Anti-spastin antibodies Sp/AAA, Sp3G11/1, and Sp6C6 were diluted 1:1000, 1:100, and 1:100, respectively. Antibodies to GM130 and tubulin were diluted 1:100 and 1:20, respectively. Cy3-conjugated anti-mouse and anti-rabbit antibodies were diluted 1:500. DY 488–conjugated anti-mouse and anti-rabbit antibodies were diluted 1:100. Fluorescein isothiocyanate–conjugated phalloidin (Sigma-Aldrich) was used at a concentration of 0.2 μg/ml to detect microfilaments. 4,6-Diamidino-2-phenylindole was used to label cell nuclei. Preparations were mounted in MOWIOL 4–88 (Calbiochem, San Diego, CA) and examined with a microscope (A70 Provis; Olympus Optical Co., Hamburg, Germany). Conjugates alone did not give any detectable immunoreactivity.

Time-Lapse Imaging

T98G cells were transfected with either spastin-specific siRNA or negative control siRNA as described previously. Seventy-two hours after transfection, cells were detached, counted, and diluted in culture media. A total of 2×10^4 transfected cells were plated in a single well of a 6-well tissue culture dish and allowed to adhere for 24 hours. Cells were thereafter incubated in medium containing Hoechst 33342 (Sigma-Aldrich) at a final concentration of 0.5 μg/mL and imaged by 10×/NA 0.30 dry objective on a microscope (IX-81; Olympus) equipped with platform for live cell imaging, motorized stage and objectives, and a temperature-controlled chamber at 37°C and 5% CO_2. Images were obtained in a bright-field channel to visualize whole cells and in a fluorescence channel (excitation, 350 nm; emission: 460 nm) to visualize nuclei. The total imaging time was 10 hours with 10-minute intervals. For each experiment, time-lapse sequences of 10 different fields were acquired for negative control or spastin-depleted cells (n = 3). Time-lapse sequences were adjusted, and nuclei movement was analyzed using an object-tracking plug-in written in-house; 8-bit grayscale images were used for nuclei detection. Images were initially smoothed by Gaussian filter (σ = 2 pixels) to increase the signal-to-noise ratio. Then the morphologic opening by octagon (16 pixels wide) grayscale opening with cone (slope = 4 gray levels per pixel) and Gaussian smoothing (σ = 2 pixels) were applied to simplify the images and to filter out small artifacts. Maxima of the image intensity were then detected by morphologic reconstruction, and coordinates of nuclei were calculated as centers of mass of the maxima dilated by an octagon 20 pixels wide (34). The corresponding nuclei in subsequent images were detected by pairing the mutually closest particles with a distance less than 100 pixels. The particle trajectories were constructed from corresponding particles connecting the mutually closest ends and origins of trajectories with a time interval less than 6 frames and with a distance less than 100 pixels. The speed of particles was calculated as the ratio of the particle trajectory length to the trajectory duration. The algorithms were implemented as plug-in modules of the Ellipse program, version 2.07 (ViDiTo Systems, Košice, Slovakia). Statistical analysis was performed with the Student 2-tailed unpaired *t*-test using Microsoft Excel (Microsoft Corp, Redmond, WA).

Evaluation of Cell Growth

Cell proliferation was assessed by manual cell counting of T98G cells transfected with either spastin-specific siRNA or negative control siRNA. Twenty-four hours after transfection, cells were detached, diluted in culture medium, and counted. A total of 2×10^5 transfected cells were plated on a 6-cm-diameter Petri dish. Cells were counted at various time intervals from 2 to 6 days after transfection. Samples were counted in doublets in a total of 3 independent experiments.

Clinical Tumor Samples

Formaldehyde-fixed, paraffin-embedded biopsy/resection samples from adults (n = 37) and children (n = 8) representative of all World Health Organization (WHO) grades of astrocytic gliomas (WHO grades I–IV; n = 45) were collected retrospectively from the Gade Institute, Department of Pathology, University of Bergen, Haukeland Hospital (Bergen, Norway); Department of Pathology, University of Patras Hospital (Rion, Patras, Greece); and St. Christopher's Hospital for Children (Philadelphia, PA) under the approval by an institutional review board (IRB) exempt review (Drexel University IRB protocol no. 16660). A number of tumor specimens used in this study were also used in previous studies (35–37).

Histologic classification was according to the recommendations of the 2007 WHO classification of tumors of the CNS (38). Tumor specimens from adult patients included low-grade diffuse astrocytomas (WHO grade II; n = 7), anaplastic astrocytomas (WHO grade III; n = 5), and GBM (WHO grade IV; n = 25). Pediatric glioma specimens included diffuse gliomas (WHO grade II) of the cerebral hemispheric white matter (n = 2) and brainstem (n = 2) and anaplastic gliomas of the thalamus and brainstem (WHO grade III; n = 4). Histologic features of the tumor samples were evaluated independently by 2 neuropathologists (Sverre J. Mörk and Christos D. Katsetos) and a pediatric pathologist (Jean-Pierre de Chadarévian) who were blinded to the original histopathologic diagnosis for each specimen.

Five-micrometer-thick microtome sections from archived formalin-fixed, paraffin-embedded tissue blocks were placed on electromagnetically charged slides and stained with hematoxylin and eosin for morphologic evaluation. Adjacent, serially cut, and sequentially numbered sections were processed for immunohistochemistry.

Control tissues included surgical and autopsy tissue samples from cases devoid of tumor (n = 10). Nonneoplastic cerebral and cerebellar autopsy tissue samples (n = 10) were examined from 3 infants (aged 2, 4, and 8 months), 2 children (6 and 7 years old), and 5 adults (21, 49, 54, 59, and 63 years old) who had died of nonneurologic conditions and the postmortem CNS examination of whom was devoid of pathologic findings. Some of these tissues have been used in previous studies (27). The use of existing autopsy tissue specimens was approved by an IRB exempt review protocol (Drexel University IRB protocol no. 17148). No patient identifiers were used.

Immunohistochemistry

Immunohistochemistry was performed according to the avidin-biotin complex (ABC) peroxidase method using Rabbit and Mouse IgG ABC Elite Detection Kits (Vector Labs, Burlingame, CA), as previously described (35–37). Five-micrometer-thick paraffin-embedded tissue sections were subjected to nonenzymatic antigen retrieval using 0.01 mol/L sodium citrate buffer (pH 6.0) (for immunostaining with Sp6C6 and Sp/AAA antibodies) and Tris-EDTA (pH 9.0) (for immunostaining with Sp3G11/1 monoclonal antibody) at 95 to 100°C for 30 minutes. Slides were then allowed to cool to room temperature and endogenous peroxide activity quenched with 3% H_2O_2 (vol/vol) in methanol for 30 minutes.

Tissues were incubated at room temperature in corresponding blocking solution (5% normal horse serum or 5% normal goat serum in 0.1% PBS–bovine serum albumin for mouse monoclonal antibodies or rabbit polyclonal antibodies, respectively) for 2 hours. Tissues were then incubated overnight at room temperature in primary antibodies diluted in blocking solution diluted as follows: Sp/AAA 1:2000, Sp3G11/1 1:20, and Sp6C6 1:50 to 1:100. Prediluted secondary antibodies from the ABC Elite Detection Kits were applied at room temperature for 1 hour, followed by a 1-hour incubation with ABC solution under the same condition. Negative controls included omission of primary antibody, as well as substitution with nonspecific mouse IgG2a or nonspecific rabbit antibody (Becton Dickinson, Franklin Lakes, NJ). Experiments using isotype-matched control antibodies did not show any nonspecific binding of secondary antibodies.

Immunodetection visualizations were performed using 3′3-diaminobenzidine solution (DAB Substrate Kit; Vector Labs) and were allowed to develop on tissues for 3 to 7 minutes. Slides were counterstained for 4 minutes in Harris hematoxylin (Fisher, Norristown, PA), dehydrated through a graded alcohol-water sequence, cleared in xylene, and mounted with cover slides (Fisher) using Permount (Fisher).

Cell Counting

Manual cell counting of spastin-labeled tumor cells in immunohistochemical preparations was performed independently by 3 observers (Christos D. Katsetos, Pei S. Liu, and Kandan Kulandaivel). Cell counting and statistical analysis were carried out on preparations immunostained with Sp3G11/1 and Sp/AAA only in the adult group of diffuse astrocytic gliomas for which clear spastin immunoreactivity was detected (n = 27). Preparations stained with Sp6C6 were evaluated qualitatively/semiquantitatively. Between 568 and 928 tumor cells were evaluated per case in 20 nonoverlapping high-power (40×) fields, and a labeling index was determined for each case. The labeling index was expressed as the percentage (%) of spastin-labeled cells of the total number of tumor cells counted in each case and for each antibody, as previously described (35). The level of interobserver agreement was quantitated using generalized κ and pairwise κ statistics (39, 40). Immunohistochemical preparations were reviewed at a multiheaded microscope to achieve consensus. Interobserver agreement was substantial ($\kappa = 0.65$). For purposes of labeling index recording, the consensus opinion was considered as conclusive. The median labeling index (MLI) and the interquartile range (IQR)—delimited by the 25th and 75th percentiles—were determined for the set of cases in each histologic grade using one-way analysis of variance

(SigmaStat; SPSS, Chicago, IL). The statistical significance of differences in labeling indices between WHO histologic grades was examined with nonparametric statistical techniques using Kruskal-Wallis analysis of variance tests. A p value of less than 0.05 was considered as statistically significant. Because of the small number of pediatric gliomas with spastin immunoreactivity included in this study, only qualitative assessment was performed in these cases.

RESULTS

Subcellular Distribution and Expression of Spastin in Human GBM Cell Lines

Immunofluorescence staining of various cell lines was first performed using the Sp3G11/1 anti-spastin monoclonal antibody. In NHA, a faint granular staining was observed throughout the cytoplasm (Fig. 2A). In contrast, there was more prominent and widespread spastin localization in the form of confluent punctate and diffuse cytoplasmic aggregates in human GBM cell lines (T98G, U138MG, U87MG) (Figs. 2B, D). Comparable staining patterns were observed for T98G cells stained with the anti-spastin monoclonal antibody Sp6C6 (Fig. 2E) or the polyclonal antibody Sp/AAA (Fig. 2F). In control human neuroblastoma cell lines (SHSY5Y, SK-N-SH), both prominent cytoplasmic diffuse and granular staining were observed (Figs. 2G, H).

When SH-SY5Y cells are grown for 4 days in the presence of 1 μmol/L of all *trans*-retinoic acid, prominent neurites are generated (26). Spastin labeling was detectable along these neurites and in the cell periphery (Figs. 3A–C). Interestingly, vesicle-like immunoreactivity for spastin was also observed at the leading edges of migrating T98G cells, a cellular compartment where few microtubules are present (Figs. 3D–I). The association of spastin with leading edges was confirmed by double-label fluorescence in T98G cells with an antibody to spastin and fluorescein isothiocyanate–conjugated phalloidin as a marker of microfilaments. The distribution of spastin and microfilaments is shown in Figure, Supplemental Digital Content 1, http://links.lww.com/NEN/A262. Spatial dissociation of spastin and GM-130 was noted in GBM cells (Figs. 4A–C). Interestingly, strong spastin staining was observed near mitotic spindle microtubules, as well as the cytoplasm of round GBM cells undergoing mitosis (Figs. 4D–F). All 3 anti-spastin antibodies used in this study rendered similar patterns of immunoreactivity in T98G cells (data not shown).

Differences in the staining intensity with anti-spastin antibodies between NHA (Fig. 2A) and GBMs (Figs. 2B–D) were confirmed by immunoblotting experiments. Under our SDS-PAGE Tris-glycine conditions, antibodies Sp6C6 and Sp3G11/1 recognized a major band of ~54 kd when probed against T98G human GBM cell lysates (Fig. 5A). The antibody Sp/AAA stained only very faintly blotted proteins in the 70- to 50-kd region (not shown). To verify that the band recognized by Sp6C6 and Sp3G11/1 antibodies indeed corresponds to endogenous spastin, T98G cells were treated with either control or spastin-specific siRNAs, and lysates derived from these cells were probed by immunoblotting. Immunoreactivity of the ~54-kd band was substantially diminished by spastin-specific siRNA 1 and siRNA 2, but not by control siRNA, confirming its identity as endogenous spastin (Fig. 5B). Immunoblotting experiments showed higher levels of spastin expression in GBM cell lines compared with NHA cells (Fig. 5C), consistent with results from immunocytochemical experiments (Fig. 2). Immunoblots of HEK cell

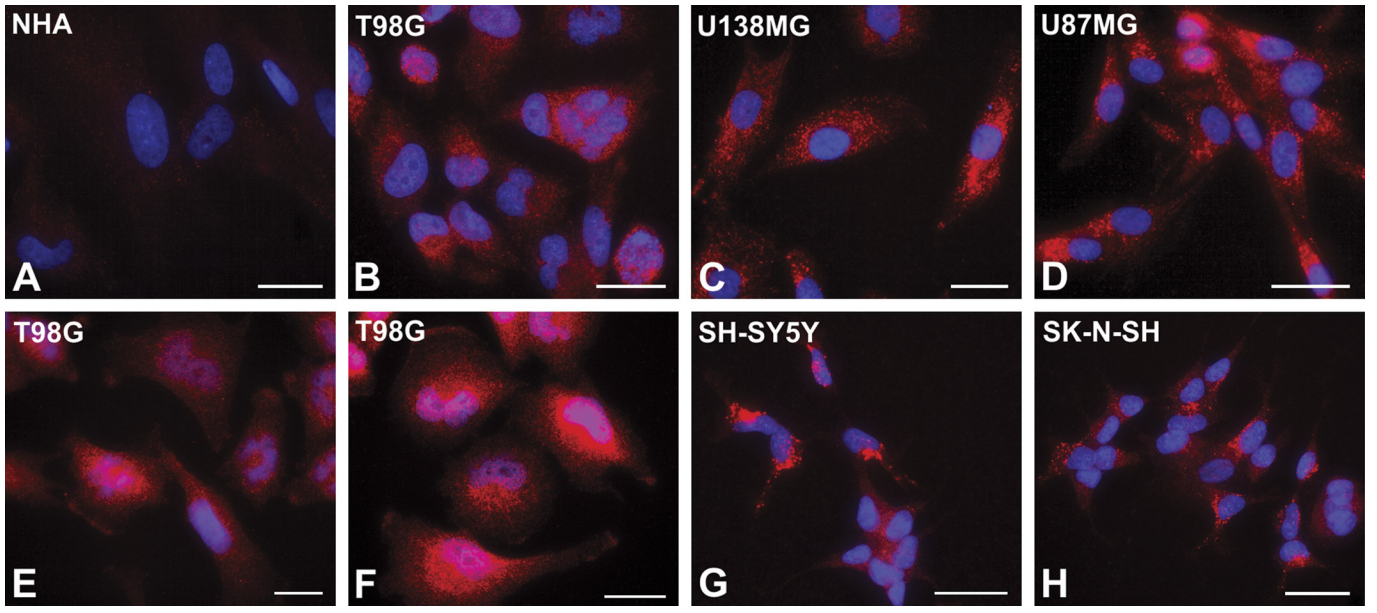

FIGURE 2. Spastin localization in human astrocytes (NHA), human glioblastoma cell lines (T98G, U138MG, U87MG), and human neuroblastoma cell lines (SH-SY5Y, SK-N-S H). **(A–H)** Cells were stained with monoclonal antibody Sp3G11/1 **(A–D, G–H)**, monoclonal antibody Sp6C6 **(E)**, or polyclonal antibody Sp/AAA **(F)**. DNA in nuclei was stained by 4,6-diamidino-2-phenylindole. Fluorescence images were captured and processed in the same manner. Scale bar = 20 μm.

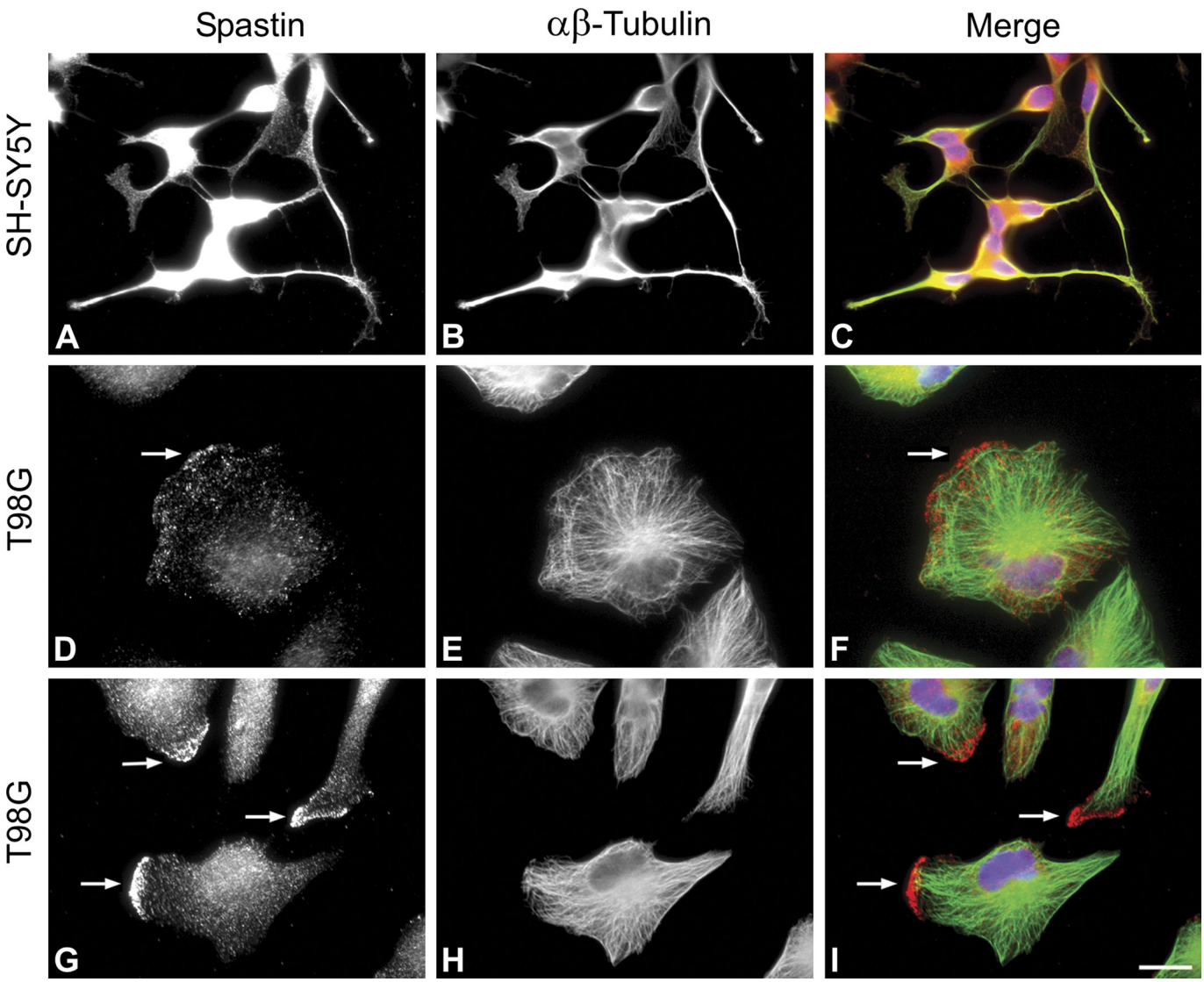

FIGURE 3. Spastin localization in differentiated SH-SY5Y cells **(A–C)** and migrating glioblastoma T98G cells **(D–I)**. Cells were double-labeled with antibodies to spastin Sp6C6 **(A, D, G)** and tubulin dimer **(B, E, H)**. Superposition of spastin and tubulin staining after DNA staining with 4,6-diamidino-2-phenylindole is shown in **(C, F, I)**. An enrichment of spastin in the cell periphery (arrows in **D, F, G, I**) was observed for populations of glioblastoma cells. Scale bar = **(I)** 20 μm.

lysates overexpressing full-length versions of human M1 and M87 spastin isoforms showed that all anti-spastin antibodies used in this study similarly recognized both M1 and M87 spastin isoforms (Fig. 1A). Moreover, immunoblots of T98G, NHA, and cortical cell lysates indicate that the main spastin isoform predominantly expressed in these cells corresponds to M87 (Fig. 1B). A weaker immunoreactive band running at a slightly lower molecular weight than M87 was also observed, likely corresponding to M87 lacking exon 4 (Fig. 1B) (20).

Consistent with results from immunoblotting experiments, quantitative real-time PCR experiments showed increased expression of spastin transcripts in human GBM (U138MG, U87MG, and T98G) and neuroblastoma (SK-N-SH) cell lines compared with NHA (Fig. 6). Collectively, these results indicated increased expression of spastin in human GBM cell lines.

Spastin Depletion Affects Cell Motility and Proliferation in T98G Cells

To determine whether spastin affects cell motility, this protein was depleted in T98G cells using spastin-specific siRNA, and cell motility was monitored using time-lapse imaging for 10 hours. When compared with cells transfected with control siRNA, spastin-depleted cells displayed lower migration velocities (Fig. 7A). Velocities in control and spastin-depleted cells were 21.7 ± 13.48, and 16.5 ± 8.37 μm/h (mean ± SD; n = 503 in control cells, n = 615 in spastin-depleted cells), respectively ($p < 1 \times 10^{-14}$) (Fig. 7A). When compared with controls, spastin-depleted cells also had shorter mean trajectory length. Mean track lengths during the 10-hour time-lapse imaging in control and spastin-depleted cells were 176 ± 114 and 139 ± 80 μm (mean ± SD; n = 503 in control cells, n = 615 in spastin-depleted

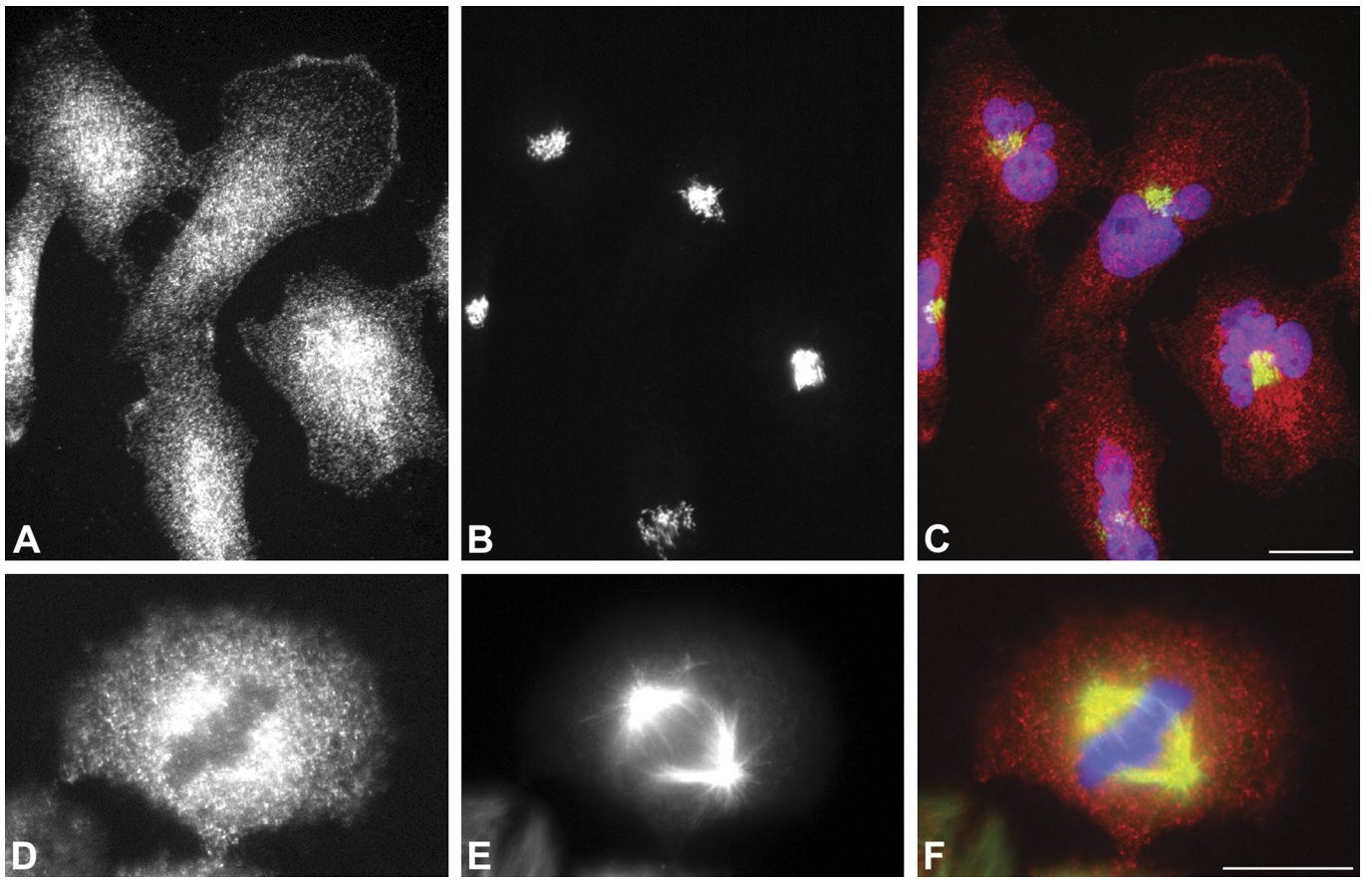

FIGURE 4. Double-label immunofluorescence staining of glioblastoma cell line T98G for spastin, GM130 and microtubules. **(A–C)** Interphase cells were stained with antibodies to spastin Sp/AAA **(A)** and the Golgi marker protein GM130 **(B)**. Superposition of images after DNA staining with 4,6-diamidino-2-phenylindole is shown in **(C)**. **(D–F)** A cell undergoing mitosis was stained with antibody Sp6C6 to spastin **(D)** and an antibody to tubulin dimer **(E)**. Superposition of images after DNA staining with 4,6-diamidino-2-phenylindole is shown in **F**. Scale bars = 20 μm.

cells), respectively ($p < 1 \times 10^{-9}$) (Figure, Supplemental Digital Content 2, http://links.lww.com/NEN/A264). Examples of cell trajectories in control and spastin-depleted cells are shown in Figure 7B. Time-lapse imaging of control and spastin-depleted T98G cells revealed that some cells within the spastin-depleted cell population had distinctively long protrusions. Video, Supplemental Digital Content 3, http://links.lww.com/NEN/A265, demonstrates motility in control and spastin-depleted cells. One long protrusion was observed typically per moving cell, as documented by still images from time-lapse experiments (Figs. 8A, B). These protrusions, characteristic of spastin-depleted T98G cells, were packed by dense arrays of microtubules (Fig. 8D). Protrusions and changes in the organization of microtubules were not detected in control cells (Fig. 8C).

To assess the effect of spastin depletion on cell division, growth curves were determined in control and spastin-depleted cells (Days 1–6 after siRNA transfection) together with immunoblot analysis of spastin expression. The number of viable cells was clearly higher in spastin-depleted cells; statistically significant differences were observed on Day 3 after transfection (Fig. 9A); effective spastin depletion at this time point was confirmed by immunoblotting (Fig. 9B). Higher proliferation of spastin-depleted cells was also confirmed by demonstrating a higher amount of kinesin-like protein KIF11 (Eg5), which associates with mitotic spindles and represents a marker of mitotic cells (Figure, Supplemental Digital Content 4, http://links.lww.com/NEN/A266). Collectively, these results document substantial changes in cell motility and proliferation in spastin-depleted GBM T98G cells.

Distribution of Spastin in the Normal Brain

In the normal brain, antibodies Sp/AAA, Sp3G11/1, and Sp6C6 produced similar, yet not identical, immunoreactivity profiles. In the cerebellum, Sp/AAA rendered widespread staining in Purkinje cell perikarya and apical dendrites in the molecular layer (Fig. 10A), Golgi II neurons (Fig. 10B), and, to a lesser extent, glial cells of the molecular layer (Fig. 10C). In contrast, antibodies Sp3G11/1 and Sp6C6 did not stain Purkinje cell bodies but instead rendered discrete punctate staining in the neuropil of the Purkinje cell and molecular layers (Fig. 10D) and in the cerebellar white matter (Fig. 10E, arrows), suggesting localization in axodendritic or axoaxonal synapses. Scant cytoplasmic staining was

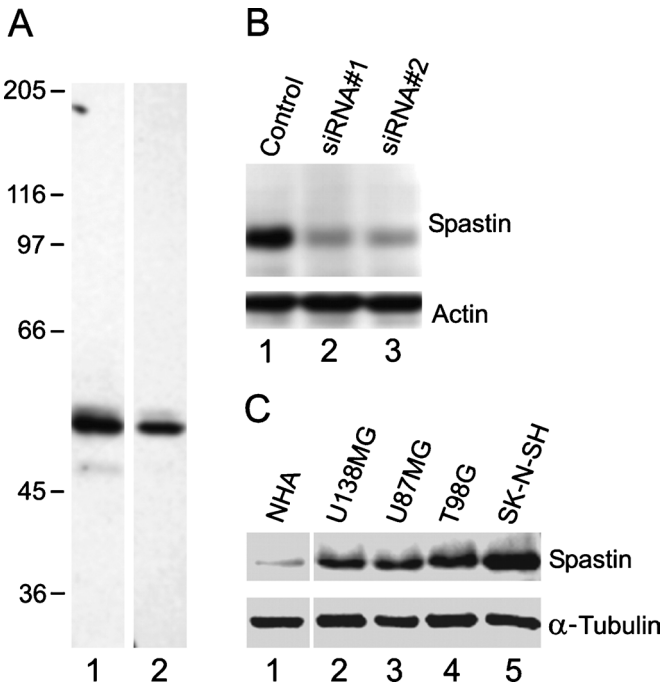

FIGURE 5. Immunoblot analysis of cell extracts with anti-spastin antibodies. **(A)** Immunoblot of whole cell extracts from T98G cells using anti-spastin antibodies Sp6C6 (lane 1) and Sp3G11/1 (lane 2). Bars on the left margin denote position of molecular weight markers in kilodalton. **(B)** Immunoblots of whole cell extracts from T98G cells transfected with negative control or spastin-specific siRNAs were revealed using antibodies against spastin (Sp6C6) and actin. **(C)** Quantitative immunoblot of whole cell extracts from human astrocytes (NHA) (1), human glioblastoma cell lines U138MG (2), U87MG (3), T98G (4), and human neuroblastoma cell line SK-N-SH (5) using anti-spastin antibody Sp6C6. There is a marked increase in spastin expression in glioblastoma and SK-N-SH cells versus NHA. Immunoblotting with an anti–α-tubulin antibody served as a loading control.

detected in glial cells with Sp3G11/1 (Fig. 10F), much as observed with the Sp6C6 antibody.

Expression and Cellular Distribution of Spastin in Clinical Tumor Samples

Compared with the normal brain, spastin immunoreactivity profiles were significantly increased in diffuse astrocytic gliomas according to an ascending gradient of malignancy. Immunolabeling with all 3 anti-spastin antibodies used in this study was detected in 27 of 37 adult diffuse astrocytic gliomas. Ten of 37 tumor specimens (9 GBM and 1 grade III anaplastic astrocytoma) showed no spastin immunoreactivity. Grade for grade, spastin immunoreactivity was significantly increased in GBM ($p < 0.05$ vs grade II astrocytoma). Among the 27 tumor specimens exhibiting positive labeling by immunohistochemistry, the spastin MLI for GBM was 17.2% (IQR = 6.4%–38.4%) and 15.4% (IQR = 5.5%–36.7%) using antibodies Sp3G11/1 and Sp/AAA, respectively, compared with the low-grade (grade II) diffuse astrocytomas (MLI = 2.1%, IQR = 1.4%–5.6% and MLI = 1.7%, IQR = 0.7%–3.8%) also with antibodies Sp3G11/1 and Sp/AAA, respectively ($p < 0.05$). A similar trend was noted in pediatric tumors, but the number of available cases was too small for statistical analysis.

Spastin immunoreactivity profiles varied widely among different tumor specimens of the same histologic grade and among different areas within individual samples, consistent with marked intratumoral staining heterogeneity. In diffuse low-grade astrocytomas (Figs. 11A, B, D, E) and anaplastic astrocytomas (Figs. 11C, F, I, J), spastin staining was detected in randomly dispersed tumor cells (Figs. 11B, D), including in areas of gray matter infiltration (Figs. 11A, B, G, H). Aside from robust somatodendritic spastin labeling in entrapped neurons of the cerebral cortex and deep gray nuclei (Figs. 11A–C, G, H), overlapping diffuse and punctate localizations (Figs. 11E, F) (some with a distinctive tendency for the cell periphery) were noted in neoplastic glial cells (Figs. 11F, I, J). As a consistent trend (but not invariably), distinctive punctate staining (with a predilection for the cell periphery) was present in large pleomorphic/multinucleated ("ganglioid") tumor cells with ample cytoplasm (Figs. 11F, I, J). Immunostaining of such tumor cells was almost indistinguishable from the punctate pattern of spastin localization in entrapped indigenous neurons (Figs. 11G, H), except for the presence of supernumerary and/or atypical nuclei in neoplastic glial cells (Figs. 11F, I, J).

Robust, mostly diffuse and multipunctate spastin immunoreactivity was detected in tumor cells clustered around tumor blood vessels in GBM (Figs. 12A–C) but was also variously distributed throughout the tumor parenchyma (Figs. 12D–K). In contrast to spastin-expressing neoplastic cells, there was a paucity of spastin labeling in hypertrophic endothelial cells in foci of angiogenesis (Figs. 12A-C). There was a diffuse and dense cytoplasmic staining pattern in the preponderant nondescript tumor cells (Figs. 12E, F). Randomly scattered

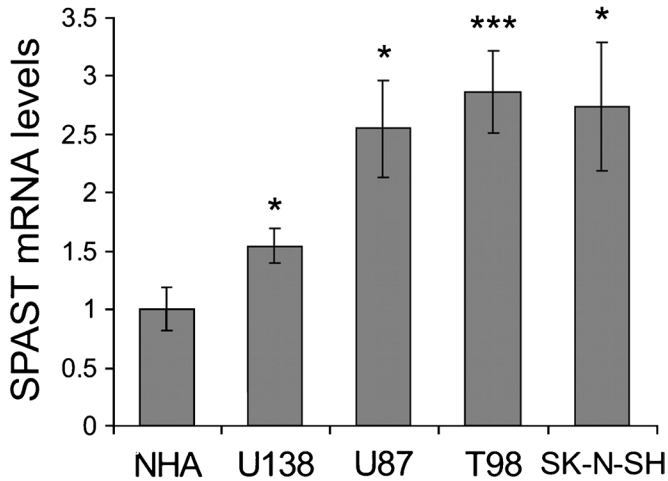

FIGURE 6. Analysis of spastin (SPAST) mRNA levels. Spastin transcripts were increased in the glioblastoma cell lines U138MG, U87MG, and T98G and in neuroblastoma cell line SK-N-SH relative to normal human astrocytes (NHAs). Data are presented as the mean fold change ± SD obtained from 2 independent experiments with triplicate samples. Mean values different from NHA levels are indicated: ***, $p < 0.005$, *, $p < 0.05$.

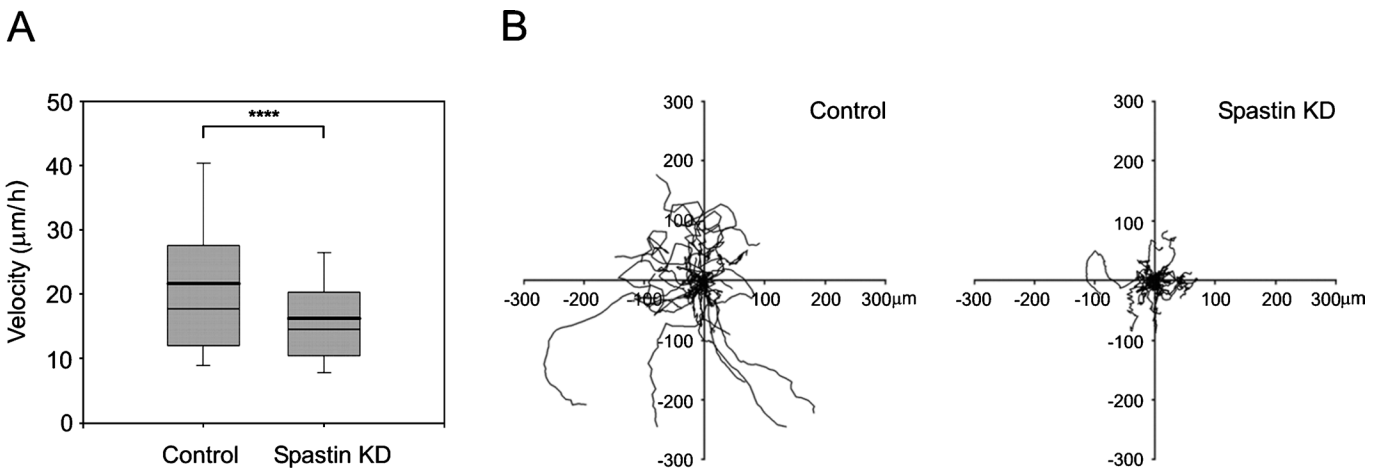

FIGURE 7. Effect of spastin depletion on migration of T98G cells. **(A)** Box plot of migration velocities in negative control and spastin-depleted glioblastoma cells (Spastin KD). Bold and thin lines within the box represent mean and median (the 50th percentile), respectively. The bottom and top of the box represent the 25th and 75th percentiles. Whiskers below and above the box indicate the 10th and 90th percentiles; n = 503 (control), n = 615 (Spastin KD). ****, $p < 1 \times 10^{-14}$. **(B)** Migration tracks in negative control and spastin-depleted glioblastoma cells (Spastin KD). Randomly chosen time-lapse sequences were analyzed, and all tracks were aligned, with their starting points at the coordinate position [0, 0]. Tracks resulting from detection errors and tracks crossing the border of the image were not included (<10% of all tracks). Thirty-eight trajectories were analyzed in control and spastin-depleted cells.

tumor cells with an irregular multipolar astroglial-like morphology exhibited a variant robust fibrillary/filamentous staining (Fig. 12G). Strong, diffuse, and/or micropunctate, juxtanuclear staining was also noted in small ("anaplastic") GBM cells and in the intervening tumor-infiltrated brain parenchyma in areas of pseudopalisading necrosis (Figs. 12H–J). Mitotic figures were, for the most part, spastin-negative in these sections (Fig. 11C), although weak spastin labeling was noted in a small number of mitoses (Fig. 12L). There was an overall trend for increased spastin expression in overtly astroglial morphologic phenotypes compared with neoplastic cells with spindle cell/sarcomatoid features (not shown).

Immunoreactivity with Sp3G11/1 and Sp/AAA was qualitatively and semiquantitatively more robust than that of Sp6C6. The labeling pattern with Sp3G11/1 was also more micropunctate compared with that of Sp/AAA on paraffin sections. However, no statistically significant differences were detected in tumor labeling indices obtained using Sp3G11/1 and Sp/AAA antibodies.

Collectively, the immunohistochemical findings on the tumor samples suggest that increased spastin expression represents a distinct feature of neoplastic glial phenotypes, especially in GBM.

DISCUSSION

This study demonstrates that in the context of human gliomas, the microtubule-severing ATPase spastin is expressed at higher levels in neoplastic glial phenotypes, especially in GBM, than in normal brain tissue. In the latter, spastin localization is predominantly neuronal and, only to a lesser extent, glia-associated. Increased spastin protein and transcripts levels were confirmed by immunofluorescence, immunoblotting, and quantitative RT-PCR experiments in 3 human GBM cell lines compared with cultured NHA. Notably, all 3 antibodies used in this study yielded similar immunofluorescence profiles on cultured GBM cell lines. The lack of colocalization of spastin and GM-130 in these cells suggests that spastin does not undergo trafficking along the early secretory pathway. By immunohistochemistry, the anti-spastin antibodies Sp3G11/1 and Sp/AAA gave statistically significant increases in spastin labeling indices in primary, surgically excised, GBM specimens versus grade II diffuse astrocytic gliomas. Collectively, these results indicate that increased expression of spastin is linked to an overall tendency toward high-grade glioma malignancy.

Spastin Expression in Brain

Spastin expression has been documented in brain, spinal cord, heart, kidney, liver, lung, pancreas, placenta, and skeletal muscle (23). Our results in the normal human CNS confirm previous studies reporting a predominantly neuronal trend for spastin localization (24, 25). Our immunohistochemical studies also revealed different patterns of spastin immunoreactivity for different spastin antibodies in neuronal cells in situ. Specifically, the antibody Sp/AAA gave strong somatodendritic and axonal Purkinje cell immunoreactivity. In contrast, antibodies Sp3G11/1 and Sp6C6 produce no Purkinje cell staining but instead rendered discrete punctalike localizations in the neuropil, for example, at the boundary of Purkinje and molecular layers near the basket fibers and the white matter. Because spastin localization has also been described in synapses (41), we speculate that these spastin-immunopositive puncta may represent axodendritic and/or axoaxonal synaptic sites. Also, the Sp/AAA antibody stained glial cell populations in the cerebellar molecular layer and white matter, whereas the Sp3G11/1 and Sp6C6 showed no significant glial cell immunoreactivity besides weak/scanty labeling in occasional astrocytes. Consistent with these

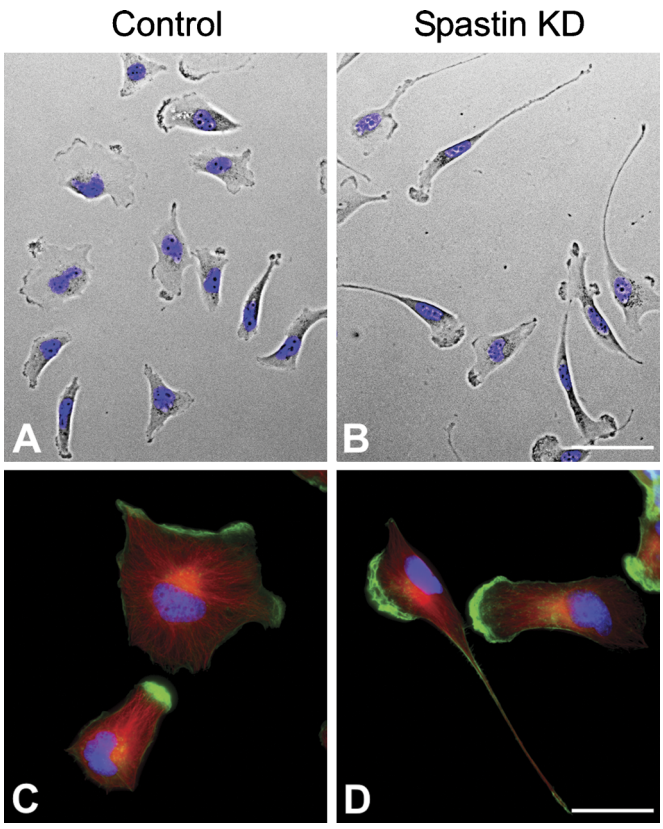

FIGURE 8. Effect of spastin depletion on morphology of T98G cells. **(A, B)** Still images from time-lapse imaging of negative control **(A)** and spastin-depleted glioblastoma cells **(B)**. Combination of bright field and fluorescence; nuclei are visualized with Hoechst 33342 labeling. **(C, D)** Distribution of microtubules (red) and microfilaments (green) in control cells **(C)** and glioblastoma cells with depleted spastin **(D)**. DNA staining with 4,6-diamidino-2-phenylindole. Scale bars = **(B)** 100 μm; **(D)** 20 μm.

observations, deletion experiments mapped the Sp3G11/1 and Sp6C6 epitopes to a region within a.a. 87 and 274, far away from the Sp/AAA epitope(s) located between a.a. 337 and 465 (M. A. Burns and G. Morfini, unpublished data). Thus, differences in Sp3G11/1-Sp6C6 versus Sp/AAA immunoreactivity most likely result from differential epitope availability in situ.

Spastin Isoform Expression in GBM Cells

The human spastin gene yields 2 major isoforms (M1 and M87) that result from 2 different translational start sites (18, 21). The exclusion of specific exons (exons 4, 9, and 15) further increases the heterogeneity of spastin isoforms in different tissues (20). In normal human brain, 2 major spastin transcripts have been identified by RT-PCR, the most prominent one corresponding to full-length M87 and a less abundant one corresponding to M87 lacking exon 4 (20). Previous immunoblotting studies established selective expression of M87, but not M1, in the adult rat hippocampus and cerebral cortex (22). These observations, coupled with immunoblotting data herein, strongly suggest that NHA and GBM cells mainly express M87 spastin. A weaker spastin-immunoreactive band running at a slightly lower molecular weight than full-length M87 was also observed. On the basis of prior studies, this band likely represents M87 lacking exon 4 (20). However, the expression of M87 spastin isoform variants was not directly evaluated in the present study.

Role of Spastin in Cell Motility and Proliferation of GBM Cells

Overlapping punctate and diffuse patterns of spastin localization were identified in primary tumors and in interphase cells of GBM cell lines, independent of Golgi staining, as well as in mitoses. Intriguingly, recruitment of spastin to the leading edges of growing tumor cells, where few microtubules are present, was detected both in T98G cells and in tumor cells from clinical samples. Aside from actin-driven protrusions, including α-actinin–enriched ruffled membranes and lamelipodia (42), a similar recruitment to the leading edges of GBM cells has been observed with the intermediate filament protein synemin, which contributes to the migratory properties of astrocytoma cells by influencing the dynamics of the actin cytoskeleton (43). We observed a substantial decrease in cell motility in spastin-depleted versus control

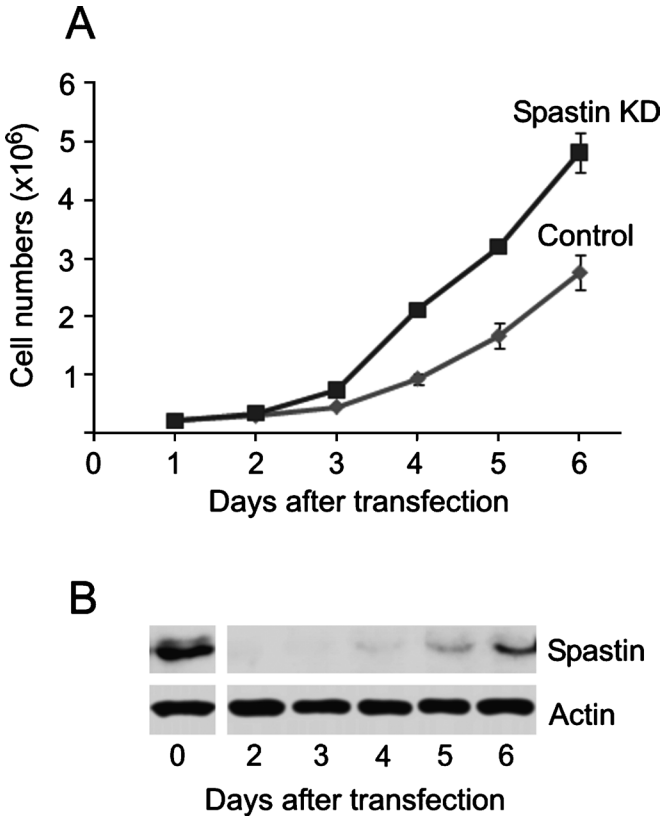

FIGURE 9. Effect of spastin depletion on cell proliferation of T98G cells. **(A)** Growth curves in negative control and spastin-depleted glioblastoma cells (Spastin KD). A total of 2×10^5 cells were plated 1 day after transfection both in control and spastin-depleted cells. Values indicate mean ± SD; n = 3. **(B)** Immunoblots of whole cell extracts from T98G cells transfected with spastin-specific siRNAi were probed with antibodies to spastin (Sp6C6) and actin (loading control).

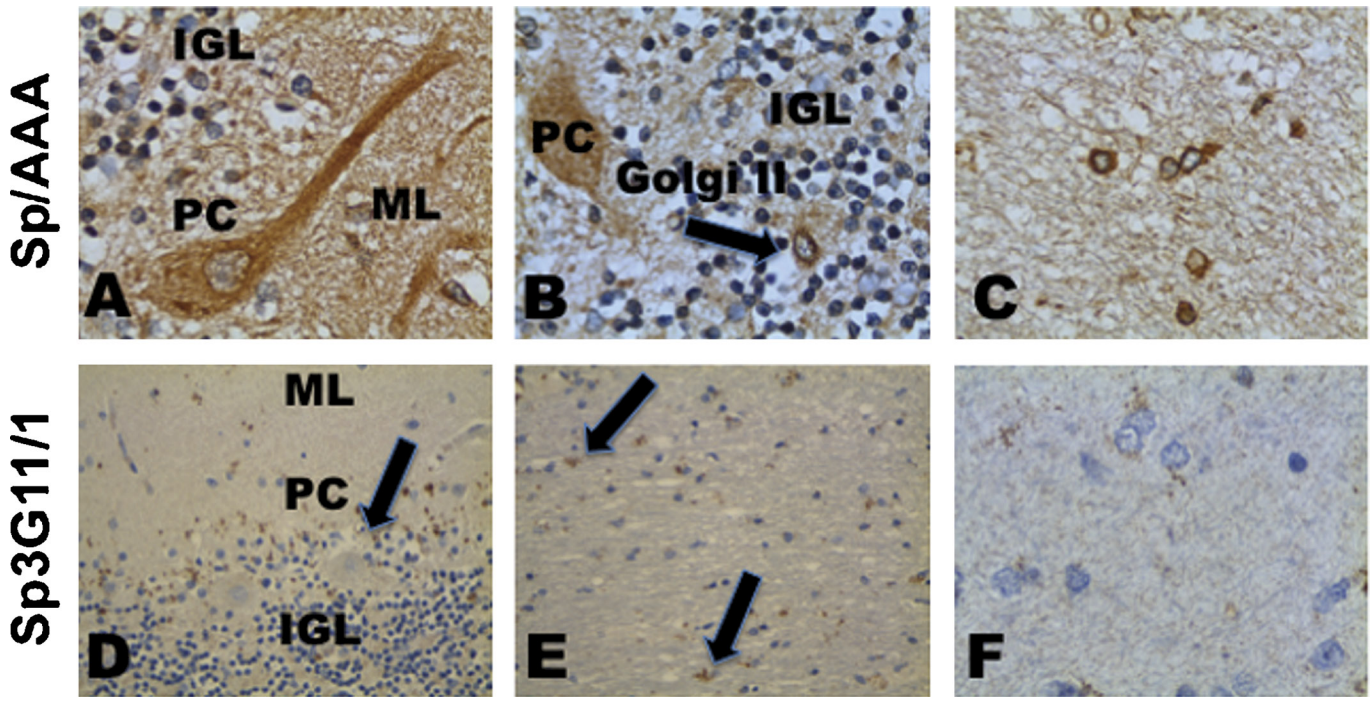

FIGURE 10. Spastin immunoreactivity in normal brain. **(A–F)** Immunohistochemical staining of normal brain with anti-spastin Sp/AAA **(A–C)** and Sp3G11/1 antibodies **(D–F)**. Sp/AAA renders widespread staining in Purkinje cell (PC) perikarya and apical dendrites in the molecular layer (ML), as well as fibers of the ML **(A)**, PC and Golgi II neurons **(B)**, and, to a lesser extent, glia in the molecular layer **(C)**. In contrast, Sp3G11/1 antibody renders discrete staining in neuropil puncta near the Purkinje and molecular layers **(D)** and cerebellar white matter **(E)** as well as scanty cytoplasmic staining in glial cells **(F)**. Note the lack of Sp3G11/1 immunoreactivity in PC or Golgi II neurons (**D**, arrow). IGL indicates internal granule layer; ML, molecular layer; PC, Purkinje cell. Avidin-biotin complex (ABC) peroxidase with hematoxylin counterstain. Original magnifications: **(A–C, F)** 500×; **(D, E)** 100×.

cells. These results were also supported by a radial cell migration assay (44) using T98G cells attached on laminin (E. Dráberová, unpublished data). In some cells, spastin depletion resulted in generation of long protrusions but immunofluorescence microscopy in T98G cells did not reveal overt changes in microtubule organization in the close vicinity of plasma membranes. On the other hand, depletion of katanin, another microtubule-severing protein, in addition to affecting cell migration, reportedly results also in the generation of dense arrays of microtubules running parallel to the inner face of the plasma membrane (cell cortex) (45). Both proteins might therefore regulate different microtubule functions in moving cells. To our knowledge, there are no previous reports indicating involvement of spastin in cell motility.

Gene expression profiling experiments in gliomas have shown upregulation of genes related to motility, and functional studies demonstrated that increased cell motility may be the main contributor to the invasive phenotype of diffuse gliomas (46). Similarly, the commitment of glioma cells to migrate and invade seems to be inversely related to proliferative activity (47). Intriguingly, depletion of spastin in T98G cells in the present study also resulted in inhibition of cell migration and stimulation of cellular proliferation. These data suggest that spastin levels may correlate with changes in proliferation and migratory rates, thus making spastin a novel determinant in the emergence of divergent proliferating or invasive cell populations in gliomas. Accordingly, the inverse and dichotomous role(s) of spastin in cell motility versus proliferation in GBM cells are consistent with the concept that migration and proliferation constitute antagonistic cellular behaviors within a glioma cell population (46). Further studies are needed to elucidate the role of spastin in the growth and invasion of gliomas because this microtubule-severing enzyme may be subject to differential regulation by divergent signaling effectors within the brain tumor microenvironment. The permissiveness of the cellular environment may promote migration and decrease proliferation and proapoptotic disposition in tumor cells; collectively, these effects may contribute to tumor resistance to chemotherapy and radiation therapy (46).

Role of Spastin-Mediated Microtubule Severing in Brain Cancer Cells

Abnormalities in microtubule dynamics and organization underlie a common mechanism for genetic instability in cancer cells and for altered tumor cell architecture; however, the molecular mechanisms underlying such changes are poorly understood (48). In normal CNS development, spatial control of microtubule severing is important for mobilizing large numbers of microtubules at growth-related sites, such as centrosomes/microtubule-organizing centers (49), sites of branch formation (50), and growth cones (51). Previous studies have shown that spastin is enriched in cell regions containing dynamic microtubules including the spindle pole, the central

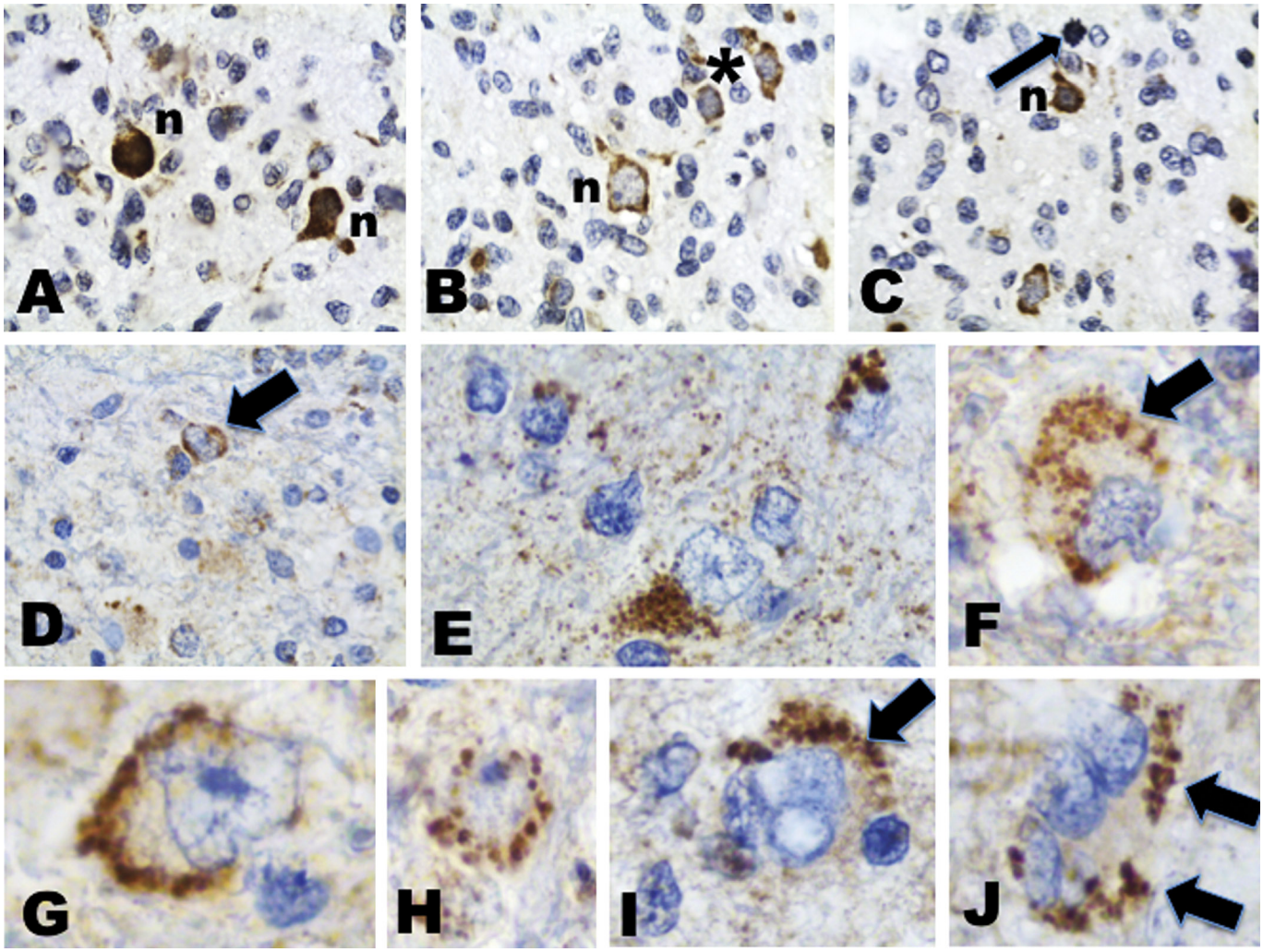

FIGURE 11. Spastin immunoreactivity profiles in diffuse low-grade (grade II) and anaplastic (grade III) astrocytomas. **(A–J)** Immunohistochemical staining of diffuse astrocytoma (grade II) infiltrating gray matter **(A, B, D, E)** and anaplastic astrocytomas (grade III) also infiltrating gray matter **(C, F–J)**. Staining with antibodies Sp/AAA **(A–C)** and Sp3G11/1 **(D–J)**. Compared with normal brain, spastin immunoreactivity is markedly increased in diffuse astrocytic gliomas **(A–F, I, J)**. Note overlapping of diffuse **(E)** and micropunctate localizations with a tendency for the periphery of tumor cells (**F, I, J**, arrows). **(G, H)** Presumed entrapped neurons with spastin localization in the cell periphery **(G)** or perikaryal puncta **(H)**. Arrow in **C** depicts spastin-negative mitosis and that in **D** depicts an immunoreactive tumor cell. Avidin-biotin complex (ABC) peroxidase with hematoxylin counterstain. n indicates neuron. **B**: *, cluster of immunoreactive tumor cells. Original magnification: **(A–J)** 500×.

spindle, and the midbody, as well as the distal axon and the branching points (52).

Microtubule severing may increase polymer mass by generating shorter microtubules that can serve as seeds for nucleating new microtubules (53, 54). In previous studies, we and others demonstrated overexpression and aberrant patterns of noncentrosomal γ-tubulin compartmentalization in diffuse astrocytic gliomas and GBMs (36, 37, 55), as well as in breast cancer cell lines (56), suggesting ectopic microtubule nucleation in cancer cells (55, 56). Interestingly, spastin interacts with centrosomal proteins and cofractionates with γ-tubulin (52), a form of tubulin essential for centrosomal (57, 58) and noncentrosomal (59, 60) microtubule nucleation. Future studies are warranted to determine whether γ-tubulin overexpression may affect abnormal microtubule severing activity and aberrant microtubule nucleation in cancerous glial cells.

Intratumoral Staining Heterogeneity in Clinical Tumor Samples

Spastin labeling was present in both human cell lines and tumor cells of surgically excised GBM, but more robust and widespread labeling was consistently encountered the former. A striking feature in GBM specimens was markedly heterogeneous immunoreactivity profiles associated with large areas of nonstaining of the tumors. This cellular distribution pattern contrasts with that of perivascular and/or randomly dispersed aggregates of tumor cells that exhibited unequivocal spastin staining. This again raises the question of differential epitope availability. Moreover, hindered detection of spastin by

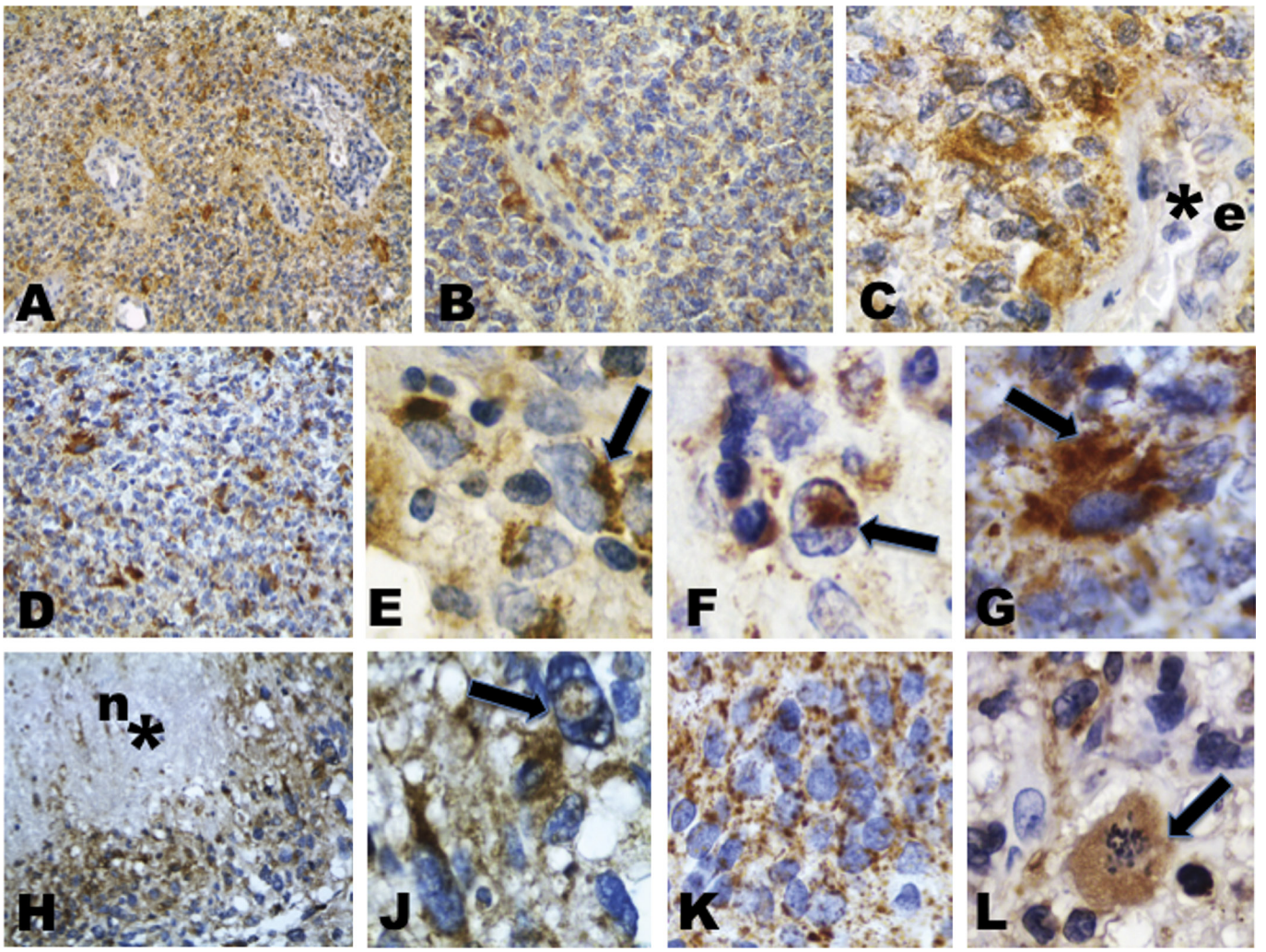

FIGURE 12. Spastin immunoreactivity profiles in glioblastoma. **(A–L)** Staining with antibodies Sp3G11/1 **(A–G, K)** and Sp/AAA **(H, J, L)**. Perivascular distribution of tumor cells and lack of labeling in foci of angiogenesis **(A–C)**. Asterisk in **C** depicts a tumor blood vessel with endothelial hypertrophy (e). Spastin labeling in primary tumors **(D–G)**. Arrow in **F** depicts diffuse staining in small anaplastic cells; arrow in **G** depicts fibrillary/filamentous staining in a multipolar cell. Spastin immunoreactive tumor cells from areas of pseudopalisading necrosis **(H, J**; asterisk denotes necrotic center [n]**)**. Higher magnification of **H** with the arrow pointing to a spastin-positive nuclear pseudoinclusion **(J)**. **(K)** Juxtanuclear labeling in small (anaplastic) cells. **(L)** Weak spastin labeling of a mitotic cell (arrow). Avidin-biotin complex (ABC) peroxidase with hematoxylin counterstain. Original magnifications: **(A)** 100×; **(B, D, H)** 200×; **(C, E–G, J–L)** 500×.

immunohistochemistry in formalin-fixed tissues may be due to epitope loss as a consequence of proteolysis in deeper portions of surgically excised or biopsy tissue samples because of slower tissue penetration by the fixative. Alternatively, it may be related to epitope masking due to protein conformational changes by formaldehyde-induced cross linkages or other factors related to histologic processing and/or embedding.

SUMMARY AND FUTURE DIRECTIONS

To our knowledge, this is the first study to demonstrate increased levels of spastin expression in human GBM cell lines versus NHA. Moreover, greater spastin immunoreactivity was found in clinical samples of GBM compared with low-grade diffuse astrocytic gliomas or nascent indigenous astrocytes, albeit with markedly heterogeneous cellular distribution. These results indicate that spastin overexpression in GBM is linked to a trend toward high-grade malignancy and aggressive growth potential. Although aberrant upregulation of spastin in a subset of tumor cells may not necessarily have functional significance, the observation of spastin enrichment in the leading edges of GBM cells in vitro and in situ, coupled with results from functional experiments, calls for future investigations into the possible role of spastin in tumor cell motility and invasion. Because increased spastin expression may promote cellular migration in the face of decreasing proliferation, targeting spastin may offer a promising therapeutic strategy directed against glioma cell invasion with a potentially added benefit on tumor cell response(s) to conventional cytotoxic and/or tubulin-targeted treatments.

REFERENCES

1. Ohgaki H, Kleihues P. Population-based studies on incidence, survival rates, and genetic alterations in astrocytic and oligodendroglial gliomas. J Neuropathol Exp Neurol 2005;64:479–89
2. Jordan MA, Wilson L. Microtubules and actin filaments: Dynamic targets for cancer chemotherapy. Curr Opin Cell Biol 1998;10:123–30
3. Pasquier E, Kavallaris M. Microtubules: A dynamic target in cancer therapy. IUBMB Life 2008;60:165–70
4. Dumontet C, Jordan MA. Microtubule-binding agents: A dynamic field of cancer therapeutics. Nat Rev Drug Discov 2010;9:790–803
5. Baas PW, Karabay A, Qiang L. Microtubules cut and run. Trends Cell Biol 2005;15:518–24
6. Whipple RA, Cheung AM, Martin SS. Detyrosinated microtubule protrusions in suspended mammary epithelial cells promote reattachment. Exp Cell Res 2007;313:1326–36
7. Schoumacher M, Goldman RD, Louvard D, et al. Actin, microtubules, and vimentin intermediate filaments cooperate for elongation of invadopodia. J Cell Biol 2010;189:541–56
8. Liaw TY, Chang MH, Kavallaris M. The cytoskeleton as a therapeutic target in childhood acute leukemia: Obstacles and opportunities. Curr Drug Targets 2007;8:739–49
9. Ferlini C, Raspaglio G, Cicchillitti L, et al. Looking at drug resistance mechanisms for microtubule interacting drugs: Does TUBB3 work? Curr Cancer Drug Targets 2007;7:704–12
10. Katsetos CD, Dráberová E, Legido A, et al. Tubulin targets in the pathobiology and therapy of glioblastoma multiforme. I. Class III β-tubulin. J Cell Physiol 2009;221:505–13
11. Kavallaris M. Microtubules and resistance to tubulin-binding agents. Nat Rev Cancer 2010;10:194–204
12. Régina A, Demeule M, Ché C, et al. Antitumour activity of ANG1005, a conjugate between paclitaxel and the new brain delivery vector Angiopep-2. Br J Pharmacol 2008;155:185–97
13. Mielke S, Sparreboom A, Mross K. Peripheral neuropathy: A persisting challenge in paclitaxel-based regimes. Eur J Cancer 2006;42:24–30
14. Richter-Landsberg C. The cytoskeleton in oligodendrocytes. Microtubule dynamics in health and disease. J Mol Neurosci 2008;35:55–63
15. Shi J, Orth JD, Mitchison T. Cell type variation in responses to antimitotic drugs that target microtubules and kinesin-5. Cancer Res 2008;68:3269–76
16. Hornick JE, Karanjeet K, Collins ES, et al. Kinesins to the core: The role of microtubule-based motor proteins in building the mitotic spindle midzone. Semin Cell Dev Biol 2010;21:290–99
17. Baas PW, Sudo H. More microtubule severing proteins: More microtubules. Cell Cycle 2010;9:2271–74
18. Claudiani P, Riano E, Errico A, et al. Spastin subcellular localization is regulated through usage of different translation start sites and active export from the nucleus. Exp Cell Res 2005;309:358–69
19. White SR, Evans KJ, Lary J, et al. Recognition of C-terminal amino acids in tubulin by pore loops in Spastin is important for microtubule severing. J Cell Biol 2007;176:995–1005
20. Svenson IK, Ashley-Koch AE, Gaskell PC, et al. Identification and expression analysis of spastin gene mutations in hereditary spastic paraplegia. Am J Hum Genet 2001;68:1077–85
21. Salinas S, Carazo-Salas RE, Proukakis C, et al. Human spastin has multiple microtubule-related functions. J Neurochem 2005;95:1411–20
22. Solowska JM, Morfini G, Falnikar A, et al. Quantitative and functional analyses of spastin in the nervous system: Implications for hereditary spastic paraplegia. J Neurosci 2008;28:2147–57
23. Hazan J, Fonknechten N, Mavel D, et al. Spastin, a new AAA protein, is altered in the most frequent form of autosomal dominant spastic paraplegia. Nat Genet 1999;23:296–303
24. Wharton SB, McDermott CJ, Grierson AJ, et al. The cellular and molecular pathology of the motor system in hereditary spastic paraparesis due to mutation of the spastin gene. J Neuropathol Exp Neurol 2003;62:1166–77
25. Ma DL, Chia SC, Tang YC, et al. Spastin in the human and mouse central nervous system with special reference to its expression in the hippocampus of mouse pilocarpine model of status epilepticus and temporal lobe epilepsy. Neurochem Int 2006;49:651–64
26. Encinas M, Iglesias M, Liu Y, et al. Sequential treatment of SH-SY5Y cells with retinoic acid and brain-derived neurotrophic factor gives rise to fully differentiated, neurotrophic factor–dependent, human neuron-like cells. J Neurochem 2000;75:991–1003
27. Dráberová E, Del Valle L, Gordon J, et al. Class III β-tubulin is constitutively coexpressed with glial fibrillary acidic protein and nestin in midgestational human fetal astrocytes: Implications for phenotypic identity. J Neuropathol Exp Neurol 2008;67:341–54
28. Viklický V, Dráber P, Hašek J, et al. Production and characterization of a monoclonal antitubulin antibody. Cell Biol Int Rep 1982;6:725–31
29. Dráber P, Dráberová E, Zicconi D, et al. Heterogeneity of microtubules recognized by monoclonal antibodies to α-tubulin. Eur J Cell Biol 1986;41:82–88
30. Dráber P, Dráberová E, Viklický V. Immunostaining of human spermatozoa with tubulin domain-specific monoclonal antibodies. Recognition of a unique β-tubulin epitope in the sperm head. Histochemistry 1991;95:519–24
31. Laemmli UK. Cleavage of structural proteins during the assembly of the head of bacteriophage T4. Nature 1970;227:680–85
32. Dráber P, Lagunowich LA, Dráberová E, et al. Heterogeneity of tubulin epitopes in mouse fetal tissues. Histochemistry 1988;89:485–92
33. Dráberová E, Dráber P. A microtubule-interacting protein involved in coalignment of vimentin intermediate filaments with microtubules. J Cell Sci 1993;106:1263–73
34. Soile P. *Morphological Image Analysis*. 2nd ed. Berlin, Germany: Springer, 2003
35. Katsetos CD, Del Valle L, Geddes JF, et al. Aberrant localization of the neuronal class III β-tubulin in astrocytomas. Arch Pathol Lab Med 2001;125:613–24
36. Katsetos CD, Reddy G, Dráberová E, et al. Altered cellular distribution and subcellular sorting of γ-tubulin in diffuse astrocytic gliomas and human glioblastoma cell lines. J Neuropathol Exp Neurol 2006;65:465–77
37. Katsetos CD, Dráberová E, Šmejkalová B, et al. Class III β-tubulin and γ-tubulin are co-expressed and form complexes in human glioblastoma cells. Neurochem Res 2007;32:1387–98
38. Louis DN, Ohgaki H, Wiestler OD, et al. The 2007 WHO classification of tumours of the central nervous system. Acta Neuropathol 2007;114:97–109
39. Fleiss JG. *Statistical Methods for Rates and Proportions*. New York, NY: Wiley, 1981:225–32
40. Landis JR, Koch GG. The measurement of observer agreement for categorical data. Biometrics 1977;33:159–74
41. Trotta N, Orso G, Rossetto MG, et al. The hereditary spastic paraplegia gene, spastin, regulates microtubule stability to modulate synaptic structure and function. Curr Biol 2004;14:1135–47
42. Quick Q, Skalli O. α-Actinin 1 and α-actinin 4: Contrasting roles in the survival, motility, and RhoA signaling of astrocytoma cells. Exp Cell Res 2010;316:1137–47
43. Pan Y, Jing R, Pitre A, et al. Intermediate filament protein synemin contributes to the migratory properties of astrocytoma cells by influencing the dynamics of the actin cytoskeleton. FASEB J 2008;22:3196–206
44. Berens ME, Beaudry C. Radial monolayer cell migration assay. Methods Mol Med 2004;88:219–24
45. Zhang D, Grode KD, Stewman SF, et al. *Drosophila katanin* is a microtubule depolymerase that regulates cortical-microtubule plus-end interactions and cell migration. Nat Cell Biol 2011;13:361–70
46. Giese A, Bjerkvig R, Berens ME, et al. Cost of migration: Invasion of malignant gliomas and implications for treatment. J Clin Oncol 2003;21:1624–36
47. Berens ME, Giese A. "…those left behind." Biology and oncology of invasive glioma cells. Neoplasia 1999;1:208–19
48. Nigg EA. Centrosome aberrations: Cause or consequence of cancer progression? Nat Rev Cancer 2002;2:815–25
49. Ahmad FJ, Yu W, McNally FJ, et al. An essential role for katanin in severing microtubules in the neuron. J Cell Biol 1999;145:305–15
50. Yu W, Ahmad FJ, Baas PW. Microtubule fragmentation and partitioning in the axon during collateral branch formation. J Neurosci 1994;14:5872–84
51. Dent EW, Callaway JL, Szebenyi G, et al. Reorganization and movement of microtubules in axonal growth cones and developing interstitial branches. J Neurosci 1999;19:8894–908
52. Errico A, Claudiani P, D'Addio M, et al. Spastin interacts with the centrosomal protein NA14, and is enriched in the spindle pole, the midbody and the distal axon. Hum Mol Genet 2004;13:2121–32

53. Roll-Mecak A, Vale RD. Making more microtubules by severing: A common theme of noncentrosomal microtubule arrays? J Cell Biol 2006; 175:849–51
54. Roll-Mecak A, McNally FJ. Microtubule-severing enzymes. Curr Opin Cell Biol 2010;22:96–103
55. Katsetos CD, Dráberová E, Legido A, et al. Tubulin targets in the pathobiology and therapy of glioblastoma multiforme. II. γ-Tubulin. J Cell Physiol 2009;221:514–20
56. Cho EH, Whipple RA, Matrone MA, et al. Delocalization of γ-tubulin due to increased solubility in human breast cancer cell lines. Cancer Biol Ther 2010;9:66–76
57. Joshi HC, Palacios MJ, McNamara L, et al. γ-Tubulin is a centrosomal protein required for cell cycle–dependent microtubule nucleation. Nature 1992;356:80–83
58. Zheng Y, Wong ML, Alberts B, et al. Nucleation of microtubule assembly by a γ-tubulin–containing ring complex. Nature 1995;378:578–83
59. Chabin-Brion K, Marceiller J, Perez F, et al. The Golgi complex is a microtubule-organizing organelle. Mol Biol Cell 2001;12:2047–60
60. Macurek L, Dráberová E, Richterová V, et al. Regulation of microtubule nucleation in differentiating embryonal carcinoma cells by complexes of membrane-bound γ-tubulin with Fyn kinase and phosphoinositide 3-kinase. Biochem J 2008;416:421–30

VI.2.1

Supplementary data for:

Dráberová E., **Vinopal S**., Morfini G., Liu P.S., Sládková V., Sulimenko T., Burns M.R., Solowska J., Kulandaivel K., de Chadarévian J.P., Legido A., Mörk S.J., Janáček J., Baas P.W., Dráber P., Katsetos C.D. (2011). Microtubule-severing ATPase spastin in glioblastoma: increased expression in human glioblastoma cell lines and inverse roles in cell motility and proliferation. J Neuropathol Exp Neurol. *70*, 811-826.

Supplemental Digital Content 1. Figure demonstrating codistribution of spastin and microfilaments in migrating glioblastoma cells.jpg

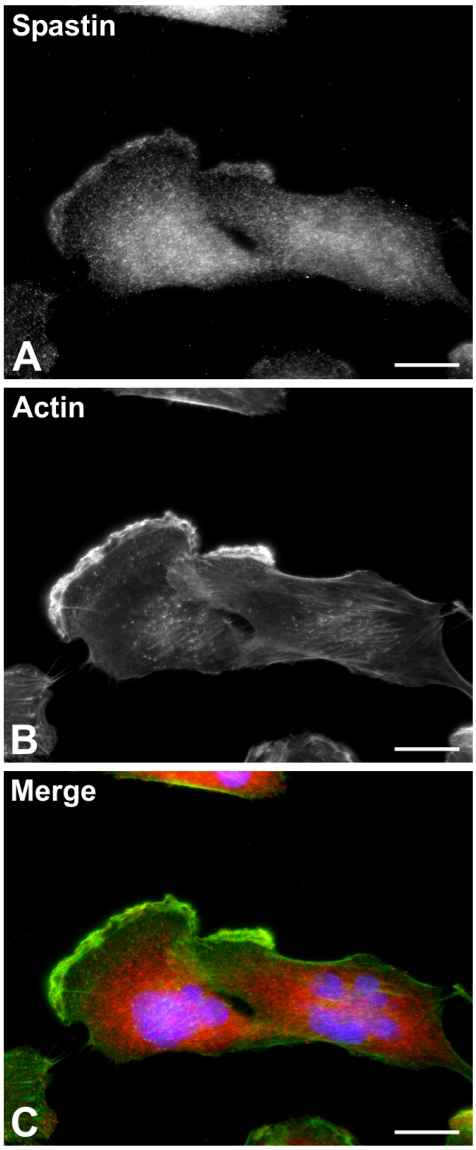

Double-label fluorescence staining of glioblastoma cell line T98G for spastin and microfilaments. (A-C) Glioblastoma interphase cells were stained with an antibody to spastin Sp6C6 (A) and FITC-conjugated phalloidin as a marker for microfilaments (B). Superposition of images after DNA staining with DAPI is shown in (C). Scale bar: 20 μm.

Supplemental Digital Content 2. Figure demonstrating track length in control and spastin-depleted glioblastoma cells.jpg

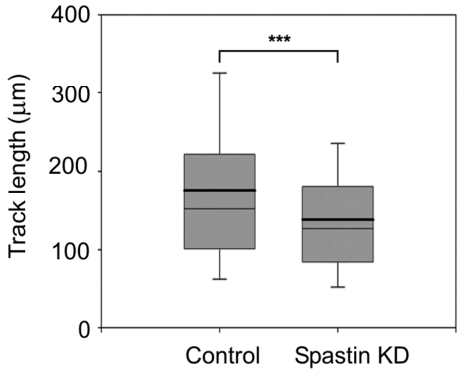

Effect of spastin depletion on track length of T98G glioblastoma cells. Box plot of track length in control and spastin-depleted cells (Spastin-KD). Bold and thin lines within the box represent, respectively, mean and median (the 50^{th} percentile). The bottom and top of the box represent the 25^{th} and the 75^{th} percentile. Whiskers below and above the box indicate the 10^{th} and the 90^{th} percentiles. n=503 (Control), n=615 (Spastin-KD). ***$p < 1x10^{-9}$.

Supplemental Digital Content 3. Video illustrating motility in control and spastin-depleted glioblastoma cells. mov (http://links.lww.com/NEN/A265)

Supplemental Digital Content 4. Figure demonstrating higher amount of Eg5 in spastin-depleted glioblastoma cells.jpg

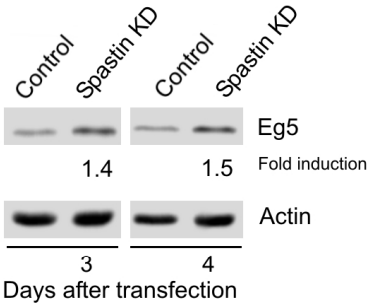

Effect of spastin depletion on cell proliferation of T98G glioblastoma cells. Immunoblots of whole extracts from negative control or spastin-depleted cells (Spastin KD) were probed with antibodies to Eg5 and actin (loading control). Numbers under the blots indicate relative amounts of Eg5 normalized to control cells.

VI.3

Hořejší B., **Vinopal S.**, Sládková V., Dráberová E., Sulimenko V., Sulimenko T., Vosecká V., Philimonenko A., Hozák P., Katsetos C. D., Dráber P. (2012). Nuclear γ-tubulin associates with nucleoli and interacts with tumor suppressor protein C53. J Cell Physiol. *227*, 367-382.

Journal of Cellular Physiology

Nuclear γ-Tubulin Associates With Nucleoli and Interacts With Tumor Suppressor Protein C53

BARBORA HOŘEJŠÍ,[1] STANISLAV VINOPAL,[1] VLADIMÍRA SLÁDKOVÁ,[1] EDUARDA DRÁBEROVÁ,[1] VADYM SULIMENKO,[1] TETYANA SULIMENKO,[1] VĚRA VOSECKÁ,[1] ANATOLY PHILIMONENKO,[2] PAVEL HOZÁK,[2] CHRISTOS D. KATSETOS,[3,4,5] AND PAVEL DRÁBER[1]*

[1]*Department of Biology of Cytoskeleton, Institute of Molecular Genetics, Academy of Sciences of the Czech Republic, Czech Republic*

[2]*Department of Biology of the Cell Nucleus, Institute of Molecular Genetics, Academy of Sciences of the Czech Republic, Czech Republic*

[3]*Department of Pediatrics, Drexel University College of Medicine, St. Christopher's Hospital for Children, Philadelphia, Pennsylvania*

[4]*Department of Pathology and Laboratory Medicine, Drexel University College of Medicine, St. Christopher's Hospital for Children, Philadelphia, Pennsylvania*

[5]*Department of Neurology, Drexel University College of Medicine, Philadelphia, Pennsylvania*

γ-Tubulin is assumed to be a typical cytosolic protein necessary for nucleation of microtubules from microtubule organizing centers. Using immunolocalization and cell fractionation techniques in combination with siRNAi and expression of FLAG-tagged constructs, we have obtained evidence that γ-tubulin is also present in nucleoli of mammalian interphase cells of diverse cellular origins. Immunoelectron microscopy has revealed γ-tubulin localization outside fibrillar centers where transcription of ribosomal DNA takes place. γ-Tubulin was associated with nucleolar remnants after nuclear envelope breakdown and could be translocated to nucleoli during mitosis. Pretreatment of cells with leptomycin B did not affect the distribution of nuclear γ-tubulin, making it unlikely that rapid active transport via nuclear pores participates in the transport of γ-tubulin into the nucleus. This finding was confirmed by heterokaryon assay and time-lapse imaging of photoconvertible protein Dendra2 tagged to γ-tubulin. Immunoprecipitation from nuclear extracts combined with mass spectrometry revealed an association of γ-tubulin with tumor suppressor protein C53 located at multiple subcellular compartments including nucleoli. The notion of an interaction between γ-tubulin and C53 was corroborated by pull-down and co-immunoprecipitation experiments. Overexpression of γ-tubulin antagonized the inhibitory effect of C53 on DNA damage G_2/M checkpoint activation. The combined results indicate that aside from its known role in microtubule nucleation, γ-tubulin may also have nuclear-specific function(s).

J. Cell. Physiol. 227: 367–382, 2012.

Microtubules, assembled from αβ-tubulin heterodimers, play a decisive role in many cellular functions such as intracellular transport, cell organization, and cell division. One of the key components required for microtubule organization is γ-tubulin (Oakley and Oakley, 1989), a highly conserved, albeit minor, member of the tubulin superfamily concentrated mainly in microtubule organizing centers (MTOCs) (Stearns et al., 1991). In mitotic cells γ-tubulin is distributed along spindle fibers (Lajoie-Mazenc et al., 1994) and is found in midbodies during cytokinesis (Julian et al., 1993). However, the greater part of γ-tubulin is associated in cytoplasmic complexes with other proteins. Large γ-tubulin-ring complexes (γTuRCs) are formed by γ-tubulin small complexes (γTuSCs), comprising two molecules of γ-tubulin and one molecule each of γ-tubulin complex protein 2 (GCP2) and γ-tubulin complex protein 3 (GCP3), along with other proteins, including GCP4, 5, and 6 (Raynaud-Messina and Merdes, 2007). The γTuRCs embedded in MTOC matrix then nucleate microtubules. In addition to nucleation from MTOC, γTuRCs are also involved in the regulation of microtubule minus-end dynamics (Wiese and Zheng, 2000). We and others have demonstrated that γ-tubulin is associated with cellular membranes (Chabin-Brion et al., 2001; Dryková et al., 2003; Bugnard et al., 2005) where it can participate in non-centrosomal microtubule nucleation (Chabin-Brion et al., 2001; Efimov et al., 2007; Macurek et al., 2008). γ-Tubulin complexes apparently also play a role in the regulation of microtubule plus-end dynamics and in the spindle

Additional Supporting Information may be found in the online version of this article.

Contract grant sponsor: Grant Agency of the Czech Republic;
Contract grant numbers: 204/09/1777 (P.D.), 204/09/H084 (B.H.), P302/10/1701 (E.D).
Contract grant sponsor: Ministry of Education, Youth and Sports of the Czech Republic;
Contract grant numbers: LC545 (A.P., P.H., P.D.), 1M6837805001(V.V.).
Contract grant sponsor: Grant Agency of the Czech Academy of Sciences;
Contract grant number: KAN200520701 (V.S., T.S.).
Contract grant sponsor: Institutional Research Support;
Contract grant number: AVOZ 50520514 (P.D.).
Contract grant sponsor: Grant Agency of Charles University;
Contract grant number: 11109 (S.V.).
Contract grant sponsor: St Christopher's Foundation for Children (Philadelphia);
Contract grant number: 203 (C.D.K.).

*Correspondence to: Dr. Pavel Dráber, Department of Biology of Cytoskeleton, Institute of Molecular Genetics, Academy of Sciences of the Czech Republic, Vídeňská 1083, 142 20 Prague 4, Czech Republic. E-mail: paveldra@img.cas.cz

Received 6 December 2010; Accepted 24 March 2011

Published online in Wiley Online Library (wileyonlinelibrary.com), 4 April 2011.
DOI: 10.1002/jcp.22772

assembly checkpoint signaling (Raynaud-Messina and Merdes, 2007).

Whereas multiple families encode the α- and β-tubulins, there are only two functional genes in mammalian cells (TUBG1, TUBG2) that code very similar γ-tubulins (Wise et al., 2000; Yuba-Kubo et al., 2005). γ-Tubulin is post-translationally modified (Moudjou et al., 1996; Sulimenko et al., 2002), and phosphorylation (Vogel et al., 2001; Kukharskyy et al., 2004) as well as mono-ubiquitination (Starita et al., 2004) of γ-tubulin have been described.

Notwithstanding the entrenched view that γ-tubulin constitutes a typical cytosolic protein, there is a growing body of evidence documenting that γ-tubulin interacts with nuclear proteins which take part in DNA damage checkpoint and repair. γ-Tubulin co-immunoprecipitated from nuclear fraction the DNA damage checkpoint kinase ATR (Zhang et al., 2007) as well as the Rad51, protein involved in recombination repair (Lesca et al., 2005). The role(s) of γ-tubulin in these assemblies are not fully understood, and the mechanism responsible for the translocation of γ-tubulin into nucleus is unknown. Interestingly, aberrant presence of class II β-tubulin in the nucleus has been linked to cancerous transformation (Walss-Bass et al., 2002; Yeh and Luduena, 2004).

Previously we have demonstrated excessive and ectopic accumulation of γ-tubulin in glioblastoma cell lines and in primary gliomas corresponding to the acquisition of a malignant state (Katsetos et al., 2006; Katsetos et al., 2009). To gain a deeper insight into the function of γ-tubulin in malignant cells, we have examined the expression, distribution, and compartmentalization of this protein in glioblastoma cell lines. Here we report evidence of an enhanced expression and nucleolar accumulation of γ-tubulin in tumor cells. However, unlike overexpression of γ-tubulin in glioblastoma cells, nucleolar localization was not limited to neoplastic cells, as it was also found in both transformed and non-transformed cultured mammalian cells. Interestingly, both endogenous and exogenous γ-tubulins were detected in the nucleoli. Our data also indicate that γ-tubulin can be translocated into nucleoli during mitosis while rapid active transport of γ-tubulin via nuclear pores during interphase was not detected. Finally, we report on interaction of nucleolar γ-tubulin with tumor suppressor protein C53. Collectively, our findings indicate that aside from microtubule nucleation γ-tubulin might also be engaged in nuclear-specific function(s).

Material and Methods

Cell cultures and transfections

Human glioblastoma cell lines U138MG, U118MG, and T98G, human osteogenic sarcoma cells U2OS, human epitheloid carcinoma HeLa S3 cells, mouse embryonal carcinoma cells P19, mouse neuroblastoma Neuro-2a, mouse embryonal fibroblasts NIH 3T3 and Madin-Darby canine kidney cells MDCK were obtained from the American Type Culture Collection (Manassas, VA). Human kidney embryonal cells HEK293-FT (HEK) were from Promega Biotec (Madison, WI). Cells were cultured in Dulbecco's modified Eagle's medium (DMEM) containing 10% fetal bovine serum, penicillin (100 units/ml), and streptomycin (0.1 mg/ml). Cells were grown at 37°C in 5% CO_2 in air and passaged every 2 or 3 days using 0.25% trypsin/0.01% EDTA in PBS, pH 7.5. Proliferating non-immortalized, non-transformed normal human fetal astrocytes (NHA; Clonetics® Astrocyte Cell Systems), were from Cambrex Bio Science (Walkersville, MD) and were maintained as described (Dráberová et al., 2008). Proliferating non-immortalized, non-transformed normal human small airway epithelial cells (SAEC) were from Lonza (Cologne, Germany), and were maintained in supplemented SAEC Basal Medium according to manufacturer's directions. In some cases, U2OS cells were incubated for 3 h with 20 nM leptomycin B (LMB; Sigma, St. Louis, MO) before fixation. To induce genotoxic stress, U2OS cells were incubated for 3 or 20 h in 20 μM etoposide (Sigma, St. Louis, MO).

U138MG cells were transfected with 500 ng DNA/well in a 24-well plate using Lipofectamine LTX reagent and Opti MEM medium according to the manufacturer's instructions (Invitrogen, Carlsbad, CA). After 5 h, the transfection mixture was replaced with fresh complete medium, and cells were incubated for 48 h. U2OS cells were transfected with 2.5 μg DNA per 3.5-cm tissue culture dish using Lipofectamine LTX reagent. HEK cells were transfected with 17 μg DNA per 9-cm tissue culture dish using 51 μg polyethylenimine (Polysciences, Warrington, PA) and serum-free DMEM. After 24 h, the transfection mixture was replaced with fresh medium supplemented with serum, and cells were incubated for additional 24 h.

DNA constructs

C-terminally FLAG-tagged γ-tubulin 1 was constructed by PCR amplification of full length cDNA of human γ-tubulin 1 from pH3-16 vector (Zheng et al., 1991) using forward 5′-ACGAATTCTGCCTGAGGAGCGATGC-3′ and reverse 5′-TCAAGTCGACCTGCTCCTGGGTGCC-3′ primers (restriction sites underlined) to allow subcloning into the pFLAG-CMV-5a vector (Sigma). For preparation of the construct expressing N-terminally FLAG-tagged γ-tubulin 1, forward 5′-AGTCAAGCTTCCGAGGGAAATCATCACC-3′ and reverse 5′-CCGAGATCTACCAGTAAGGCAGAT GAGG-3′ primers were used for PCR amplification. The PCR product was then cloned into pFLAG-CMV-4 (Sigma). TUBG1, digested from pH3-16 by *Eco*RI, was also subcloned into pCI-NEO expression vector (Promega). For preparation of the construct expressing C-terminally Dendra2-tagged γ-tubulin 1, forward 5′-CAAGATCTACCATGCCGAGGGAAATCATC-3′ and reverse 5′-ATTGGTACCTTCTGCTCCTGGGTGCC-3′ primers were used for amplification from pH3-16 vector. The PCR product was then cloned into pDendra2-N1 vector (pEGFP-N1 vector from Clontech in which EGFP sequence has been replaced by Dendra2 sequence). GST-tagged g-tubulin 1 was described (Macurek et al., 2008).

Full length cDNA of mouse protein tyrosine kinase $p59^{Fyn}$ (Fyn) was amplified from pBSRαEN vector (Gauen et al., 1992) by PCR using forward 5′-ACGAATTCATGGGCTGTGTGCA ATG-3′ and reverse 5′-CGTCGTCTAGATCACAGG TTTTC ACCG-3′ primers, and the isolated fragment was ligated into pCI-NEO vector. The constructed vector served as template for additional PCR amplification of Fyn, using forward 5′-ACGAATTCATGGGCTGTGTGCAATG-3′ and reverse 5′-ACTGTCGACTAACAGGTTTTCACCG-3′ primers. C-terminally FLAG-tagged Fyn was generated by the insertion of isolated fragment into pFLAG-CMV5a vector. N-terminally FLAG-tagged human nucleophosmin was described previously (Bertwistle et al., 2004).

Total RNA from BALB/c adult mouse brain was isolated by the RNeasy Mini kit (QIAGEN, Valencia, CA) and reverse transcription was performed with oligo(dT) primers and ImProm-II RT kit (Promega). The fragment coding mouse GCP5 (TUBGCP5, Refseq ID: NM_1469) was amplified by PCR using forward 5′-AGTCGGATCCAAAGCTGCTAGTTGGAAG AG-3′ and reverse 5′-AAGCGTCGACTCTCGGAAGCG CCTGGTTGTC-3′ primers and total cell cDNA as template. The isolated fragment was ligated into pGEX-6P-1 vector (Amersham Biosciences, Freiburg, Germany) for preparation of GST-tagged fusion protein. All constructs were verified by sequencing.

N-terminally GST-tagged CDK5 regulatory subunit-associated protein 3 (C53) was prepared by PCR amplification

of full length cDNA of C-terminally Myc-FLAG-tagged human C53 clone (#RC209901; Origene, Rockville, MD) using forward 5′TAATCCCGGGTGAGGACCATCAGCAC-3′ and reverse 5′-ATTATGCGGCCGCTCACAGAGAGGTTC-3′ primers. Isolated fragment was ligated into pGEX-6P-1 vector (Amersham Biosciences). C-terminally EGFP-tagged C53 (pC53-EGFP) was prepared by PCR amplification of full length cDNA of human C53 clone (#RC209901; Origene) using forward 5′-TGCTAGCGGAGGAAAGATGGAGGAC-3′ and reverse 5′-TGTCGACCAGAGAGGTTCCCATCAG-3′ primers carrying *Nhe*I and *Sal*I restriction sites, respectively. PCR product was inserted in the pCR-2.1-TOPO vector (Invitrogen). Coding sequence of C53 was digested from this vector using *Nhe*I and *Sal*I restriction enzymes and the isolated fragment was ligated into EGFP-N3 vector (Clontech, Laboratories, Mountain View, CA). C-terminally FLAG-tagged α-tubulin was constructed by PCR amplification of full-length cDNA of human α-tubulin from pEGFP-Tub vector (Clontech Laboratories) using forward 5′-CAAGATCTATGCGTGAGT GCATCTCCA-3′ and reverse 5′-CTGGTACCGTATTCCT CTCCTTCTTCCTC-3′ primers to allow subcloning into the pFLAG-CMV-5a vector (Sigma).

U2OS cells stably expressing C53-EGFP were obtained by transfection of cells with pC53-EGFP, and selection in 1.1 mg/ml geneticin (G418, Sigma) for 2 weeks. Cells were then diluted to one cell/well on 96-well plate and allowed to grow for 2 weeks. Homogenous colonies expressing C53-EGFP were propagated and used for further studies.

Antibodies

The following anti-peptide antibodies (Abs) to human γ-tubulin were used: monoclonal antibodies (mAbs) TU-30, TU-31, and TU-32 to the sequence 434–449 (Nováková et al., 1996); Ab DQ-19 to the sequence 433-451 (Sigma, T3195) and Ab (Sigma, T5192) to the sequence 38–53. α-Tubulin and β-tubulin were detected with mAbs TU-01 and TU-06, respectively (Dráber et al., 1989). Microtubule structures were visualized by Ab to αβ-tubulin dimer (Dráber et al., 1991). Pericentrin was detected with Ab M8 (Doxsey et al., 1994) and centrin 2 with Ab from Biolegend (San Diego, CA; 628801). Abs to coilin (C1862), nucleolin (N2662), GAPDH (G9545), actin (A2066), FLAG peptide (F1804 and F7425), and p53 (P5813) were from Sigma. Abs to UBF (sc-9131), fibrillarin (sc-25937), and Cdk1-p-Y15 (sc-136014) were from Santa Cruz Biotechnology (Santa Cruz, CA). Abs to C53 were from Novus Biologicals (Littleton, CO; NB110-40617) or Abcam (Cambridge, MA; ab70776), mAb to C53 was from Santa Cruz (sc-101093). Abs to cyclin B1 (4138), H2AX-p-S139 (ab18311), myosin (BT-561), and Fyn (1562-1) were from Cell Signaling (Danvers, MA), Abcam, Biomedical Technologies (Stoughton, MA) and Epitomics (Burlingame, CA), respectively. Ab to cyclophilin A was from Millipore (Schwalbach/Ts, Germany; 07-313). MAb to fibrillarin (ab4566) and Ab to ATM-p-S1981 (ab8192) were from Abcam. MAbs NF-09 to neurofilament NF-M protein (Dráberová et al., 1999) and VI-01 to vimentin (Dráberová et al., 1986) served as controls. Secondary Cy3-conjugated and FITC-conjugated Abs were from Jackson Immunoresearch Laboratories (West Grove, PA). Anti-rabbit Ab conjugated with Alexa 488 was from Invitrogen. Secondary horseradish peroxidase-conjugated Abs were from Promega. The anti-rabbit Ab conjugated with 10 nm gold particles was from British Biocell International (Cardiff, United Kingdom). Anti-mouse Ab conjugated with 6 nm gold particles was from Jackson Immunoresearch Laboratories.

To prepare mAbs specific for GCP2, GST-tagged fragment coding mouse GCP2 (Swiss-Prot accession no. Q921G8) polypeptide (a.a. 2-194), was prepared (Macurek et al., 2008) and used as antigen. Immunization of F1(B10AxBALBc) mice, fusion with mouse myeloma cells Sp2/0, screening by ELISA and cloning have been described previously (Viklický et al., 1982; Dráber et al., 1988). The mAb GCP2-01 (IgG2b) stained MTOC in cell lines of various origin and recognized GCP2 on blots from total cell lysates or after immunoprecipitation with anti-γ-tubulin Ab.

Anti-GCP5 rabbit Ab was prepared according to a method described previously (Dráber et al., 1991), and was affinity-purified on GST-GCP5 coupled to CNBr-activated Sepharose (Amersham). The Ab was eluted using 3.5 M $MgCl_2$ in 5% dioxane and dialyzed against PBS, pH 7.5. The Ab specificity was verified by immunoblotting and immunofluorescence microscopy.

RNA silencing

U2OS cells in 24-well plates were transfected with siRNAs (final concentration 10 nM) using Lipofectamine RNAi MAX (Invitrogen) according to the manufacturer′s instructions. Two siRNAs (Dharmacon, Lafayette, CO) that target regions present in human γ-tubulin 1 and γ-tubulin 2 isoforms at nucleotide positions 1230-1247 (5′-GGAGGACAUGUUCAA GGA-3′; siRNA#1) and 259-279 (5′-AACCCAGAGA ACAUCUACCUG-3′; siRNA#2) were used. dTdT overhangs were added to the 3′ of the oligomers. Maximal depletion was reached by transfecting the siRNA twice with a 96-h time interval and with harvesting cells 48 h after the second transfection (Haren et al., 2006). siRNA (Ambion) that targets the region present in human C53 at nucleotide positions 438-456 (5′- GGUUCGGAAUGUCAACUAU-3′) was used. dTdT overhang was added to the 3′ of the oligomer. Cells were harvested 48 h after transfection with siRNA. Negative control siRNA was from Applied Biosystems (Prague, Czech Republic; Silencer Negative Control #1 siRNA).

Quantitative real-time PCR (qRT-PCR) analysis

Total cellular RNA from cultured cells was extracted as described above. Aliquots of total RNA were converted to cDNA using the ImProm-II RT kit (Promega) with oligo(dT) primers. Amplifications were performed with gene-specific primers for human γ-tubulin 1 (TUBG1, NM_001070), γ-tubulin 2 (TUBG2, NM_016437), or β-actin (ACTB, NM_001101). Primer sequences are summarized in Supplemental Table S1). Oligonucleotides were from East Port (Prague, Czech Republic). qRT-PCRs were carried out on Master-cycler realplex (Eppendorf, Wesseling-Berzdorf, Germany) as decribed (Dráberová et al., 2008). The expression of analyzed genes was normalized to the expression of β-actin. Levels of β-actin did not differ significantly between glioblastoma cell lines and NHA. Identity of PCR products was verified by sequencing. Statistical analysis was performed with the Student′s unpaired *t*-test.

Cell fractionation

Nucleoli were prepared from T98G cells at 4°C essentially as described (Andersen et al., 2002). Briefly, washed cells were resuspended in buffer A (Andersen et al., 2002), supplemented with protease (Protease inhibitor cocktail tabletes; Roche, Basel Switzerland) and phosphatase (1 mM Na_3VO_4 and 1 mM NaF) inhibitors, disrupted in Dounce homogenizer and centrifuged at 228 *g* for 5 min. Supernatant represented the cytosolic fraction. The pellet was resuspended in 10 mM $MgCl_2$ in 0.25 M sucrose and layered over 0.35 M sucrose containing 0.5 mM $MgCl_2$. After centrifugation at 1,430 *g* for 5 min, the pellet (nuclear fraction) was resuspended in 0.35 M sucrose containing 0.5 mM $MgCl_2$ and sonicated. Absence of intact nuclei was verified by phase contrast microscopy. Sonicated sample was layered over 0.88 M sucrose containing 0.5 mM $MgCl_2$ and centrifuged at 2,800 *g* for 10 min. Supernatant represents the nucleoplasmic fraction. The pellet was

resuspended in 0.35 M sucrose containing 0.5 mM $MgCl_2$ and centrifuged at 2,000 *g* for 2 min to obtain highly purified nucleoli.

For immunoprecipitation experiments or gel filtration chromatography nuclei or nucleoli were extracted by RIPA buffer (50 mM Tris pH 8.0, 150 mM NaCl, 1% NP-40, 0.5% sodium deoxycholate and 0.1% SDS) supplemented with protease and phosphatase inhibitors.

Whole-cell extracts for GST pull-down assays were prepared in 1% NP-40 in Hepes buffer (50 mM Hepes pH 7.6, 75 mM NaCl, 1 mM $MgCl_2$ and 1 mM EGTA) supplemented with inhibitors. Whole-cell extracts for sodium dodecyl sulfate-polyacrylamide gel electrophoresis (SDS-PAGE) were prepared solubilizing cells in hot SDS-sample buffer.

Gel filtration chromatography

Gel filtration was performed using fast protein liquid chromatography (AKTA-FPLC system, Amersham) on Superose 6 10/300 GL column (Amersham). Column equilibration and chromatography was performed in RIPA buffer. Column was eluted at 30 ml/hod, and 0.5-ml aliquots were collected. Samples for SDS-PAGE were prepared by mixing with 5x concentrated SDS-sample buffer. The following molecular mass standards were used: immunoglobulin IgM (900 kDa), thyroglobulin (669 kDa), ferritin (440 kDa), catalase (232 kDa), and BSA (66 kDa).

Immunoprecipitation, GST pull-down assay, gel electrophoresis, and immunoblotting

Immunoprecipitation was performed as described (Kukharskyy et al., 2004). Cell extracts were incubated with beads of protein A (Pierce, Rockford, IL) saturated with: (i) mAb TU-31 (IgG2b) to γ-tubulin, (ii) rabbit Ab to C53, (iii) rabbit Ab to non-muscle myosin (negative control), (iv) mAb NF-09 (IgG2a; negative control), or with (v) immobilized protein A alone.

For large-scale immunoprecipitation experiments, HeLa S3 cells grown in suspension to cell density 3.5×10^5 cells/ml (total 1.5 L) were collected and nuclei isolated as described above. Nuclei were solubilized in 2 ml RIPA buffer with inhibitors for 10 min at 4°C, and suspension centrifuged at 28,000 g for 10 min at 4°C. Supernatant was thereafter incubated with anti-peptide mAb TU-31 immobilized onto 500 μl of protein A-Sepharose. After extensive washing, protein A with bound proteins was loaded into column and eluted with immunizing peptide (Nováková et al., 1996) at concentration 200 μg/ml in dd water. Fractions containing γ-tubulin were collected and concentrated to 25 μl in vacuum concentrator (SpeedVac SC 110, Savant).

GST pull-down assays with whole-cell extracts were performed as described (Kukharskyy et al., 2004). Gel electrophoresis and immunoblotting were performed using standard protocols. Two-dimensional electrophoresis (2D-PAGE) was performed as described (Sulimenko et al., 2002).

For immunoblotting Abs to γ-tubulin (Sigma T5192), cyclophilin A, FLAG, Fyn, GCP5, and UBF were diluted 1:10,000, 1:5,000, 1:5,000, 1:500, 1:500, and 1:200, respectively. Abs to GAPDH, fibrillarin and centrin 2 were diluted 1:10,000, 1:5,000, and 1:3,000, respectively. Abs to cyclin B1, Cdk1-p-Y15, ATM-p-S1981 and H2AX-p-S139 and were diluted 1:1,000, 1:1,000, 1:1,000, and 1:5,000, respectively. MAbs to α-tubulin (TU-01), β-tubulin (TU-06), γ-tubulin (TU-32), GCP2 (GCP2-01), and vimentin (VI-01), in the form of spent culture supernatants, were diluted 1:10. MAb to C53 was diluted 1:1000. Peroxidase-conjugated secondary Abs were diluted 1:10,000. Bound Abs were detected by SuperSignal WestPico Chemiluminescent reagents (Pierce).

Mass spectrometry

Following large-scale immunoprecipitation, concentrated samples after peptide elution were dissolved in 2x Laemmli sample buffer and separated on 8% SDS-PAGE (50 μl sample/well) using Multigel-Long electrophoretic system (Biometra, Goettingen, Germany). Gels were stained by Coomassie Brilliant Blue G-250. The spots of interest were cut out from the gel, and trypsin gel-in digestion, peptide extraction, and spotting on matrix-assisted laser desorption ionization (MALDI) plate (Bruker Daltonics, Billerica, MA) were performed as described (Heneberg et al., 2010). Samples were ionized using Dual II ion source (Bruker Daltonics). Mass spectra were acquired on an APEX-Qe Fourier transformation mass spectrometry instrument equipped with 9.4 tesla superconducting magnet (Bruker Daltonics) at the Core facility of Biomedical Institutes, Prague-Krc, Czech Republic. The spectra were processed by Data Analysis 4.0 software (Bruker Daltonics) and searched by Mascot search engine against the data base (SwissProt) created from all known *Homo sapiens* proteins.

Heterokaryon assay

Heterokaryon assay was performed as described (Ma et al., 2008). Shortly, transfected human U2OS cells (5×10^5) in a 3.5-cm tissue culture dish with coverslips were cultured for 24 h, washed, and then overlaid with mouse NIH 3T3 cells (5×10^5), and cultured for another 12 h. Cycloheximide (Sigma) was then added to final concentration 100 μg/ml for 30 min in order to block proteosynthesis. Cells were washed with PBS and fused with 50% polyethylene glycol 3350 (Sigma) in PBS for 2 min, washed again three times in PBS and incubated for 2 h in culture medium containing cycloheximide (100 μg/ml). Cells were then fixed for immunostaining. Murine nuclei were easily recognized by the presence of bright chromatin aggregates (Hache et al., 1999).

Immunofluorescence

Immunofluorescence microscopy was performed as previously described (Dráberová and Dráber, 1993). A brief description of the fixation protocols, with abbreviations in parentheses, follows. Cells on coverslips were rinsed with microtubule-stabilizing buffer (MSB; 1 M Mes, pH 6.9, 2 mM EGTA, 2 mM $MgCl_2$), fixed in 3% formaldehyde in MSB and extracted with 0.5% Triton X-100 in MSB (F/Tx). Preparations were further post-fixed in methanol (F/Tx/M). Alternatively, cells were extracted with 0.2% Triton X-100 in MSB, fixed in 3% formaldehyde, and post-fixed in methanol (Tx/F/M); or cells were directly fixed in methanol (M). Cells were also extracted for 1 min with 0.2% Triton X-100 in MSB at 37°C and thereafter incubated (2×5 min) with 3:1 mixture of glacial acetic acid and methanol at 4°C (Tx/HAc/M). Samples were then washed in PBS.

Abs to γ-tubulin (Sigma, T3195 and T5192) and αβ-tubulin dimer were diluted 1:300 and 1:10, respectively. Abs to nucleolin, Fyn, cyclophilin A, and GCP5 were diluted 1:800, 1:100, 1:500, and 1:500, respectively. Abs to fibrillarin (Santa Cruz, sc-25937), pericentrin, C53 (Abcam ab70776) and UBF were diluted 1:200. MAbs TU-30, TU-31, and TU-32 to γ-tubulin, as well as TU-01 to α-tubulin and TU-06 to β-tubulin, were used as undiluted spent culture medium. MAbs to FLAG peptide, coilin, p53, and fibrillarin were diluted 1:1,000, 1:100, 1:200, and 1:200, respectively. Cy3-conjugated, FITC-conjugated, and Alexa 488 secondary Abs were diluted 1:500, 1:200, and 1:200, respectively.

For double-label immunofluorescence, the coverslips were incubated separately with the primary Abs, and simultaneously with the secondary conjugated Abs. The preparations were mounted in MOWIOL 4-88 (Calbiochem, San Diego, CA) supplemented with 4,6-diamidino-2-phenylindole (DAPI) to label nuclei, and examined with Olympus A70 Provis

microscope equipped with 40x or 60x water-immersion and 100x oil-immersion objectives. Conjugates alone did not give any detectable staining. Alternatively, samples were examined with a confocal laser scanning microscope Leica TCS SP5 (Leica) equipped with 63x oil-immersion objective. Excitation and emission wavelengths were 405 nm and 408–532 nm for DAPI (UV diode laser), 488 nm and 492–542 nm for Alexa 488 (Argon laser) and 561 nm and 565–633 nm for Cy3 (diode pumped solid-state laser). Optical sections were acquired in 0.2 μm steps, and z-series were made from 25 to 30 sections.

Quantification of immunofluorescence was performed on Olympus Scan^R screening station equipped with 40x (1.3 N.A.) oil-immersion objective. Control and LMB-treated cells were stained for γ-tubulin, p53, or DAPI, and 500 images (~3,000–10,000 cells) were collected. Acquired images were segmented and evaluated using Scan^R analysis software. Mean intensity of fluorescence signals for γ-tubulin or p53 was measured in nuclei (defined by DAPI) and cytoplasm (defined as 4.8 μm wide area around nuclei), and ratios of nucleoplasmic to cytoplasmic signals (localization indexes) were calculated.

In some experiments, the TU-30 mAb was preabsorbed with peptides corresponding to the human γ-tubulin sequence 434–449 (peptide used for immunization) or to the sequence 38–53 (negative control). Two molar Ab to peptide ratios were used, 1:10 and 1:100. Mixtures of Abs and peptides were incubated for 30 min at room temperature.

Time-lapse imaging

For time-lapse imaging, U2OS cells expressing green to red photoconvertible γ-tubulin-Dendra2 protein or Dendra2 alone were grown on glass-bottom-dishes (MatTek). Time-lapse sequences were collected at 15 sec intervals with Delta Vision Core system (Applied Precision) equipped with 40x/1.35 NA oil-immersion objective. At each time point 3 optical sections in 0.75 μm steps were collected. Dendra2 was activated with 405 nm diode laser line (75% laser power) 30 sec after starting the time-lapse imaging. The intensity of red fluorescence was determined in nuclei and cytoplasm (ROI ~100 μm^2), and ratios of nucleoplasmic to cytoplasmic signals were calculated.

Immunoelectron microscopy

Cells on coverslips were fixed for 30 min in 3% paraformaldehyde, 0.1% glutaraldehyde in Sörensen buffer (SB; 0.1 M Na/K phosphate buffer, pH 7.3). They were washed (2 × 10 min) in SB and then incubated in 0.2 M glycin in SB for 10 min. Samples were then dehydrated in ethanol. Ethanol was replaced in two steps with LR White resin (Polysciences), and the resin was polymerized by UV light (48 h, 4°C). Alternatively, cells were grown on sapphire discs (Leica, 1.4 mm), immersed quickly in 20% dextran in culture medium, transferred to the membrane specimen carrier (Leica, 1.5 mm cavity diameter), and frozen in the Leica EM PACT2 high pressure freezer. Frozen samples in the carriers were transferred under liquid nitrogen to the Leica AFS2 automatic freeze substitution machine equipped with Leica EM FSP. Cells were freeze substituted in acetone at −90°C for 2 days, the temperature was then elevated at a rate of 5°C/h to −50°C, and the samples were incubated for the next 24 h. The samples were then infiltrated in 2:1 (v/v), 1:1 (v/v), and 1:2 (v/v) acetone/Lowicryl HM20 (Polysciences) mixtures (3 h each at −50°C), followed by five changes of pure Lowicryl HM20 at −50°C, for 32 h in total. After a next change of pure resin, the temperature was elevated to −10°C at a rate of 1.7°C/h (24 h in total), and the samples were covered with fresh resin. Polymerization was effected by UV light (48 h, −10°C) and by gradual temperature elevation to 20°C in the course of the following 32 h.

After cutting 80 nm sections, non-specific labeling was blocked by preincubation with 10% normal goat serum (British BioCell International), 1% BSA and 0.1% Tween 20 in PBS for 30 min at room temperature. The sections were incubated with anti-γ-tubulin Ab DQ-19 or anti-C53 mAb diluted 1:200 and 1:100, respectively, washed three times in PBT (0.005% Tween 20 in PBS), incubated with 10 nm gold-conjugated anti-rabbit Ab or 6 nm gold-conjugated anti-mouse Ab, diluted 1:50, washed twice in PBT, and twice in bidistilled water, and then air-dried. Finally, sections were contrasted with a saturated solution of uranyl acetate in water (4 min) and inspected in Morgagni 268 electron microscope (FEI) equipped with SIS MegaView III digital camera. Control incubations without primary Ab proved that the signal was highly specific.

Results

Differential expression of γ-tubulins in human astrocytes versus glioblastoma cell lines

First, we compared the subcellular distribution of γ-tubulin in non-immortalized, non-transformed human fetal astrocytes, hereafter referred as normal human astrocytes (NHA) and human glioblastoma cell lines. In the former, γ-tubulin was localized mainly to MTOC (Fig. 1A, a), while in the latter it showed a robust, dense and diffuse distribution of γ-tubulin throughout the cytoplasm extending into the cell periphery (Fig. 1A, c). In contrast, the spatial distribution of microtubules in glioblastoma cells T98G (Fig. 1A, d) and NHA (Fig. 1A, b) was similar. Prominent punctuate cytoplasmic γ-tubulin staining was observed in all three tested cell lines (T98G, U138MG, U118MG) prepared under different conditions of fixation. Immunofluorescence labeling for γ-tubulin was strikingly more robust and widespread in glioblastoma cells as compared to NHA when probed with a panel of five well-characterized Abs recognizing distinct epitopes in the C-terminal region mAbs TU-30, TU-31, TU-32, and polyclonal Ab from Sigma T3195) as well as in the N-terminal region (polyclonal Ab from Sigma T5192) of the γ-tubulin molecule (data not shown).

To compare the expression of γ-tubulin in NHA and glioblastoma cell lines, blots of whole cell extracts were probed with Abs to γ-tubulin and vimentin. A higher amount of γ-tubulin was detected in glioblastoma cell lines (Fig. 1B, γ-Tb), while no substantial differences were observed in the expression level of vimentin (Fig. 1B, Vim) or α-tubulin (results not shown). Densitometry measurements of immunoblots showed that the amount of γ-tubulin was approximately threefold in glioblastoma cell lines.

To decide whether both γ-tubulin genes (TUBG1 and TUBG2) are expressed in NHA and glioblastoma cell lines, the expression levels of mRNA for γ-tubulin 1 and γ-tubulin 2 were determined using qRT-PCR. The expression of both γ-tubulin 1 and γ-tubulin 2 mRNA significantly rose in all three glioblastoma cell lines tested as compared to NHA (Fig. 1C).

Collectively taken, these data demonstrate that the significant increase in transcripts for γ-tubulin 1 and γ-tubulin 2 in glioblastoma cell lines, as compared to NHA, is associated with higher amounts of γ-tubulin protein, as determined by both immunoblotting and immunofluorescence.

Nucleolar localization of γ-tubulin

Immunofluorescence experiments on glioblastoma cell lines subjected to various types of fixations revealed discrete nuclear regions very faintly stained with anti-γ-tubulin Abs in preparations fixed by cold methanol. This staining was more prominent when methanol-fixed samples were stored for prolonged time (up to 5 days) in PBS at 4°C. Bright nuclear staining for γ-tubulin was directly observed when samples were extracted with Triton X-100 and then fixed in a mixture of methanol and acetic acid (Tx/HAc/M). A comparison of the staining intensities obtained in preparations fixed by methanol or by Tx/HAc/M and immediately stained by anti-γ-tubulin Ab is

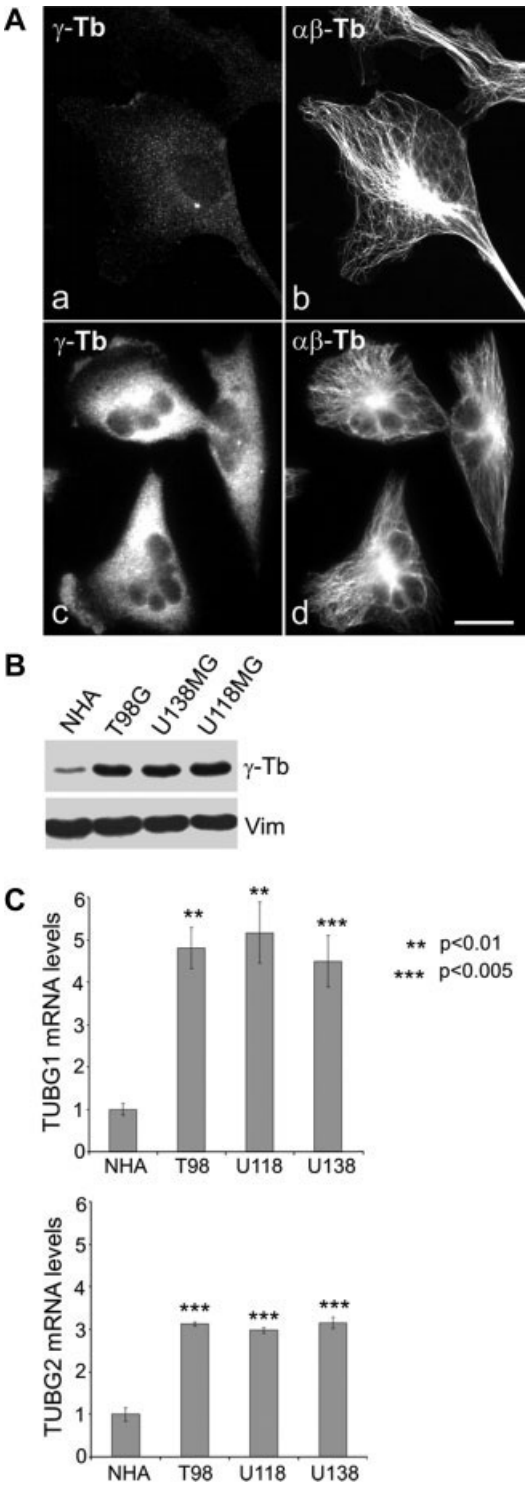

Fig. 1. Comparison of γ-tubulin expression in NHA and glioblastoma cell lines. A: NHA (a–b) and T98G cells (c–d) were stained with mAb to γ-tubulin (a, c) and Ab to αβ-tubulin dimer (b, d). Images were collected and processed in exactly the same manner. Fixation F/Tx/M. Scale bar 20 μm. B: Immunoblot analysis of whole cell extracts from NHA and glioblastoma cell lines. Staining with mAbs to γ-tubulin (γ-Tb) and vimentin (Vim). C: Transcription of genes for γ-tubulin 1 (TUBG1) and γ-tubulin 2 (TUBG2) in cell lines T98G (T98), U118MG (U118), and U138MG (U138) relative to the level in NHA. Data are presented as the mean fold change ± s.e.m. obtained from two independent experiments with triplicate samples.

illustrated in Figure 2-I. Double-label experiments with nucleolar markers were designed to improve the accuracy of γ-tubulin localization in the nucleus. Labeling with mAb to γ-tubulin and Abs to nucleolin (Fig. 2-II, A–C), UBF (Fig. 2-II, D–F), or fibrillarin (Fig. 2-II, G–I) clearly demonstrated that γ-tubulin was concentrated in the nucleoli. Staining of MTOC was preserved (arrows in Fig. 2-II, A, D, G). The Abs to α-tubulin, β-tubulin, pericentrin, GCP5, and cyclophilin A failed to decorate nucleoli. Interestingly, the mAb to GCP2 decorated nucleoli (not shown). Upon closer inspection diffuse γ-tubulin staining was also detectable in the nucleoplasm. Double-labeling with Abs to γ-tubulin and coilin revealed that γ-tubulin staining was clearly located outside the Cajal bodies, which are characterized by the presence of coilin (results not shown). Higher magnification of double-label stained nucleolus with Abs to γ-tubulin and fibrillarin is shown in Figure 3A. Fluorescence intensity scanning did not reveal co-localization either in the combination of γ-tubulin and fibrillarin (Fig. 3B) or γ-tubulin and UBF (data not shown). When anti-peptide mAb TU-30 was preabsorbed with its immunization peptide, no staining of nucleoli was observed. On the other hand, preabsorption of the TU-30 with γ-tubulin peptide derived from a different part of γ-tubulin molecule did not extinguish the staining, thus confirming the specificity of immunolabeling. Interestingly, nucleolar localization of γ-tubulin was more prominent with Abs directed to epitopes located in the C-terminal region of the γ-tubulin molecule (TU-30, TU-31, TU-32, polyclonal Ab DQ19), while polyclonal Ab T5192 directed against an epitope in the N-terminal region rendered a much weaker staining. This suggests a preferential exposure of the C-terminal region of γ-tubulin in nucleoli after fixation.

The nucleolus consists of three different regions: fibrillar centers (FC), dense fibrillar components (DFC), and granular components (GC) (Raška et al., 2006). To obtain data on subnucleolar localization of γ-tubulin, post-embedding immunoelectron microscopy was carried out on 80 nm sections of T98G cells. Electron microscopy examination of formaldehyde-fixed preparation disclosed that γ-tubulin in interphase T98G cells was located in GC or on the boundary between DFC and GC, and did not accumulate in FC where transcription of ribosomal DNA takes place (Fig. 3C). Large clusters of gold particles were occasionally also detected (Fig. 3C, insert). Different samples from three experiments on T98G cells were tested, and the labeling pattern was similar. The same staining pattern was obtained with cryofixation (Fig. 3D).

Nucleolar localization of γ-tubulin was not limited to glioblastoma cell lines with high expression of γ-tubulin, but was also detected in human NHA, SAEC, U2OS, and HEK cells, in canine MDCK as well as in murine P19 and Neuro-2a cells. This suggests that nucleolar γ-tubulin is present both in transformed and non-transformed cells of divergent cell and tissue origins. Immunostaining of nucleolar γ-tubulin in NHA, SAEC, U2OS, HEK, and MDCK cells is shown in Fig. S1.

To strengthen the evidence of nucleolar localization of γ-tubulin, U2OS cells were transfected with siRNAs that target γ-tubulin 1 and γ-tubulin 2. The level of γ-tubulin, including nucleolar γ-tubulin, in transfected cells was substantially lower, as revealed by immunofluorescence microscopy (Fig. S2A). γ-Tubulin knock-down was also confirmed by immunoblotting results (Fig. S2B) and by qRT-PCR (Fig. S2C). No marked impairment of nucleolar integrity was detectable in cells with knock-down of γ-tubulin on the basis of immunostaining with Ab to fibrillarin (Fig. S2D).

Distribution of γ-tubulin upon subcellular fractionation

To corroborate independently the presence of γ-tubulin in nucleoli, immunoblotting experiments were performed with

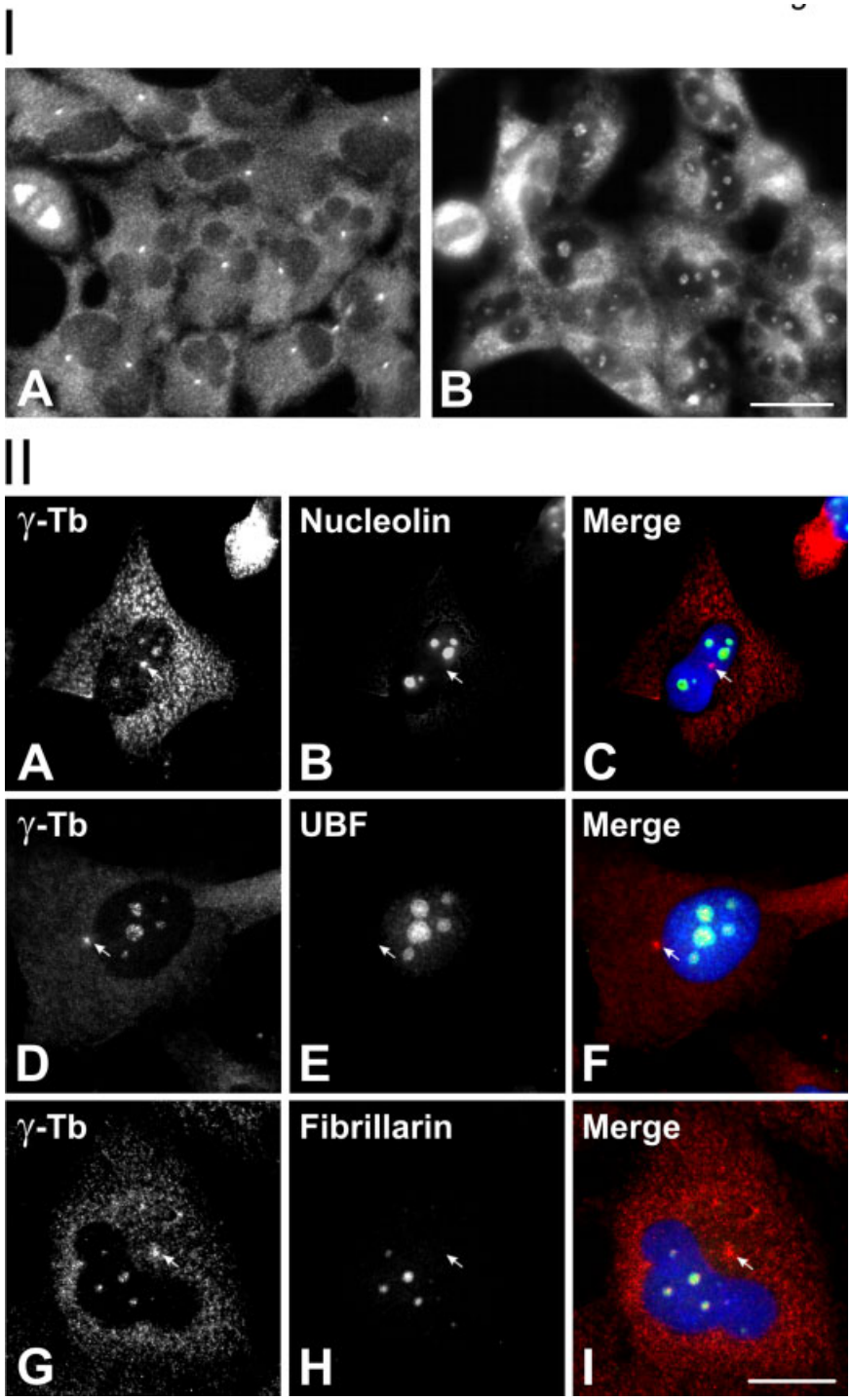

Fig. 2. Immunofluorescence staining of nucleolar γ-tubulin in T98G cells. I: Effect of fixation on γ-tubulin localization. A: Cells fixed by methanol. B: Cells extracted with Triton X-100 and then fixed by methanol/acetic acid mixture (Tx/HAc/M). Fixed cells were immediately stained with mAb TU-30 to γ-tubulin. Scale bar 25 μm. (II) Nucleolar localization of γ-tubulin. Cells were double-label stained with mAb TU-30 (A, D, G; red) and polyclonal Abs to nucleolar markers (green): nucleolin (B), UBF (E), fibrillarin (H). DAPI (C, F, I; blue). Arrows denote positions of MTOC. Fixation Tx/HAc/M. Scale bar 20 μm.

cytosolic, nuclear, and nucleolar extracts from T98G cells. The purity of isolated nucleolar preparations was checked by phase contrast light microscopy. When blots were probed with different Abs to γ-tubulin, a single band with relative mobility corresponding to γ-tubulin was obtained in tested fractions (Fig. 4A, γ-Tb). When the blots were probed with Ab to UBF, immunoreactivity was substantially higher in the nucleolar fraction (Fig. 4A, UBF). Stronger signal in nucleolar fraction was also detected with Abs to fibrillarin and nucleolin (not shown). No signal in nucleolar fraction was detected with Ab to cyclophilin A (Fig. 4A, Cycl.), indicating that the nucleolar fraction was free of cytosolic contaminants. Similarly, when Abs

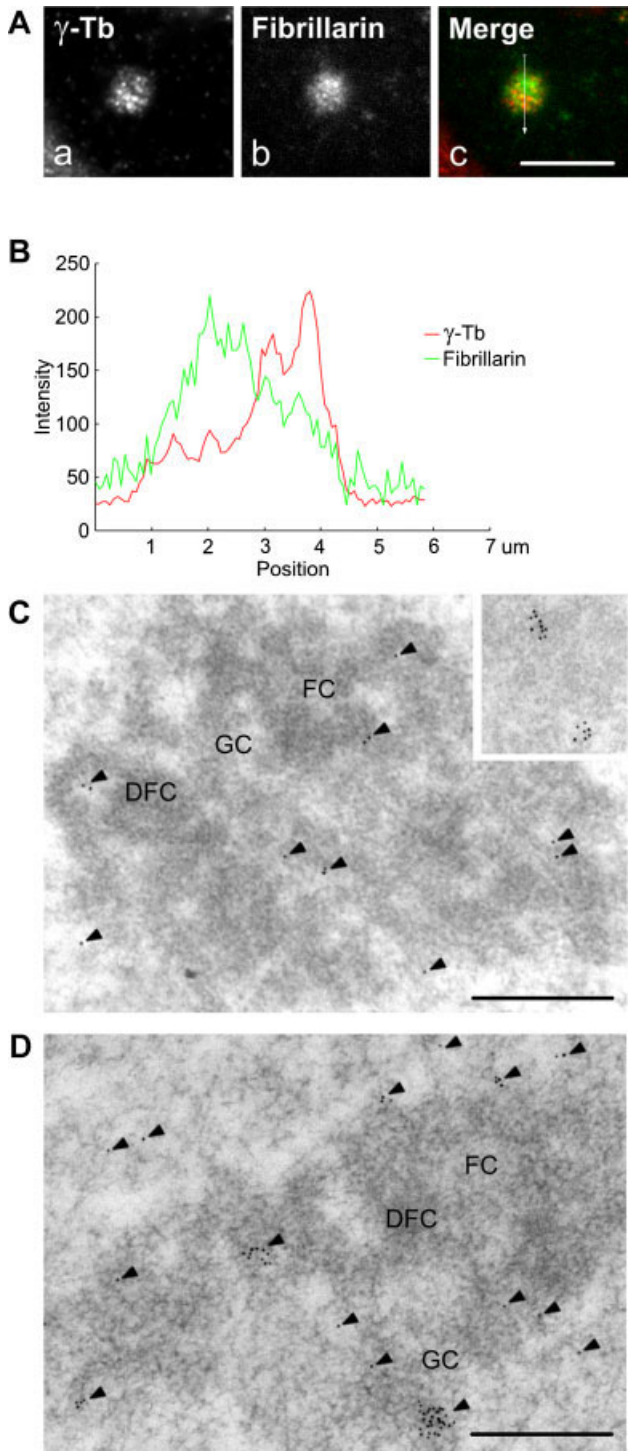

Fig. 3. Ultrastructural localization of γ-tubulin in nucleolus of T98G cells. A: Double-label staining with mAb TU-30 to γ-tubulin (a; red) and polyclonal Ab to fibrillarin (b; green). Fixation Tx/HAc/M. Scale bar 7 μm. (B) A plot of the change in intensity along the white line in Figure 3A. C: Immunoelectron microscopy with Ab DQ-19 to γ-tubulin on a sample prepared by aldehyde fixation. Clusters of gold particles are shown in the insert. D: Immunoelectron microscopy with Ab DQ-19 on a sample prepared by cryofixation. Arrowheads in C and D indicate position of gold particles. FC, fibrillar center; DFC, dense fibrillar component; GC, granular component. Scale bar 0.5 μm.

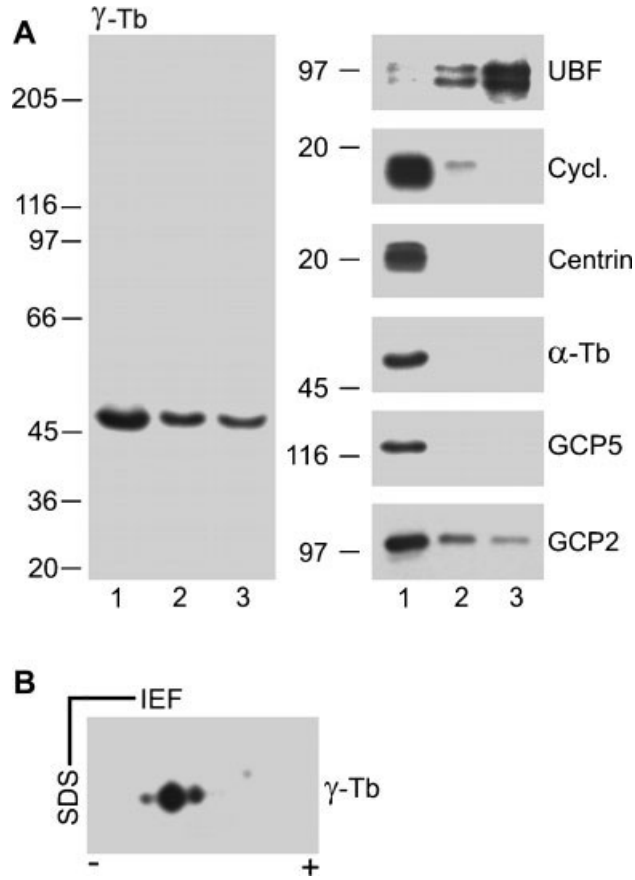

Fig. 4. Immunoblot analysis of subcellular fractions. A: Immunoblotting of cytosolic (1), nuclear (2), and nucleolar (3) fractions of T98G cells with Abs to γ-tubulin (γ-Tb), UBF, cyclophilin A (Cycl.), centrin-2 (Centrin), α-tubulin (α-Tb), GCP5, and GCP2. The same amount of proteins was loaded into each lane. Bars on the margins indicate positions of molecular mass markers in kDa. B: Immunoblotting of nucleolar fraction separated by 2D-PAGE with Ab to γ-tubulin.

to centrin 2 (Fig. 4A, Centrin), α-tubulin (Fig. 4A, α-Tb), or GCP5 (Fig. 4A, GCP5) were applied, no staining was detected in the nucleolar fraction. Nor was any staining observed with Abs to β-tubulin (not shown). These data suggest that αβ-tubulin dimers do not co-distribute with γ-tubulin in nucleoli in T98G cells. Interestingly, GCP2 characteristic for γTuSCs was detected in the nucleolar fraction (Fig. 4A, GCP2). After separation of nucleolar fraction by 2D-PAGE, at least three charge variants of γ-tubulin were distinguished by immunoblotting (Fig. 4B). This suggests that nucleolar γ-tubulin is post-translationally modified.

Exogenous γ-tubulin associates with nucleoli

FLAG-tagged human γ-tubulin expression constructs served to further prove that γ-tubulin is indeed associated with nucleoli. γ-Tubulin-FLAG had lower electrophoretic mobility compared with endogenous γ-tubulin (Fig. 5-I, γ-Tb) as confirmed by anti-FLAG Ab (Fig. 5-I, FLAG). FLAG-tagged protein tyrosine kinase $p59^{Fyn}$ (Fyn) served as a negative control (Fig. 5-I, Fyn). To verify proper localization of tagged γ-tubulin, U138MG cells expressing γ-tubulin-FLAG were first fixed by methanol and then directly processed for immunostaining. In such case, exogenous γ-tubulin was located on centrosomes of interphase

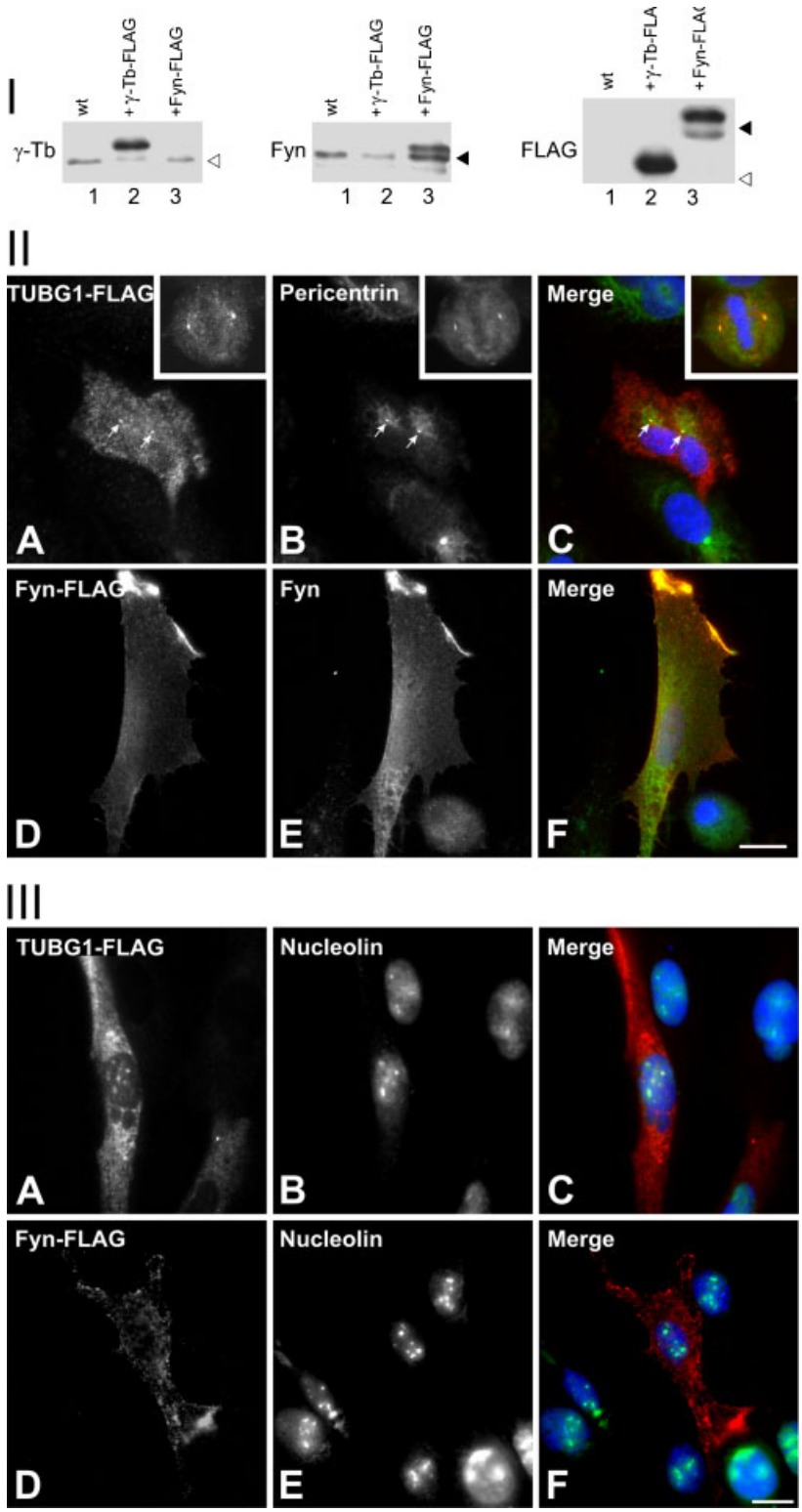

Fig. 5. Effect of fixation on subcellular localization of FLAG-tagged γ-tubulin. I: Immunoblot analysis of U138MG cells expressing γ-tubulin-FLAG or control Fyn-FLAG. Wild-type cells (1), cells expressing γ-tubulin-FLAG (2), or Fyn-FLAG (3) were probed with Abs to γ-tubulin (γ-Tb), Fyn or FLAG. White and black arrowheads point to position of endogenous γ-tubulin and Fyn kinase, respectively. II: Cells fixed by methanol were double-label stained with Abs to FLAG (A, D; red) pericentrin (B; green) or Fyn (E; green). DAPI (C, F; blue). γ-Tubulin-FLAG concentrates at centrosomes in interphase cells and on spindle poles in mitotic cells (insert in A) in contrast to Fyn-FLAG. Scale bar 20 μm. III: Cells fixed by Tx/HAc/M were double-label stained with Abs to FLAG (A, D; red) and nucleolin (B, E; green). DAPI (C, F; blue). γ-Tubulin-FLAG (A) was detected in nucleoli in contrast to Fyn-FLAG (D). Scale bar 20 μm.

cells and spindle poles of mitotic cells (Fig. 5-II, A), as confirmed by staining with Ab to pericentrin that served as a marker of MTOC (Fig. 5-II, B). Diffuse cytoplasmic staining was also detectable. On the other hand, FLAG-tagged Fyn was concentrated on cell periphery and did not localize to centrosomes (Fig. 5-II, D–E) or spindle poles (results not shown). When transfected cells were subjected to Tx/HAc/M fixation, γ-tubulin-FLAG was localized both to the cytoplasm and the nucleoli (Fig. 5-III, A). Nucleolin served as a marker of nucleoli (Fig. 5-III, B). On the other hand, Fyn-FLAG was not detected in nucleoli (Fig. 5-III, D–E). Nucleolar localization of γ-tubulin was also discernible in fixed U2OS cells expressing green to red photoconvertible γ-tubulin-Dendra2 protein (data not shown).

Additional evidence of exogenous γ-tubulin association with nucleoli was obtained when nucleoli were isolated from cells expressing untagged γ-tubulin in pCI-NEO vector. γ-Tubulin and Fyn (control) were overexpressed in HEK cells, and blots were prepared from cytosol and isolated nucleoli of transfected and not transfected cells. Higher amounts of the two proteins were found in cytoplasm of transfected cells, and increased amount of γ-tubulin was detected in nucleoli isolated from transfected cells (Fig. S3), while Fyn was not detected in isolated nucleoli (results not shown). Collectively, these data strongly suggest that exogenous γ-tubulin can associate with nucleoli.

Mechanism of localization of γ-tubulin into the nucleoli

To test whether or not γ-tubulin can shuttle between the nucleus and cytoplasm via nuclear pores, cells were pretreated with LMB, an effective inhibitor of nuclear export (Ullman et al., 1997). The p53 protein, which is known to shuttle between nucleus and cytoplasm and to contain both the nuclear location signals (NLS) and the nuclear export signals (NES) (Zhang and Xiong, 2001) served as a positive control. Whereas p53 clearly accumulated in the nucleus of LMB-treated U2OS cells, enrichment of γ-tubulin was lacking (Fig. 6A). These observations were verified by screening of a large number of cells (~3,000–10,000). Localization indexes (ratio of nucleoplasmic to cytoplasmic mean fluorescence intensity) of γ-tubulin and p53 in control and LMB-treated cells were calculated to compare the distribution of those proteins (Fig. 6B). Whereas the index for p53 significantly increased (1.33 ± 0.16-fold; mean ± s.d., $n = 4$, $P < 0.05$) after LMB treatment, its value for γ-tubulin remained unchanged (1.01 ± 0.18-fold; mean ± s.d., $n = 4$, $P < 0.05$). Possible nucleocytoplasmic shuttling was also tested by means of heterokaryon analysis. Human U2OS cells were transfected with vectors encoding either FLAG-tagged γ-tubulin or nucleophosmin (positive control). Two hours after fusion of transfected U2OS cells with mouse NIH 3T3 cells, nucleophosmin-FLAG was clearly detected in nucleoli of NIH 3T3 cells (Fig. 6C, a), while γ-tubulin-FLAG was absent in nucleoli of NIH 3T3 cells (Fig. 6C, c). However, faint staining of γ-tubulin-FLAG in nuclear region of NIH 3T3 was detectable 6 h after fusion (data not shown). The dynamics of γ-tubulin was also followed in living cells by time-lapse imaging using U2OS cells expressing green to red photoconvertible protein Dendra2 tagged to γ-tubulin. When γ-tubulin was

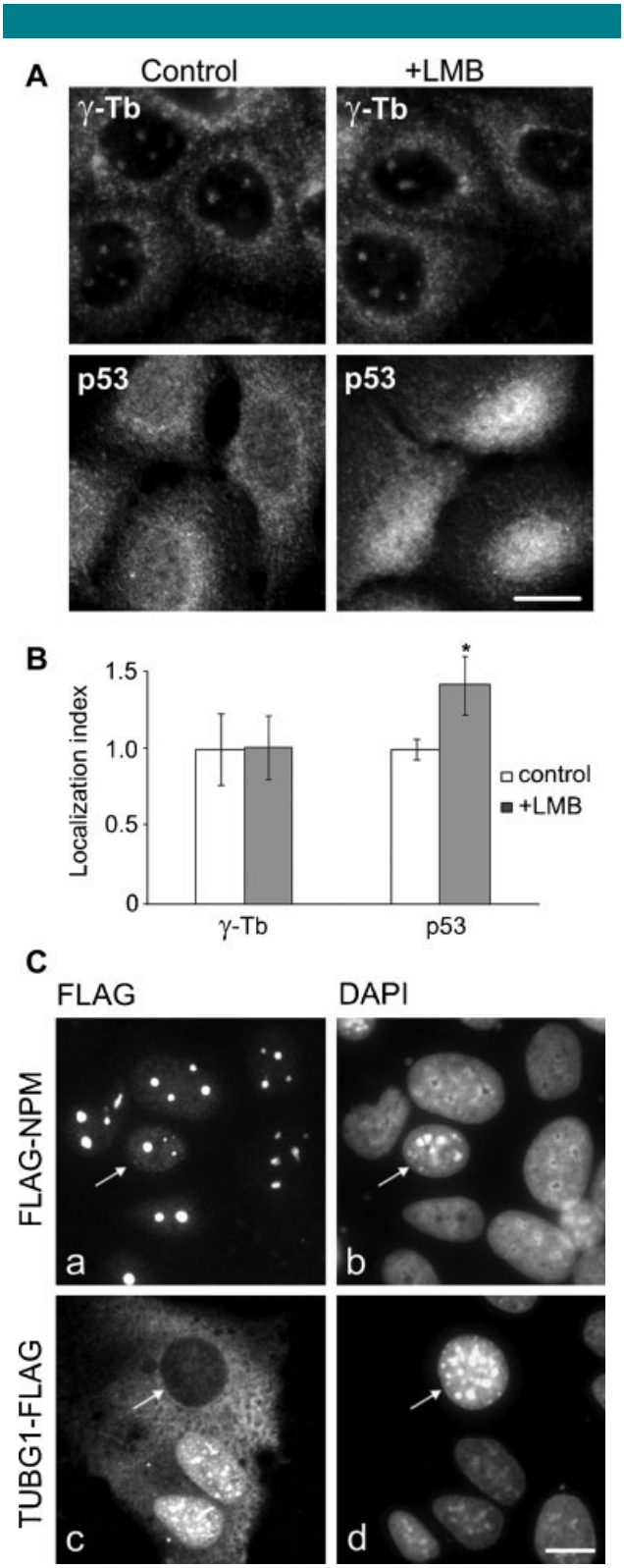

Fig. 6. Evaluation of nucleocytoplasmic shuttling of γ-tubulin. A: Effect of nuclear transport inhibition on the distribution of nucleolar γ-tubulin. Immunostaining of control or leptomycin B-treated (+LMB) U2OS cells with TU-30 to γ-tubulin (γ-Tb) and Ab to p53. Methanol fixation. Scale bar 10 μm. B: Quantification of immunofluorescence signals for γ-tubulin and p53 in LMB-treated cells relative to the level in control cells. Mean intensity was determined in nuclei and cytoplasm, and the ratio of nucleoplasmic to cytoplasmic signals was calculated (localization index). Data are presented as the mean fold change ± s.d. obtained from four independent experiments. *$P < 0.05$. C: Subcellular distribution of FLAG-tagged γ-tubulin in heterokaryon assay. U2OS cells transfected with FLAG-nucleophosmin (FLAG-NPM) or γ-tubulin-FLAG (TUBG1-FLAG) were fused with NIH 3T3 cells and fixed after 2 h with methanol. Immunofluorescence staining with Ab to FLAG (a, c). DAPI (b, d). NIH 3T3 nuclei in heterokaryons, recognized by bright chromatin aggregates, are marked by arrows. Scale bar 10 μm.

photoactivated in cytoplasm, red γ-tubulin was detected in cytoplasm but not in nuclei for as long as 2 h after activation. Photoactivated Dendra2 without γ-tubulin was found in nucleus within 2 min as documented in a typical experiment shown in Fig. S4. Collectively, these data strongly suggest that rapid nucleocytoplasmic transport of γ-tubulin, detectable by fluorescence microscopy, does not take place in interphase cells. On the other hand, the possibility that γ-tubulin can reach nucleus in interphase cells by yet another mechanism cannot be ruled out.

The nucleolus is a dynamic structure that assembles around the clusters of rRNA gene repeats during late telophase, persists throughout interphase, and then disassembles as the cells enter mitosis (Lam et al., 2005). During the nuclear envelope breakdown, nucleolar proteins are still associated with nucleoli remnants that are shifted to mitotic spindle and form a new nucleoli after cytokinesis (Raška et al., 2006). To determine whether γ-tubulin also can follow such trail, double label staining for γ-tubulin and nucleolin was performed at different stages of the cell cycle. In all stages, interphase, prophase, metaphase, and telophase, γ-tubulin was found to co-distribute with nucleolin (Fig. 7). This suggests that γ-tubulin is able to translocate to nucleolus via mitosis.

Nucleolar γ-tubulin associates with tumor suppressor protein C53

To identify the potential nuclear/nucleolar binding partner for γ-tubulin, nuclei were isolated from HeLa S3 cells growing in suspension. Extract from nuclei was precipitated with anti-

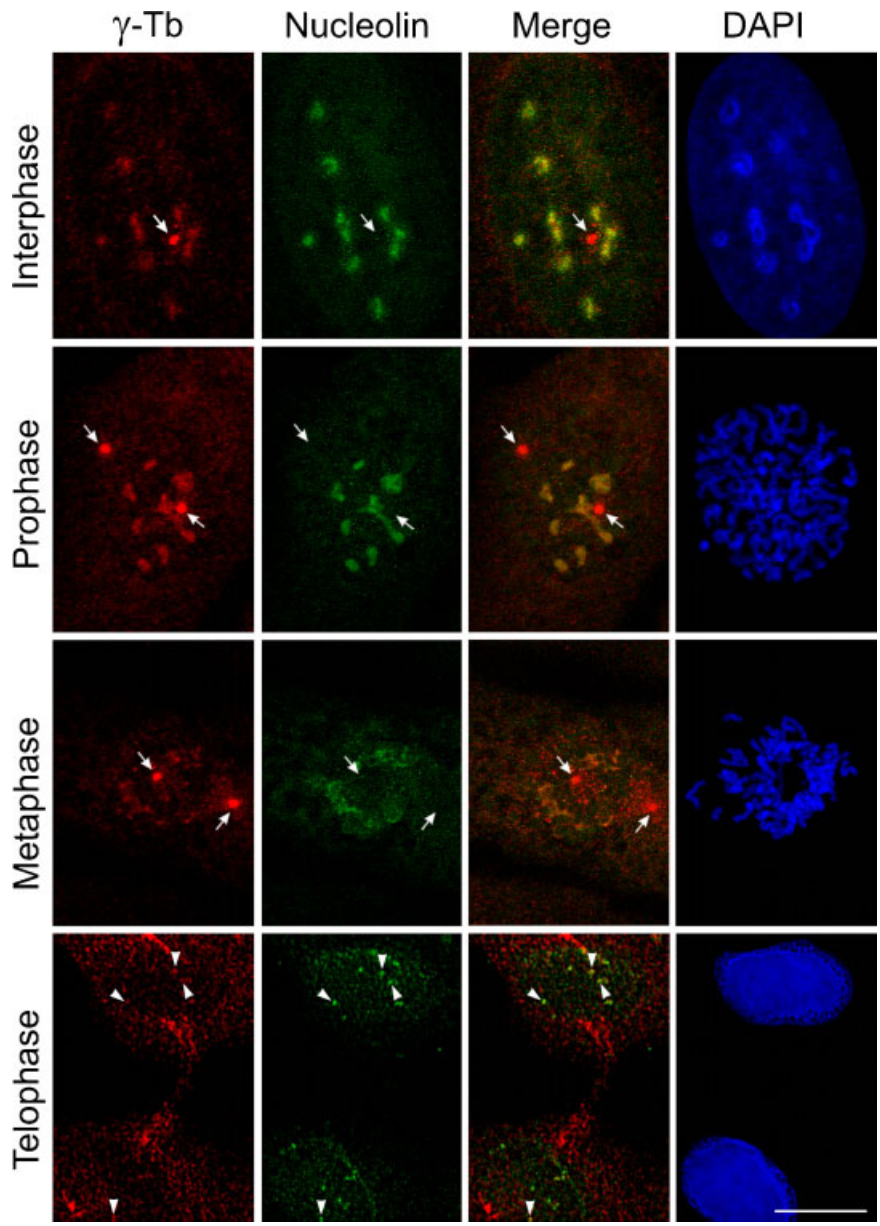

Fig. 7. Confocal laser scanning microscopy of γ-tubulin and nucleolin in different stages of cell cycle. Immunofluorescence staining of U2OS cells in interphase, prophase, metaphase, and telophase with mAb TU-30 to γ-tubulin (γ-Tb, red) and polyclonal Ab to nucleolin (green). DAPI (blue). Images represent maximum intensity projections of z-series made from 25–30 optical sections. Arrows indicates the positions of MTOCs, arrowheads the same positions in telophase cells. Fixation methanol. Scale bar 10 μm.

peptide mAb TU-31 to γ-tubulin and the bound proteins were eluted with peptide used for immunization. Proteins were separated on SDS-PAGE and subjected to MALDI/MS fingerprint analysis. Out of three independent experiments CDK5 regulatory subunit-associated protein 3 (also known as C53, Cdk5rap3, or LZAP; Swiss-Prot identifier Q96JB5), hereafter denoted as C53, was identified three times. Typical example of mass spectrometry identification is shown in Table S2. To ascertain whether C53 associates with γ-tubulin, immunoprecipitation experiments were performed with Ab to C53 from nuclear extracts. Immunoblot analysis revealed co-immunoprecipitation of γ-tubulin with C53 (Fig. 8A, left part, lane 3). In addition, the reciprocal precipitation with Ab to γ-tubulin confirmed an interaction of C53 with γ-tubulin (Fig. 8A, right part, lane 3). Relatively low amounts of C53 and γ-tubulin in the extract (Fig. 8A, right part, lane 1) reflect

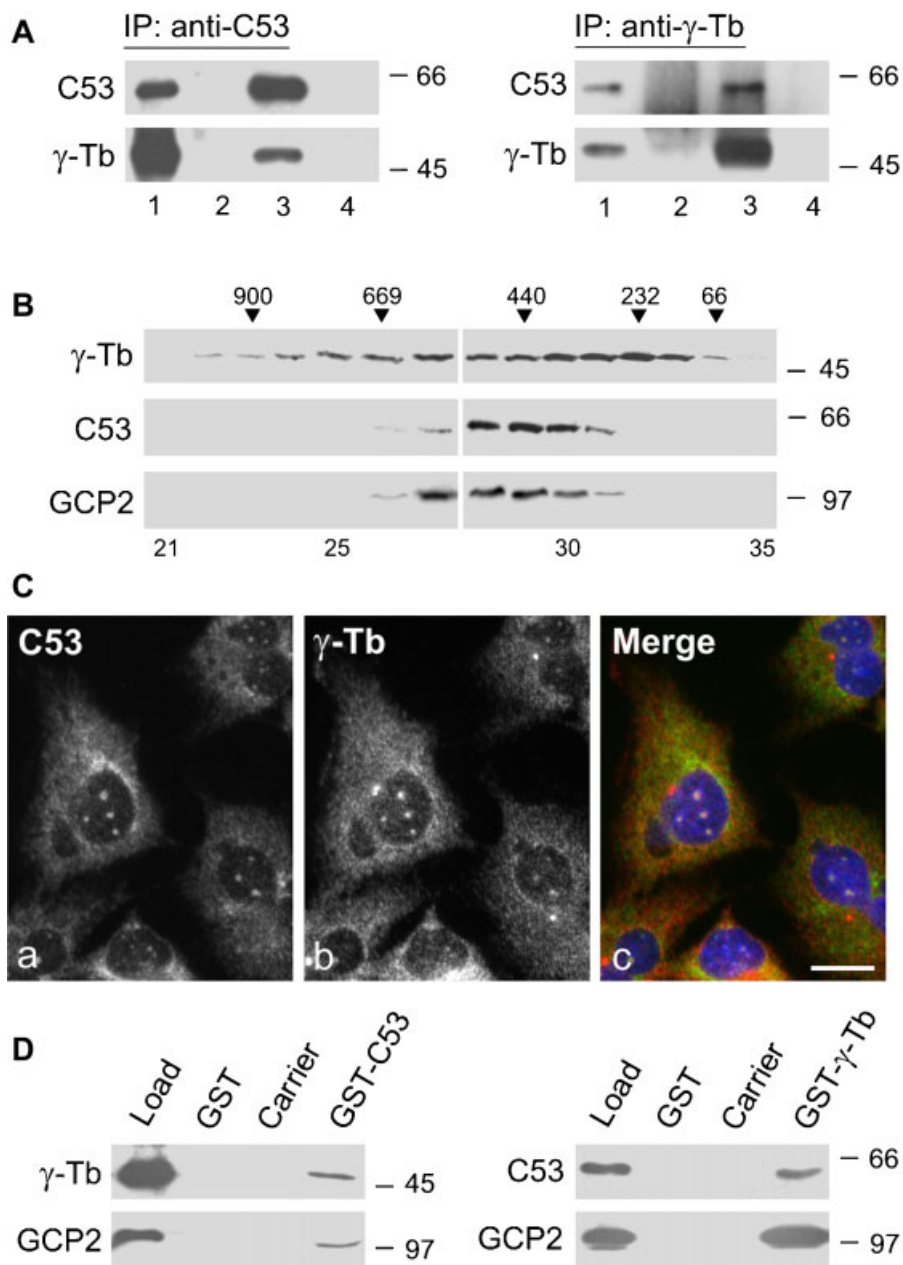

Fig. 8. Association of γ-tubulin with C53 in T98G cells. A: Co-immunoprecipitation of γ-tubulin and C53. Nuclear extracts were immunoprecipitated with Abs to C53 or γ-tubulin. Blots were probed with Abs to C53 or γ-tubulin (γ-Tb). Extracts (1), immobilized Abs not incubated with extract (2), immunoprecipitated proteins (3), protein A without Abs incubated with extracts (4). B: Size distribution of nucleolar proteins. Proteins extracted from nucleoli were fractionated on Superose 6. Blots of collected fractions were probed with Abs to γ-tubulin (g-Tb). C53 and GCP2. Calibration standards (in kDa) are indicated on the top. Numbers at the bottom denote individual fractions. C: Nucleolar localization of C53 and γ-tubulin. Cells were double-label stained with mAb TU-31 to γ-tubulin (a; red) and polyclonal Ab to C53 (Abcam) (b; green). DAPI (c; blue). Fixation with methanol. Scale bar 20 μm. D: Interaction of γ-tubulin with C53 in GST pull-down assay. Whole-cell lysates (Load) were incubated with immobilized GST alone (GST), beads used for immobilization (Carrier), or immobilized GST-fusion proteins (GST-C53; GST-γ-tubulin). Blots of bound proteins were probed with Abs to γ-tubulin (γ-Tb), C53, and GCP2. Position of molecular mass markers (in kDa) is indicated on the right in A, B, and D.

dilution of the extract (1:5) used for precipitation. The similar co-immunoprecipitation results were obtained when nucleolar extracts were used (Fig. S5). On the other hand, negative control Abs did not co-immunoprecipitate C53 or γ-tubulin (data not shown).

Evidence of exogenous C53 association with nucleoli was obtained when nucleoli were isolated from cells expressing FLAG-tagged C53 or FLAG-tagged α-tubulin (control). The FLAG-tagged proteins were expressed in HEK cells, and blots were prepared from cytosol and isolated nucleoli of transfected and non-transfected cells. Both FLAG-tagged proteins were found in cytoplasm of transfected cells, whereas only FLAG-tagged C53 was detected in nucleoli isolated from transfected cells (Fig. S6A).

In order to decide whether nucleolar γ-tubulin and C53 appear in the form of complexes, nucleolar extracts were subjected to gel filtration chromatography on Superose 6 column. γ-Tubulin was distributed through a large zone in complexes of various sizes. Large complexes of ~2 MDa, that could possibly represent γTuRCs, were not detected. Interestingly, C53 was also present in complexes, but their distribution only partially overlapped with γ-tubulin. Similarly, GCP2 also appeared in complexes that only partially overlapped with those of γ-tubulin (Fig. 8B).

To estimate the localization of C53, T98G cells were double-label stained with Abs to C53 and γ-tubulin. Under the fixation conditions when γ-tubulin was detectable in nucleoli (Fig. 8C, b), the C53 was located in cytoplasm, nucleoplasm, and co-distributed with γ-tubulin in nucleolar regions (Fig. 8C, a). No obvious concentration of C53 in MTOC was detected (Fig. 8C, c). Localization of C53 in nucleoli was further confirmed by immunofluorescence double-label staining of cells with Abs to C53 and fibrillarin (Fig. S6B). Besides, electron microscopy examination of formaldehyde-fixed preparations disclosed that C53 was located in GC or on the boundary between DFC and GC (Fig. S6C). Large clusters of gold particles were also detected (Fig. S6, insert).

To confirm independently the interaction of C53 and γ-tubulin, pull-down assays were performed, using whole-cell extracts and GST-tagged C53 and γ-tubulin fusion proteins. The experiments revealed that both γ-tubulin and GCP2 bound to GST-C53, but not to GST alone (Fig. 8D, left part). Similarly, both C53 and GCP2 bound to GST-γ-tubulin (Fig. 8D, right part). The amounts of immobilized GST fusion proteins were similar, as evidenced by staining with anti-GST Ab (data not shown). Collectively, these data strongly suggest that γ-tubulin interacts with C53, and both proteins are able to localize to nuclei and nucleoli.

γ-Tubulin antagonizes the inhibitory effect of C53 on DNA damage G_2/M checkpoint activation

Cyclin-dependent kinase 1 (Cdk1)/cyclin B1 complex is the driving force for mitotic entry. In response to DNA damage G_2/M checkpoint system (ATM/ATR and checkpoint kinases) inactivates phosphatase Cdc25C by phosphorylation, which in turn leads to accumulation of Cdk1 phoshorylated at Y15 and inactivation of Cdk1 (Lindqvist et al., 2009). It has previously been demonstrated that C53 overexpression overrides the G_2/M DNA damage checkpoint induced by genotoxic agents as etoposide (Jiang et al., 2005). As shown in Figure 9, treatment of U2OS cells with etoposide (20 h) caused Cdk1 inactivation indicated by the increase in inhibitory phosphorylation of Cdk1 at Y15. The C53 overexpression (U2OS-C53 cells) attenuated the inhibitory phosphorylation of Cdk1. Intriguingly, the overexpression of FLAG-tagged γ-tubulin in U2OS-C53 antagonized the C53 action and led to accumulation of Cdk1-p-Y15. With control plasmid for FLAG-tagged Fyn, the accumulation was absent (Fig. 9, Cdk1-p-Y15). No obvious changes in the amount of endogenous γ-tubulin (Fig. 9, γ-Tb) or

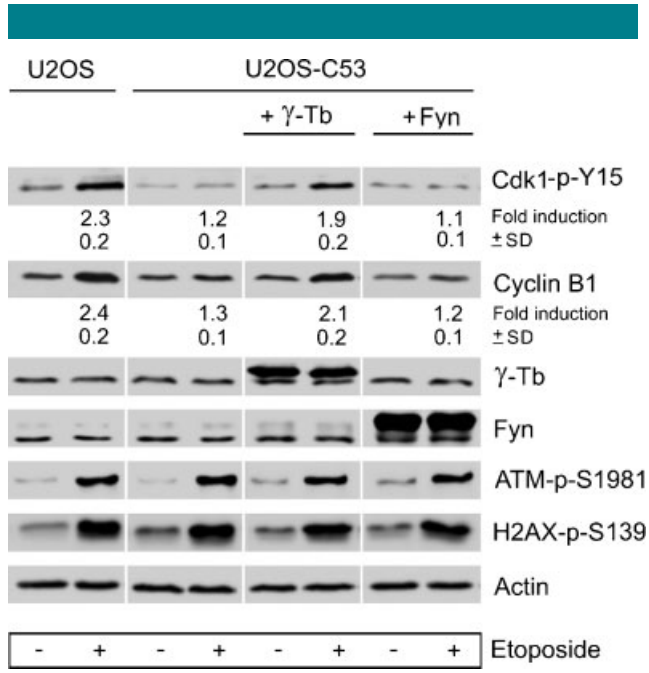

Fig. 9. Overexpression of γ-tubulin antagonizes the inhibitory effect of C53 on DNA damage G_2/M checkpoint activation. U2OS cells expressing GFP-C53 were transfected with vector encoding γ-tubulin (+γ-Tb) or control vector encoding Fyn (+Fyn). After 48 h the cells were treated with 20 μM etoposide for 20 h. U2OS cells served as control. Immunoblot analysis of whole cell extracts with Abs to Cdk1-p-Y15, cyclin B1, γ-tubulin (γ-Tb), Fyn, ATM-p-S1981, H2AX-p-S139, and actin. Numbers under the blots indicate relative amounts of proteins normalized to cells not treated with etoposide. Means ± s.d. were calculated from three experiments.

its nucleolar localization were detected in etoposide-treated U2OS cells. It has been reported that C53 overexpression promotes Cdk1/cyclin B1 activation which is followed by cyclin B1 degradation at the exit of mitosis (Jiang et al., 2005). In the course of etoposide treatment, cyclin B1 accumulated in U2OS but its amount was significantly lower in U2OS-C53 cells. Overexpression of γ-tubulin in U2OS-C53 cells restored cyclin B1 accumulation (Fig. 9, Cyclin B1). This result indirectly shows that activation of Cdk1/cyclin B1 by C53 overexpression is diminished by an excess of γ-tubulin. Phosphorylation of ATM at S1981 and histone H2AX at S139 were used as indicators of ATM/ATR activity responsible for phosphorylation of checkpoint kinases (Fig. 9, ATM-p-S1981 and H2AX-p-S139); actin served as loading control (Fig. 9, Actin). Shorter etoposide treatment (3 h) provided similar results, however the differences between control and etoposide-treated cells were less prominent (Fig. S7). Similar results were obtained when nuclei isolated from control or etoposide-treated HEK cells were used for the immunoblotting. In this case overexpression of γ-tubulin also antagonized the C53 action (data not shown). In etoposide-treated U2OS cells depletion of γ-tubulin inhibited accumulation of Cdk1-p-Y15, while depletion of C53 led to more pronounced accumulation of Cdk1-p-Y15 (Fig. S8).

Collectively taken, the data suggest that interaction between γ-tubulin and C53 is functionally relevant and that γ-tubulin can modulate the C53 activity during G_2/M DNA damage checkpoint.

Discussion

γ-Tubulin is the key protein for microtubule nucleation from MTOCs. According to a long-standing and deeply entrenched view, γ-tubulin is a typical cytosolic protein in mammalian cells.

Contrary to that view, novel data generated in the present study show that γ-tubulin is also located in nucleoli of cultured cells. Several lines of new evidence support this conclusion. First, nucleolar γ-tubulin was detected by double-labeling immunofluorescence microscopy using different Abs to γ-tubulin and Abs to nucleolar markers. Second, the immunofluorescence staining was inhibited by preabsorption of Abs with immunizing peptide or by knock-down of γ-tubulin. Third, nucleolar γ-tubulin was visualized by immunoelectron microscopy on fixed and cryofixed samples. Fourth, immunoblot analysis of isolated nucleoli has confirmed that they contain γ-tubulin but not cytosolic proteins. Fifth, exogenous FLAG-tagged γ-tubulins were detected in nucleoli using anti-FLAG Ab, ruling out the possibility that nucleolar staining of γ-tubulin reflects the cross-reactivity of Abs to γ-tubulin with nucleolar proteins. Moreover, untagged exogenous γ-tubulin accumulated in nucleoli. Finally, nucleolar γ-tubulin was detected in cultured cells of diverse cellular origins and cells in primary culture.

It is well documented that fixation conditions can substantially influence the exposition of epitopes on αβ-tubulin dimers in microtubule wall (Dráberová et al., 2000). The same holds true for γ-tubulin labeling of MTOCs as it is variable, depending on the Ab used and the employed fixation protocol (Lajoie-Mazenc et al., 1994; Moudjou et al., 1996; Nováková et al., 1996; Robinson and Vandre, 2001). Similarly, immunofluorescence detection of γ-tubulin in nucleoli is dependent on the used Abs, fixation procedure and cell type examined. We have first noted the presence of nucleolar γ-tubulin in glioblastoma cell lines with substantially enhanced expression of γ-tubulin. Nucleolar γ-tubulin was detected after acetic alcohol fixation when, however, microtubule structures are not properly preserved. Alternatively, nucleolar γ-tubulin was detected after prolonged washing of methanol-fixed preparations. The most likely explanation for the observed findings is an unmasking of γ-tubulin epitopes within the compact structure of interphase nucleolus. This might explain why in general nucleolar γ-tubulin is not detected by immunofluorescence microscopy in mammalian cells. Moreover, a GFP-tag on either end of the protein prevented γ-tubulin visualization in nucleoli of living cells (E. Dráberová, unpublished). Reports on γ-tubulin presence in nucleoli are very scarce. γ-Tubulin was found in the nucleolus by proteomic analysis (Andersen et al., 2002); besides, there is just one tangential remark on nucleolar γ-tubulin detected by immunoelectron microscopy of formaldehyde fixed CHO cells overproducing Rad51 protein (Lesca et al., 2005). Our data corroborate these findings and provide the first direct visualization of nucleolar γ-tubulin in cultured mammalian cells. Multiple charge variants of γ-tubulin indicate that interactions of nucleolar γ-tubulin might be modulated by its post-translational modification(s). While the presence of γ-tubulin in nuclei/nucleoli of mammalian cells is unexpected, we have already documented nuclear γ-tubulin in plants that have a higher amount of γ-tubulin (Binarová et al., 2000).

γ-Tubulin associates with GCP2 in γTuSCs and with GCP5 in γTuRCs. We have clearly detected GCP2 in isolated nucleoli by immunoblotting, while the signal for GCP5 was undetectable. The fractionation of nucleoli by gel filtration failed to reveal large complexes corresponding to γTuRCs, but GCP2 complexes of intermediate sizes were detected. Considering the data obtained so far, it is unlikely that γTuRCs are present in nucleoli, but the presence of γTuSCs cannot be completely excluded. Stabilizing effect of nucleolar and centrosomal protein HCA66 on γTuSCs was reported (Fant et al., 2009).

In agreement with the overexpression of γ-tubulin in glioblastoma cell lines, a significant increase in γ-tubulin staining was detected by immunohistochemistry on tissue sections from glioblastoma multiforme, the most prevalent form of brain cancer (Katsetos et al., 2006; Katsetos et al., 2007). Increased γ-tubulin expression occurs in thyroid carcinoma (Montero-Conde et al., 2007) and carcinomas of breast (Niu et al., 2009). Interestingly, the βII isotype of tubulin has been detected in the nuclei of a variety of human cancer cell lines (Walss-Bass et al., 2002), denoting that the presence of nuclear βII-tubulin may correlate with the cancerous state of cells (Yeh and Luduena, 2004). However, nucleolar γ-tubulin does not necessarily signify a malignant state in cells as it was also detected in proliferating non-immortalized, non-transformed fetal astrocytes and SAECs.

There are several main mechanisms as to how tubulin can enter into the nucleus. In principle, it can be transported (i) actively via nuclear pore complex, (ii) passively by diffusion through nuclear pore complex, or (iii) during mitosis. Since there is putative NLS (http://www.rostlab.org) and NES (http://www.cbs.dtu.dk) in human γ-tubulin, it might be actively transported via nuclear pores. Alternatively, it could "hitchhike" on other proteins that are endowed with such signals. Inhibition of nuclear export should lead to a rapid accumulation of γ-tubulin in the nucleus. However, when nuclear export was inhibited by LMB, the distribution of γ-tubulin was unchanged, while the control p53 protein readily accumulated in nucleus. Similarly in heterokaryon assay, FLAG-tagged γ-tubulin did not rapidly accumulate in nuclei of NIH 3T3 cells, in contrast to FLAG-tagged nucleophosmin/B23. Finally, time-lapse imaging of cells expressing green to red photoconvertible Dendra2 protein tagged to γ-tubulin failed to reveal translocation of red signal from cytoplasm to nucleus when photoactivation occurred in cytoplasm. Protein kinase D3, which shuttles between cytoplasm and nucleus, appeared in the nucleus within a few minutes when photoactivated in cytoplasm (Rey et al., 2006). Collectively, these data suggest that neither rapid diffusion nor rapid active shuttling based on exportin1/CRM1 pathway (Ohno et al., 1998) are the major mechanisms accounting for the localization of γ-tubulin in the nucleus. On the other hand, during nuclear envelope breakdown, γ-tubulin was associated with nucleolar remnants that were later detected on the mitotic spindle and formed new nucleoli after cytokinesis. Thus, in principle, γ-tubulin can enter the nuclei of daughter cells through mitosis. A similar mechanism was described for βII-tubulin in transformed cells (Walss-Bass et al., 2001). However, one cannot exclude the possibility that additional γ-tubulin might get into the nucleus via passive diffusion after dilation of the pore gate. Such mechanism was proposed for nuclear import of αβ-tubulin dimers in cells under conditions when the amount of soluble tubulin in the cytoplasm was increased by depolymerization of microtubules (Schwarzerová et al., 2006; Akoumianaki et al., 2009).

Combination of immunoprecipitation with mass spectrometry revealed that nuclear γ-tubulin interacted with C53, and this interaction was confirmed by co-immunoprecipitation and pull-down experiments. It has been previously reported that C53 localizes at multiple subcellular compartments, including cytosol, nucleus, centrosome, endoplasmic reticulum and microtubules (Jiang et al., 2009). In the present study we have noted localization of endogenous C53 in cytosol and nucleus/nucleolus. Observed staining was specific, since the immunoreactivity was substantially diminished after knock-down of C53 (E. Dráberová, unpublished result). The differences in immunofluorescence localization of C53 could reflect an exposition of epitopes for used Abs. It was found that in U2OS cells overexpressing C53 and tumor suppressor ARF, the C53 was located both in nucleus and nucleolus while its cytoplasmic localization was substantially reduced (Wang et al., 2006). Differential subcellular distribution indicates that C53 may be a multifunctional protein. The C53 plays a role in modulation of

Cdk1/cyclin B1 complex both in G_2/M DNA damage checkpoint activation (Jiang et al., 2005) and in unperturbed cells (Jiang et al., 2009). However, C53 is also associated with regulation of tumor suppressor ARF functions (Wang et al., 2006) and regulation of transcriptional activity of nuclear factor-κB (NF-κB) by direct binding and inhibition of DNA-binding protein RelA (Wang et al., 2007). While our data indicate that γ-tubulin can modulate C53 function during DNA damage G_2/M checkpoint activation in U2OS cells (Fig. 9), it remains unclear whether γ-tubulin affects other C53 functions.

In conclusion, we show here that in transformed as well as in non-transformed interphase mammalian cells γ-tubulin is present not only in cytoplasm but also in nuclei and nucleoli where it can be translocated during mitosis. Nuclear γ-tubulin interacts with tumor suppressor protein C53 that is involved in regulation of DNA damage G_2/M checkpoint activation, and γ-tubulin affects this C53 function. We suggest that next to its well-established role in microtubule nucleation, γ-tubulin also participates in nuclear-specific function(s).

Acknowledgments

We thank Drs. B. Oakley (Ohio State University, Columbus, USA) for cDNA of γ-tubulin, C. J. Sherr (HHMI, St. Jude Children's Research Hospital, Memphis, USA) for cDNA of nucleophosmin, Petr Dráber and D. Staněk (Institute of Molecular Genetics, Prague, Czech Republic) for, respectively, cDNA of Fyn and pDendra2-N1 vector. The Ab against pericentrin was kindly donated by Dr. S. J. Doxsey (University of Massachusetts Medical School, Worcester, USA). Stanislav Vinopal was supported in part by the Department of Cell Biology, Faculty of Science, Charles University, Prague, Czech Republic.

Literature Cited

Akoumianaki T, Kardassis D, Polioudaki H, Georgatos SD, Theodoropoulos PA. 2009. Nucleocytoplasmic shuttling of soluble tubulin in mammalian cells. J Cell Sci 122:1111–1118.

Andersen JS, Lyon CE, Fox AH, Leung AKL, Lam YW, Steen H, Mann M, Lamond AI. 2002. Directed proteomic analysis of the human nucleolus. Curr Biol 12:1–11.

Bertwistle D, Sugimoto M, Sherr CJ. 2004. Physical and functional interactions of the Arf tumor suppressor protein with nucleophosmin/B23. Mol Cell Biol 24:985–996.

Binarová P, Cenklová V, Hause B, Kubátová E, Lysák M, Doležel J, Bögre L, Dráber P. 2000. Nuclear γ-tubulin during acentriolar plant mitosis. Plant Cell 12:433–442.

Bugnard E, Zaal KJM, Ralston E. 2005. Reorganization of microtubule nucleation during muscle differentiation. Cell Motil Cytoskel 60:1–13.

Chabin-Brion K, Marceiller J, Perez F, Settegrana C, Drechou A, Durand G, Pous C. 2001. The Golgi complex is a microtubule-organizing organelle. Mol Biol Cell 12:2047–2060.

Doxsey SJ, Stein P, Evans L, Calarco P, Kirschner M. 1994. Pericentrin, a highly conserved protein of centrosomes involved in microtubule organization. Cell 76:639–650.

Dráber P, Lagunowich LA, Dráberová E, Viklický V, Damjanov I. 1988. Heterogeneity of tubulin epitopes in mouse fetal tissues. Histochemistry 89:485–492.

Dráber P, Dráberová E, Linhartová I, Viklický V. 1989. Differences in the exposure of C- and N-terminal tubulin domains in cytoplasmic microtubules detected with domain-specific monoclonal antibodies. J Cell Sci 92:519–528.

Dráber P, Dráberová E, Viklický V. 1991. Immunostaining of human spermatozoa with tubulin domain-specific monoclonal antibodies. Histochemistry 195:519–524.

Dráberová E, Dráber P. 1993. A microtubule-interacting protein involved in coalignment of vimentin intermediate filaments with microtubules. J Cell Sci 106:1263–1273.

Dráberová E, Dráber P, Havlíček F, Viklický V. 1986. A common antigenic determinant of vimentin and desmin defined by monoclonal antibody. Folia Biol (Prague) 32:295–303.

Dráberová E, Sulimenko V, Kukharskyy V, Dráber P. 1999. Monoclonal antibody NF-09 specific for neurofilament protein NF-M. Folia Biol (Prague) 45:163–165.

Dráberová E, Viklický V, Dráber P. 2000. Exposure of lumenal microtubule sites after mild fixation. Eur J Cell Biol 79:982–985.

Dráberová E, Del Valle L, Gordon J, Marková V, Šmejkalová B, Bertrand L, de Chadarevian JP, Agamanolis DP, Legido A, Khalili K, Dráber P, Katsetos CD. 2008. Class III β-tubulin is constitutively coexpressed with glial fibrillary acidic protein and nestin in midgestational human fetal astrocytes: Implications for phenotypic identity. J Neuropathol Exp Neurol 67:341–354.

Dryková D, Sulimenko V, Cenklová V, Volc J, Dráber P, Binarová P. 2003. Plant γ-tubulin interacts with ab-tubulin dimers and forms membrane-associated complexes. Plant Cell 15:465–480.

Efimov A, Kharitonov A, Efimova N, Loncarek J, Miller PM, Andreyeva N, Gleeson P, Galjart N, Maia ARR, Mcleod IX, Yates JR, Maiato H, Khodjakov A, Akhmanova A, Kaverina I. 2007. Asymmetric CLASP-dependent nucleation of noncentrosomal microtubules at the trans-Golgi network. Dev Cell 12:917–930.

Fant X, Gnadt N, Haren L, Merdes A. 2009. Stability of the small γ-tubulin complex requires HCA66, a protein of the centrosome and the nucleolus. J Cell Sci 122:1134–1144.

Gauen LKT, Kong ANT, Samelson LE, Shaw AS. 1992. P59Fyn tyrosine kinase associates with multiple T-cell receptor subunits through its unique amino-terminal domain. Mol Cell Biol 12:5438–5446.

Hache RJ, Tse R, Reich T, Savory JG, Lefebvre YA. 1999. Nucleocytoplasmic trafficking of steroid-free glucocorticoid receptor. J Biol Chem 274:1432–1439.

Haren L, Remy MH, Bazin I, Callebaut I, Wright M, Merdes A. 2006. NEDD1-dependent recruitment of the γ-tubulin ring complex to the centrosome is necessary for centriole duplication and spindle assembly. J Cell Biol 172:505–515.

Heneberg P, Dráberová L, Bambousková M, Pompach P, Dráber P. 2010. Down-regulation of protein-tyrosine phosphatases activates an immune receptor in the absence of its translocation into lipid rafts. J Biol Chem 285:12787–12802.

Jiang H, Luo S, Li H. 2005. Cdk5 activator-binding protein C53 regulates apoptosis induced by genotoxic stress via modulating the G2/M DNA damage checkpoint. J Biol Chem 280:20651–20659.

Jiang H, Wu J, He C, Yang W, Li H. 2009. A tumor suppressor C53 protein antagonizes checkpoint kinases to promote cyclin-dependent kinase 1 activation. Cell Res 19:458–468.

Julian M, Tollon Y, Lajoie-Mazenc I, Moisand A, Mazarguil H, Puget A, Wright M. 1993. γ-Tubulin participates in the formation of midbody during cytokinesis in mammalian cells. J Cell Sci 105:145–156.

Katsetos CD, Reddy G, Dráberová E, Šmejkalová B, Del Valle L, Ashraf Q, Tradevosyan A, Yelin K, Maraziotis T, Mishra OP, Mork S, Legido A, Nissanov J, Baas PW, de Chadarevian JP, Dráber P. 2006. Altered cellular distribution and subcellular sorting of γ-tubulin in diffuse astrocytic gliomas and human glioblastoma cell lines. J Neuropathol Exp Neurol 65:465–477.

Katsetos CD, Dráberová E, Šmejkalová B, Reddy G, Bertrand L, de Chadarevian JP, Legido A, Nissanov J, Baas PW, Dráber P. 2007. Class III β-tubulin and γ-tubulin are co-expressed and form complexes in human glioblastoma cells. Neurochem Res 32:1387–1398.

Katsetos CD, Dráberová E, Legido A, Dráber P. 2009. Tubulin targets in the pathobiology and therapy of glioblastoma multiforme. II. γ-Tubulin. J Cell Physiol 221:514–520.

Kukharskyy V, Sulimenko V, Macůrek L, Sulimenko T, Dráberová E, Dráber P. 2004. Complexes of γ-tubulin with non-receptor protein tyrosine kinases Src and Fyn in differentiating P19 embryonal carcinoma cells. Exp Cell Res 298:218–228.

Lajoie-Mazenc I, Tollon I, Détraves C, Julian M, Moisand A, Gueth-Hallonet C, Debec A, Salles-Passador I, Puget A, Mazarguil H, Raynaud-Messina B, Wright M. 1994. Recruitment of antigenic gamma-tubulin during mitosis in animal cells: Presence of gamma-tubulin in the mitotic spindle. J Cell Sci 107:2825–2837.

Lam YW, Trinkle-Mulcahy L, Lamond AI. 2005. The nucleolus. J Cell Sci 118: 1335–1337.

Lesca C, Germanier M, Raynaud-Messina B, Pichereaux C, Etievant C, Emond S, Burlet-Schiltz O, Monsarrat B, Wright M, Defais M. 2005. DNA damage induce g-tubulin-RAD51 nuclear complexes in mammalian cells. Oncogene 24:5165–5172.

Lindqvist A, Rodriguez-Bravo V, Medema RH. 2009. The decision to enter mitosis: Feedback and redundancy in the mitotic entry network. J Cell Biol 185:193–202.

Ma XM, Yoon SO, Richardson CJ, Julich K, Blenis J. 2008. SKAR links pre-mRNA splicing to mTOR/S6K1-mediated enhanced translation efficiency of spliced mRNAs. Cell 133:303–313.

Macurek L, Dráberová E, Richterová V, Sulimenko V, Sulimenko T, Dráberová L, Marková V, Dráber P. 2008. Regulation of microtubule nucleation in differentiating embryonal carcinoma cells by complexes of membrane-bound γ-tubulin with Fyn kinase and phosphoinositide 3-kinase. Biochem J 416:421–430.

Montero-Conde C, Martin-Camposo JM, Lerma E, Martinez-Guitarte JL, Combalia N, Montaner D, Matias-Guiu X, Dopazo J, de Leiva A, Robledo M, Mauricio D. 2007. Molecular profiling related to poor prognosis in thyroid carcinoma. Combining gene expression data and biological information. Oncogene 26:1–8.

Moudjou M, Bordes N, Paintrand M, Bornens M. 1996. γ-Tubulin in mammalian cells: The centrosomal and the cytosolic forms. J Cell Sci 109:875–887.

Niu Y, Liu T, Tse GM, Sun B, Niu R, Li HM, Wang H, Yang Y, Ye X, Wang Y, Yu Q, Zhang F. 2009. Increased expression of centrosomal α, γ-tubulin in atypical ductal hyperplasia and carcinoma of the breast. Cancer Sci 100:580–587.

Nováková M, Dráberová E, Schürmann W, Czihak G, Viklický V, Dráber P. 1996. γ-Tubulin redistribution in taxol-treated mitotic cells probed by monoclonal antibodies. Cell Motil Cytoskeleton 33:38–51.

Oakley CE, Oakley BR. 1989. Identification of γ-tubulin, a new member of the tubulin superfamily encoded by mipA gene of *Aspergillus nidulans*. Nature 338:662–664.

Ohno M, Fornerod M, Mattaj IW. 1998. Nucleocytoplasmic transport: The last 200 nanometers. Cell 92:327–336.

Raška I, Shaw PJ, Cmarko D. 2006. New insights into nucleolar architecture and activity. Int Rev Cytol 225:177–235.

Raynaud-Messina B, Merdes A. 2007. γ-tubulin complexes and microtubule organization. Curr Opin Cell Biol 19:24–30.

Rey O, Papazyan R, Waldron RT, Young SH, Lippincott-Schwartz J, Jacamo R, Rozengurt E. 2006. The nuclear import of protein kinase D3 requires its catalytic activity. J Biol Chem 281:5149–5157.

Robinson JM, Vandre DD. 2001. Antigen retrieval in cells and tissues: Enhancement with sodium dodecyl sulfate. Histochem Cell Biol 116:119–130.

Schwarzerová K, Petrášek J, Panigrahi KC, Zelenková S, Opatrný Z, Nick P. 2006. Intranuclear accumulation of plant tubulin in response to low temperature. Protoplasma 227:185–196.

Starita LM, Machida Y, Sankaran S, Elias JE, Griffin K, Schlegel BP, Gygi SP, Parvin JD. 2004. BRCA1-dependent ubiquitination of γ-tubulin regulates centrosome number. Mol Cell Biol 24:8457–8466.

Stearns T, Evans L, Kirschner M. 1991. γ-Tubulin is highly conserved component of the centrosome. Cell 65:825–836.

Sulimenko V, Sulimenko T, Poznanovic S, Nechiporuk-Zloy V, Böhm JK, Macůrek L, Unger E, Dráber P. 2002. Association of brain γ-tubulins with αβ-tubulin dimers. Biochem J 365:889–895.

Ullman KS, Powers MA, Forbes DJ. 1997. Nuclear export receptors: From importin to exportin. Cell 90:967–970.

Viklický V, Dráber P, Hašek J, Bártek J. 1982. Production and characterization of a monoclonal antitubulin antibody. Cell Biol Int Rep 6:725–731.

Vogel J, Drapkin B, Oomen J, Beach D, Bloom K, Snyder M. 2001. Phosphorylation of γ-tubulin regulates microtubule organization in budding yeast. Dev Cell 1: 621–631.

Walss-Bass C, Kreisberg JI, Ludueña RF. 2001. Mechanism of localization of βII-tubulin in the nuclei of cultured rat kidney mesangial cells. Cell Motil Cytoskeleton 49: 208–217.

Walss-Bass C, Xu K, David S, Fellous A, Ludueña RF. 2002. Occurrence of nuclear βII-tubulin in cultured cells. Cell Tissue Res 308:215–223.

Wang J, He X, Luo Y, Yarbrough WG. 2006. A novel ARF-binding protein (LZAP) alters ARF regulation of HDM2. Biochem J 393:489–501.

Wang J, An H, Mayo MW, Baldwin AS, Yarbrough WG. 2007. LZAP, a putative tumor suppressor, selectively inhibits NF-kappaB. Cancer Cell 12:239–251.
Wiese C, Zheng Y. 2000. A new function for the γ-tubulin ring complex as a microtubule minus-end cap. Nat Cell Biol 2:358–364.
Wise DO, Krahe R, Oakley BR. 2000. The γ-tubulin gene family in humans. Genomics 67:164–170.
Yeh IT, Luduena RF. 2004. The βII isotype of tubulin is present in the cell nuclei of a variety of cancers. Cell Motil Cytoskeleton 57:96–106.
Yuba-Kubo A, Kubo A, Hata M, Tsukita S. 2005. Gene knockout analysis of two γ-tubulin isoforms in mice. Develop Biol 282:361–373.
Zhang YP, Xiong Y. 2001. A p53 amino-terminal nuclear export signal inhibited by DNA damage-induced phosphorylation. Science 292:1910–1915.
Zhang S, Hernmerich P, Grosse F. 2007. Centrosomal localization of DNA damage checkpoint proteins. J Cell Biochem 101:451–465.
Zheng Y, Jung MK, Oakley BR. 1991. Gamma-tubulin is present in *Drosophila melanogaster* and *Homo sapiens* and is associated with centrosome. Cell 65:817–823.

VI.3.1

Supplementary data for:

Hořejší B., **Vinopal S.**, Sládková V., Dráberová E., Sulimenko V., Sulimenko T., Vosecká V., Philimonenko A., Hozák P., Katsetos C. D., Dráber P. (2012). Nuclear γ-tubulin associates with nucleoli and interacts with tumor suppressor protein C53. J Cell Physiol. *227*, 367-382.

Fig. S1

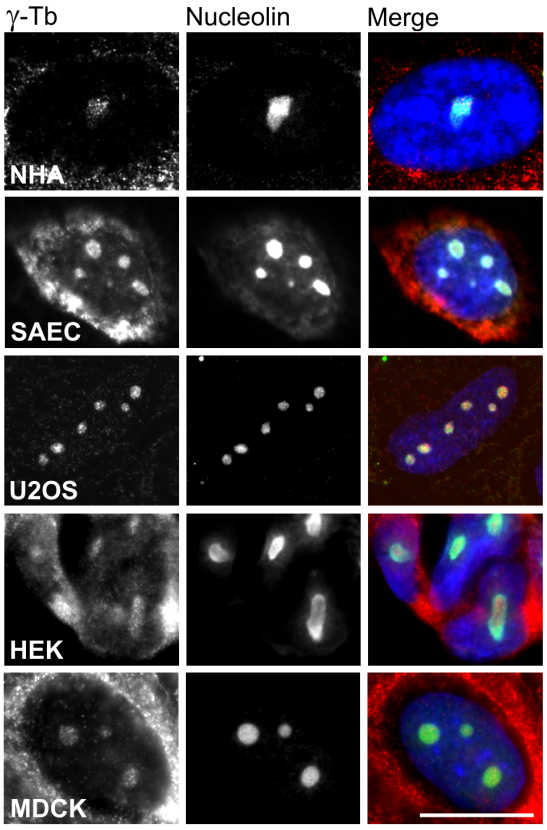

Fig. S1. Immunofluorescence detection of nucleolar γ-tubulin in various cell types. Normal human astrocytes (NHA), normal human small airway epithelial cells (SAEC), human osteogenic sarcoma cells (U2OS), human embryonal kidney cells HEK and Madin-Darby canine kidney cells (MDCK) were double-label stained with mAb TU-30 to γ-tubulin (γ-Tb; red) and Ab to nucleolin (green). DAPI (blue). Fixation Tx/HAc/M. Scale bar 20 μm.

Fig. S2

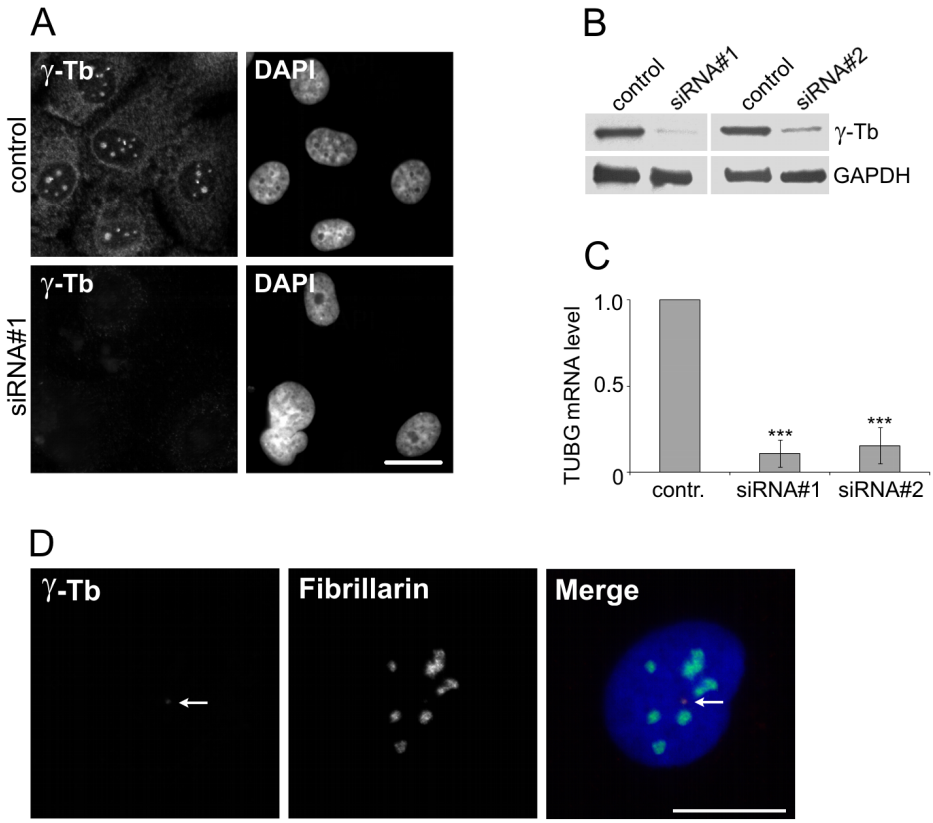

Fig. S2. Effect of γ-tubulin knock-down on nucleolar integrity. (A) Comparison of γ-tubulin distribution in U2OS cells transfected with negative control siRNA (control) and with γ-tubulin specific siRNA (siRNA#1). Cells were stained with anti-γ-tubulin Ab TU-30 (γ-Tb), DNA was labelled with DAPI. Methanol fixation. Fluorescence images of cells stained for γ-tubulin were captured under identical conditions and processed in exactly the same manner. Scale bar 20 μm. (B) Immunoblot analysis of whole cell extracts from cells transfected with negative control or γ-tubulin specific siRNAs. Staining with Abs to γ-tubulin (γ-Tb) and GAPDH. (C) Transcription of γ-tubulin genes in cells transfected with γ-tubulin specific siRNA#1 and siRNA#2 relative to the level in cells transfected with negative control siRNA (contr.) Data are presented as the fold change ± s.e.m. ***, $P<0.005$. (D) Immunofluorescence staining of U2OS cells after γ-tubulin knock-down with Ab TU-30 to γ-tubulin (γ-Tb; red) and polyclonal Ab to fibrillarin (green). DAPI (blue). Arrows point to remnants of γ-tubulin concentrated in the MTOC region. Methanol fixation. Scale bar 20 μm.

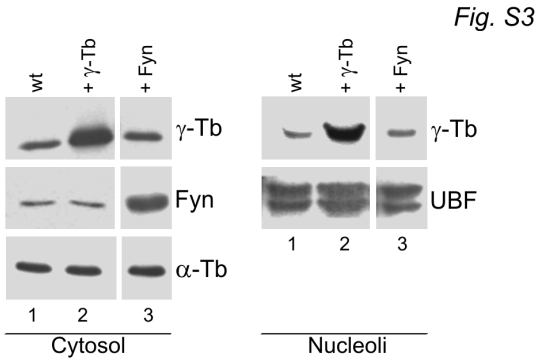

Fig. S3. Enrichment of γ-tubulin in nucleoli isolated from cells transfected with γ-tubulin. Immunoblot analysis of cytosolic and nucleolar fractions from non-transfected HEK cells or cells expressing exogenous γ-tubulin or Fyn (control). Wild-type cells (1, wt), cells expressing exogenous γ-tubulin (2, + γ-Tb) or exogenous Fyn (3, + Fyn) were stained with Abs to γ-tubulin (γ-Tb), Fyn, α-tubulin (α-Tb, loading control for cytosolic fractions) and UBF (loading control for nucleolar fraction).

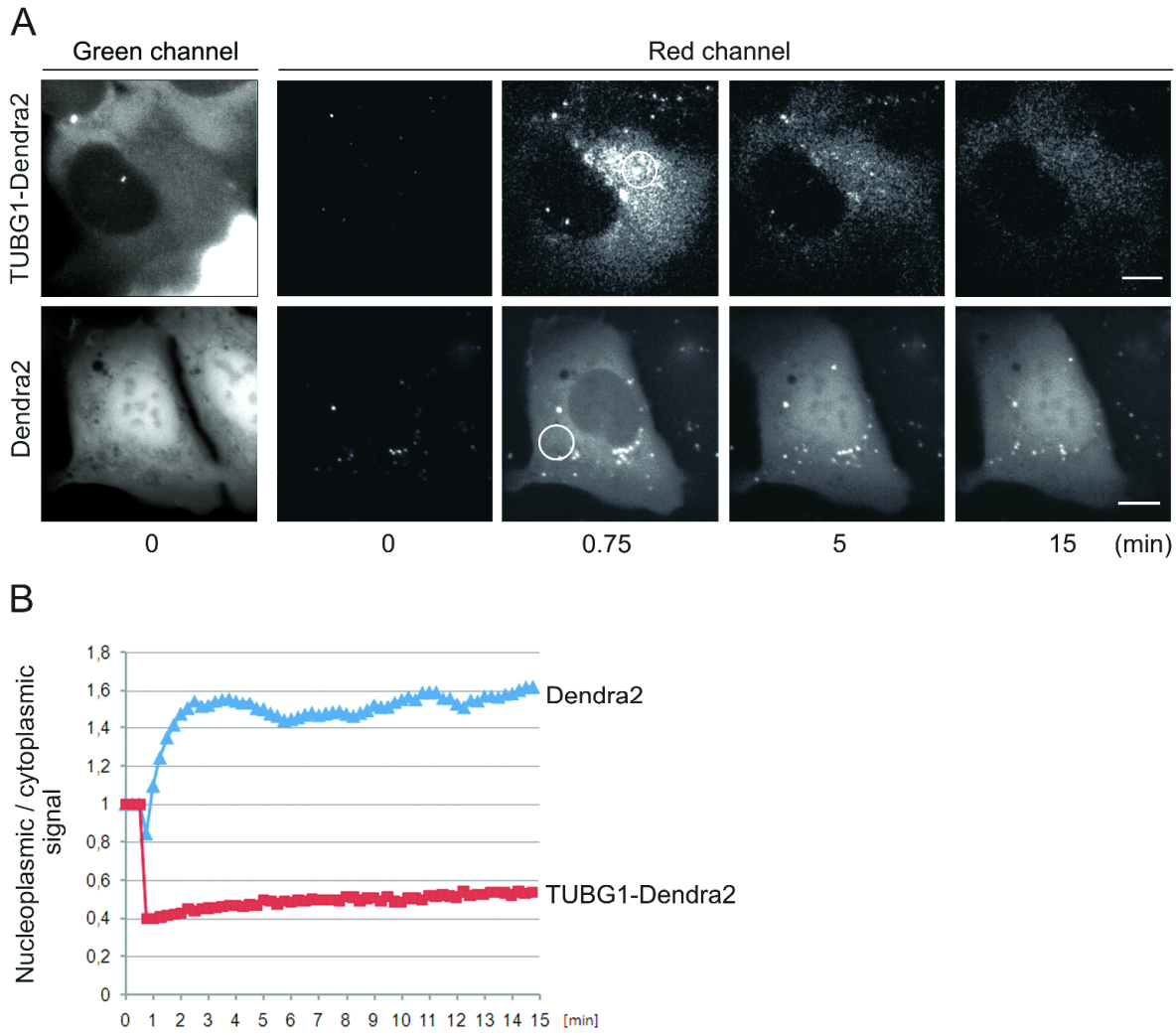

Fig. S4. **Distribution of photoactivated γ-tubulin-Dendra2.** U2OS cells expressing green to red photoconvertible γ-tubulin-Dendra2 protein or Dendra2 alone were photoactivated and time-lapse sequences were collected for 15 minutes at 15 second intervals. Dendra2 in cytoplasm was activated in depicted regions (white circles) 30 seconds after starting the time-lapse imaging. (A) Still images of fluorescence at various time points. (B) Quantification of red fluorescence, ratio of nucleoplasmic to cytoplasmic intensity during time-lapse experiment shown in panel A. Scale bar 10 μm.

Fig. S5

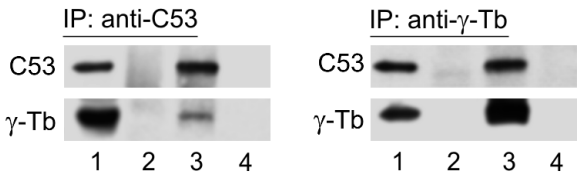

Fig. S5. Co-immunoprecipitation of γ-tubulin with C53 in nucleolar fraction of T98G cells. Nucleolar extracts were immunoprecipitated with Abs to C53 or γ-tubulin, and blots were probed with Abs to C53 or γ-tubulin (γ-Tb). Extracts (1), immobilized Abs not incubated with extract (2), immunoprecipitated proteins (3), protein A without Abs incubated with extracts (4).

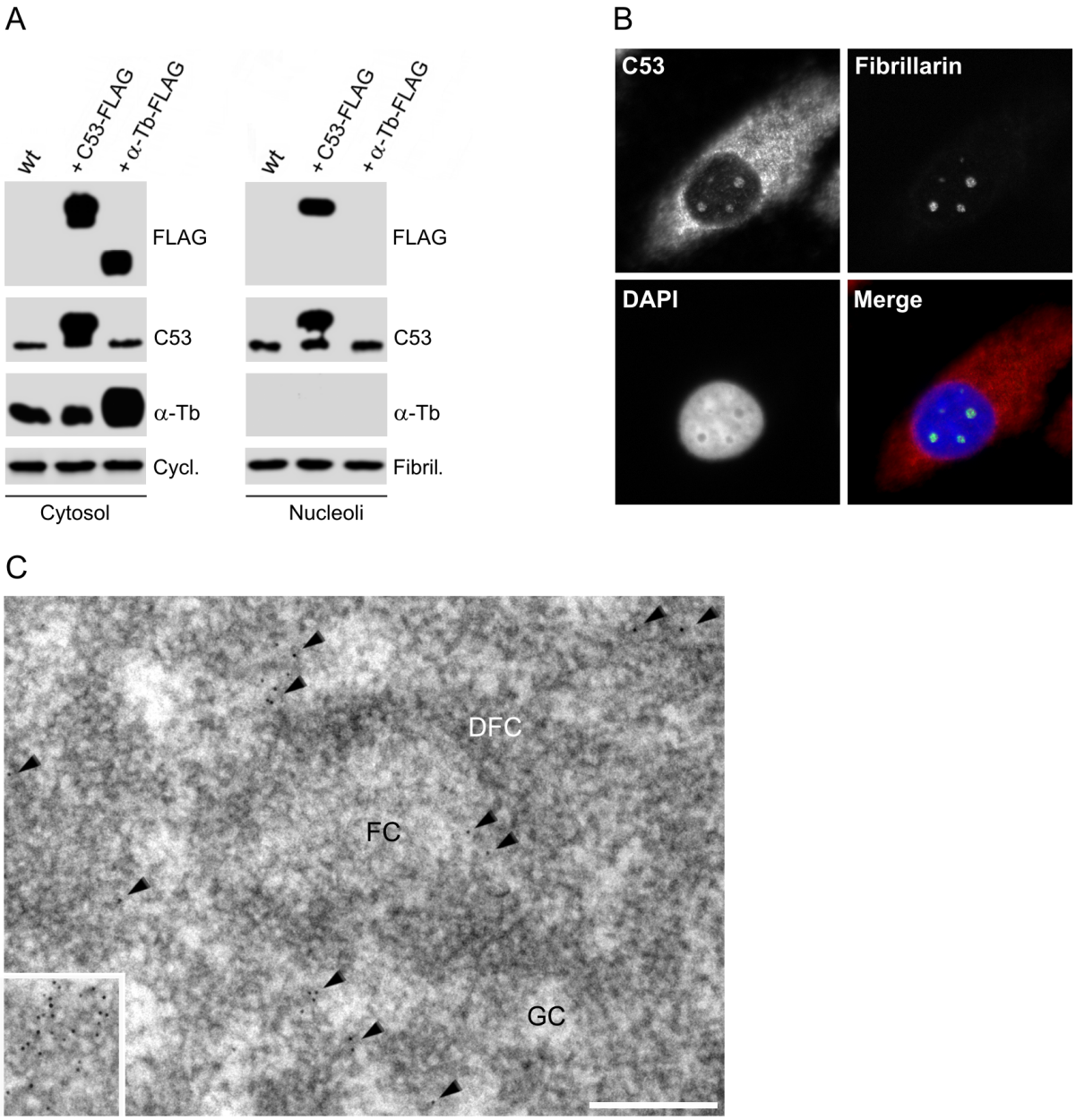

Fig. S6. C53 associates with nucleoli. (A) Immunoblot analysis of cytosolic and nucleolar fractions from non-transfected HEK cells (wt), cells expressing FLAG-tagged C53 or control FLAG-tagged α-tubulin. Blots were probed with Abs to FLAG, C53, α-tubulin (α-Tb), cyclophilin A (Cycl.) and fibrillarin (Fibril.) (B) Immunofluorescence microscopy. T98G cells were double-label stained with polyclonal Ab to C53 (red) and mAb to fibrillarin (green). DAPI (blue). Fixation with methanol. Scale bar 20 μm. (C) Ultrastructural localization of C53 in nucleolus of T98G cells. Immunoelectron microscopy with mAb to C53 on a sample prepared by aldehyde fixation. Clusters of gold particles are shown in the insert. Arrowheads indicate position of gold particles. FC, fibrillar center; DFC, dense fibrillar component; GC, granular component. Scale bar 0.2 μm.

Fig. S7

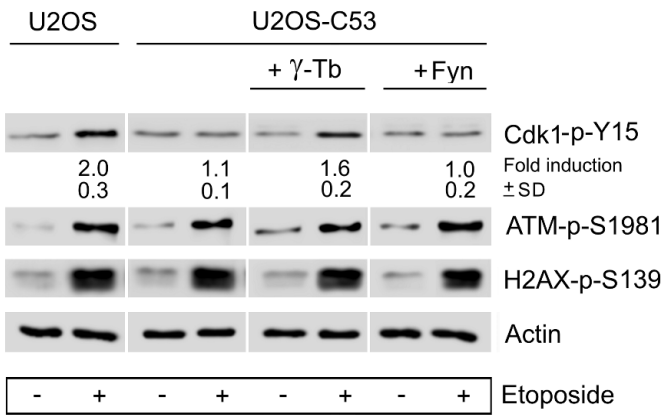

Fig. S7. Overexpression of γ-tubulin antagonizes the inhibitory effect of C53 on DNA damage G_2/M checkpoint activation. U2OS cells expressing GFP-C53 were transfected with vector encoding γ-tubulin (+ γ-Tb) or control vector encoding Fyn (+Fyn). After 48 hours the cells were treated with 20 μM etoposide for 3 h. U2OS cells served as control. Immunoblot analysis of whole cell extracts with Abs to Cdk1-p-Y15, H2AX-p-S139 and actin. Numbers under the blots indicate relative amounts of proteins normalized to cells not treated with etoposide. Means ± s.d. were calculated from three experiments.

Fig. S8

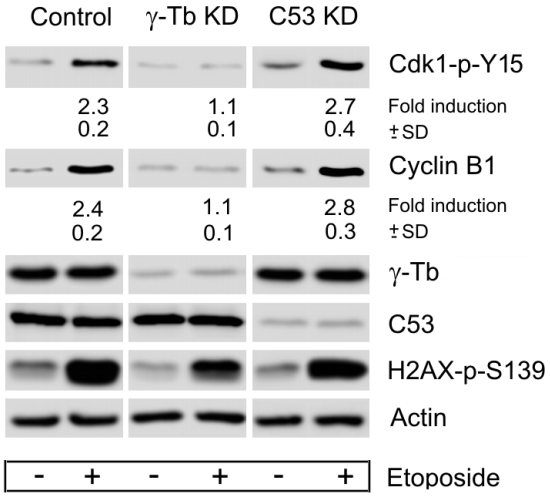

Fig. S8. Effect of γ-tubulin or C53 depletion on DNA damage G_2/M checkpoint activation. U2OS cells were transfected with γ-tubulin or C53 specific siRNAs or corresponding negative controls. Cells with depleted γ-tubulin (γ-Tb KD) or C53 (C53 KD) were treated with 20 μM etoposide for 3 h. Immunoblot analysis of whole cell extracts with Abs to Cdk1-p-Y15, cyclin B1, γ-tubulin (γ-Tb), C53, H2AX-p-S139 and actin. Negative control for γ-Tb KD is shown (negative control for C53 KD gave similar results). Numbers under the blots indicate relative amounts of proteins normalized to cells not treated with etoposide. Means ± s.d. were calculated from three experiments.

TABLE S1. Sequence of oligonucleotides used for quantitative RT-PCR analysis

Name	Sequence
γ-tubulin 1, forward	5'-ATCGCCATCCTCAACATCATCCAG-3'
γ-tubulin 1, reverse	5'-GTGTTTGCAGGCCAACAGAGAGTC-3'
γ-tubulin 2, forward	5'-CTGCGGAAGCGGGATGC-3'
γ-tubulin 2, reverse	5'-CACGGGCTGGAGATGAACC-3'
γ-tubulin 1+2, forward	5'-TGGGTTCGAGTTCTGGAAA-3'
γ-tubulin 1+2, reverse	5'-CATCGTCTGCCTGGTAGAAA-3'
β-actin, forward	5'-TCCTTCCTGGGCATGGAGT-3'
β-actin, reverse	5'-AAAGCCATGCCAATCTCATC-3'

TABLE S2. Mass spectrometry identification of the C53

Measured mass [M+H]	Computed mass [M+H]	Error (ppm)	Peptide sequence	Peptide position
1028.566	1028.565	1	LLDWLVDR	16 - 23
1110.509	1110.509	0	GNSTVYEWR	234 - 242
1114.649	1114.649	0	WQSLVLTIR	30 - 38
1175.618	1175.618	0	NVNYEIPSLK	121 - 130
1184.667	1184.666	1	LLDWLVDRR	16 - 24
1409.695	1409.697	1	YSGRPVNLMGTSL	494 - 506
1577.791	1577.793	1	GPDALTLLEYTETR	337 - 350
1620.872	1620.872	0	DNTYLVELSSLLVR	107 - 120
1681.839	1681.838	1	MKDWQEIIALYEK	94 - 106

1 MEDHQHVPID IQTSK**LLDWL VDRR**HCSLK**W QSLVLTIR**EK INAAIQDMPE SEEIAQLLSG

61 SYIHYFHCLR ILDLLKGTEA STKNIFGRYS SQR**MKDWQEI IALYEKDNTY LVELSSLLVR**

121 **NVNYEIPSLK** KQIAKCQQLQ QEYSRKEEEC QAGAAEMREQ FYHSCKQYGI TGENVRGELL

181 ALVKDLPSQL AEIGAAAQQS LGEAIDVYQA SVGFVCESPT EQVLPMLRFV **QKRGNSTVYE**

241 **WR**TGTEPSVV ERPHLEELPE QVAEDAIDWG DFGVEAVSEG TDSGISAEAA GIDWGIFPES

301 DSKDPGGDGI DWGDDAVALQ ITVLEAGTQA PEGVAR**GPDA LTLLEYTETR** NQFLDELMEL

361 EIFLAQRAVE LSEEADVLSV SQFQLAPAIL QGQTKEKMVT MVSVLEDLIG KLTSLQLQHL

421 FMILASPRYV DRVTEFLQQK LKQSQLLALK KELMVQKQQE ALEEQAALEP KLDLLLEKTK

481 ELQKLIEADI SKR**YSGRPVN LMGTSL**

Amino acids of the identified peptides in the human CDK5 regulatory subunit-associated protein 3 (UniProtKB/Swiss-Prot Q96JB5) are indicated in bold and underlined (bottom part of the table). The matched peptides cover 18% of the protein sequence.

VI.4

Vinopal S., Černohorská M., Sulimenko V., Sulimenko T., Vosecká V., Flemr M., Dráberová E., Dráber P. (2012). γ-Tubulin 2 nucleates microtubules and is downregulated in mouse early embryogenesis. PLoS ONE *7*: e29919.

OPEN ACCESS Freely available online

PLoS one

γ-Tubulin 2 Nucleates Microtubules and Is Downregulated in Mouse Early Embryogenesis

Stanislav Vinopal[1], Markéta Černohorská[1], Vadym Sulimenko[1], Tetyana Sulimenko[1], Věra Vosecká[1], Matyáš Flemr[2], Eduarda Dráberová[1], Pavel Dráber[1]*

1 Department of Biology of Cytoskeleton, Institute of Molecular Genetics, Academy of Sciences of the Czech Republic, Prague, Czech Republic, **2** Department of Epigenetic Regulations, Institute of Molecular Genetics, Academy of Sciences of the Czech Republic, Prague, Czech Republic

Abstract

γ-Tubulin is the key protein for microtubule nucleation. Duplication of the γ-tubulin gene occurred several times during evolution, and in mammals γ-tubulin genes encode proteins which share ~97% sequence identity. Previous analysis of *Tubg1* and *Tubg2* knock-out mice has suggested that γ-tubulins are not functionally equivalent. *Tubg1* knock-out mice died at the blastocyst stage, whereas *Tubg2* knock-out mice developed normally and were fertile. It was proposed that γ-tubulin 1 represents ubiquitous γ-tubulin, while γ-tubulin 2 may have some specific functions and cannot substitute for γ-tubulin 1 deficiency in blastocysts. The molecular basis of the suggested functional difference between γ-tubulins remains unknown. Here we show that exogenous γ-tubulin 2 is targeted to centrosomes and interacts with γ-tubulin complex proteins 2 and 4. Depletion of γ-tubulin 1 by RNAi in U2OS cells causes impaired microtubule nucleation and metaphase arrest. Wild-type phenotype in γ-tubulin 1-depleted cells is restored by expression of exogenous mouse or human γ-tubulin 2. Further, we show at both mRNA and protein levels using RT-qPCR and 2D-PAGE, respectively, that in contrast to *Tubg1*, the *Tubg2* expression is dramatically reduced in mouse blastocysts. This indicates that γ-tubulin 2 cannot rescue γ-tubulin 1 deficiency in knock-out blastocysts, owing to its very low amount. The combined data suggest that γ-tubulin 2 is able to nucleate microtubules and substitute for γ-tubulin 1. We propose that mammalian γ-tubulins are functionally redundant with respect to the nucleation activity.

Citation: Vinopal S, Černohorská M, Sulimenko V, Sulimenko T, Vosecká V, et al. (2012) γ-Tubulin 2 Nucleates Microtubules and Is Downregulated in Mouse Early Embryogenesis. PLoS ONE 7(1): e29919. doi:10.1371/journal.pone.0029919

Editor: Claude Prigent, Institut de Génétique et Développement de Rennes, France

Received August 23, 2011; **Accepted** December 6, 2011; **Published** January 3, 2012

Funding: This work was supported in part by Grants 204/09/H084 (SV, MČ), 204/09/1777 (PD), and P302/10/1759 (ED) from the Grant Agency of the Czech Republic, Grants LC545 (TS) and 1M6837805001 (VV) from Ministry of Education, Youth and Sports of the Czech Republic, KAN200520701 (VS) from the Grant Agency of the Czech Academy of Sciences, Grant 11109 from the Grant Agency of Charles University (SV), and by the Institutional Research Support Grant AVOZ50520514 (PD). The funders had no role in study design, data collection and analysis, decision to publish, or preparation of the manuscript.

Competing Interests: The authors have declared that no competing interests exist.

* E-mail: paveldra@img.cas.cz

Introduction

γ-Tubulin is a highly conserved member of the tubulin superfamily essential for microtubule nucleation in all eukaryotes [1–3]. It assembles together with other proteins, named Gamma-tubulin Complex Proteins (GCPs) in human, into two main γ-Tubulin Complexes (γTuCs): the γ-Tubulin Small Complex (γTuSC) and the γ-Tubulin Ring Complex (γTuRC). The γTuSC, a vital component of microtubule nucleation machinery in all eukaryotes, is composed of two molecules of γ-tubulin and one copy each of GCP2 and GCP3. The γTuRCs are found only in metazoa and consist of seven γTuSCs and additional GCPs, including GCP4-6 [4,5]. The γTuRC is a ring structure with an arrangement of γ-tubulin molecules that matches the 13-fold symmetry of a microtubule. It serves as a template for microtubule polymerization [6]. It has recently been shown that the budding yeast γTuSCs alone form *in vitro* ring structures similar to γTuRCs [7]; it supports the general template model of microtubule nucleation [6].

γTuCs are concentrated at Microtubule Organizing Centers (MTOCs) such as centrosomes and basal bodies in animals or spindle pole bodies in fungi. They are also found on nuclear membranes in acentrosomal plants and on Golgi membranes, condensed mitotic chromosomes, midbodies and along microtubules in mitotic spindles [8]. We have recently reported nucleolar localization of γ-tubulin [9]. However, the majority of γTuCs exist in cytoplasm in soluble form [10]. In addition to its function in microtubule nucleation, γ-tubulin is also involved in centriole biogenesis [11,12], regulation of microtubule (+) end dynamics [13–15], regulation of the anaphase-promoting complex/cyclosome during interphase in *Aspergillus* [16] or regulation of bipolar spindle assembly in fission yeast [17].

Many organisms including *Arabidopsis* [18], *Paramecium* [19], *Euplotes* [20], *Drosophila* [21] and mammals [22–24] possess two genes encoding γ-tubulin. Nevertheless, phylogenetic analyses revealed that γ-tubulin gene duplication in mammals occurred independent of the others [23,24]. Mammalian γ-tubulin genes are located on the same chromosome in tandem, and their coding sequences share very high sequence similarity (>94% in human)[22]. Although it was initially assumed that γ-tubulin genes are functionally redundant [22], gene knock-out analysis of *Tubg1* and *Tubg2* in mice suggested that they might have different functions [23]. While *Tubg1* was expressed ubiquitously, *Tubg2* was primarily detected in brain and also in blastocysts. $Tubg1^{-/-}$ embryos stopped their development at the morula/blastocyst stage because of severe mitotic defects. $Tubg2^{-/-}$ mice developed

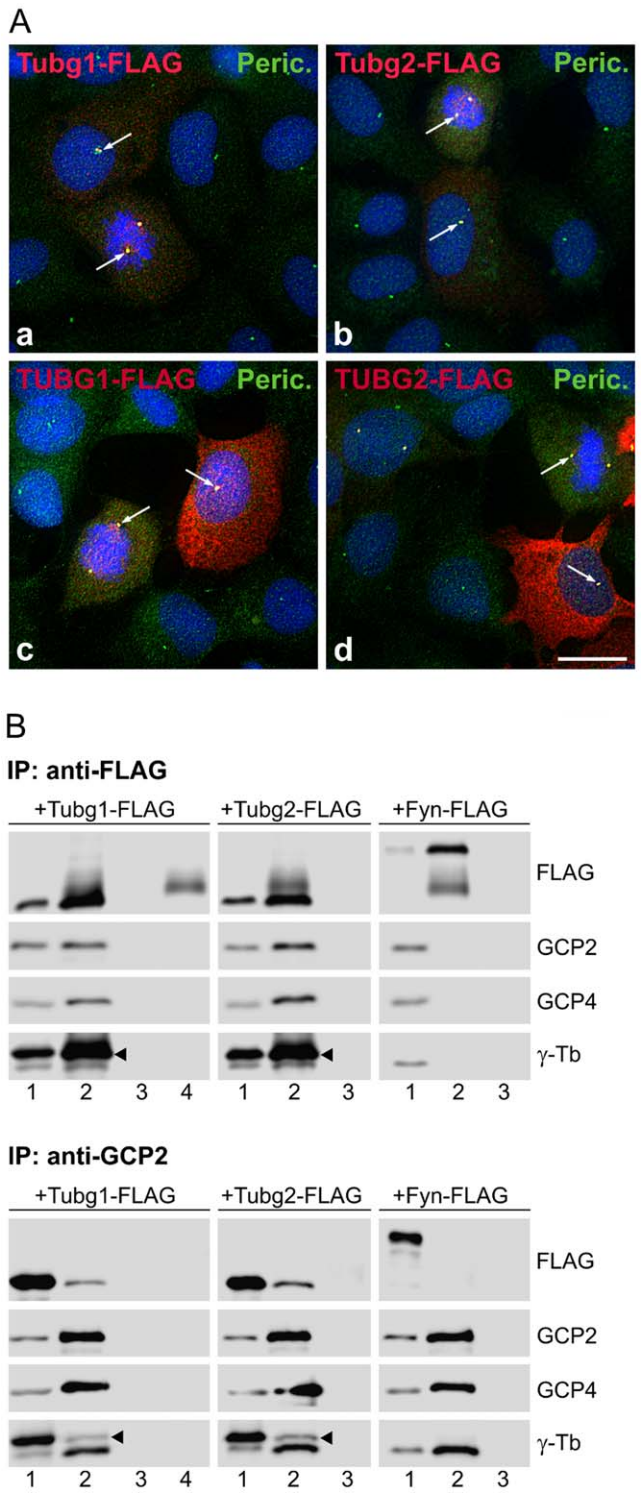

Figure 1. Exogenous γ-tubulin 2 locates to centrosomes and interacts with GCPs. (A) Localization of FLAG-tagged γ-tubulins. Human U2OS cells expressing mouse γ-tubulin 1 (a, Tubg1-FLAG), mouse γ-tubulin 2 (b, Tubg2-FLAG), human γ-tubulin 1 (c, TUBG1-FLAG) and human γ-tubulin 2 (d, TUBG2-FLAG) were stained for FLAG (red) and pericentrin (green). DNA was stained with DAPI (blue). Arrows denote positions of MTOCs where FLAG-tagged γ-tubulins co-localize with pericentrin. Final images were made by maximum intensity projection of 3 deconvolved z-sections spaced at 0.25 μm. Scale bar 10 μm. (B) Coimmunoprecipitation of mouse γ-tubulins with GCP2 and GCP4 proteins. Extracts from HEK cells expressing FLAG-tagged γ-tubulin 1 (Tubg1-FLAG), γ-tubulin 2 (Tubg2-FLAG) or control mouse Fyn (Fyn-FLAG) were immunoprecipitated with antibodies to FLAG or GCP2, and blots were probed with antibodies to FLAG, GCP2, GCP4 and γ-tubulin (γ-Tb). Extracts (1), immunoprecipitated proteins (2), protein A without antibodies incubated with extracts (3), immobilized antibodies not incubated with extracts (4). Arrowheads indicate the positions of exogenous γ-tubulins.
doi:10.1371/journal.pone.0029919.g001

normally and produced fertile offspring. However, adults exhibited some behavioral changes including abnormalities in circadian rhythm and different reaction to painful stimulations. These findings led to a conclusion that γ-tubulin 1 is the conventional γ-tubulin, whereas γ-tubulin 2, which lacks the capability to rescue the consequences of γ-tubulin 1 deficiency, might have specific function(s) in the brain [23]. Nevertheless, the molecular basis of suggested functional differences between γ-tubulin 1 and γ-tubulin 2 is unknown.

To gain a deeper insight into the potential functional differences of mammalian γ-tubulins, we have examined subcellular distribution of γ-tubulin 2 in cultured cells, its interactions with GCPs, capability to nucleate microtubules and substitute for γ-tubulin 1. We have also analyzed γ-tubulin 2 expression in the course of mouse preimplantation development. Our results indicate that even though γ-tubulins are differentially expressed during mouse early embryogenesis and in adult tissues, they are functionally redundant with respect to their nucleation activity.

Results

γ-Tubulin 2 is indistinguishable from γ-tubulin 1 in subcellular localization and interactions with GCPs

To decide whether or not γ-tubulin 2 differs from γ-tubulin 1 in subcellular localization, we examined U2OS cells expressing FLAG-tagged mouse or human γ-tubulin 2 (Tubg2-FLAG, TUBG2-FLAG) by immunofluorescence microscopy with anti-FLAG antibody. Centrosomes were marked with antibody to pericentrin. U2OS cells expressing FLAG-tagged mouse and human γ-tubulin 1 (Tubg1-FLAG, TUBG1-FLAG) served as controls. As expected, exogenous mouse (Fig. 1A, a) and human (Fig. 1A, c) γ-tubulin 1 localized to the centrosomes in both interphase and mitotic cells. FLAG-tagged γ-tubulin 1 was also found along mitotic spindle and diffusely in cytoplasm. The same staining pattern was detected in cells expressing exogenous mouse (Fig. 1A, b) and human (Fig. 1A, d) γ-tubulin 2. Fully displayed immunofluorescence of Fig. 1A appears in Fig. S1.

Next we checked by coimmunoprecipitation the ability of γ-tubulin 2 to interact with GCP2 (γTuSC marker) and GCP4 (γTuRC marker). FLAG-tagged mouse γ-tubulin 1, γ-tubulin 2 or Fyn kinase (negative control) were immunoprecipitated from HEK 293FT cells with rabbit anti-FLAG antibody. Immunoblot analysis revealed that both FLAG-tagged γ-tubulins interacted with GCP2 and GCP4, yet no coimmunoprecipitation was observed in case of FLAG-tagged Fyn kinase (Fig. 1B, upper panel). Negative control rabbit antibody failed to coimmunoprecipitate GCP proteins (not shown). In addition, the reciprocal precipitation with antibody to GCP2 (IgG2b), confirmed the interaction of FLAG-tagged γ-tubulins with GCP2 (Fig. 1B, lower panel). Again, negative control antibody (IgG2b) did not coimmunoprecipitate FLAG-tagged γ-tubulins (not shown). We obtained the same results when lysates from HEK 293FT cells expressing FLAG-tagged human γ-tubulin 1 and γ-tubulin 2 were used for immunoprecipitation with anti-FLAG and anti-GCP2 antibodies (Fig. S2). Altogether the data indicate that mammalian γ-tubulin 2 is indiscernible from γ-tubulin 1 as far as the subcellular distribution and interactions

with components of small and large γ-tubulin complexes are concerned.

γ-Tubulin 2 rescues mitotic progression in γ-tubulin 1-depleted cells

To find out whether or not γ-tubulin 2 is able to take the place of γ-tubulin 1, we performed phenotypic rescue experiments in U2OS cells depleted of γ-tubulin 1 by RNAi. As demonstrated by immunoblotting, transfection of TUBG1-specific siRNAs (KD1 and KD2) led to a substantial reduction of total γ-tubulin content when compared to negative control cells (Fig. S3A). Noticeably, it means that γ-tubulin 1 is the dominant γ-tubulin in U2OS cells, because the specificity of both KD1 and KD2 siRNAs was verified *in silico* (NCBI BLAST) and by means of RT-qPCR (data not shown). Since KD2 siRNA proved to be more efficient, it was used in further experiments. Effective γ-tubulin depletion by KD2 siRNA was further confirmed by immunofluorescence microscopy (Fig. 2A). The most prominent phenotypic feature of γ-tubulin 1 depletion was mitotic arrest in metaphase (Fig. 2B), most likely induced by severe mitotic spindle defects (Fig 2C). Basically, cells in anaphase, telophase or cytokinesis were absent in the population of γ-tubulin 1-depleted cells.

FLAG-tagged mouse γ-tubulin 1, used as a positive control, restored the original phenotype in γ-tubulin 1-depleted U2OS. Cells expressing exogenous γ-tubulin 1 were able to pass the spindle assembly checkpoint, as demonstrated by the presence of cells in anaphase, whereas the untrasfected cells were not (Fig. 3, a–d). Interestingly, FLAG-tagged mouse γ-tubulin 2 (Fig. 3, e–h) and FLAG-tagged human γ-tubulin 2 (Fig. 3, i–l) also rescued the normal mitotic division similarly to mouse γ-tubulin 1. Detailed microscopic examination of rescued cells revealed that they regained the ability to build properly arranged metaphase (Fig. S4, a–c) and anaphase (Fig. S4, d–f) mitotic spindles. Importantly, we failed to detect any mitotic spindle defects in the rescued cells.

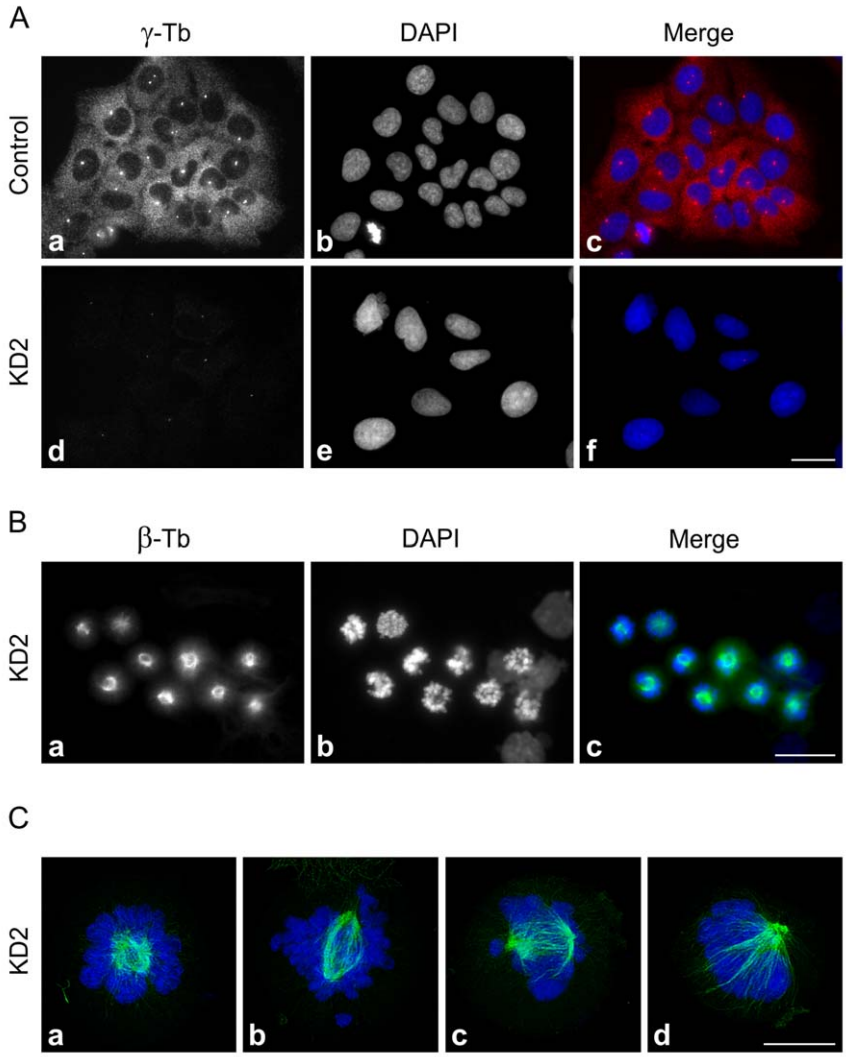

Figure 2. Depletion of human γ-tubulin 1 leads to mitotic spindle defects and metaphase arrest. (A) Interphase U2OS cells transfected with negative control siRNA (Control) or with γ-tubulin 1 specific siRNA (KD2). Cells were stained for γ-tubulin (a, d; red). DNA was stained with DAPI (b, e; blue). Images of cells stained for γ-tubulin were captured under identical conditions and processed in exactly the same way. Scale bar 20 μm. (B) Aberrant spindle formation and metaphase arrest in U2OS cells depleted of γ-tubulin 1 (KD2). Cells were stained for β-tubulin (a; green). DNA was stained with DAPI (b; blue). Scale bar 20 μm. (C) Detailed images of aberrant mitotic spindles. Cells were stained for β-tubulin (a–d; green). DNA was stained with DAPI (a–d; blue).Maximum intensity projections of 30–40 deconvolved confocal z-sections spaced at 0.125 μm. Scale bar 10 μm.
doi:10.1371/journal.pone.0029919.g002

Immunoblot tests in performed rescue experiments confirmed an effective expression of FLAG-tagged γ-tubulins in γ-tubulin 1-depleted cells (Fig. S3B). These findings suggest that γ-tubulin 2 is capable of replacing γ-tubulin 1 during mitosis.

γ-Tubulin 2 nucleates microtubules

Taking advantage of the above described phenotypic rescue experimental set-up, we further investigated the microtubule nucleating capability of γ-tubulin 2 in microtubule regrowth experiments. The amount of γ-tubulin on prophase/metaphase centrosomes is significantly higher than that in interphase due to the process called centrosome maturation [25,26]. We therefore first focused on mitotic centrosomes, where one could expect a prominent effect of γ-tubulin depletion on microtubule nucleation. Microtubules were depolymerized by nocodazole, washed by ice-cold PBS, and allowed to regrow before fixation and staining for β-tubulin. Mitotic cells became more abundant in the course of nocodazole treatment. While the regrowth of microtubules from centrosomes was easily observable in cells transfected with negative control siRNA (Fig. 4A, a–d), it was substantially delayed and/or impaired in γ-tubulin 1-depleted cells (Fig. 4A, e–h). Clearly recognizable microtubule asters were seen in 97% (n = 369) of negative control mitotic cells. In γ-tubulin 1-depleted cells, however, microtubule asters were indistinct and formed in only 18% (n = 274) of mitotic cells. As expected, FLAG-tagged mouse γ-tubulin 1 (positive control) rescued the microtubule aster formation in γ-tubulin 1-depleted cells (Fig. 4B, a–d). In accordance with our previous results, both FLAG-tagged mouse γ-tubulin 2 (Fig. 4B, e–h) and FLAG-tagged human γ-tubulin 2 (Fig. 4B, i–l) also rescued aster formation. Clear microtubule regrowth was observed in all γ-tubulin 1-depleted cells expressing exogenous γ-tubulin 2; it indicates that γ-tubulin 2 is capable of centrosomal microtubule nucleation in mitotic cells.

In order to strengthen the evidence of microtubule nucleation capability of γ-tubulin 2, we quantified microtubule formation *in vivo* by the tracking microtubule (+) ends marked by EB1-GFP in interphase U2OS cells (U2OS-EB1). For live cell imaging we used the shRNA system based on pLKO.1 vectors. Puromycin selection for 6 days made it possible to analyze only γ-tubulin-depleted cells. We constructed TUBG1-specific shRNA expressing vectors based on siRNAs (KD1 and KD2), and tested their effectivity by immunoblotting (Fig S5A). Since KD2 shRNA was found more efficient, further experiments were limited to that. Substantial γ-tubulin depletion by KD2 shRNA was confirmed by immunofluorescence microscopy (Fig. S5B). Additionally, we prepared TagRFP-tagged mouse γ-tubulin 1 (pmTubg1-TagRFP) and TagRFP-tagged human γ-tubulin 2 (phTUBG2-TagRFP) for phenotypic rescue experiments. TagRFP (pCI-TagRFP) served as control.

Following puromycin selection, transfected U2OS-EB1 cells were subjected to live cell imaging; time-lapse sequences of EB1-GFP dynamics were acquired only from cells coexpressing TagRFP or TagRFP-tagged proteins. Immunoblotting confirmed an effective expression of tagged γ-tubulins in γ-tubulin 1-depleted cells (Fig. S6). Results of typical experiments are presented in Fig. 5, where single-frame (Fig. 5, a–d) as well as 60-frame projections (Fig. 5, e–h) of time-lapse sequences are shown. While TagRFP was found in both cytoplasm and nuclei (Fig 5, a–b), TagRFP-tagged γ-tubulins were concentrated to MTOC (Fig. 5, c–d). This is more distinctly demonstrated in Fig. S7, where green and red channels are depicted separately. The density of microtubule (+) end tracks, reconstructed by maximum intensity projection of time-lapse sequences, was markedly reduced in γ-

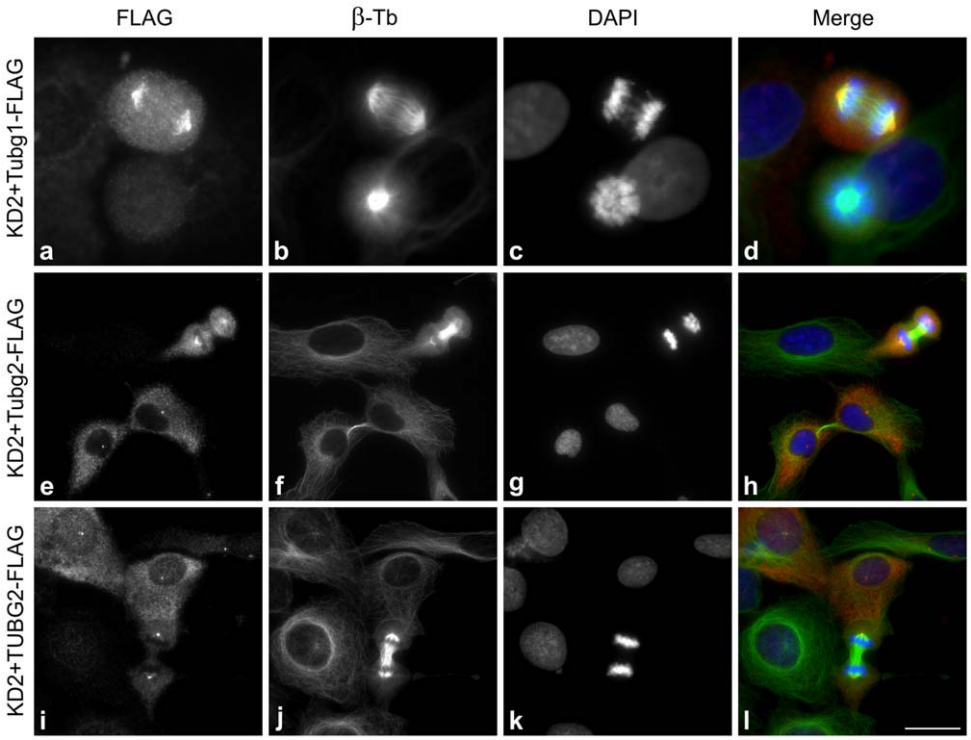

Figure 3. γ-Tubulin 2 restores normal mitotic spindle functioning in γ-tubulin 1-depleted cells. U2OS cells depleted of γ-tubulin 1 and expressing FLAG-tagged mouse γ-tubulin 1 (a-d, Tubg1-FLAG), mouse γ-tubulin 2 (e-h, Tubg2-FLAG) or human γ-tubulin 2 (i–l, TUBG2-FLAG) were stained for FLAG (a, e, i; red) and β-tubulin (b, f, j; green). DNA was stained with DAPI (c, g, k; blue). Scale bar 20 μm.
doi:10.1371/journal.pone.0029919.g003

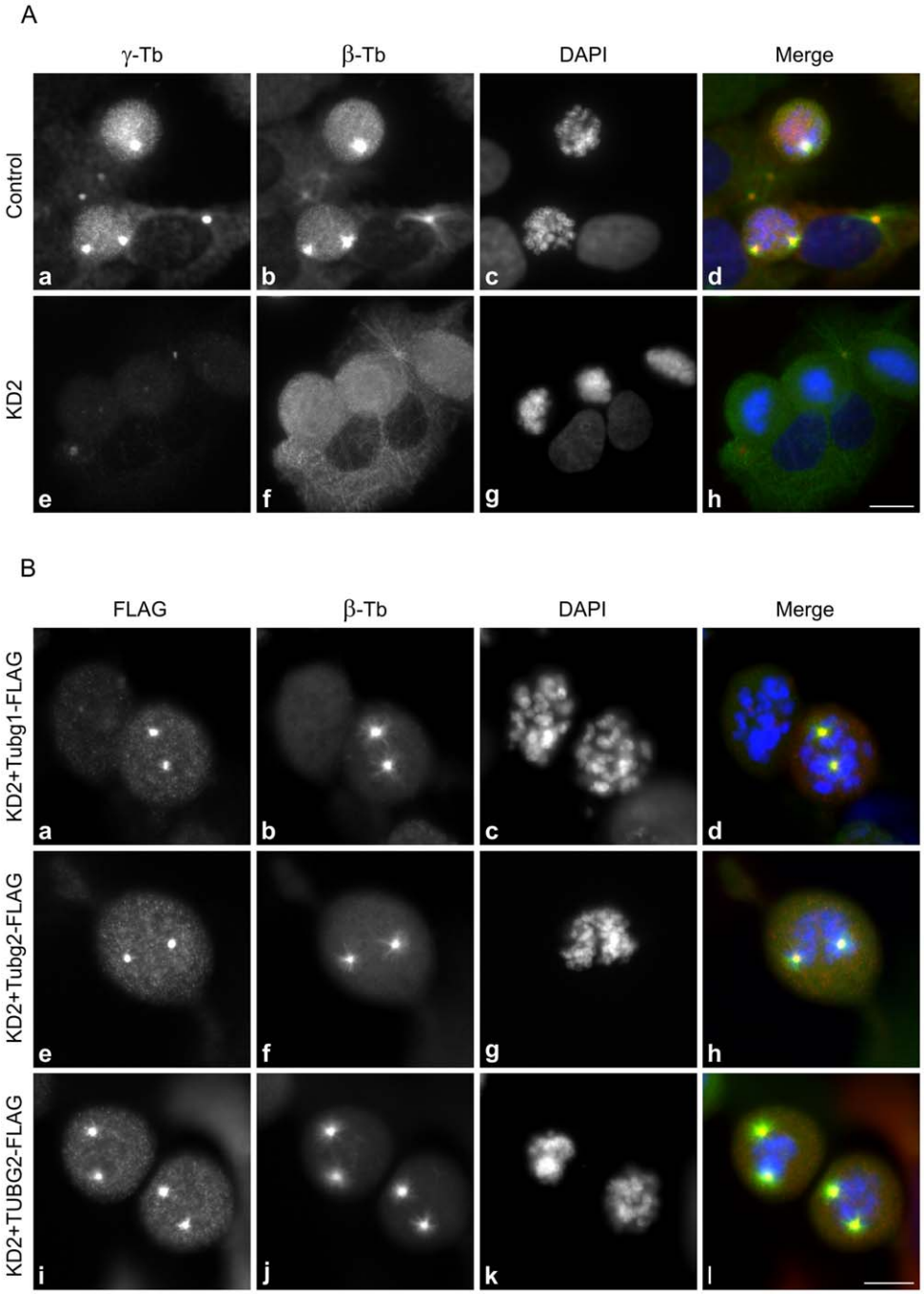

Figure 4. γ-Tubulin 2 rescues centrosomal microtubule nucleation in γ-tubulin 1-depleted mitotic cells. A) U2OS cells transfected with negative control siRNA (Control) or with γ-tubulin 1 specific siRNA (KD2) were treated with 10 μM nocodazole for 6 h and fixed after 3 min incubation in medium without nocodazole. Cells were stained for γ-tubulin (a, e; red) and β-tubulin (b, f; green). DNA was stained with DAPI (c, g; blue). Fluorescence images of cells stained for γ-tubulin were captured under identical conditions and processed in exactly the same way. Scale bar 10 μm. (B) U2OS cells depleted of γ-tubulin 1 and expressing FLAG-tagged mouse γ-tubulin 1 (a–d, Tubg1-FLAG), mouse γ-tubulin 2 (e–h, Tubg2-FLAG) or human γ-tubulin 2 (i–l, TUBG2-FLAG) were treated with 10 μM nocodazole for 6 h and fixed after 3 min incubation in medium without nocodazole. Cells were stained for FLAG (a, e, i; red) and β-tubulin (b, f, j; green). DNA was stained with DAPI (c, g, k; blue). Scale bar 10 μm.
doi:10.1371/journal.pone.0029919.g004

tubulin 1-depleted cells (Fig. 5, f) when compared with negative control cells (Fig. 5, e). This most likely reflects an impaired microtubule nucleation. In contrast, the density of EB1 tracks in cells rescued by exogenous mouse γ-tubulin 1 (Fig. 5, g) resembled that seen in negative controls cells (Fig. 5, e). Clear phenotypic rescue was also observed in cells expressing exogenous human γ-tubulin 2 (Fig. 5, h). These findings were confirmed by evaluation of statistical data as documented in histograms of the microtubule growth rates, where the number of EB1 tracks was normalized by the cell area and tracking time (Fig. 6). To compare whole populations of EB1 tracks in analyzed cells, we applied Bonferroni correction of p-values to velocity histograms (Fig. 6).

Calculated p-values for differences among individual growth velocity groups were multiplied by the number of all growth velocity groups in the histogram (n = 13). Based on this correction, the number of EB1 tracks was significantly reduced in γ-tubulin 1-depleted cells when compared with negative control cells ($p<0.0001$, Fig. 6A). Conversely, the number of EB1 tracks was significantly higher in cells rescued by exogenous mouse γ-tubulin 1 ($p<1.10^{-6}$, Fig. 6B) or human γ-tubulin 2 ($p<1.10^{-5}$, Fig. 6C) than in γ-tubulin 1-depleted cells. Differences between negative control (blue columns in Fig. 6A) and γ-tubulin 2 expressing cells (blue columns in Fig. 6C) were statistically insignificant. Interestingly, the number of EB1 tracks in cells expressing exogenous mouse γ-tubulin 1 (blue columns in Fig. 6B) exceeded that seen in negative control ($p<0.05$; blue columns in Fig. 6A) or in cells expressing exogenous γ-tubulin 2 ($p<0.05$; blue columns in Fig. 6C). Taken collectively, our experimental data demonstrate that mammalian γ-tubulin 2 is able to nucleate microtubules and substitute for γ-tubulin 1 even in interphase cells.

Tubg2 is downregulated in mouse preimplantation development

Since γ-tubulin 2 was capable to substitute for γ-tubulin 1 in cultured cells, its inability to do so in blastocysts [23] is intriguing. We therefore quantified by RT-qPCR the mRNA levels of *Tubg1* and *Tubg2* in mouse oocytes, 2-cell stage embryos, 8-cell stage embryos and blastocysts. Adult mouse liver and brain tissues served as controls, because *Tubg2* expression is high in brain and low in liver [23,24]. Geometric mean of mouse peptidylprolyl isomerase A (*Ppia*) and mouse glyceraldehyde-3-phosphate dehydrogenase (*Gapdh*) mRNA levels were used for normalization. *Tubg1* mRNA level decreased 17 times, when 2-cell stage embryos were compared with blastocysts, and was almost equal in liver and brain (Fig 7A). In contrast, *Tubg2* mRNA level decreased dramatically by almost three orders of magnitude (815 times), when these two developmental stages were compared. *Tubg2* expression in blastocysts was comparable to that in liver and was 38 times lower than in brain (Fig. 7B). For comparison, mRNA levels were also ascertained for *Tubgcp2* and *Tubgcp5* that encode, respectively, GCP2 and GCP5 proteins. While *Tubgcp2* mRNA level remained relatively stable (Fig. 7C), that of *Tubgcp5* decreased 9 times when comparing the 2-cell stage embryos and blastocysts (Fig. 7D). Notably, the highest mRNA levels of tested genes were detected in oocytes, which probably reflects the high content of stored maternal mRNA [27]. Taken together, our data clearly show that *Tubg2* mRNA level is appreciably decreasing during mouse preimplantation development.

RT-qPCR analysis disclosed that blastocyst contains a very low amount of *Tubg2* mRNA. However, γ-tubulin 2 protein might still be present. To analyze the expression of *Tubg2* at the protein level, we first identified the positions of mouse γ-tubulin 1 and γ-tubulin 2 in samples separated by 2D-PAGE. Different antibodies reacting with both γ-tubulins were used for immunoblotting. The exact positions of γ-tubulin 1 and γ-tubulin 2 were determined by overexpression of, respectively, untagged mouse γ-tubulin 1 and γ-tubulin 2 in P19 cells, where *Tubg2* was undetectable by RT-qPCR (Fig. S8). Immunoblotting of untransfected and transfected cells with anti-γ-tubulin antibodies revealed that the signal of main γ-tubulin isoforms in P19 cells (Fig. 8, wt) was enhanced in cells overexpressing the γ-tubulin 1 (Fig. 8, +γ-Tb1). In cells overexpressing γ-tubulin 2, a new signal appeared in a more basic position compared to γ-tubulin1 isoforms (Fig. 8, +γ-Tb2). This was in agreement with theoretical isoelectric points for γ-tubulin 1 (5.66) and γ-tubulin 2 (5.80). These experiments demonstrate that mouse γ-tubulins can be easily discriminated on 2D-PAGE.

To rule out the possibility that the isoelectric point of exogenous γ-tubulin 2 expressed in P19 cells substantially differs from that in mouse tissues, we compared the expression of γ-tubulins in mouse

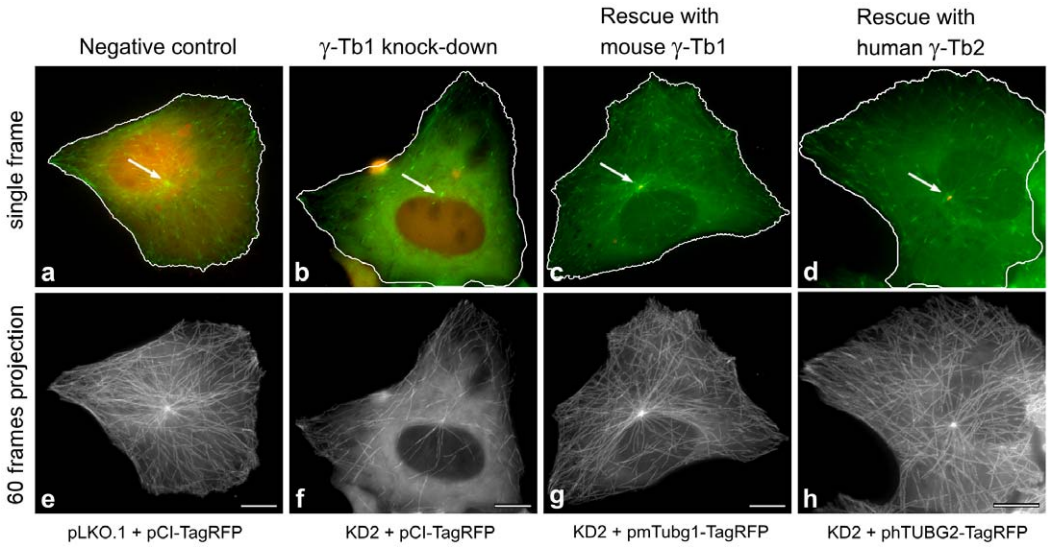

Figure 5. γ-Tubulin 2 rescues microtubule formation in γ-tubulin 1-depleted cells during interphase. Time-lapse imaging of U2OS-EB1 cells for quantitative evaluation of microtubule (+) end dynamics. Cells with depleted γ-tubulin 1 (KD2) expressing either TagRFP (pCI-TagRFP), mouse γ-tubulin 1 (pmTubg1-TagRFP) or human γ-tubulin 2 (phTUBG2-TagRFP). Cells with empty vector (pLKO.1) expressing TagRFP (pCI-TagRFP) served as negative control. (a–d) Still images of typical cells selected for evaluation. Only cells expressing both EB1-GFP (green) and TagRFP (red) or γ-tubulin-TagRFP fusions (red) were evaluated. In contrast to freely diffusible TagRFP (a, b), γ-tubulin-TagRFP fusions properly localized to MTOCs (c, d) marked by white arrows. (e–f) Maximum intensity projections of 60 consecutive time-frames from acquired time-lapse sequences. Note the markedly lower density of microtubule tracks in cell with depleted human γ-tubulin 1 (f). Microtubule track density is rescued in cells expressing exogenous mouse γ-tubulin 1 (g) or exogenous human γ-tubulin 2 (h). Scale bar 10 μm.
doi:10.1371/journal.pone.0029919.g005

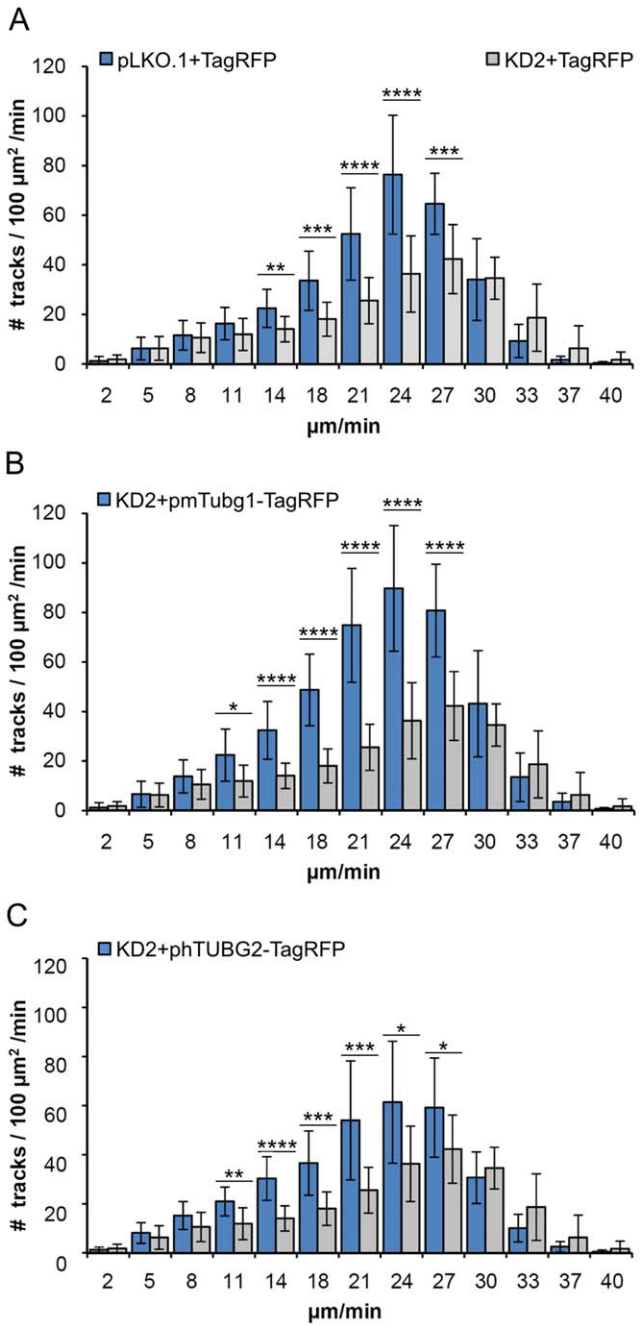

Figure 6. Quantitative evaluation of microtubule formation in phenotypic rescue experiments. Microtubule (+) end dynamics in U2OS-EB1 cells presented as velocity histograms. Cells with depleted γ-tubulin 1 (KD2) or negative control cells (pLKO.1), expressing either TagRFP (pCI-TagRFP), mouse γ-tubulin 1 (pmTubg1-TagRFP) or human γ-tubulin 2 (phTUBG2-TagRFP). (A) Comparison of negative control cells (pLKO.1+pCI-TagRFP; n = 19) with γ-tubulin 1 depleted cells (KD2+pCI-TagRFP; n = 15). (B) Comparison of cells rescued with mouse γ-tubulin 1 (positive control; KD2+pmTubg1-TagRFP; n = 18) with γ-tubulin 1 depleted cells. (C) Comparison of cells rescued with human γ-tubulin 2 (KD2+hTubg2-TagRFP; n = 19) with γ-tubulin 1 depleted cells. Data are from 3 independent experiments. Bars represent means±SD. Asterisks represent the p-values (p) of two-sided unpaired t-test (****, $p < 0.00001$; ***, $p < 0.0001$; **, $p < 0.001$; *, $p < 0.01$).
doi:10.1371/journal.pone.0029919.g006

brain and mouse liver, where *Tubg2* expression is high and low, respectively [23,24]. For this, we used immunoblotting after 2D-PAGE separation of samples containing similar total protein amounts. γ-Tubulin 1 was clearly detectable in both brain and liver. In contrast, a strong signal in the position of γ-tubulin 2 was detected merely in brain, whereas it was undetectable in liver (Fig. 9A). Again, these results correlated with data obtained in RT-qPCR experiments (Fig. 7B). The performed experiments confirmed that γ-tubulin 2 can be discriminated by 2D-PAGE also in mouse tissues. Using the same approach, we compared the expression of γ-tubulin 1 and γ-tubulin 2 in mouse oocytes and blastocysts. Samples were prepared from 150 fully grown oocytes at the GV stage and from 197 early blastocysts to ensure that the total protein amount in blastocyst sample was not underestimated. A fully grown oocyte (from adult animals) at GV stage contains approximately 30 ng of protein. Zona pellucida contributes to this amount some 4–5 ng [28]. An early blastocyst contains approximately 25 ng of protein [29]. γ-Tubulin 1 was clearly detectable in both oocytes and blastocysts. On the other hand, while there was a strong signal detectable in the position of γ-tubulin 2 in oocytes, the relevant signal in this position was dramatically reduced in blastocysts (Fig. 9B). Expression of γ-tubulin 2 at the protein level in oocytes and blastocysts thus correlated with its mRNA level (Fig. 7B). Collectively taken, these data strongly indicate that a very low amount of γ-tubulin 2 is present in wild-type blastocysts due to its transcriptional downregulation.

Discussion

Mammalian γ-tubulins are encoded by two closely related genes [22,24], and specific functions have been attributed to them. [23]. The molecular basis of suggested functional differences between γ-tubulins is however unknown. In this study we document that mammalian γ-tubulin 2 is able to nucleate microtubules and substitute for γ-tubulin 1. In addition, we show that *Tubg1* and *Tubg2* are differentially transcribed during mouse early embryogenesis, with *Tubg2* transcription being progressively downregulated.

In general, γ-tubulins are highly conserved proteins in all eukaryotes. At the amino acid sequence level, human γ-tubulin 1 and γ-tubulin 2, respectively, show 98.9% and 97.6% identity with the corresponding mouse isoforms (Table S1) [23]. To study the subcellular localization and function of human and mouse γ-tubulin 2, we have chosen human osteosarcoma cells U2OS. Because of their flat shape, they are excellent for immunofluorescence analysis and are easily transfectable. Moreover, the the selection of U2OS made it possible to answer the question whether or not the mouse γ-tubulin 2 is capable of replacing human γ-tubulin 1. We have used exogenously expressed FLAG-tagged mouse and human γ-tubulins to evaluate the subcellular localization of γ-tubulin 2 proteins and their interactions with GCPs. It was reported previously that exogenous mouse γ-tubulin 2 located to interphase and mitotic centrosomes in mouse Eph4 epithelial cells [23]. Our data corroborate this finding by showing that both human and mouse γ-tubulin 2 are recruited to interphase and mitotic centrosomes in human U2OS cells. By immunoprecipitation experiments we found that γ-tubulin 2 interacted with GCP2, an integral component of γTuSCs. Reciprocal coimmunoprecipitations of γ-tubulin 2 and GCP4 (T. Sulimenko, unpublished data) indicated that γ-tubulin 2 normally also incorporated in γTuRCs. We found no differences between γ-tubulin 1 and γ-tubulin 2 with regard to their localization and interactions. Intriguingly, antibody to GCP2 coimmunoprecipitated more endogenous than exogenous γ-tubulins (Fig. 1B, Fig. S2). A similar result was obtained with

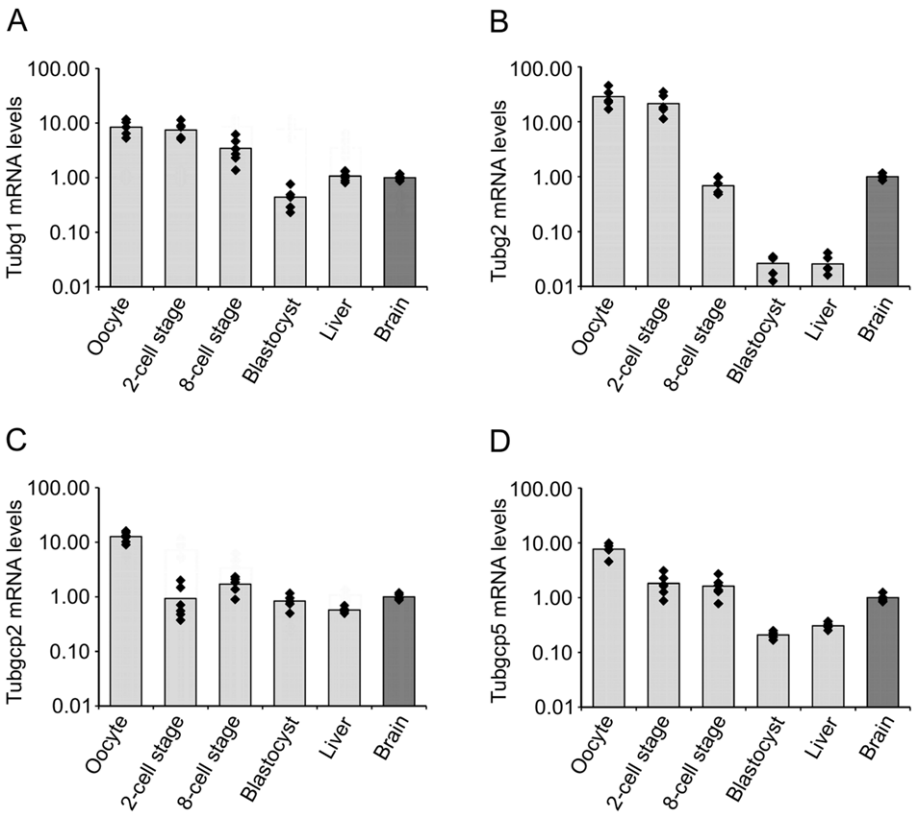

Figure 7. *Tubg2* mRNA level is decreasing during mouse preimplantation development. mRNA levels of *Tubg1* (A), *Tubg2* (B), *Tubgcp2* (C) and *Tubgcp5* (D) in mouse oocyte, 2-cell stage embryo, 8-cell stage embryo, blastocyst and liver relative to the level found in brain. Data are presented as mean fold change (columns) with individual samples displayed (diamonds). Three biological replicates were measured twice under identical conditions. Note that the Y-axis is in the logarithmic scale.
doi:10.1371/journal.pone.0029919.g007

antibody to GCP4 (T. Sulimenko, unpublished data). This fact might indicate a slow turnover of γTuCs, because precipitations were performed 48 hours after transfection. Alternatively, FLAG tags might interfere with interaction of γ-tubulin with GCPs. However, this seems unlikely as FLAG tags were fused to the C-termini of γ-tubulins, which probably is not involved in the interaction with GCP2 and GCP3 [30]. Moreover, FLAG-tagged γ-tubulins rescued normal mitotic progression in γ-tubulin 1-depleted cells (Fig. 3).

The most remarkable phenotypic sign of γ-tubulin 1-depleted U2OS cells was arrest in metaphase caused by mitotic spindle defects such as monopolar or collapsed spindles (Fig. 2C), previously described in mammalian cells depleted of γ-tubulin [11,23,31]. Similar defects were detected in cells in which γ-tubulin localization to centrosomes, mitotic spindle and mitotic chromatin was damaged by depletion of γTuRC recruitment factors like GCP-WD/NEDD1 [11,31] or components of augmin complex [32,33]. As expected, the observed phenotype was reverted by expression of mouse γ-tubulin 1. Both human and mouse γ-tubulin 2 likewise rescued the normal mitotic progression in γ-tubulin 1-depleted cells, indicating that mammalian γ-tubulin 2 is able to substitute for γ-tubulin 1 *in vivo* (Fig. 3). Consistent with these findings are the results of microtubule regrowth experiments on mitotic cells which reveal that γ-tubulin 2 does have microtubule nucleating capability (Fig. 4). We used only KD2 siRNA and corresponding shRNA for phenotypic rescue experiments, because it was more efficient than KD1 (Fig. S3A, Fig. S5A) and its specificity was verified in an independent study [34]. Rescue experiments also ruled out potential off-target RNAi effects.

When testing the microtubule (+) end dynamics in γ-tubulin 1-depleted cells, we observed a significant reduction in the number of EB1 tracks in interphase cells (Fig. 5, f; Fig. 6A), a sign of impaired microtubule nucleation. Alternatively, reduction in the EB1 track number might be explained by changes in microtubule dynamics; the nucleation is not affected but the fraction of growing microtubules relative to pausing or depolymerizing microtubules is diminished. Although one cannot exclude a potential contribution of impaired microtubule (+) ends dynamics to the observed phenotype, we consider this possibility much less probable because it has been previously demonstrated by regrowth experiments that microtubule nucleation is impaired and/or delayed in interphase cells depleted of γ-tubulin [31]. We therefore conclude that γ-tubulin 2 is able to nucleate microtubules also in interphase cells. Interestingly, a higher number of EB1 tracks was in γ-tubulin 1-depleted cells expressing exogenous γ-tubulin 1 than in cells expressing exogenous γ-tubulin 2 (Fig. 6). It might imply that for interphase cells γ-tubulin 1 is a more potent nucleator of microtubules than γ-tubulin 2. However, no corresponding differences in microtubule regrowth were observed in mitotic cells (Fig. 4), where centrosomes are highly enriched with γTuCs [25,26], and where consequently the potential differences in nucleation capability ought to be stronger. In addition, statistical significance ($p<0.05$) of this difference is relatively low. We therefore do not think that γ-tubulin 1 and γ-tubulin 2 substantially differ in nucleation activity.

Functional redundancy of mammalian γ-tubulins was expected because of their high sequence similarity [22]. Importantly, only 6

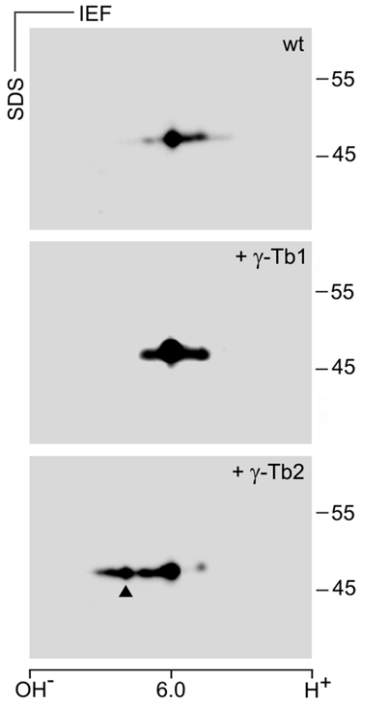

Figure 8. Electrophoretic distinction of mouse γ-tubulins on 2D-PAGE. Immunoblots of mouse P19 cell extracts separated by 2D-PAGE probed with antibody to γ-tubulin. Wild-type cells (wt), cells expressing exogenous untagged mouse γ-tubulin 1 (+γ-Tb1) or mouse γ-tubulin 2 (+γ-Tb2). Molecular mass markers (in kDa) are indicated on the right. The pI scale is shown along the bottom of the figure. IEF, isoelectric focusing. Arrowhead indicates the position of mouse γ-tubulin 2.
doi:10.1371/journal.pone.0029919.g008

amino acids specific for γ-tubulin 1- or γ-tubulin 2 are conserved in the majority of mammalian species. They are located in two clusters in helixes H11 (3 amino acids) and H12 (3 amino acids) of γ-tubulins (Table S2). These regions might be important for hypothetical divergent functions of mammalian γ-tubulins. However, when γ-tubulin in fission yeast was replaced by human γ-tubulin 1, with all three γ-tubulin 1-specific amino acids in helix H11 (R390, T391, R393) or one amino acid in helix H12 (I427) mutated to alanines, no deleterious effect on cell viability was observed [35]. It indicates that these regions are not essential for conserved γ-tubulin functions; this is in line with our data suggesting that γ-tubulin 2 is able to substitute for γ-tubulin 1.

Yuba-Kubo et al. reported that γ-tubulin 2 is expressed in the wild-type mouse blastocyst [23]. In contrast, our 2D-PAGE analysis indicates that there is very low level of γ-tubulin 2 protein in the wild-type blastocyst, whereas γ-tubulin 1 is abundant (Fig. 9). This is in a good agreement with our RT-qPCR data, indicating that *Tubg2* mRNA level is dramatically decreasing during preimplantation development unlike mRNA levels of *Tubg1*, *Tubgcp2* and *Tubgcp5* (Fig. 7). The reason for such discrepancy is unclear. Previously blastocysts were analyzed only by immunoblotting after one-dimensional PAGE. Anti-γ-tubulin antibody recognized two bands that were supposed to represent γ-tubulin 1 and γ-tubulin 2 [23]. However, reported separation of γ-tubulins in blastocysts by SDS-PAGE need not reflect only the presence of different genes, but proteolysis or posttranslational modification(s) as well.

A common fate of the members of duplicate-gene pairs is the partitioning of tissue-specific patterns of expression of the ancestral

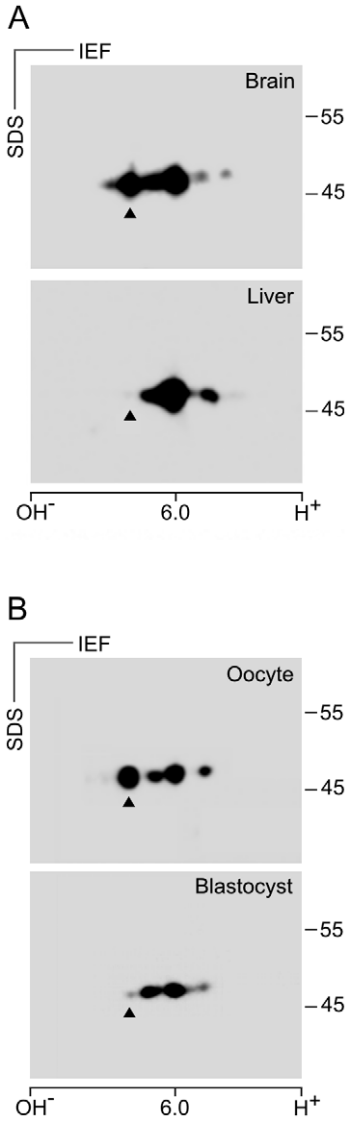

Figure 9. Differences in the expression of mouse γ-tubulin 2 protein in oocytes and blastocysts. Immunoblot analysis of tissue and cell extracts separated by 2D-PAGE with antibody to γ-tubulin. (A) Comparison of control adult mouse brain and liver. (B) Comparison of mouse oocytes and blastocysts. Molecular mass markers (in kDa) are indicated on the right. The pI scale is shown along the bottom of the figure. IEF, isoelectric focusing. Arrowheads indicate the position of γ-tubulin 2 as defined in Fig. 8.
doi:10.1371/journal.pone.0029919.g009

gene [36]. Analyses of expression of mammalian γ-tubulin genes showed differential expression in many tissues [23,24]; the same holds also for this study. It suggests that an important mechanism acting on γ-tubulin gene pair is the subfunctionalization. It was reported that some gene segments of γ-tubulin genes had been evolving together in the process known as "concerted evolution" [24]. It was proposed that concerted evolution might have been operative to maintain perfect homology at essential binding sites. Indeed, exons 2–3 and 7–10 of the two γ-tubulin genes homogenized by concerted evolution [24] encode regions which are probably critical for interaction of γ-tubulin with GCP2 and GCP3 [30]. Thus, concerted evolution together with subfunctionalization foster the preservation of highly similar and functionally redundant γ-tubulin genes in mammalian genomes [24].

Our data allow an alternative interpretation of *Tubg1*$^{-/-}$ and *Tubg2*$^{-/-}$ phenotypes previously described in mice [23]. Endogenous γ-tubulin 2 cannot rescue γ-tubulin 1 deficiency in Tubg1$^{-/-}$ blastocyst, even though it can nucleate microtubules, because it is not present in a sufficient amount. It was previously reported that knock out of single gene resulted in overexpression of related genes [37–39]. Our data do not strictly exclude the possibility that γ-tubulin 2 expression could be up-regulated in *Tubg1*$^{-/-}$ blastocysts, however, γ-tubulin 2 may be insufficient to fully replacer the lacking γ-tubulin 1. On the other hand, whole-mount immunostaining with anti-γ-tubulin antibody in Tubg1$^{-/-}$ blastocyst cells did not identify any γ-tubulin 2-positive foci, even though one pericentrin-positive focus occurred in each cell [23]. It was suggested that γ-tubulin 1 was necessary for recruitment of γ-tubulin 2 to blastocyst centrosomes [23]. We propose that such observation can be alternatively explained by the absence of γ-tubulin 2 at the blastocyst stage both both in wild type and Tubg1$^{-/-}$ embryos. Behavioral abnormalities of Tubg2 $^{-/-}$ mice do not necessarily imply unknown function(s) of γ-tubulin 2. They might also reflect a reduction of total γ-tubulin in brain of *Tubg2*$^{-/-}$ mice, since *Tubg2* is highly expressed in the brain [23,24] as demonstrated also in this study. Yet, we cannot exclude the possibility that brain γ-tubulin 2 has some additional still unknown function(s). Thorough phenotype analysis of *Tubg2*$^{-/-}$ mice could shed more light on γ-tubulin 2 function(s) in brain and its development. Further, elucidation of transcriptional regulation of γ-tubulin genes would by very important not only from the developmental point of view but also with respect to tumorigenesis. Significantly higher expression of γ-tubulin was found in high- versus low-grade gliomas, common brain cancers [40,41].

In conclusion, the findings indicate that mammalian γ-tubulin 2 is able to nucleate microtubules and substitute for γ-tubulin 1. Although γ-tubulins are differentially expressed during mouse early embryogenesis and in adult tissues, they are functionally redundant with respect to their nucleation activity.

Materials and Methods

Ethics statement

All mice were maintained in accordance with the Institute of Molecular Genetics Guidelines. Experiments were approved by the Committee on the Ethics of Animal Experiments of the Institute of Molecular Genetics (permit number 18/2009).

Cell cultures and transfections

Human osteogenic sarcoma cells U2OS, human glioblastoma cell line T98G, mouse embryonal carcinoma cells P19, mouse neuroblastoma Neuro-2a and mouse embryonal fibroblasts NIH 3T3 were obtained from the American Type Culture Collection. Human kidney embryonal cells HEK293-FT (HEK) were from Promega Biotec. Mouse bone marrow-derived mast cell line (BMMC) was kindly provided by M. Hibbs (Ludwig Institute for Cancer Research, Melbourne, Australia). Cells were cultured in Dulbecco's modified Eagle's medium (DMEM) containing 10% fetal bovine serum, penicillin (100 units/ml), and streptomycin (0.1 mg/ml). Cells were grown at 37°C in 5% CO_2 in air, and passaged every 2 or 3 days using 0.25% trypsin/0.01% EDTA in PBS. BMMC were cultured in RPMI 1640 medium supplemented with serum, antibiotics and interleukin 3 (PeproTech) as described previously [42].

U2OS cells were transfected with 2.5 μg (single plasmid) or 4 μg (cotransfection of 2 plasmids) DNA/well in a 6-well plate using Lipofectamine LTX reagent (Invitrogen) (DNA[μg]: LTX [μl] ratio was 1:2.5) and Opti MEM medium (Gibco) according to the manufacturer's instruction. After 12 h, the transfection mixture was replaced with fresh complete medium, and cells were incubated for 48 h. HEK cells were transfected with 17 μg DNA per 9-cm tissue culture dish using 51 μg polyethylenimine (Polysciences) and serum-free DMEM. After 24 h, the transfection mixture was replaced with fresh medium supplemented with serum, and cells were incubated for additional 24 h.

Some of the U2OS cells, growing on coverslips, were treated with 10 μM nocodazole (Sigma) for 6 h. Afterwards, cells were washed 5 times in ice-cold PBS, transferred to new medium and incubated for 3 min at 28°C before fixation.

Mouse oocytes, embryos and tissues

Oocytes and embryos were obtained from 6–8 week old C57BL/6 mice. Fully grown germinal vesicle (GV) oocytes were liberated from ovaries by puncturing the antral follicles with syringe needle and collected in M2 medium (Sigma) containing 0.2 mM isobutylmethylxanthine (IBMX; Sigma). To obtain preimplantation embryos, mice were superovulated with 5 IU of Folligon (pregnant mare serum gonadotropin; PMSG) (Intervet) followed by stimulation with 5 IU of human chorionic gonadotrophin (hCG, Sigma) 47 hours post-PMSG. The stimulated mice were mated with 8–10 week old C57BL/6 males immediately after hCG injection. Two-cell and eight-cell stage embryos were collected 48 and 68 hours post-hCG, respectively, by flushing the oviducts with M2 medium. Blastocyst stage embryos were collected 96 hours post-hCG by flushing the uteri with M2 medium. Oocytes and embryos were washed 5 times in PBS prior to transfer into TRI reagent (Ambion) for RNA isolation or into buffer for 2D-PAGE. Liver and brain were dissected from 6–8 week old female C57BL/6 mice.

DNA constructs

Total RNA from BALB/c adult mouse brain or from human cell line T98G was isolated by the RNeasy Mini kit (QIAGEN) according to the manufacturer's directions. The purity and integrity of the RNA preparations were checked using Experion automated electrophoresis system for microfluidic chip-based analysis and RNA StdSens analysis kit (Bio-Rad Laboratories). The quantity of RNA was checked by Nanodrop spectrophotometer (NanoDrop Technologies). Reverse transcription was performed with oligo(dT) primers and SuperScript III Reverse Transcriptase kit (Invitrogen).

The full length human γ-tubulin 2 (*TUBG2*, Refseq ID: NM_016437) was amplified by PCR using forward 5′-GCCCACGTCTGAAGAGCGATGC-3′ and reverse 5′-CTGGAGATGAACCAAGAAGGGTTG-3′ primers and T98G cell cDNA as template. The full length mouse γ-tubulin 1 (*Tubg1*, Refseq ID: NM_134024) and mouse γ-tubulin 2 (*Tubg2*, Refseq ID: NM_134028) were amplified by PCR using the following specific primers - *Tubg1*: forward 5′-GAGAGACTGCAACGCCGATGTCTG-3′ and reverse 5′-TTGTGAGGTCCCTGATCTGTGCTC-3′; *Tubg2*, forward 5′- GGCAGGAGTTCCTCTCAGTCGTGAC-3′ and reverse 5′-TGTGAGGCGAAGTTGGGTCAGAG-3′ - and mouse brain cDNA as template.

PCR products were ligated into pCR 3.1 vector (Invitrogen) by TA-cloning method. Sequencing revealed that the M413V variant of human γ-tubulin 2 was isolated (refSNP ID: rs1046097). The constructed vectors (pCR-hTUBG2, pCR-mTubg1, pCR-mTubg2) served as templates for additional PCRs with following specific forward and reverse primers carrying *Eco*RI/*Sal*I restriction sites (underlined): human *TUBG2*, forward 5′-CTGAATTCCACGTCTGAAGAGCGATGC-3′ and reverse 5′-TCAAGTCGACCTGCTCCTGGGTGCC-3′; mouse *Tubg1*: forward

5′-ACGAATTCTGCCTGAGGAGCGATGC-3′ and reverse 5′-TCAAGTCGACCTGCTCCTGGGTGCC-3′; mouse *Tubg2*: forward 5′- CTGAATTCGGTCTGATCGGCGATGC-3′ and reverse 5′-TCAAGTCGACCTGCTCCTGGGTGCC-3′. PCR products without stop codon were digested with *Eco*RI/*Sal*I restriction enzymes and inserted into pFLAG-CMV5a vector (Sigma) resulting in C-terminally FLAG-tagged human γ-tubulin 2 (phTUBG2-FLAG), mouse γ-tubulin 1 (pmTubg1-FLAG) and mouse γ-tubulin 2 (pmTubg2-FLAG). Constructs encoding C-terminally FLAG-tagged human γ-tubulin 1 (phTUBG1-FLAG) or mouse Fyn (pFyn-FLAG) were described previously [9].

Complete coding sequences of mouse *Tubg1* and *Tubg2* were cut out from pCR-mTubg1 and pCR-mTubg2, respectively, by *Eco*RI and inserted into pCI-NEO (Promega) to create vectors expressing untagged mouse γ-tubulin 1 (pCI-mTubg1) and γ-tubulin 2 (pCI-mTubg2).

Coding sequence of monomeric red fluorescent protein TagRFP-T (GenBank: EU582019.1) was amplified from pcDNA3.1-TagRFP (kind gift of Dr. R.Y. Tsien, HHMI at the University of California, San Diego, USA) by PCR with the following specific forward and reverse primers carrying *Sal*I and *Not*I restriction sites (underlined): forward 5′-AGTCGAC*GGAGGTGGTGGAGGT*ATGGTGTCTAAGGGCGAAGA-3′ (added 5x glycine coding motif in *italic*) and reverse 5′- TGCGGCCGCTTACTTGTACAGCTCGTCCATGCCA -3′. PCR products were ligated into pCR 2.1 vector (Invitrogen) by TA-cloning method. TagRFP coding sequence was digested from this vector using *Sal*I/*Not*I restriction enzymes and inserted into pCI-Neo (Promega) resulting in a vector encoding TagRFP (pCI-TagRFP) and allowing construction of C-terminally TagRFP-tagged fusion proteins. Coding sequences of mouse *Tubg1* and human *TUBG2* without stop codon were cut out from pmTubg1-FLAG and phTUBG2-FLAG, respectively, by *Eco*RI/*Sal*I restriction enzymes and ligated into pCI-TagRFP resulting in vectors encoding TagRFP-tagged mouse γ-tubulin 1 (pmTubg1-TagRFP) and human γ-tubulin 2 (phTUBG2-TagRFP). All constructs were verified by sequencing.

U2OS cells stably expressing EB1-GFP (U2OS-EB1) were obtained by transfection of cells with pEB1-GFP, obtained from Dr. Y. Mimori-Kiyosue [43], and selection in 1.1 mg/ml geneticin (G418, Sigma) for 2 weeks. Cells were then diluted to one cell/well on 96-well plate and allowed to grow for 2 weeks. Homogeneous colonies expressing EB1-GFP were propagated.

Antibodies

The following anti-peptide antibodies prepared to human γ-tubulin were used: mouse monoclonal antibodies TU-30 (IgG1) and TU-32 (IgG1) to the sequence 434–449 [44]; monoclonal antibody GTU 88 (IgG1; Sigma, T6657) and rabbit antibody (Sigma, T5192) to the sequence 38–53. The anti-γ-tubulin antibodies react with both γ-tubulin 1 and γ-tubulin 2 in mouse and human. β-Tubulin was detected with monoclonal antibody TUB 2.1 conjugated with FITC (IgG1; Sigma F2043) and pericentrin with rabbit antibody (Covance PRB-432C). Rabbit antibodies to GAPDH (G9545) and FLAG peptide (F7425) as well as monoclonal antibody M2 (IgG1) to FLAG peptide (F1804) were from Sigma. Monoclonal antibodies to GCP2 protein, GCP2-01 (IgG2b) and GCP2-02 (IgG1), were described previously [9]. Monoclonal antibody to GCP4 (IgG1) was from Santa Cruz (sc-271876). Monoclonal antibody NF-09 (IgG2b) to neurofilament NF-M protein [45] and rabbit antibody to non-muscle myosin BT-561 (Biomed Techn. Inc) served as controls.

The Cy3-conjugated anti-mouse and anti-rabbit antibodies were from Jackson Immunoresearch Laboratories. Anti-rabbit antibody conjugated with Alexa 488 was from Invitrogen. Secondary horseradish peroxidase-conjugated antibodies were from Promega.

RNAi

U2OS cells in 6-well plates were transfected with siRNAs (final concentration 20 nM) using Lipofectamine RNAi MAX (Invitrogen) according to the manufacturer's instruction. Five siRNAs (Ambion/Applied Biosystems) that target the regions present in human γ-tubulin 1, namely, (5′-GGGAGAAAAGATCCATGAG-3′; siRNA ID #9227), (5′-CGCATCTCTTTCTCATATA-3′; siRNA ID #120194), (5′-GGACATTTTTGACATCATA -3′; siRNA ID #9317), (5′-GAACCTGTCGCCAGTATGA-3′; siRNA ID #120784), (5′-GGTATCCTAAGAAGCTGGT-3′; siRNA ID #9396) were tested. Maximal depletion was reached by transfecting the siRNA twice with a 72-h time interval and harvesting cells 72 h after the second transfection. Negative control siRNA was from Ambion/Applied Biosystems (Silencer Negative Control #1 siRNA).

Immunoblotting and immunofluorescence analyses revealed that the highest reduction of γ-tubulin was obtained with siRNA ID#9396 (KD1) and siRNA ID#120194 (KD2; results not shown). These siRNAs were used for some phenotypic rescue experiments. In that case siRNA was mixed with the plasmid of interest and transfected into cells which already underwent the first round of 72 h-long siRNA treatment, using Lipofectamine LTX. Cells were analyzed 72 h after the second transfection.

The selected siRNAs were also used for construction of shRNA vectors based on pLKO.1 (Addgene, #8453) that enabled puromycin selection. Corresponding sense and antisense oligonucleotides were synthetized by Sigma-Aldrich: 9396sh-sense 5′-CCGGGGTATCCTAAGAAGCTGGTTTCTCGAGACCAGCTTCTTAGGATACCTGTTTTTG-3′, 9396-antisense 5′-AATTCAAAAACAGGTATCCTAAGAAGCTGGTCTCGAGAAACCAGCTTCTTAGGATACC-3′; 120194sh-sense 5′- CCGGCGCATCTCTTTCTCATATATTCTCGAGTATATGAGAAAGAGATGCGTGTTTTTG-3′, 120194sh-antisense 5′- AATTCAAAAACACGCATCTCTTTCTCATATACTCGAGAATATATGAGAAAGAGATGCG-3′. Sense and antisense oligonucleotides, at final concentration 45 μM of each, were annealed in 1x NEB 2 buffer (New England Biolabs) by initial warming up to 95°C followed by slow (3 h) cooling down to the room temperature. Annealed oligonucleotides were inserted into pLKO.1 previously linearized with *Age*I/*Eco*RI resulting in human TUBG1 shRNA expressing vectors p9396sh (KD1) and p120194sh (KD2). Correct sequences of all vectors were verified by sequencing.

shRNA vectors were transfected in the same way as other plasmids used in the study. To select shRNA expressing cells, the transfection mixture was replaced with fresh complete medium 12 h later. Puromycin (Sigma) at final concentration 2.5 μg/ml was added after 12 h incubation, and cells were selected in puromycin for 6 days before analysis.

Reverse transcription quantitative real-time PCR (RT-qPCR) analysis

Total cellular RNA was extracted in three independent isolations from 20 mouse oocytes and 5–10 embryos using TRI reagent (Ambion) according to manufacturer's instructions. Three independent isolations of total cellular RNA were also made from four mouse cell lines Neuro2a, P19, BMMC and 3T3 using RNeasy Mini kit (QIAGEN). In three independent experiments mouse livers and brains were frozen in liquid nitrogen, homogenized under liquid nitrogen using mortar and pestle, and total RNA was extracted from 10–15 mg of homogenized tissue

using RNeasy Minikit (QIAGEN). Concentration of the purified RNA was determined with spectrophotometer NanoDrop (Thermo Scientific). The quality of RNA was checked on Agilent 2100 Bioanalyzer. All RNA samples were of good qPCR quality (RNA integrity number [RIN] ≥7.6 for all tissue samples; RIN≥9.8 for all cell lines samples). Purified RNA was stored at −70°C. Purified RNAs from oocytes and embryos were converted to cDNA immediately after isolation. RNA from each sample was converted to cDNA using the ImProm-II RT kit (Promega). For tissues and cell lines, each reaction sample (20 µl) contained 1 µg RNA, random hexamer primers (25 ng/ µl), ImPROM-II reaction buffer, 5.6 mM $MgCl_2$, dNTP mix (0.5 mM each dNTP), 0.5 µl RNasin and 1 µl ImProm-II reverse transcriptase. For oocytes and embryos, all isolated RNA was used for reverse transcription.

Quantitative PCR was performed with gene-specific primers for mouse γ-tubulin 1 (*Tubg1*, NM_134024), mouse γ-tubulin 2 (*Tubg2*, NM_134028), mouse GCP2 (*Tubgcp2*, NM_133755), mouse GCP5 (*Tubgcp5*, NM_146190), mouse peptidylprolyl isomerase A (*Ppia*, NM_008907) and mouse glyceraldehyde-3-phosphate dehydrogenase (*Gapdh*, NM_008084). All primers were tested *in silico* by NCBI BLAST to amplify specific targets. Primer sequences are summarized in Table S3. Oligonucleotides were from East Port (Prague, Czech Republic).

Quantitative PCRs were carried out on LightCycler 480 System (Roche). Each reaction (5 µl) consisted of 2.5 µl LightCycler® 480 SYBR Green I Master (Roche), 0.5 µl mixed gene-specific forward and reverse primers (5 µM each) and 2 µl diluted cDNA. cDNA samples from brain, liver and cell lines were diluted 1:50. In case of oocyte and embryonal cDNA samples, the used amounts of cDNA per reaction corresponded to 1/4 of oocyte, 1/2 of 2-cell stage embryo, 1/10 of 8-cell stage embryo and 1/10 of blastocyst. Calibration curves for tested genes were made by serial dilutions (dilution factor 4) of brain cDNA. Each sample was run in duplicate. Thermocycling parametres are described in Text S1. Identity of PCR products was verified by sequencing.

Preparation of cell extracts

Whole-cell extracts for SDS-PAGE were prepared by rinsing the cells twice in Hepes buffer (50 mM Hepes adjusted to pH 7.6 with NaOH, 75 mM NaCl, 1 mM $MgCl_2$ and 1 mM EGTA), scraping them into Hepes buffer supplemented with protease (Roche; Complete EDTA-free protease mixture) and phosphatase (1 mM Na_3VO_4 and 1 mM NaF) inhibitors, and solubilizing in hot SDS-sample buffer [46] without bromphenol blue and boiling for 5 min.

When preparing the extracts for immunoprecipitation, cells were rinsed twice in cold Hepes buffer and extracted for 10 min at 4°C with Hepes buffer supplemented with protease and phosphatase inhibitors and 1% Nonidet P-40. The suspension was then spun down (20,000 *g*, 15 min, 4°C).

For preparation of samples for 2D-PAGE, oocytes and blastocysts were directly lysed in 2D-PAGE sample buffer [47]. Brain and liver were mixed with cold Hepes buffer supplemented with protease and phosphatase inhibitors in tissue/buffer ratio 1:10 and homogenized in teflon/glass grinder. The suspension was then spun down (20,000 *g*, 15 min, 4°C) and 10–15 µl aliquots of supernatant were mixed with 200 µl of sample buffer. Similarly, 20 µl aliquots of supernatants from 1% NP-40 extracts of P19 cells were mixed with 200 µl of sample buffer.

Protein quantifications in lysates and SDS-PAGE-samples were performed, respectively, with bicinchoninic acid assay and silver dot assay [48].

Immunoprecipitation, gel electrophoresis and immunoblotting

Immunoprecipitation from 1% NP-40 extracts was performed as described [49]. Cell extracts were incubated with beads of protein A (Pierce, Rockford, IL) saturated with: (I) rabbit antibody to FLAG, (II) monoclonal antibody GCP2-01 (IgG2b) to GCP2 (III) rabbit antibody to non-muscle myosin (negative control), (IV) monoclonal antibody NF-09 (IgG2a; negative control) or with (V) immobilized protein A alone. Gel electrophoresis and immunoblotting were performed using standard protocols. Two-dimensional electrophoresis (2D-PAGE) was performed as described [47] using for the first dimension 7 cm long Immobiline DryStrip gels with a linear pH 4-7 gradient (Amersham Biosciences). Comparable protein amounts were loaded in case of P19, liver and brain extracts (~25 µg).

For immunoblotting, rabbit antibodies to GAPDH, γ-tubulin (Sigma T5192) and FLAG peptide (Sigma F7425) were diluted 1:20,000, 1:5,000 and 1:2,000, respectively. Monoclonal antibodies to γ-tubulin (GTU88) and GCP4 were diluted 1:10,000 and 1:2,000, respectively. Monoclonal antibodies to γ-tubulin (TU-32) and GCP2 (GCP2-02), in the form of spent culture supernatants, were diluted 1:10. Peroxidase-conjugated secondary antibodies were diluted 1:10,000. Bound antibodies were detected by SuperSignal WestPico Chemiluminescent reagents (Pierce).

Immunofluorescence

Immunofluorescence staining was performed as previously described [50]. Samples were fixed in methanol at −20°C, air-dried and washed in PBS. Rabbit antibodies to FLAG peptide and pericentrin were diluted 1:1000 and 1:750, respectively. Monoclonal antibodies to FLAG peptide and β-tubulin were diluted 1:1,000 and 1:100, respectively. Monoclonal antibody TU-30 to γ-tubulin was used as spent culture medium diluted 1:50. Cy3-conjugated anti-mouse and ant-rabbit antibodies were diluted 1:1,000, Alexa 488-conjugated anti-rabbit antibody was diluted 1:200. For double-label immunofluorescence, coverslips were incubated separately with the primary antibodies, and simultaneously with the secondary conjugated antibodies. The preparations were mounted in MOWIOL 4–88 (Calbiochem) supplemented with 4,6-diamidino-2-phenylindole (DAPI, Sigma) to label nuclei, and examined on Delta Vision Core system (Applied Precision) equipped with 60x/1.42 NA oil-immersion objective. Optical z-sections were acquired in 0.25–0.30 µm steps. Z-stacks were deconvolved by a built-in deconvolution program (Softworx) using default parameters. Alternatively, some preparations were examined on Olympus AX-70 equipped with 40x/1.0 NA water objective. Some preparations were also examined on confocal microscope Leica SP5 with 60x/1.4 NA oil objective. Optical z-sections were acquired at 0.125 µm. Z-stacks were deconvolved by Huygens Professional software (SVI, The Netherlands). All presented Maximum Intensity Projections (MIP) of deconvolved z-stacks were prepared in ImageJ (NIH/USA). Conjugates alone gave no significant staining.

Time-lapse imaging

For time-lapse imaging, U2OS cells expressing EB1-GFP were grown on glass-bottom-dishes (MatTek) and transfected with different sets of plasmids, as specified in Result section. Before imaging, DMEM was replaced with medium for live cell imaging (DMEM without phenol red, riboflavin, folic acid, pyridoxal, $Fe[NO_3]_3$ and puromycin). Only cells expressing TagRFP or TagRPF-fusion proteins were selected for time-lapse imaging.

Time-lapse sequences of EB1-GFP dynamics were collected for 2 min at 1 sec intervals on Delta Vision Core system (Applied

Precision) equipped with 60x/1.42 NA oil-immersion objective. The focus plane was near the coverslip where the best resolution of EB1 comets was observed. Time-lapse sequences were adjusted in ImageJ (NIH, USA) by manual cropping of individual cells, enhancement of brightness and contrast, and converting sequences to a depth of 8 bits. Adjusted time-lapse sequences of individual cells were analyzed by in-house-written particle tracking plug-in implemented in Ellipse program version 2.07 (ViDiTo, Systems, Košice Slovakia; http://www.ellipse.sk) as described [42]. The particle speed was calculated as the ratio of particle trajectory length and trajectory duration. Statistical analysis was performed with the Student's two-tailed unpaired t-test using Microsoft Excel.

Supporting Information

Figure S1 Exogenous γ-tubulin 2 locates to centrosomes. Human U2OS cells expressing FLAG-tagged mouse γ-tubulin 1 (a–d, Tubg1-FLAG), mouse γ-tubulin 2 (e–h, Tubg2-FLAG), human γ-tubulin 1 (i–l, TUBG1-FLAG) and human γ-tubulin 2 (m–p, TUBG2-FLAG) were stained for FLAG (red) and pericentrin (green). DNA was stained with DAPI (blue). Final images were made by maximum intensity projection of 3 deconvolved z-sections spaced at 0.25 μm. Scale bar 10 μm.
(TIF)

Figure S2 Coimmunoprecipitation of human γ-tubulins with GCP2 and GCP4 proteins. Extracts from HEK cells expressing FLAG-tagged human γ-tubulin 1 (TUBG1-FLAG), human γ-tubulin 2 (TUBG2-FLAG) or control mouse Fyn (Fyn-FLAG) were immunoprecipitated with antibodies to FLAG or GCP2, and blots were probed with antibodies to FLAG, GCP2, GCP4 and γ-tubulin (γ-Tb). Extracts (1), immunoprecipitated proteins (2), protein A without antibodies incubated with extracts (3), immobilized antibodies not incubated with extracts (4). Arrowheads indicate the positions of exogenous γ-tubulins.
(TIF)

Figure S3 Immunoblot analysis of U2OS cells in phenotypic rescue experiments with FLAG-tagged γ-tubulins. (A) Immunoblot analysis of whole cell extracts from cells transfected with negative control (Control) or γ-tubulin specific siRNAs (KD1 and KD2). Staining with antibodies to γ-tubulin (γ-Tb) and GAPDH. (B) Cells with depleted γ-tubulin 1 (KD2), expressing FLAG-tagged mouse γ-tubulin 1 (Tubg1-FLAG), mouse γ-tubulin 2 (Tubg2-FLAG) or human γ-tubulin 2 (TUBG2-FLAG). Immunoblots of whole cell lysates probed with antibodies to γ-tubulin (γ-Tb), FLAG and GAPDH (loading control). Arrowhead indicates the position of endogenous γ-tubulin.
(TIF)

Figure S4 γ-Tubulin 2 rescues mitotic spindle organization and function in γ-tubulin 1-depleted cells. U2OS cells depleted of γ-tubulin 1 and expressing FLAG-tagged mouse γ-tubulin 1 (a, d; Tubg1-FLAG), mouse γ-tubulin 2 (b, e; Tubg2-FLAG) or human γ-tubulin 2 (c, f; TUBG2-FLAG). Cells were stained for FLAG (red) and β-tubulin (green). DNA was stained with DAPI (blue). Final images were made by maximum intensity projection of 30–40 deconvolved confocal z-sections spaced at 0.125 μm. Scale bars 5 μm.
(TIF)

Figure S5 Depletion of γ-tubulin 1 in U2OS cells by shRNA. Cells transfected with empty pLKO.1 vector (Control), TUBG1 shRNA expressing vectors p9396sh (KD1) or p120194sh (KD2). (A) Immunoblots of whole cell lysates probed with antibodies to γ-tubulin (γ-Tb) and GAPDH (loading control). (B) Immunofluorescence staining with antibody to γ-tubulin (red) and with DAPI (blue). Fluorescence images of cells stained for γ-tubulin were captured under identical conditions and processed in exactly the same manner. Scale bar 20 μm.
(TIF)

Figure S6 Immunoblot analysis of U2OS cells in phenotypic rescue experiments with TagRFP-tagged γ-tubulins. U2OS-EB1 cells with depleted γ-tubulin 1 (KD2; shRNA) or negative control cells (NC; pLKO.1), expressing TagRFP, tagged mouse γ-tubulin 1 (Tubg1-TagRFP) or tagged human γ-tubulin 2 (TUBG2-TagRFP). Immunoblots of whole cell lysates probed with antibodies to γ-tubulin (γ-Tb) and GAPDH (loading control). Arrowhead indicates the position of endogenous γ-tubulin.
(TIF)

Figure S7 γ-Tubulin 2 rescues microtubule formation in γ-tubulin 1-depleted cells during interphase. Time-lapse imaging of U2OS-EB1 cells for quantitative evaluation of microtubule (+) end dynamics. Cells with depleted γ-tubulin 1 (KD2) expressing either mouse γ-tubulin 1 (pmTubg1-TagRFP) or human γ-tubulin 2 (phTUBG2-TagRFP). Single frame coloured images Fig 5c and Fig. 5d were separated to red and green channels for a better evaluation of γ-tubulin-TagRFP fusions (red) and EB1-GFP (green). White arrows mark MTOCs.
(TIF)

Figure S8 Comparison of γ-tubulin 2 expression in mouse brain and cell lines. Expression of gene for γ-tubulin 2 (Tubg2) in neuroblastoma (Neuro2a), bone marrow mast cells (BMMC), embryonal fibroblasts (3T3) and embryonic carcinoma cells (P19) relative to the level in brain. Data are presented as mean fold change (columns) with individual samples displayed (diamonds). Three biological replicates were quantified twice under identical conditions. *, undetectable level in P19 cells.
(TIF)

Table S1 Sequence alignments of human and mouse γ-tubulins.
(PDF)

Table S2 Multiple sequence alignment of carboxy-terminal domains of mammalian γ-tubulins.
(PDF)

Table S3 Sequences of primers used for RT-qPCR analysis of mouse genes.
(PDF)

Text S1 Thermocycling parameters at quantitative PCR.
(PDF)

Acknowledgments

We thank Dr. Y. Mimori-Kiyosue (KAN Research Institute, Kyoto, Japan) for EB1-GFP construct, Dr. R.Y. Tsien (HHMI at the University of California, San Diego, USA) for pcDNA3.1-TagRFP construct and Dr. M. Hibbs (Ludwig Institute for Cancer Research, Melbourne, Australia) for BMMC cells. We thank Dr. Petr Svoboda (Institute of Molecular Genetics AS CR, Prague, Czech Republic) for critical reading of the manuscript. S. Vinopal was supported in part by the Department of Cell Biology, Faculty of Science, Charles University, Prague, Czech Republic.

Author Contributions

Conceived and designed the experiments: SV ED PD. Performed the experiments: SV MČ VS TS ED VV MF. Analyzed the data: SV VS TS ED PD. Wrote the paper: SV PD.

References

1. Oakley BR, Oakley CE, Yoon Y, Jung M (1990) γ-Tubulin is a component of the spindle pole body that is essential for microtubule function in *Aspergillus nidulans*. Cell 61: 1289–1301.
2. Stearns T, Evans L, Kirschner M (1991) γ-Tubulin is highly conserved component of the centrosome. Cell 65: 825–836.
3. Joshi HC, Palacios MJ, McNamara L, Cleveland DW (1992) γ-Tubulin is a centrosomal protein required for cell cycle-dependent microtubule nucleation. Nature 356: 80–83.
4. Wiese C, Zheng Y (2006) Microtubule nucleation: gamma-tubulin and beyond. J Cell Sci 119: 4143–4153.
5. Raynaud-Messina B, Merdes A (2007) γ-Tubulin complexes and microtubule organization. Curr Opin Cell Biol 19: 24–30.
6. Moritz M, Braunfeld MB, Guenebaut V, Heuser J, Agard DA (2000) Structure of the γ-tubulin ring complex: a template for microtubule nucleation. Nat Cell Biol 2: 365–370.
7. Kollman JM, Polka JK, Zelter A, Davis TN, Agard DA (2010) Microtubule nucleating γ-TuSC assembles structures with 13-fold microtubule-like symmetry. Nature 466: 879–882.
8. Lüders J, Stearns T (2007) Microtubule-organizing centres: a re-evaluation. Nat Rev Mol Cell Biol 8: 161–167.
9. Hořejší B, Vinopal S, Sládková V, Dráberová E, Sulimenko V, et al. (2011) Nuclear γ-tubulin associates with nucleoli and interacts with tumor suppressor protein C53. J Cell Physiol 227: 367–382.
10. Moudjou M, Bordes N, Paintrand M, Bornens M (1996) γ-Tubulin in mammalian cells: the centrosomal and the cytosolic forms. J Cell Sci 109: 875–887.
11. Haren L, Remy MH, Bazin I, Callebaut I, Wright M, et al. (2006) NEDD1-dependent recruitment of the γ-tubulin ring complex to the centrosome is necessary for centriole duplication and spindle assembly. J Cell Biol 172: 505–515.
12. Dammermann A, Maddox PS, Desai A, Oegema K (2008) SAS-4 is recruited to a dynamic structure in newly forming centrioles that is stabilized by the gamma-tubulin-mediated addition of centriolar microtubules. J Cell Biol 180: 771–785.
13. Zimmerman S, Chang F (2005) Effects of γ-tubulin complex proteins on microtubule nucleation and catastrophe in fission yeast. Mol Biol Cell 16: 2719–2733.
14. Cuschieri L, Miller R, Vogel J (2006) Gamma-tubulin is required for proper recruitment and assembly of Kar9-Bim1 complexes in budding yeast. Mol Biol Cell 17: 4420–4434.
15. Bouissou A, Verollet C, Sousa A, Sampaio P, Wright M, et al. (2009) γ-Tubulin ring complexes regulate microtubule plus end dynamics. J Cell Biol 187: 327–334.
16. Nayak T, Edgerton-Morgan H, Horio T, Xiong Y, De Souza CP, et al. (2010) Gamma-tubulin regulates the anaphase-promoting complex/cyclosome during interphase. J Cell Biol 190: 317–330.
17. Rodriguez AS, Batac J, Killilea AN, Filopei J, Simeonov DR, et al. (2008) Protein complexes at the microtubule organizing center regulate bipolar spindle assembly. Cell Cycle 7: 1246–1253.
18. Liu B, Joshi HC, Wilson TJ, Silflow CD, Palevitz BA, et al. (1994) γ-Tubulin in Arabidopsis: gene sequence, immunoblot, and immunofluorescence studies. Plant Cell 6: 303–314.
19. Ruiz F, Beisson J, Rossier J, Dupuis-Williams P (1999) Basal body duplication in Paramecium requires gamma-tubulin. Current Biology 9: 43–46.
20. Tan M, Heckmann K (1998) The two gamma-tubulin-encoding genes of the ciliate Euplotes crassus differ in their sequences, codon usage, transcription initiation sites and poly(A) addition sites. Gene 210: 53–60.
21. Wilson PG, Zheng Y, Oakley CE, Oakley BR, Borisy GG, et al. (1997) Differential expression of two γ-tubulin isoforms during gametogenesis and development in *Drosophila*. Dev Biol 184: 207–221.
22. Wise DO, Krahe R, Oakley BR (2000) The γ-tubulin gene family in humans. Genomics 67: 164–170.
23. Yuba-Kubo A, Kubo A, Hata M, Tsukita S (2005) Gene knockout analysis of two γ-tubulin isoforms in mice. Develop Biol 282: 361–373.
24. Carson AR, Scherer SW (2009) Identifying concerted evolution and gene conversion in mammalian gene pairs lasting over 100 million years. BMC Evol Biol 9: 156.
25. Khodjakov A, Rieder CL (1999) The sudden recruitment of γ-tubulin to the centrosome at the onset of mitosis and its dynamic exchange throughout the cell cycle, do not require microtubules. J Cell Biol 146: 585–596.
26. Piehl M, Tulu US, Wadsworth P, Cassimeris L (2004) Centrosome maturation: Measurement of microtubule nucleation throughout the cell cycle by using GFP-tagged EB1. Proc Natl Acad Sci USA 101: 1584–1588.
27. Piko L, Clegg KB (1982) Quantitative changes in total RNA, total poly(A), and ribosomes in early mouse embryos. Dev Biol 89: 362–378.
28. Schultz RM, Wassarman PM (1977) Biochemical studies of mammalian oogenesis: Protein synthesis during oocyte growth and meiotic maturation in the mouse. J Cell Sci 24: 167–194.
29. Sellens MH, Stein S, Sherman MI (1981) Protein and free amino acid content in preimplantation mouse embryos and in blastocysts under various culture conditions. J Reprod Fertil 61: 307–315.
30. Guillet V, Knibiehler M, Gregory-Pauron L, Remy MH, Chemin C, et al. (2011) Crystal structure of gamma-tubulin complex protein GCP4 provides insight into microtubule nucleation. Nat Struct Mol Biol 18: 915–919.
31. Lüders J, Patel UK, Stearns T (2006) GCP-WD is a γ-tubulin targeting factor required for centrosomal and chromatin mediated microtubule nucleation. Nature Cell Biol 8: 137–147.
32. Uehara R, Nozawa RS, Tomioka A, Petry S, Vale RD, et al. (2009) The augmin complex plays a critical role in spindle microtubule generation for mitotic progression and cytokinesis in human cells. Proc Natl Acad Sci U S A 106: 6998–7003.
33. Uehara R, Goshima G (2010) Functional central spindle assembly requires de novo microtubule generation in the interchromosomal region during anaphase. J Cell Biol 191: 259–267.
34. Hutchins JR, Toyoda Y, Hegemann B, Poser I, Heriche JK, et al. (2010) Systematic analysis of human protein complexes identifies chromosome segregation proteins. Science 328: 593–599.
35. Hendrickson TW, Yao J, Bhadury S, Corbett AH, Joshi HC (2001) Conditional mutations in gamma-tubulin reveal its involvement in chromosome segregation and cytokinesis. Mol Biol Cell 12: 2469–2481.
36. Lynch M, Force A (2000) The probability of duplicate gene preservation by subfunctionalization. Genetics 154: 459–473.
37. Lam EW, Glassford J, Banerji L, Thomas NS, Sicinski P, et al. (2000) Cyclin D3 compensates for loss of cyclin D2 in mouse B-lymphocytes activated via the antigen receptor and CD40. J Biol Chem 275: 3479–3484.
38. Kafri R, Levy M, Pilpel Y (2006) The regulatory utilization of genetic redundancy through responsive backup circuits. Proc Natl Acad Sci U S A 103: 11653–11658.
39. DeLuna A, Springer M, KIrschner MW, Kishony R (2010) Need-based up-regulation of protein levels in response to deletion of their duplicate genes. PLoS Biol 8: e1000347.
40. Katsetos CD, Reddy G, Dráberová E, Šmejkalová B, Del Valle L, et al. (2006) Altered cellular distribution and subcellular sorting of γ-tubulin in diffuse astrocytic gliomas and human glioblastoma cell lines. J Neuropathol Exp Neurol 65: 465–477.
41. Loh JK, Lieu AS, Chou CH, Lin FY, Wu CH, et al. (2010) Differential expression of centrosomal proteins at different stages of human glioma. Bmc Cancer 10: 268.
42. Hájková Z, Bugajev V, Dráberová E, Vinopal S, Dráberová L, et al. (2011) STIM1-directed reorganization of microtubules in activated cells. J Immunol 186: 913–923.
43. Mimori-Kiyosue Y, Shiina N, Tsukita S (2004) The dynamic behavior of the APC-binding protein EB1 on the distal ends of microtubules. Curr Biol 10: 865–868.
44. Nováková M, Dráberová E, Schürmann W, Czihak G, Viklický V, et al. (1996) γ-Tubulin redistribution in taxol-treated mitotic cells probed by monoclonal antibodies. Cell Motil Cytoskel 33: 38–51.
45. Dráberová E, Sulimenko V, Kukharskyy V, Dráber P (1999) Monoclonal antibody NF-09 specific for neurofilament protein NF-M. Folia Biol (Prague) 45: 163–165.
46. Laemmli UK (1970) Cleavage of structural proteins during the assembly of the head of bacteriophage T_4. Nature 227: 680–685.
47. Sulimenko V, Sulimenko T, Poznanovic S, Nechiporuk-Zloy V, Böhm JK, et al. (2002) Association of brain γ-tubulins with αβ-tubulin dimers. Biochem J 365: 889–895.
48. Dráber P (1991) Quantitation of proteins in sample buffer for sodium dodecyl sulfate-polyacrylamide gel electrophoresis using colloidal silver. Electrophoresis 12: 453–456.
49. Kukharskyy V, Sulimenko V, Macůrek L, Sulimenko T, Dráberová E, et al. (2004) Complexes of γ-tubulin with non-receptor protein tyrosine kinases Src and Fyn in differentiating P19 embryonal carcinoma cells. Exp Cell Res 298: 218–228.
50. Dráberová E, Dráber P (1993) A microtubule-interacting protein involved in coalignment of vimentin intermediate filaments with microtubules. J Cell Sci 106: 1263–1273.

VI.4.1

Supplementary data for:

Vinopal S., Černohorská M., Sulimenko V., Sulimenko T., Vosecká V., Flemr M., Dráberová E., Dráber P. (2012). γ-Tubulin 2 nucleates microtubules and is downregulated in mouse early embryogenesis. PLoS ONE *7*: e29919.

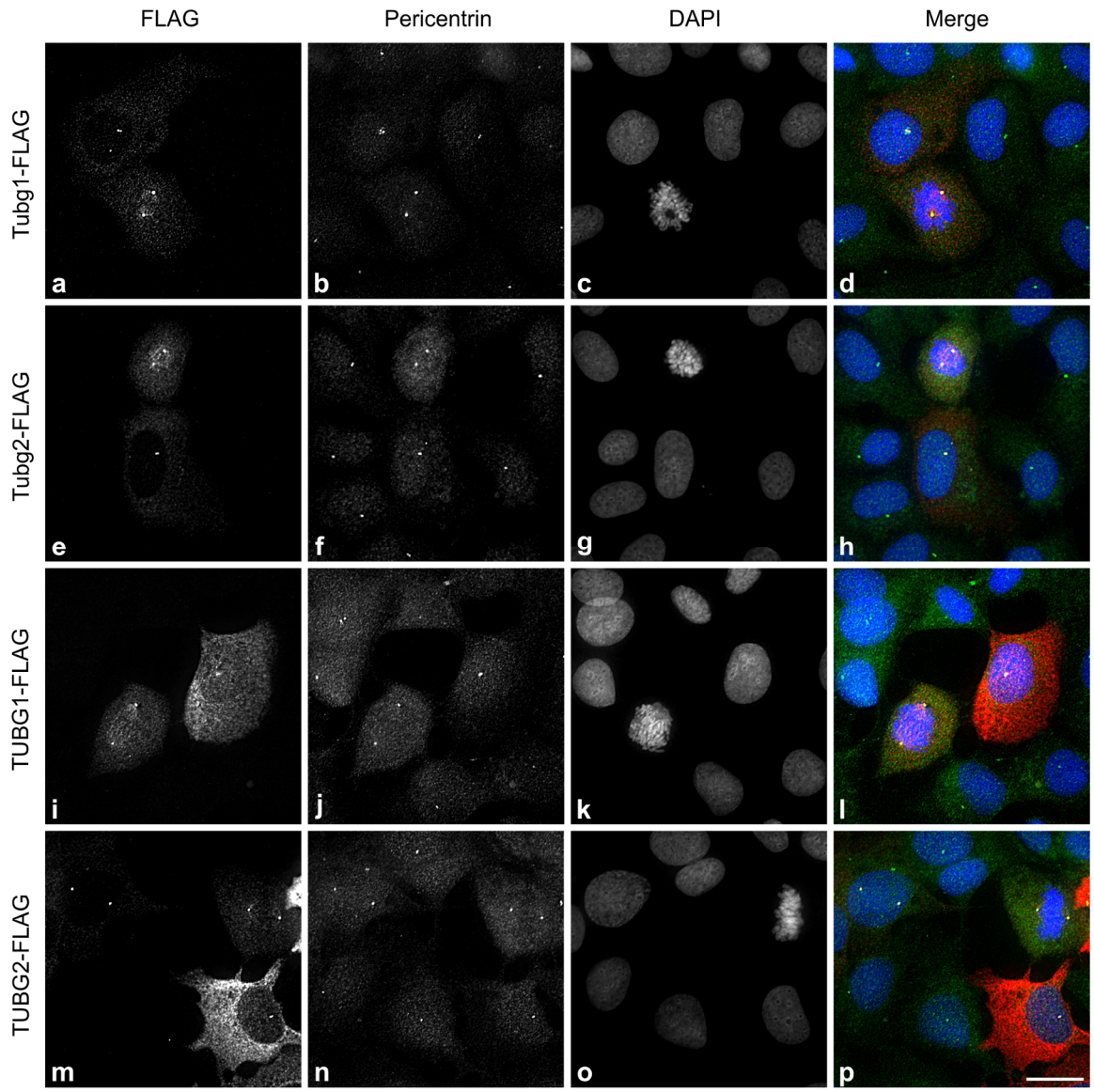

Figure S1. Exogenous γ-tubulin 2 locates to centrosomes. Human U2OS cells expressing FLAG-tagged mouse γ-tubulin 1 (a-d, Tubg1-FLAG), mouse γ-tubulin 2 (e-h, Tubg2-FLAG), human γ-tubulin 1 (i-l, TUBG1-FLAG) and human γ-tubulin 2 (m-p, TUBG2-FLAG) were stained for FLAG (red) and pericentrin (green). DNA was stained with DAPI (blue). Final images were made by maximum intensity projection of 3 deconvolved z-sections spaced at 0.25 µm. Scale bar 10 µm.

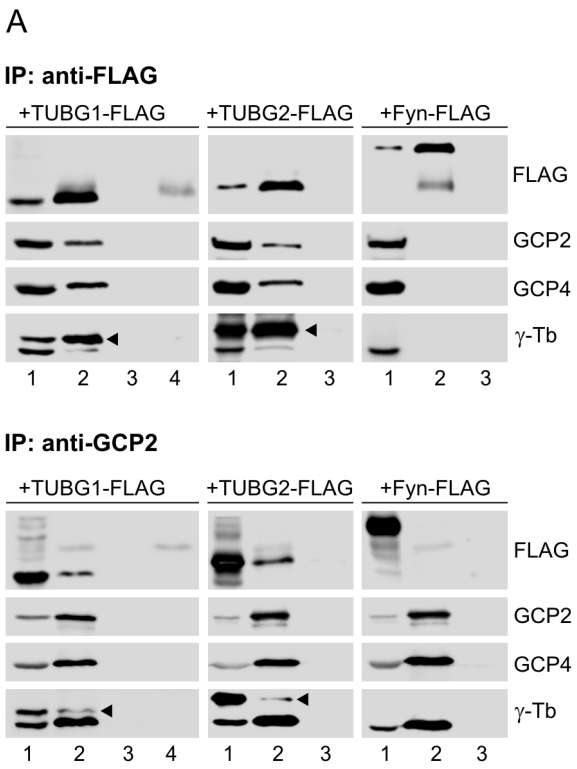

Figure S2. Coimmunoprecipitation of human γ-tubulins with GCP2 and GCP4 proteins. Extracts from HEK cells expressing FLAG-tagged human γ-tubulin 1 (TUBG1-FLAG), human γ-tubulin 2 (TUBG2-FLAG) or control mouse Fyn (Fyn-FLAG) were immunoprecipitated with antibodies to FLAG or GCP2, and blots were probed with antibodies to FLAG, GCP2, GCP4 and γ-tubulin (c-Tb). Extracts (1), immunoprecipitated proteins (2), protein A without antibodies incubated with extracts (3), immobilized antibodies not incubated with extracts (4). Arrowheads indicate the positions of exogenous γ-tubulins.

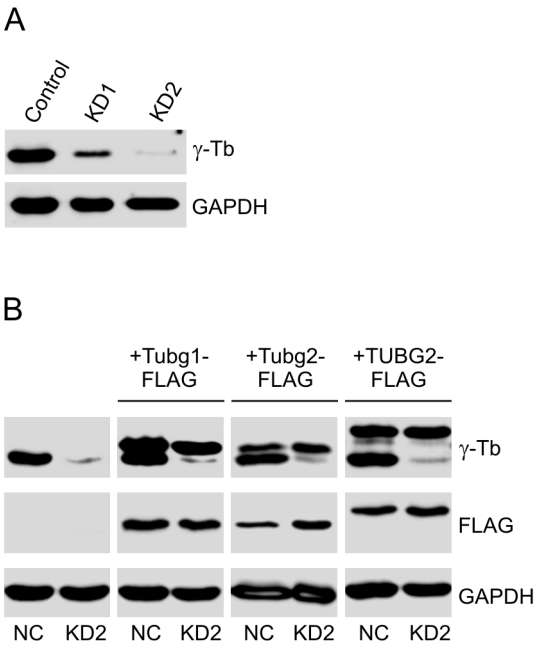

Figure S3. Immunoblot analysis of U2OS cells in phenotypic rescue experiments with FLAG-tagged γ-tubulins. (A) Immunoblot analysis of whole cell extracts from cells transfected with negative control (Control) or γ-tubulin specific siRNAs (KD1 and KD2). Staining with antibodies to γ-tubulin (γ-Tb) and GAPDH. (B) Cells with depleted c-tubulin 1 (KD2), expressing FLAG-tagged mouse γ-tubulin 1 (Tubg1-FLAG), mouse γ-tubulin 2 (Tubg2-FLAG) or human γ-tubulin 2 (TUBG2-FLAG). Immunoblots of whole cell lysates probed with antibodies to γ-tubulin (γ-Tb), FLAG and GAPDH (loading control). Arrowhead indicates the position of endogenous γ-tubulin.

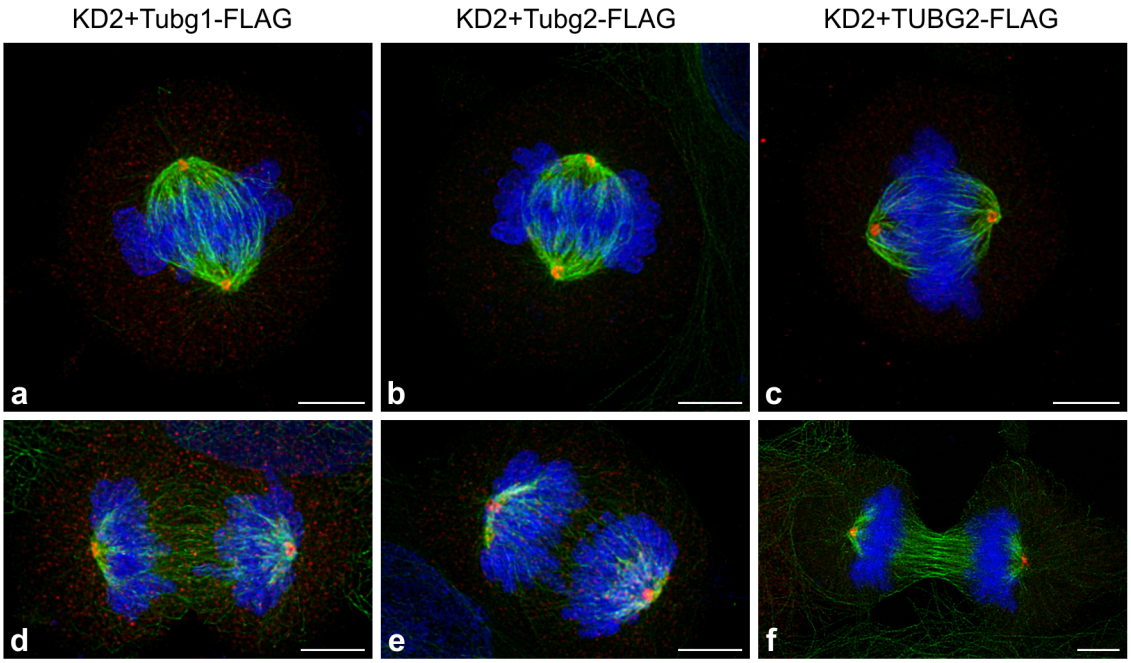

Figure S4. γ-Tubulin 2 rescues mitotic spindle organization and function in γ-tubulin 1-depleted cells. U2OS cells depleted of γ-tubulin 1 and expressing FLAG-tagged mouse γ-tubulin 1 (a, d; Tubg1-FLAG), mouse γ-tubulin 2 (b, e; Tubg2-FLAG) or human γ-tubulin 2 (c, f; TUBG2-FLAG). Cells were stained for FLAG (red) and β-tubulin (green). DNA was stained with DAPI (blue). Final images were made by maximum intensity projection of 30–40 deconvolved confocal z-sections spaced at 0.125 µm. Scale bars 5 µm.

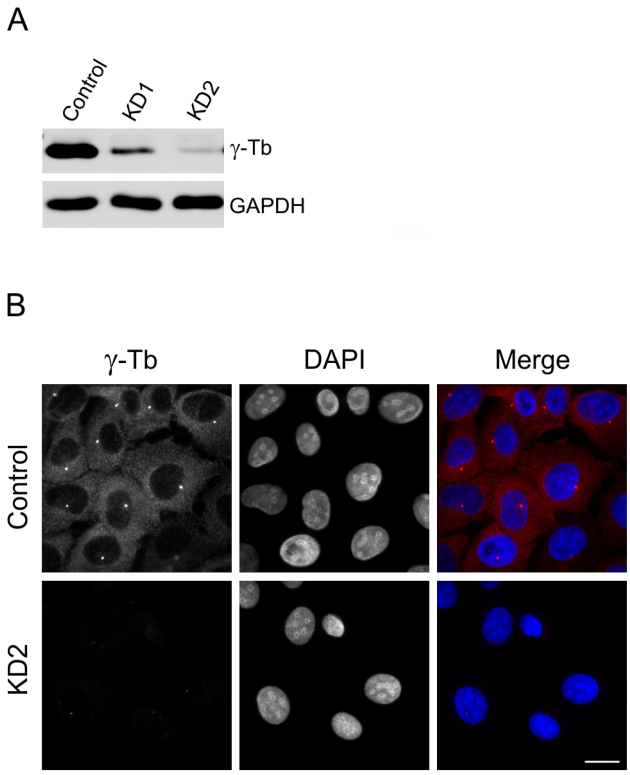

Figure S5. Depletion of γ-tubulin 1 in U2OS cells by shRNA. Cells transfected with empty pLKO.1 vector (Control), TUBG1 shRNA expressing vectors p9396sh (KD1) or p120194sh (KD2). (A) Immunoblots of whole cell lysates probed with antibodies to γ-tubulin (γ-Tb) and GAPDH (loading control). (B) Immunofluorescence staining with antibody to γ-tubulin (red) and with DAPI (blue). Fluorescence images of cells stained for γ-tubulin were captured under identical conditions and processed in exactly the same manner. Scale bar 20 μm.

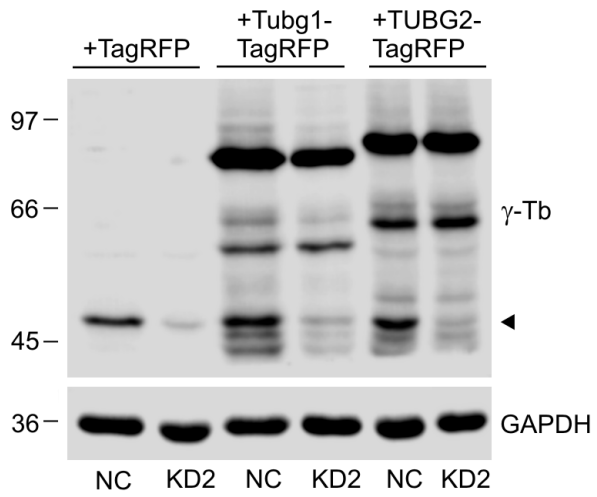

Figure S6. Immunoblot analysis of U2OS cells in phenotypic rescue experiments with TagRFP-tagged γ-tubulins. U2OS-EB1 cells with depleted γ-tubulin 1 (KD2; shRNA) or negative control cells (NC; pLKO.1), expressing TagRFP, tagged mouse γ-tubulin 1 (Tubg1-TagRFP) or tagged human γ-tubulin 2 (TUBG2-TagRFP). Immunoblots of whole cell lysates probed with antibodies to γ-tubulin (γ-Tb) and GAPDH (loading control). Arrowhead indicates the position of endogenous γ-tubulin.

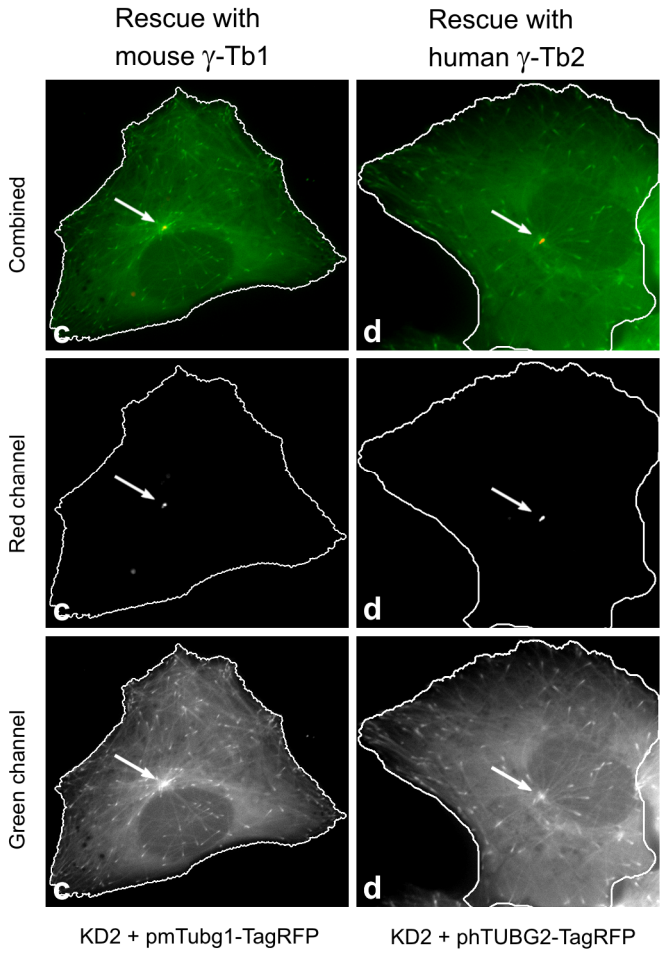

Figure S7. γ-Tubulin 2 rescues microtubule formation in γ-tubulin 1-depleted cells during interphase. Time-lapse imaging of U2OS-EB1 cells for quantitative evaluation of microtubule (+) end dynamics. Cells with depleted γ-tubulin 1 (KD2) expressing either mouse γ-tubulin 1 (pmTubg1-TagRFP) or human γ-tubulin 2 (phTUBG2-TagRFP). Single frame coloured images Fig 5c and Fig. 5d were separated to red and green channels for a better evaluation of c-tubulin-TagRFP fusions (red) and EB1-GFP (green). White arrows mark MTOC

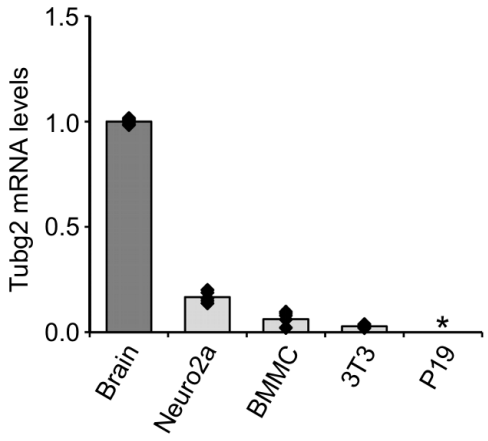

Figure S8. Comparison of γ-tubulin 2 expression in mouse brain and cell lines. Expression of gene for γ-tubulin 2 (Tubg2) in neuroblastoma (Neuro2a), bone marrow mast cells (BMMC), embryonal fibroblasts (3T3) and embryonic carcinoma cells (P19) relative to the level in brain. Data are presented as mean fold change (columns) with individual samples displayed (diamonds). Three biological replicates were quantified twice under identical conditions. *, undetectable level in P19 cells.